Formulation, characterization and processing of protein-based hydrogels

Zur Erlangung des akademischen Grades eines

DOKTORS DER INGENIEURWISSENSCHAFTEN (DR.-ING.)

von der KIT-Fakultät für Chemieingenieurwesen und Verfahrenstechnik des Karlsruher Instituts für Technologie (KIT)
genehmigte

DISSERTATION

von

Sandra Katrin Haas, M.Sc.

aus Stuttgart

Tag der mündlichen Prüfung: 28. März 2023

Erstgutachter: Prof. Dr. Jürgen Hubbuch

Zweitgutachter: Prof. Dr. rer. nat. Christoph Syldatk

Danksagung

Ohne die Mitwirkung und Unterstützung zahlreicher Menschen, denen ich im Folgenden danken möchte, wäre diese Dissertation nicht möglich gewesen.

Dazu zählt insbesondere Prof. Dr. Jürgen Hubbuch, der mir die Möglichkeit gegeben hat, Teil seiner Arbeitsgruppe am Institut für Molekulare Aufarbeitung von Bioprodukten zu werden. Vielen Dank für deine Unterstützung, dein Verständnis, dein Vertrauen, deinen Beitrag zu meiner wissenschaftlichen Arbeit und für die große Freiheit, die ich von dir während der gesamten Zeit erhalten habe.

Im Rahmen eines Kooperationsprojektes, für dessen finanzieller Förderung mein Dank der Baden-Württemberg Stiftung gilt, möchte ich mich ebenfalls bei meinem Projektpartner Prof. Dr. Stefan Schiller, und insbesondere seinen Mitarbeitern Anna Resch sowie Uwe Jonas bedanken. Dazu kamen erfolgreiche KIT-interne Kooperationen mit Prof. Dr. Gisela Guthausen vom EBI mit ihrem Mitarbeiter Nicolas Schork und weiterhin die angenehme Zusammenarbeit mit Frank Kirschhöfer (IFG) und Ralf Rössler (IAM-WK). Prof. Dr. Christoph Syldatk gilt mein Dank für die Begutachtung meiner Arbeit und seinem Interesse an meinem Thema.

Den Beitrag aller Studenten mit denen ich zusammenarbeiten durfte, sowohl durch ihre Persönlichkeit, die zahlreichen Stunden im Labor und ihrem Engagement, möchte ich an dieser Stelle ebenfalls würdigen. Namentlich sind dies Adrian Schimek, Florian Kaiser, Friederike Götz, Helin Arslan, Henri Steinweg, Monika Desombre, Laura Zintel und Saskia Körner.

Ein besonderer Dank gilt allen Kollegen und Bürokollegen am MAB - insbesondere aber der 3D-Druck Gruppe um Lukas Wenger, Barbara Schmieg, Carsten Radtke, Sarah Gretzinger, Svenja Strauß und David Grijalva - die ich im Laufe meiner Zeit am Institut kennen und schätzen lernen durfte. Durch die zahlreichen gemeinsamen Mittagspausen, Kaffee- und Kuchenpausen, eure Beiträge und gemeinsame Zeit auf Seminaren, Konferenzen und Abendveranstaltungen, habt ihr maßgeblich zur Qualität dieser Arbeit beigetragen und dafür gesorgt, dass ich die letzten Jahre im positiven Sinne wohl nie vergessen werde. Ohne euch hätte es nur halb so viel Spaß gemacht!

Neben all den fachlichen Beiträgen möchte ich mich bei meiner Familie und Freunden bedanken – ihr habt mir neben der Arbeit immer wieder gezeigt was das eigentlich Wichtige im Leben ist. Dabei gilt mein besonderer Dank meinen Eltern, meinem Bruder, meiner Schwester und meinen Schwiegereltern, für euer Vertrauen, offenes Ohr, Verständnis und die motivierenden Worte. Nicht genug für seinen Rückhalt kann ich mich bei Marius bedanken. Ohne deine Unterstützung bei jeder Entscheidung, die ich oder wir gemeinsam getroffen haben, hätte ich diese Promotion wohl nie begonnen und auch nie beendet. Neben unseren Kindern Vivien und Vincent bist du die wichtigste Person in meinem Leben und ich bin überglücklich, mit euch diesen gemeinsamen Weg gegangen zu sein!

Jeder ist ein Genie! Aber wenn Du einen Fisch danach beurteilst, ob er auf einen Baum klettern kann, wird er sein ganzes Leben glauben, dass er dumm ist.

Albert Einstein

Abstract

In recent years, there has been an increasing need for materials derived from renewable resources like proteins which has led to a lot of progress in the emerging field of protein-based materials. Right now, research in this field is focused on the development of potential applications in medical purposes, as proteins and peptides are expected to be biocompatible and biodegradable combined with specific, stimuli-responsive material characteristics. Also, advances in recombinant technologies for deoxyribonucleic acid (DNA) enabled the development of engineered peptide-based polymers based on natural role models. One example molecule that is enclosed in this dissertation are elastin-like proteins (ELPs) mimicking mammalian tropoelastin. Even though they are crucial for the design of new protein-based materials with desired properties, the influencing parameters during formulation and storage which are determining the mechanical properties of the formed hydrogels, as well as the physics underlying the formation of protein networks remain poorly understood.

The purpose of this thesis is, to increase our understanding of protein-based hydrogels during their formulation, characterization, and processing. In addition to the development of dityrosine-crosslinked protein-based hydrogel formulations for homo- and copolymers made from naturally occurring proteins and an artificially derived ELP, several challenges associated with protein-based hydrogels were addressed within this thesis. To obtain protein-based hydrogels from recombinantly expressed ELPs, their processing was examined by performing and evaluating three purification routes for a hydrophobic ELP construct with low temperature transition. In the formulation part of this work, a novel ink for extrusion printing of unmodified casein was established to demonstrate the general feasibility of using additive manufacturing to functionalize and process the hydrogel material. For the characterization of the developed materials, traditional macroscopic methods such as rheometry, uniaxial compression and weight-based swelling ratios were applied. With magnetic resonance imaging, a non-destructive analytical strategy with a high spatial resolution was established to monitor the swelling behavior of hydrogels. Using this approach, even the wetting and swelling behavior of hydrogels prepared or swollen in liquids with complex composition as well as the behavior of complex hydrogels geometries could be described, being particularly useful for the characterization of functionalized hydrogel materials.

The three topics formulation, characterization and processing were covered from different perspectives with dityrosine-crosslinked protein-based hydrogels in a total of five studies. In an initial study, three different purification routes of a novel, artificially designed hydrophobic ELP construct expressed in inclusion bodies in *Escherichia coli* were evaluated. With the objective of high target yield and purity as well as economic and scalable process design, formulation salinity and nucleic acid content were screened. The ELP construct, hexahistidine-tagged and with a lower critical solution temperature (LCST) below room temperature in water, was purified using homogenization and inclusion body dissolution, either followed by high-salt precipitation, the combination of high-salt precipitation and one cycle of inverse transition

cycling (ITC) or immobilized metal affinity chromatography (IMAC) in combination with a size-exclusion chromatography. The high-salt precipitation method had the highest yield of the target molecule, but low purity (60 %) and higher nucleic acid contamination and salinity. The ITC method increased purity and nucleic acid removal, but also reduced overall yield by 17 – 34 % during the cold spin centrifugation step as a function of the applied centrifugation time due to the low LCST temperature of the ELP construct used. IMAC had comparable purity and a slightly lower yield, but also higher nucleic acid removal. When considering scale-dependent costs and the aim to generate material for biomedical applications, ITC (high processing costs due to temperature-dependent centrifugation steps) should be weighed against IMAC (high investment costs), while salt-induced precipitation could be an option for bulk application due to its high yield and simplicity.

Before polymerizing protein-based hydrogels with the obtained ELP construct, a study with a more general approach was conducted. The aim of the study was to understand how the type and characteristics of protein in combination with formulation conditions affect the mechanical properties of dityrosine-crosslinked hydrogels. Unmodified, commercially available proteins bovine serum albumin (BSA) and casein were crosslinked under different conditions while keeping the photoinitiating system constant. The resulting hydrogel networks were stored in buffer systems with or without external stimuli applied to the network and the hydrogels analyzed for their mechanical properties. The protein folding and thus the three-dimensional (3D) arrangement and amino acid residue surface availability was varied by adding different urea concentrations to the formulation buffer and measuring the storage modulus and loss factor with oscillatory rheometry. Higher urea concentrations increased the structural strength and elasticity of the hydrogel with the exact underlaying mechanisms responsible for this effect remaining unclear. The storage modulus, fracture strain, and compressive strength all increased with protein concentration, with a concentration-dependent maximum elasticity at 60 mg/ml and the fracture strain not further increasing above 80 mg/ml. In the final substudy, the rheological behavior and weight-based swelling ratio of hydrogels containing either 100 mg/ml casein or BSA were assessed as a function of urea concentration and the net charge of BSA protein at different preparation pH values. The resulting hydrogel properties were dependent on the protein and storage medium, highlighting the importance of formulation components for the development of the desired mechanical properties of dityrosine-crosslinked protein-based hydrogels.

To demonstrate the wide variety of potentially crosslinkable proteins, these methods were also applied to four proteins ranging from the intrinsically disordered ELP construct to BSA with an ordered tertiary structure. These proteins were used to create either homopolymeric or copolymeric dityrosine-crosslinked protein-based hydrogels mixed in different ratios. The rheological properties of the resulting homopolymeric hydrogel networks differed based on the protein characteristics, while the uniaxial compression properties were comparable for all protein constructs. The second goal of this study was to find a sample way to modify the mechanical properties of dityrosine-crosslinked hydrogels, without determining the specific influence of specific protein properties on the resulting hydrogel network, which is difficult due to the many factors that vary between chemical complex protein molecules. To do this, copolymeric hydrogels were polymerized by mixing two of the four proteins in two different buffer conditions prior crosslinking, keeping the total sum of amino acids constant by using weight-dependent concentrations. The rheological properties of these copolymeric hydrogels

were dependent on the mixed protein types and concentrations, with the compressive strength and hydrogel toughness peaking for mixtures containing casein compared to their related homopolymers. Overall, within the limitations of the study, the feasibility to modify the mechanical properties of dityrosine-crosslinked protein-based hydrogels by creating copolymeric hydrogels of different proteins with known properties of their homopolymeric hydrogels, was demonstrated. This provides a simple tool for the prospective design of protein-based hydrogels for specific applications.

For the processing of bio-based materials, additive manufacturing with the ability of a layerwise generation of 3D objects with complex geometries is an emerging field. Currently, most ink formulations for bio-based materials rely on modified chemical substances. As one advantage, the photoinduced dityrosine-crosslinking potentially allows the extrusion-based printing of unmodified proteins. In one study, a photopolymerizable ink formulation based on the naturally occurring protein casein was developed for extrusion printing. This ink is made by mixing the protein, the photoinitiating system, buffer and a thickening agent to increase extrudability of the ink solution. The study showed, that the ability to manufacture such an ink heavily depends on the thickening agent and mixing procedure used. In total, eight different thickening agents were tested to find the most suitable one for increasing the viscosity of the mixed ink without introducing irreversible foaming of inhibition of the formation of stable hydrogels. For the developed ink formulation, sodium alginate was found to be the most effective thickening agent and was further used for printing functionalized hydrogel structures with up to 30 layers.

Besides the processing into functionalized hydrogel structures, the understanding and characterization of the time-dependent stimuli-responsiveness of such hydrogel is important during the development for their potential applications. Hydrogels may consist of multiple components, with salts and buffer substances accounting for more than half of the as-prepared hydrogel dry weight. These characteristics can be challenging for a meaningful interpretation of common analytical methods such as weight-based swelling ratios. Magnetic resonance imaging (MRI) is a non-destructive technique that allows for the spatially resolved 3D study of soft materials. The previously established ink formulation was 3D printed to form an auxetic geometry, dried to create comparable sample conditions, and its wetting and swelling behavior in different liquids examined using MRI. The behavior of the hydrogel was found to be different depending on the liquid it was immersed in. This study demonstrated the potential of using MRI to study complex hydrogel structural changes, monitor the immersion of liquid into, and the stimuli-dependent hydrogel reaction of hydrogels.

This work has laid the foundation for creating a tool for the development of protein-based hydrogels through a deeper understanding of the factors that influence hydrogel formulation using visible light-induced dityrosine crosslinking. An in-depth understanding of the production process of a hydrophobic elastin-like protein has also been gained, which will help to make the production of this class of proteins more efficient and cost-effective. Customized processing of the developed materials via extrusion printing allows for the creation of functionalized hydrogels with customized mechanical properties. To study complex processes in these functionalized hydrogels, MRI can be applied. Its potential was shown by monitoring the time-dependent wetting and swelling behavior of auxetic hydrogel structures.

Zusammenfassung

In den letzten Jahren ist der Bedarf an Materialien aus erneuerbaren Ressourcen gestiegen, was zu großen Fortschritten auf dem Gebiet der proteinbasierten Materialien geführt hat. Derzeit konzentriert sich die Forschung in diesem Feld dabei insbesondere auf Anwendungen im medizinischen Bereich, da Proteine und Peptide in der Regel biokompatibel und biologisch abbaubar sind und über spezifische, auf Stimuli reagierende Materialeigenschaften verfügen. Fortschritte in der Rekombinationstechnologie für Desoxyribonukleinsäure (DNA) ermöglichten die Entwicklung von Polymeren auf Peptidbasis, die auf natürlichen Vorbildern basieren. Ein Beispielmolekül, das in dieser Dissertation verwendet wird, sind elastinähnliche Proteine (ELPs), die das Tropoelastin von Säugetieren nachahmen. Obwohl sie für das Design neuer proteinbasierter Materialien mit gewünschten Eigenschaften von entscheidender Bedeutung sind, sind die Einflussparameter während der Formulierung und Lagerung, die die mechanischen Eigenschaften der gebildeten Hydrogele bestimmen, sowie die der Bildung von Proteinnetzwerken zugrunde liegende Physik nach wie vor kaum verstanden.

Das Ziel dieser Arbeit ist es, das Verständnis von proteinbasierten Hydrogelen während ihrer Formulierung, Charakterisierung und Verarbeitung zu verbessern. Neben der Entwicklung von dityrosinvernetzten proteinbasierten Hydrogelformulierungen für Homo- und Copolymere aus natürlich vorkommenden Proteinen und eines künstlich hergestellten ELPs, wurden im Rahmen dieser Arbeit auch verschiedene weitere Herausforderungen im Zusammenhang mit proteinbasierten Hydrogelen behandelt. Damit proteinbasierte Hydrogele aus rekombinant exprimierten ELP gebildet werden können, wurde zunächst deren Herstellung untersucht, indem drei Aufreinigungsprozesse für ein hydrophobes ELP-Konstrukt mit niedrigem Temperaturübergang durchgeführt und bewertet wurden. Im Formulierung- und Prozessierungsteil dieser Arbeit wurde eine neuartige Tinte für den Extrusionsdruck von unmodifiziertem Kasein entwickelt, um die prinzipielle Anwendbarkeit der additiven Fertigung zur Funktionalisierung und Verarbeitung des Hydrogelmaterials zu demonstrieren. Zur Charakterisierung der entwickelten Materialien wurden herkömmliche makroskopische Methoden wie Rheometrie, Kompression und gewichtsbasiertes Quellverhalten angewandt. Mit der Magnetresonanztomographie wurde eine zerstörungsfreie Analysestrategie mit hoher räumlicher Auflösung etabliert, um das Quellverhalten von Hydrogelen zu überwachen. Mit diesem Ansatz konnte die Flüssigkeitsaufnahme und das Quellverhalten von Hydrogelen, die in Flüssigkeiten mit komplexer Zusammensetzung hergestellt und gequollen wurden, sowie das Verhalten komplexer Hydrogelgeometrien beschrieben werden, was besonders für die Charakterisierung funktionalisierter Hydrogelmaterialien nützlich ist.

Die drei Themen Formulierung, Charakterisierung und Verarbeitung wurden in insgesamt fünf Studien mit dityrosinvernetzten Hydrogelen auf Proteinbasis aus unterschiedlichen Perspektiven behandelt. In einer ersten Studie wurden drei verschiedene Aufreinigungsprozesse für ein neuartiges, künstlich entwickeltes hydrophobes ELP-Konstrukt, das in Einschlusskörpern in *Escherichia coli* exprimiert wurde, untersucht. Neben dem Ziel einer hohen Zielausbeute und Reinheit, sowie eines wirtschaftlichen und skalierbaren Prozessdesigns

wurden zusätzlich der Salzgehalt der Formulierung und der Nukleinsäuregehalt betrachtet. Die Aufreinigung des mit Hexahistidin markierten ELP-Konstrukts mit einer unteren kritischen Lösungstemperatur (LCST) unterhalb der Raumtemperatur in Wasser wurde durch Homogenisierung und Auflösung der Einschlusskörper begonnen, entweder gefolgt von einer Hochsalzfällung, einer Kombination aus Hochsalzfällung und einem Zyklus des *inverse transition cycling* (ITC) oder einer immobilisierten Metallaffinitätschromatographie (IMAC) in Kombination mit einer Größenausschlusschromatographie. Die Methode der Hochsalzfällung hatte die höchste Ausbeute an Zielmolekülen, aber eine geringe Reinheit (60 %) und eine höhere Nukleinsäurekontamination und höheren Salzgehalt in der Endformulierung. Die ITC-Methode erhöhte die Reinheit und die Nukleinsäureentfernung, verringerte aber auch die Gesamtausbeute um 17 bis 34 % während des Niedrigtemperaturzentrifugationsschritts in Abhängigkeit von der angewandten Zentrifugationszeit aufgrund der niedrigen LCST-Temperatur des verwendeten ELP-Konstrukts. IMAC hatte eine vergleichbare Reinheit und eine etwas geringere Ausbeute, aber auch eine höhere Nukleinsäureentfernung. Unter Berücksichtigung der skalenabhängigen Kosten und dem Ziel, Material für biomedizinische Anwendungen zu erzeugen, sollte ITC (hohe Prozessierungskosten aufgrund der temperaturabhängigen Zentrifugationsschritte) gegen IMAC (hohe Investitionskosten) abgewogen werden, während die salzinduzierte Fällung aufgrund ihrer hohen Ausbeute und Einfachheit eine Option für Massenanwendungen sein könnte.
Vor der Polymerisation von proteinbasierten Hydrogelen aus diesem ELP-Konstrukt, wurde eine Studie mit einem allgemeineren Ansatz durchgeführt. Ziel der Studie war es, zu verstehen, wie die Art und die Eigenschaften des Proteins in Kombination mit den Formulierungsbedingungen die mechanischen Eigenschaften der dityrosinvernetzten Hydrogele beeinflussen. Die unmodifizierten, handelsüblichen Proteine Rinderserumalbumin (BSA) und Kasein wurden unter verschiedenen Bedingungen vernetzt, wobei das photoinitiierende System konstant gehalten wurde. Die resultierenden Hydrogelnetzwerke wurden in Puffersystemen mit oder ohne externe Stimuli gelagert und die Hydrogele auf ihre mechanischen Eigenschaften hin untersucht. Die Proteinfaltung und damit die dreidimensionale (3D) Anordnung und die Oberflächenverfügbarkeit der Aminosäurereste wurden durch Zugabe verschiedener Harnstoffkonzentrationen zum Formulierungspuffer variiert und der Speichermodul sowie der Verlustfaktor mit oszillierender Rheometrie gemessen. Höhere Harnstoffkonzentrationen verstärkten die strukturelle Festigkeit und Elastizität des Hydrogels, wobei die genauen zugrunde liegenden Mechanismen, die für diesen Effekt verantwortlich sind, unklar bleiben. Der Speichermodul, die Bruchdehnung und die Druckfestigkeit nahmen mit der Proteinkonzentration zu, während die Elastizität ein konzentrationsabhängiges Maximum bei 60 mg/ml BSA aufwies und die Bruchdehnung oberhalb von 80 mg/ml BSA nicht weiter anstieg. In der letzten Teilstudie wurden das rheologische Verhalten und das gewichtsbezogene Quellungsverhältnis von Hydrogelen, die entweder 100 mg/ml Casein oder BSA enthielten, in Abhängigkeit von der Harnstoffkonzentration und der Nettoladung des BSA-Proteins bei verschiedenen pH-Werten der Formulierung untersucht. Die sich daraus ergebenden Hydrogeleigenschaften waren vom Protein und vom Lagermedium abhängig, was die Bedeutung der Formulierungskomponenten für die Entwicklung der gewünschten mechanischen Eigenschaften von dityrosinvernetzten Hydrogelen auf Proteinbasis hervorhebt.

Um die große Vielfalt der potenziell vernetzbaren Proteine zu demonstrieren, wurden diese Methoden im weiteren Verlauf auf insgesamt vier Proteine angewandt, die vom intrinsisch ungeordneten ELP-Konstrukt bis zu BSA mit einer geordneten Tertiärstruktur reichen. Diese Proteine wurden verwendet, um entweder dityrosinvernetzte Homo- oder Copolymerhydrogele herzustellen, wobei die Proteine in unterschiedlichen Verhältnissen gemischt wurden. Die rheologischen Eigenschaften der resultierenden homopolymeren Hydrogelnetzwerke unterschieden sich je nach Proteincharakteristik, während die Eigenschaften durch Kompressionsversuche für alle Proteinkonstrukte vergleichbar waren. Das zweite Ziel dieser Studie war es, eine Möglichkeit zu finden, die mechanischen Eigenschaften von dityrosinvernetzten Hydrogelen zu modifizieren, ohne den spezifischen Einfluss bestimmter Proteineigenschaften auf das resultierende Hydrogelnetzwerk zu bestimmen, da dies aufgrund der vielen Faktoren, die zwischen den chemisch komplexen Proteinmolekülen variieren, schwierig ist. Zu diesem Zweck wurden Copolymerhydrogele polymerisiert, indem je zwei der vier Proteine vor der Vernetzung in zwei verschiedenen Pufferbedingungen gemischt wurden, wobei die Gesamtsumme der Aminosäuren durch Verwendung gewichtsabhängiger Konzentrationen konstant gehalten wurde. Die rheologischen Eigenschaften dieser copolymeren Hydrogele waren von den gemischten Proteintypen und -konzentrationen abhängig, wobei die Druckfestigkeit und die Zähigkeit des Hydrogels bei kaseinhaltigen Mischungen im Vergleich zu den entsprechenden Homopolymeren am höchsten waren. Insgesamt konnte innerhalb der Grenzen der Studie gezeigt werden, dass es möglich ist, die mechanischen Eigenschaften von dityrosinvernetzten Hydrogelen auf Proteinbasis zu verändern, indem copolymere Hydrogele aus verschiedenen Proteinen mit bekannten Eigenschaften ihrer homopolymeren Hydrogele hergestellt werden. Damit steht mit dieser Methodik ein einfaches Werkzeug für das gezielte Design mechanischer Eigenschaften von Hydrogelen auf Proteinbasis für spezifische Anwendungen zur Verfügung.

Für die Verarbeitung biobasierter Materialien ist eine mögliche Option die additive Fertigung, eine Methode zur schichtweisen Herstellung von 3D-Objekten mit komplexen Geometrien. Die meisten Tintenformulierungen für biobasierte Materialien beruhen auf modifizierten chemischen Substanzen. Ein Vorteil der photoinduzierten Dityrosinvernetzung ist, dass dadurch unter anderem der extrusionsbasierte Druck von unmodifizierten Proteinen möglich sein kann. In einer weiteren Studie wurde eine photopolymerisierbare Tintenformulierung auf der Grundlage des natürlich vorkommenden Proteins Kasein für den Extrusionsdruck entwickelt. Diese Tinte wird durch Mischen des Proteins, des Photoinitiatorsystems, eines Puffers und eines Verdickungsmittels zur Erhöhung der Extrudierbarkeit der Tintenlösung hergestellt. Die Studie zeigte, dass die Herstellbarkeit einer solchen Tinte stark von dem verwendeten Verdickungsmittel und dem verwendeten Mischverfahren abhängt. Insgesamt wurden acht verschiedene Verdickungsmittel getestet, um das am besten geeignete zu finden, das die Viskosität der gemischten Tinte erhöht, ohne dass es zu einer irreversiblen Schaumbildung oder einer Hemmung der Polymerisation formstabiler Hydrogele kommt. Für die entwickelte Tintenformulierung erwies sich Natriumalginat als das wirksamste Verdickungsmittel und wurde für den Druck funktionalisierter Hydrogelstrukturen mit bis zu 30 Schichten verwendet.

Neben der Verarbeitung zu funktionalisierten Hydrogelstrukturen ist das Verständnis und die Charakterisierung der zeitabhängigen stimulusabhängigen Verhaltens solcher Hydrogele wichtig in der Entwicklung für ihre potenziellen Anwendungen. Hydrogele können aus mehreren Komponenten bestehen, wobei Salze und Puffersubstanzen mehr als die Hälfte des Trockengewichts des Hydrogels im Ausgangszustand ausmachen können. Diese Eigenschaften können eine aussagekräftige Interpretation gängiger Analysemethoden, wie z. B. gewichtsbasierter Quellungsquotienten, erschweren. Die Magnetresonanztomographie (MRI) ist eine zerstörungsfreie Technik, die eine räumlich aufgelöste 3D-Untersuchung von weichen Materialien ermöglicht. Die zuvor entwickelte Tintenformulierung wurde als eine auxetische Struktur gedruckt, getrocknet, um vergleichbare Probenbedingungen zu schaffen, und ihr Flüssigkeitsaufnahme- und Quellverhalten in verschiedenen Flüssigkeiten mittels MRI untersucht. Es zeigte sich, dass das Verhalten des Hydrogels je nach Flüssigkeit, in die es eingetaucht war, unterschiedlich war. Diese Studie zeigte das Potenzial des Einsatzes von MRI zur Untersuchung komplexer struktureller Veränderungen von Hydrogelen, zur Überwachung der Aufnahme von Flüssigkeit in das Hydrogel und der stimulusabhängigen Hydrogelreaktion.

Diese Arbeit hat durch ein tieferes Verständnis der Faktoren, die die Hydrogelformulierung unter Verwendung der durch sichtbares Licht induzierten Dityrosinvernetzung beeinflussen, den Grundstein für die gezielte Entwicklung von Hydrogelen auf Proteinbasis gelegt. Darüber hinaus wurde ein tiefes Verständnis des Produktionsprozesses eines hydrophoben elastinähnlichen Proteins gewonnen, was dazu beitragen wird, die Produktion dieser Proteinklasse effizienter und kostengünstiger zu gestalten. Die maßgeschneiderte Verarbeitung der entwickelten Materialien durch Extrusionsdruck ermöglicht die Herstellung funktionalisierter Hydrogele mit maßgeschneiderten mechanischen Eigenschaften. Um komplexe Prozesse in diesen funktionalisierten Hydrogelen zu untersuchen, kann MRI eingesetzt werden. Ihr Potenzial wurde durch die Überwachung des zeitabhängigen Flüssigkeitsaufnahme und Quellverhaltens von auxetischen Hydrogelstrukturen gezeigt.

Table of Contents

1 Introduction

Materials derived from renewable resources have gained interest in recent years due to increasing concerns about the environment, the accumulation and disposal of waste, and the depletion of fossil resources, thus increasing the demand for materials with lower environmental impact[1,2]. In general, examples of bio-based products are forestry, agriculture, textiles, paper and paper products, bioenergy, biofuels, biopharmaceuticals, and bio-based chemicals and plastics. The latter include amino acids (e.g. essential amino acids as food additives), some organic acids (e.g. citric acid mainly used as acidulent) and bioplastics (e.g. polylactic acid (PLA) as packaging materials, in the automotive industry, and in biomedical applications)[3–5], but also natural polymers themselves such as cellulose, starch, lignin and proteins used individually or in blends and composites[1]. Proteins are organic macromolecules which perform numerous functions in living organisms, ranging from acting as antibody in the immune defense, as biocatalysts (enzymes), hormones or structural components in cells or tissues. The research and development of protein-based materials is mainly focused on films, sheets, adhesives, plastics, foams, blends, composites, and gels aiming predominantly for biomedical applications such as scaffolds for tissue engineering, drug delivery systems and biosensors[1]. Despite some recent achievements in the literature, the physics underlying the formation of protein networks are still poorly understood[6]. A profound understanding of the translation of protein properties to the formed hydrogel networks and about the influencing parameters during the hydrogel formulation on the hydrogel characteristics would be essential for a targeted development of new protein-based materials with predicted and tunable properties[7]. In addition to the characterization of different protein-based hydrogels depending on their formulation and storage conditions, this includes the need of an improved understanding for the efficient purification of recombinant proteins such as elastin-like proteins mimicking naturally occurring tropoelastin, suitable production processes to be able to obtain arbitrary three-dimensional (3D) objects of protein-based hydrogels, and analytical techniques meeting the requirements of more sophisticated hydrogel formulations or functionalized hydrogels.

1.1. Proteins

Proteins are biomolecules based on amino acid chains which are connected to polypeptides by peptide bonds. Natural proteins consist of different sequences derived from 20 amino acids with unique residues as building blocks defining their primary structure. These amino acids differ in their characteristics and are most commonly classified by a total of eight different physicochemical measures - such as their charge at physiological pH, polarity, and hydrophobicity - as proposed by Taylor[8]. Artificially designed proteins can consist of the same building blocks, but also unnatural amino acids can be used in their structure[9].

1.1.1. **Spatial structure of proteins**

Hydrogen bonding between amine and carbonyl functional group within the peptide backbone segments of the same protein molecule result in local conformational arrangements such as α-helix and β-sheets referred to as the protein secondary structure. As a next level of protein organization, the term tertiary structure describes the spatial organization of the entire protein molecule consisting of a single chain, which is determined by interactions between amino acid residues which are far apart in the molecule chain (e.g. disulfide bridges between sulfhydryl functional groups, hydrogen bonds, ionic bonds and hydrophobic interactions). Some proteins assemble from two or more separate polypeptides, so called protein subunits, which is then referred to as a quaternary structure.[10,11] During the last decades, several studies revealed biologically active, functional proteins or protein regions which do not exhibit a unique 3D and thus tertiary structure under functional conditions. In contrast to ordered proteins and domains, these protein molecules are called intrinsically disordered proteins (IDPs) or as protein molecules that show intrinsically disordered protein regions (IDPRs). Due to their non-native degradation behavior, an increasing amount of scientific literature reflects the growing interest in these classes of proteins.[12,13]

1.1.2. **Parameters influencing protein stability**

In general, the confirmation of a protein in solution and thus its solubility and stability depends on the interrelationship of physical and chemical instabilities as well as instabilities related to the bioprocessing[14]. Chemical modifications are related to a change in the chemical composition and include reactions such as oxidation, hydrolysis of amino acid residues, isomerization, and racemization, while aggregation during the bioprocessing exemplarily can be introduced by shear stress, for example due to pumping or stirring[14–16]. In addition, the conformational stability of a protein in a solution heavily depends on the characteristics of the solution environment such as pH, buffer salt type and concentration, preservatives, surfactants, and other cosolvents such as non-ionic chaotropic agents[17]. The parameters relevant to this work that influence protein stability are described in more detail in the following chapters.

1.1.2.1. **Salt concentration and type**

The influence of salts on the confirmation and solubility of proteins differs depending on the used salt type, salt concentrations used in the solution and the protein as salts modulate the strength of intra- and intermolecular electrostatic interactions[17,18]. In 1888, Franz Hofmeister divided ions according to their effect on protein solutions in kosmotropes (inducing greater order and rigidity in biomacromolecules and thus decreasing protein solubility by precipitation effects) and chaotropes (induce disorder in biological macromolecules which can finally lead to protein unfolding and denaturation)[19,20].

1.1.2.2. **Solution pH**

The solution pH determines the type of charge (positive or negative) and total surface charge on the protein, affecting the intra- and intermolecular electrostatic interactions. For highly charged proteins, this results in different effects which are opposed to each other. First, an increased charge repulsion within the protein destabilizes a folded protein conformation. Second, an increasing number of formed intramolecular salt bridges can stabilize the

conformation. Third, more repulsive interactions between protein molecules reduce the susceptibility for protein aggregation.[17]

1.1.2.3. **Non-ionic chaotropic agents**

Chaotropic reagents, such as urea, are cosolvents known to decrease hydrophobic interactions in solutions[21]. The underlying mechanism of urea-induced protein denaturation is still under investigation, for example being unclear whether urea is stabilizing unfolded confirmations or being actively unfolding proteins and whether urea is directly interacting with the peptide backbone or amino acid residues of the proteins (direct mechanism) or by alteration of the water structure (indirect mechanism).[22–24] Depending on the protein, the destabilization of the protein confirmation may decrease its solubility (e.g. for protein with an ordered tertiary structure) which may result in urea-induced gelation of proteins as for bovine serum albumin, or the protein solubility even can be increased by disrupting micelle formation for casein or by inhibition of hydrophobic aggregation[25–28].

1.2. Protein-based hydrogels

Hydrogels derived from natural or artificial proteins as material source are referred to as protein-based hydrogels. In general, hydrogels are polymeric materials with the ability to swell and absorb water within its structure due to functional groups attached to the polymeric backbone without being dissolved due to crosslinks between network chains[29]. They can be classified depending on their physical properties and stimuli-responsiveness, crosslinking mechanism, biodegradability, ionic charge, preparation method or material sources[30,31]. The classifications being relevant for the understanding of the presented thesis will be explained more detailed in the following.

1.2.1. **Proteins as building blocks for protein-based hydrogels**

Several proteins have successfully been used in the formation of protein-based hydrogels with various ways of crosslinking, including collagen, gelatin, fibrin, elastin, fibroin, whey proteins, sericin, vegetable globulins, soy proteins, egg white proteins, pea proteins, wheat proteins and more[32,33]. Those proteins are either be derived from natural sources (e.g. by separation of casein from milk[34] or bovine serum albumin (BSA) from bovine serum[35]) or can be artificially designed and produced (e.g. by recombinant expression in microorganisms, mammalian systems or in plants[36], or by total chemical protein synthesis[37]). To be able to fulfill various essential and different tasks in the living organism (e.g. as antibodies in the immune response, enzymes for catalyzing chemical reactions, separation of biochemical reaction compartments and more), natural proteins vary in their structure and characteristics. In the present thesis, the focus will be on four kind of proteins whose structure are illustrated in Figure 1.1:

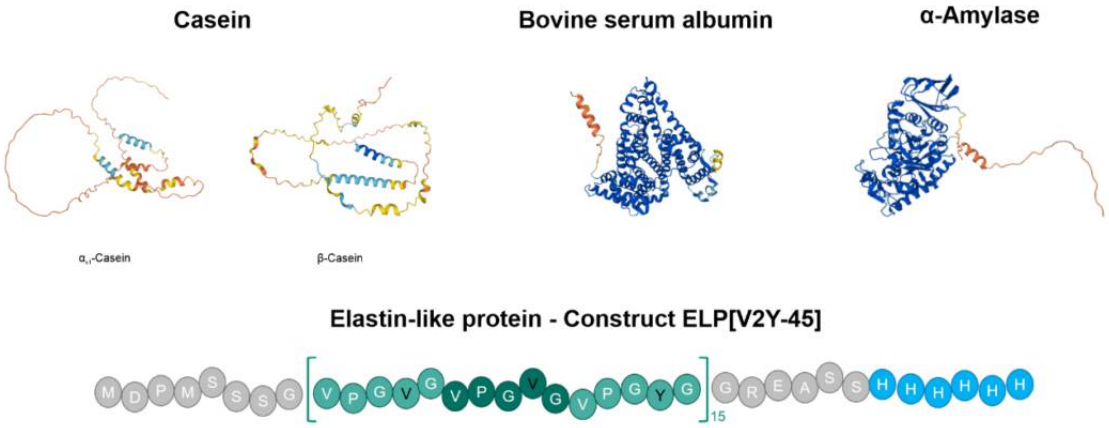

Figure 1.1 – Top: Tertiary structures of the three commercially available proteins used in this thesis with casein being represented by the two main subunits (Casein: αs1-Casein, P02662, β-Casein, P02666, Bovine Serum Albumin: A0A3Q1LNN7, α-Amylase: C8AWK4, UniProtKB/Swiss-Prot). Bottom: Schematic illustration of the amino acid sequence described in the one letter code for the ELP construct used in this thesis. The typical elastin-like polypeptide structure is highlighted in green, the guest residues in the pentapeptide structure are highlighted as black letters, the grey areas represent sequences associated with the expression vector design and the additional hexahistidine-tag is marked in blue.[38]

- Casein is an intrinsically disordered calcium(phosphate)-binding phosphoprotein without specific secondary structures and is one of the major proteins in the milk. It consists of four sub-fractions (≈ 38 % α_{s1}-, ≈ 10 % α_{s2}-, ≈ 36 % β-, ≈ 13 % κ-Casein) which all are amphiphilic with a molecular weight between 19 and 25 kDa. Due to its amphiphilic nature, a stable micellar structure tightly held together. This structure self-assembles by hydrophobic interactions and by the bridging of mineral calcium phosphate, with the exact structure of casein micelles still being under debate in the literature. While two of the four sub-fractions are able to form fibrils, casein micelles are known as chaperones for these fractions and non-casein proteins, as well as to safely transport and secrete nutrients as their biological function.[25,39–43]
- Albumin is with concentrations of up to 40 mg/ml and a share of about 60% of the total plasma protein content the most abundant soluble protein in vertebrates and contributes to the colloid osmotic pressure. It is a multifunctional protein, which transports a diverse range of metabolites, drugs, nutrients, metals and other molecules due its high ligand binding capacity. Albumin from bovine (BSA) is a globular, non-glycosylated protein with a size of around 66 kDa and its tertiary structure is stabilized by a total of 17 disulfide bridges.[44,45]
- α-Amylases belong to the class of enzymes catalyzing the hydrolysis of glycogen, starch, related polysaccharides and some oligosaccharides. They are found in a wide variety of microorganisms and tissues from animals and plants. Even though all α-Amylases possess the same catalytic function, their amino acid sequences are diverse. In the present work, bacterial α-Amylase expressed in Bacillus species with a size of around 53 kDa is used (C8AWK4, UniProtKB/Swissprot). Its tertiary structure is not stabilized by disulfide bridges.[46,47]

- Elastin-like proteins (ELPs) are intrinsically disordered engineered proteins mimicking mammalian tropoelastin - an extracellular matrix protein and key component of elastic fibres - and are based on a repetitive pentapeptide sequence with the forth guest residue representing any naturally occurring amino acid except proline. Typically, this protein class shows as lower critical solution temperature (LCST) above which they reversibly aggregate by increased hydrophobic interactions, which is manly dependent on the chemical composition and environmental stimuli. In the context of this thesis, a hydrophobic ELP construct with low temperature transition in water was used.[48–52]

1.2.2. **Preparation method**

Based on the methods of preparation, homopolymeric, copolymeric and multipolymer interpenetrating polymeric networks (IPN) are important classes of hydrogels and typical representatives are depicted in Figure 1.2[29]. Homopolymeric hydrogels are derived from a single monomer unit as building block. Depending on the nature of the monomer and polymerization technique, also the formation of skeletal structures can be achieved by homopolymeric networks[29]. Copolymers are synthesized from two or more species of monomers which can be arranged in differently – e.g. randomly, as blocks, in alternating or various more sophisticated configurations within the resulting copolymeric structure[53]. The third class of IPNs are defined as a material containing two polymers with each of them being independently crosslinked. Additionally, semi-IPN networks consisting of two polymeric materials with one component not being in a network form are reported in the literature.[54]

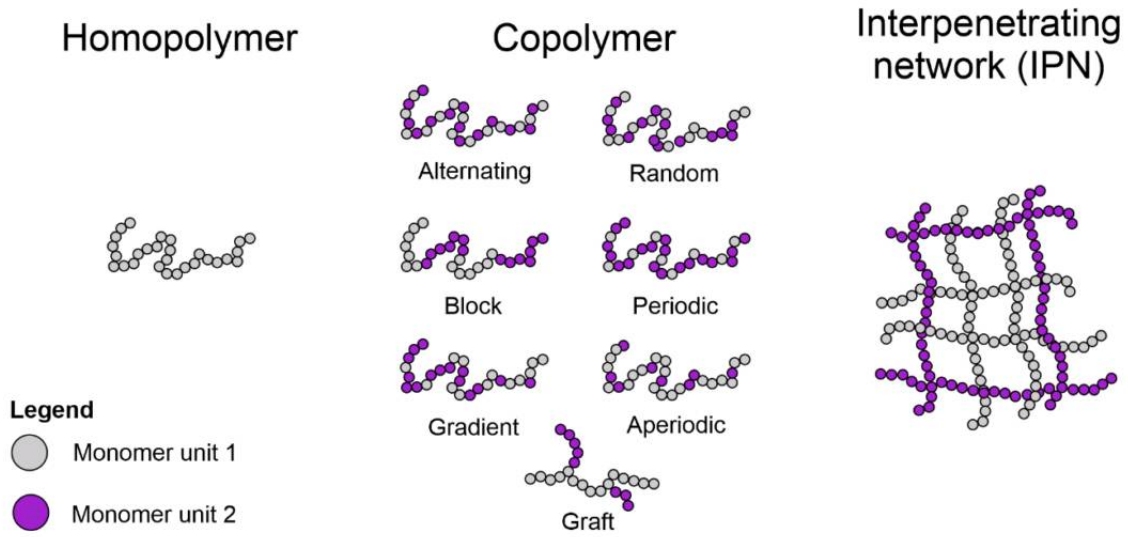

Figure 1.2 – Typical configurations of polymer networks derived from one (homopolymers) or multiple different monomer units. The latter can be either polymerized together with different arrangements of their monomer units (copolymers) or as separately formed networks (interpenetrating networks).

1.2.3. **Dityrosine-crosslinking**

Crosslinking methods for hydrogelation are based on the formation of weak or strong bonds, either within the polypeptide chains of a protein (intramolecular crosslinks) or between different protein molecules (intermolecular crosslinks)[55]. These crosslinks are forming a 3D network due to the physical or chemical reactions of active functional groups of the polymer chain[56]. Among several strategies to obtain physically or chemically crosslinked protein-based hydrogels, ruthenium-mediated dityrosine crosslinking was successfully applied for covalent protein crosslinking[57,58]. Induced by visible light and in the presence of an electron acceptor such as ammonium persulfate, the dication tris-bipyridylruthenium(II) is activated to tris-bipyridylruthenium(III), which is able to extract an electron from amino acids such as tyrosine or tryptophan (Figure 1.3). This leads to the formation of a radical species which can attack other groups, which eventually leads to covalent dityrosine crosslinking.[57] During the reaction, the potentially toxic electron acceptor is consumed, while the non-cytotoxic ruthenium complex is regenerated. Since its first introduction in 1999 by Fancy *et al.*[58], this method has been widely applied on the hydrogelation of several natural, modified natural and artificial protein constructs in different folding states[6,59–66]. Due to the fast reaction time, mild reaction conditions and biocompatibility of the photoinitiating system, it was also proven to be an applicable photoinitiating system for 3D printing of methacrylated gelatin - a protein-based material - using conventional 3D printing methods such as extrusion-based or lithography-based 3D printing[67].

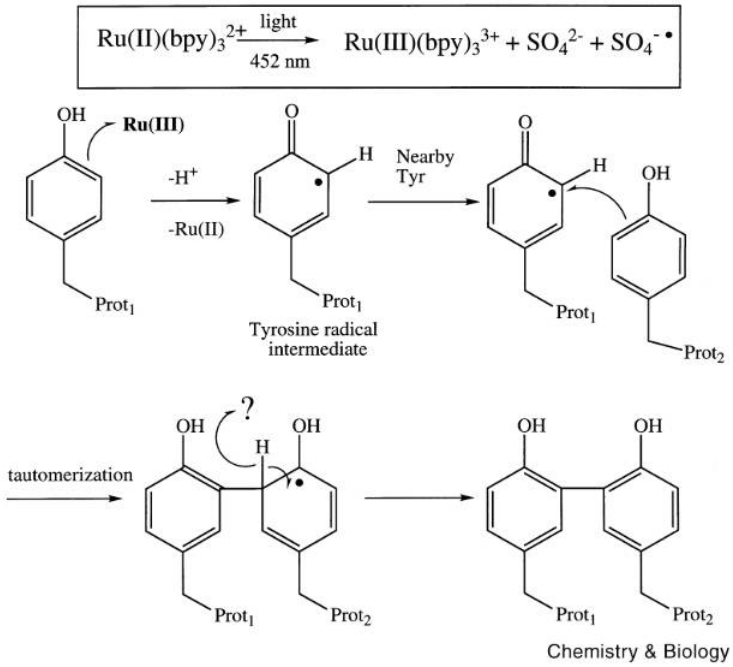

Figure 1.3 – Proposed reaction scheme of the dityrosine crosslinking of proteins. The dication of the photoinitiator tris-bypridylruthenium(II) is photolyzed with visible light in the presence of an electron acceptor (here: ammonium persulfate). In the presence of tyrosine residues of proteins, the formed trication is able to induce tyrosyl radical formation, which subsequently are crosslinked with another tyrosine residue to dityrosine.[57]

1.2.4. **Stimuli-responsiveness**

As one important subclass of hydrogels, stimuli-responsive hydrogel matrices are crosslinked networks whose physical and/or chemical properties such as their volume, network structure, mechanical strength and permeability are a function of the surrounding solution and environmental conditions[31,68,69]. According to El-Husseiny *et al.*[68], these hydrogels can respond to one or more physical (e.g. temperature, light, electric or magnetic fields, pressure, and ultrasound radiation), chemical (pH, specific chemical molecules, and ionic strength) or biological (enzymes and antibodies) stimuli. Due to these functionality, stimuli-responsive hydrogels are also called 'smart' or 'intelligent' hydrogels and show numerous potential applications, especially for biomedical applications as biosensors and drug-delivery systems[30].

1.2.5. **Functionalization of materials**

In order to expand the range of possible applications of a material, peptide- or protein-based hydrogels can be functionalized by different methods. First, they can be modified on a molecular basis (e.g. by methacrylation[70]), can be blended with other materials such as polysaccharides[71], or being formulated as nanocomposites[72]. Besides these methods, the effective properties of an material does not only arise from the bulk behavior of the materials of which it is composed, but also from the internal structuring[73]. Examples for such mechanical metamaterials are auxetics, materials showing a negative Poisson's ratio and thus are broadening under deformation stress, or origami structures, with the mechanical properties being depending on the geometry of the folded structure[74]. Examples for these two mechanisms are illustrated in Figure 1.4. Due to the complexity of their shape, additive manufacturing, casting processes and pressing methods are the manufacturing strategies of choice in research context[75].

Figure 1.4 – Internal structuring can be used to create material functionalization. As an example for an origami structure, a previously 3D printed flat star shape plate consisting of a flat polymer sheet and hinge regions by the introduction of shape memory polymers assembles into a pyramid shape upon cooling. Auxetic structures comprising of re-entrant honeycomb unit cells (highlighted in purple) are broadening when being deformed compared to their undeformed state. Adapted from Ge *et al.*[76] and Alderson & Alderson[77].

1.3. Additive manufacturing

Additive manufacturing, also known as 3D printing, is a process of generating 3D solid objects from a digital file. Traditional manufacturing methods, which typically involve the removal of material (subtractive manufacturing) through processes such as machining or drilling or formative manufacturing such as casting and forging. In contrast, 3D printing is based on the addition of successive layers from various material classes (e.g. plastics, metals, or ceramics), to build up the object layer by layer.[78] Additive manufacturing has revolutionized the way objects are designed and manufactured, enabling the creation of customized products in small quantities to the needs of individual consumers, possibly contributing to environmental sustainability by an optimized raw material usage, and offering the opportunity to reconfigure the manufacturing supply chain by on-demand manufacturing[79]. Thus, this manufacturing is used in a wide range of industries such as aerospace, medical and dental, consumer products, energy and automotive[80]. However, depending on the product and manufacturing process used, specific design limitations, the achievable spatial resolution, necessary postprocessing steps and low build speed compared to mass manufacturing methods have to be considered[80].

1.3.1. 3D Printing of hydrogels

3D printed hydrogels have many potential biomedical applications due to their deformability, flexibility and biocompatibility. These applications include drug delivery systems, implants, contact lenses, cell scaffolds, and cell cultures.[81] It is important to distinguish 3D printed hydrogels from the term *Bioprinting*, which involves the additive manufacturing of materials containing living cells using so-called bioinks[82]. The main challenges in bioprinting are the bioink properties before, during and after gelation and their impact on structural limitations and cell viability.[82] Currently, only limited ink formulations based on bio-based and renewable resources such as gelatin, sodium alginate, hyaluronic acid, methyl cellulose, or proteins, are used in 3D printing of hydrogels - even without the need of cytocompatible ink formulations. Several techniques are commonly used to print hydrogel structures, each with their own advantages and disadvantages. These modalities are schematically shown in Figure 1.5 and briefly discussed below.

1.3.1.1. Inkjet printing

Inkjet printing is a process of depositing microdroplets of ink onto a substrate using either by piezo-generated acoustic waves, pressure pulses applied in thermal inkjet systems or solenoid-actuated valves[83]. The resolution of this technique can be as fine as 10 to 50 µm. However, nozzle clogging, the use of low-viscosity inks and the small size of the orifices which are often comparable to the cells to be printed can be challenging, limiting the usage in 3D bioprinting.[82]

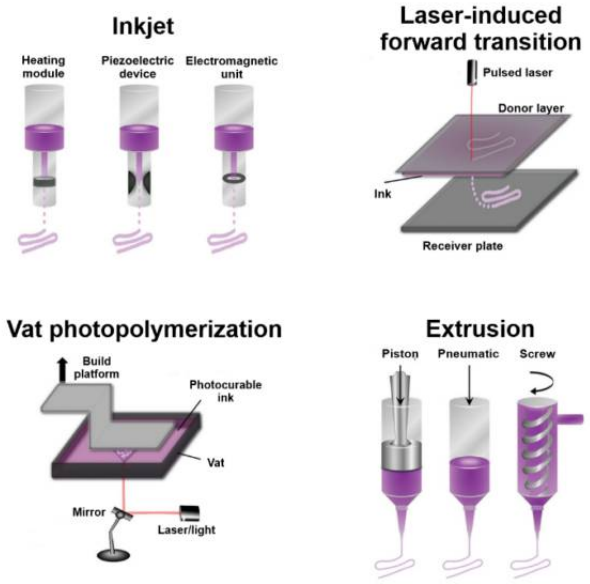

Figure 1.5 – Schematic illustration of different modalities for printing of hydrogel materials. Adapted from Ravanbakhsh *et al.*[83].

1.3.1.2. **Laser-induced forward transfer**

Laser-induced forward transfer is a printing technique that uses a laser to transfer ink droplets from a donor to a collector slide, allowing the precise deposition of materials even with high cell densities without negatively affecting cell viability and function. As it is a nozzle-free approach, it is not affected by clogging issues and has been successful applied with inks of a wide range of viscosities (1 – 300 mPa·s^{-1}). The need of rapid gelation kinetics to achieve high shape fidelity and a low overall flow rate are the main drawbacks of this modality.[84]

1.3.1.3. **Vat-photopolymerization**

Vat-photopolymerization involves the exposure of a liquid photocurable ink to a specific light wavelength to solidify it in a predetermined pattern. There are two main light-patterning methods used in this process: point-by-point exposure to a single programmed laser beam (stereolithography) and digital light processing illuminating each layer all-at-once (dynamic light processing,). These techniques allow the creation of constructs with fine details, while being limited by potential photo- and/or photoinitiator toxicity and light-triggered mutations.[83,85]

1.3.1.4. **Extrusion-based printing**

In extrusion-based printing, the hydrogel material is extruded through a nozzle to deposit layers of hydrogel material onto a substrate with the nozzle moving in a predetermined pattern to build up the desired object[83]. In general, ink formulations with shear-thinning behavior and a high viscosity are desired to obtain a good printability[86]. Pneumatic-based deposition uses compressed air to drive the ink formulation through a syringe and nozzle, while piston- and screw-based deposition are either relying on a linear moving piston or a rotating screw to mechanically extrude the ink[87]. The overall printing quality is determined by the rheological properties of the ink, the used hydrogelation mechanisms and possible enhanced printing

techniques[86]. In general, extrusion-based printing is relatively simple and inexpensive, but is limited by high shear stress in the nozzle, low flow rates and throughput and a comparable low resolution of the printed objects[83].
To address these challenges, several techniques to enhance the fabrication window of extrudable materials such as temperature-dependent printing, embedded printing, co-axial printing, and photopolymerization have been developed. Temperature-dependent printing is a variation of extrusion-based printing in which the viscosity of an ink formulation is modified by changing the cartridge – and optionally nozzle – temperature of the printer. This method is commonly applied to natural polymers such as agarose and agar, which form stable hydrogels at room temperature but can be dissolved in water at higher temperatures.[88,89] For the extrusion printing of soft or low viscosity hydrogels, in 2011, Wu *et al.*[90] developed the so-called 3D embedded printing using a support bath– mostly comprising of another hydrogel material - to physical support the printed structures. Since then, 3D embedded bioprinting has made progress in creating human-like tissues and organs, but the use of support baths in this process is still a relatively new field with limitations to be addressed, including cost, fabrication time, and safe removal of printed constructs[91]. Another technique to create structures such as two-phase filaments, hollow fibers or single-phase filaments is co-axial printing. Thereby, two or more capillaries are connected in a co-axial form to dispense material solutions, thus being limited to simple morphologies of the printed structures such as core-shell-type or hollow shapes.[87] The use of photopolymerizable ink solutions is either allowing *in situ* photopolymerization, using a cure-on-dispense setup inducing gelation during the extrusion process, or layerwise illumination of the printed material after increasing the shear viscosity of the uncrosslinked ink formulation to achieve a higher shape fidelity of the extruded strands through thickening agents[92].

1.4. Magnetic resonance imaging

Magnetic resonance imaging (MRI) is a technique based on the principles of nuclear magnetic resonance. It is used to analyze molecular structures since the 1940s and was first used for medical imaging in the 1970s, nowadays being a standard tool for the study and diagnostics of various diseases, injuries and medical conditions.[93,94] Furthermore, MRI is also used in non-biomedical fields, such as materials science, chemistry, physics, environmental science, electrochemistry and chemical engineering as it can non-invasively provide information about the composition and spatial distribution of molecules within a sample. Examples include the study of spatially heterogeneous chemical reactions, monitoring corrosion effects, and studying hydrogels.[95] In the following chapters, a brief introduction into the physical background behind this analytical technique and the image creation is given, as well as current applications to hydrogels are described.

1.4.1. Physical background

In general, MRI uses the natural magnetic properties of spinning nuclei to create images. The most commonly used nucleus in MRI is hydrogen, which has a single proton. However, other nuclei such as carbon-13, sodium, and phosphorus can also be used. These nuclei spin on their axes with their axes randomly aligned and thus exhibiting an overall net magnetic vector of zero. When a strong external magnetic field B_0 is applied, the nuclei orient themselves either

parallel or antiparallel to this field and precess around the direction of the external field with a specific frequency (Larmor frequency LF) given by the Larmor equation (Equation (1.1)) depending on the gyromagnetic ratio γ of the nucleus

$$LF = \frac{\gamma B_0}{2\pi}. \qquad (1.1)$$

To obtain the information, the nuclei need to be excited using energy with their resonance frequency, which is the Larmor frequency, with this resonance frequency lying in radio wave range. The excitation causes two effects. First, the nuclei spin is flipped and net magnetization vector changes from longitudinal to transversal direction. Second, the spins which were previously precessing in an individual phase, now precess in phase. This creates a detectable alternating current. When the radio frequency energy source is turned off, the nuclei's magnetization will return to its equilibrium state. This process is called relaxation, with the two relaxation times T1 and T2 to be distinguished. The longitudinal relaxation time T1 is the time it takes for the magnetic vector to return to its equilibrium state, while the transverse T2 relaxation time measures the time it takes for the nuclei's spinning axis to lose their alignment due to spin-spin-relaxation. While both times vary depending on the measured material, T2 is always shorter than T1.[96–99]

1.4.2. **Image creation**

To create an image of a 3D object using MRI, the following steps are performed. First, a slice of the object is selected by applying a magnetic gradient to the main magnetic field. The LF of a specific nucleus is dependent on the strength of the external magnetic field. As only the nuclei of the specific layer have the desired LF, this allows the excitation of a thin slice within the object using radiofrequency pulses. Next, frequency and phase encoding are used to determine the position of protons and generate small picture elements (voxels) by applying small temporary changes to the magnetic field. For phase encoding, a short temporary change in the magnetic field is applied between the radiofrequency excitation pulse and the signal readout, influencing the precessing phase of the spins to obtain different phase encodings. The same principle is then used to shift the resonance frequency by applying a magnetic gradient during the readout. Finally, mathematical processing of the raw data using Fourier Transformations is used to transform this data into an amplitude as a function of the frequency which determines the intensity of each voxel. To modify the image contrast, a second radiofrequency pulse is applied to flip the spin by 180 degrees and reverse the dephasing process, leading to the formation of an echo signal. The time between two radiofrequency pulses, known as the time of repetition, is chosen to be shorter than the time necessary for total longitudinal relaxation, allowing for the creation of T1 or T2-weighted images.[96–99]

1.4.3. **MRI of hydrogels**

In addition to its other uses, MRI has also been utilized in several studies in the research on hydrogels. Specifically, in the field of drug delivery, MRI is used to study the release of drugs from hydrogels over time, examining factors such as water penetration, drug release mechanisms, and the distribution and diffusion of drugs within the hydrogels. One advantage of MRI is, that these studies can be conducted both, *in vitro* and *in vivo*.[100,101] Additionally, the

distribution of cells within a hydrogel can be characterized, which is particularly useful in the field of tissue engineering. Examples include the analysis of the mixing quality of cell-laden bionks and cell distribution within the printed constructs, or the determination of the cell density in three-dimensional hydrogels.[102,103]

2 Thesis Outline

2.1. Research proposal

Polymeric elastomers are usually made from oil-derived building blocks with comparable low production costs. However, there are several natural molecules, such as certain structural proteins, that show superior mechanical properties, including high elasticity and fatigue resistance. Thus, natural protein-based components may allow to create materials with advanced mechanical properties, adding biodegradability and sustainable access as interesting features. In addition to naturally occurring proteins as building blocks, maturation of recombinant deoxyribonucleic acid (DNA) technologies allows the development of artificially designed proteins, such as elastin-like proteins based on the repetitive pentapeptide sequence of tropoelastin, with precise control of their amino acid sequence.

These proteins can be used as building blocks to generate three-dimensional hydrogel networks, either crosslinked by physical, or chemical crosslinking or a combination of both. Since physical crosslinks such as entangled chains, hydrogen bondings, hydrophobic interactions and crystallite formation usually do not lead to permanent hydrogelation, reversible hydrogels are obtained. In contrast, chemical crosslinks are formed by covalent molecular bonds. These crosslinks can be achieved by several strategies, including the crosslinking of tyrosine residues to dityrosine which was found to be contributing to the elastic properties of natural materials.

While the general feasibility of fabricating protein-based hydrogels has been demonstrated for both, commercially available and artificially derived proteins, there is still a lack of knowledge on the general properties of the mechanisms. One crucial point for understanding the crosslinking mechanisms is to describe the influence of uncrosslinked material properties on the mechanical properties of the resulting hydrogel networks. Another is the dependency on process parameters. The main focus of the present thesis is to tackle these challenges (1) by evaluating different production processes for an hydrophobic elastin-like protein, (2) by identifying parameters relevant for the resulting mechanical properties of crosslinked protein-based hydrogels, (3) by providing an ink formulation based on biologically derived materials and (4) the development of a suitable analytical method for the swelling behavior of hydrogels prepared or swelled in liquids containing high contents of salts or other buffer substances, or complex structuring as a function of different swelling medias.

For artificially designed proteins with expected superior mechanical properties, mostly no large-scale production exists. For the application in chemical industry, purification should first be developed with regard to cost-effectiveness. Especially in the context of hydrophobic ELPs exhibiting low temperature transition, limited knowledge on the process performance of different purification routes is available. Therefore, in a first study, a hydrophobic ELP construct promising distinct biomaterial properties toward its mechanical behavior and biocompatibility, will be compared and evaluated with regard to different production processes (Chapter 3).

The mechanical properties of a hydrogel network are a result of intra- and intermolecular interactions and the influence of the type of protein and reaction conditions on the mechanical properties of hydrogels is still unknown for most hydrogels prepared by visible light-induced dityrosine crosslinking. In addition, processing parameters such as the formulation buffer and storage medium are known to impact the resulting mechanical properties. The second study thus aims to extend the knowledge about protein-based hydrogels based on unmodified, commercially available proteins casein and bovine serum albumin. For this purpose, different proteins will be analyzed in dependence of the manufacturing and storage buffer consisting of different components as well as the influence of the present protein characteristics, for example by variation of intra- and intermolecular hydrophobic interactions and protein surface charge (Chapter 4).

Since artificially designed proteins in particular are usually only available in limited quantities due to manufacturing processes that have not yet been established on an industrial scale, it will also be investigated to what extent the mixture of different proteins prior to crosslinking alters the mechanical properties while the number of amino acids in the resulting copolymeric hydrogel remains constant (Chapter 5).

Besides the formulation of protein-based hydrogels, their 3D structuring remains a challenge. In the context of the protein-based hydrogels produced by visible light-induced photopolymerization, this includes among other points, the need of a light-protected ink production process, and a process either compatible with the low viscosity of uncrosslinked protein solution or the need of thickening agents. Typically, photocrosslinked hydrogels with a desired shape are produced in a mold, which requires a specific mold for each desired structure to be produced, but also limits the complexity of the hydrogel morphology and hydrogel height by the maximum penetration depth of the light. To overcome these disadvantages, an extrusion-based 3D printing process will be developed to add a large degree of freedom in the formation of arbitrary 3D objects for a hydrogel based on the unmodified protein casein prepared by dityrosine crosslinking. Using this printing process, the applicability of the whole developed system including material optimization and ink processing will be demonstrated (Chapter 6).

In addition to the mechanical properties of a hydrogel, further functionalization can be achieved by macroscopic structuring, for instance by using a re-entrant honeycomb structure to obtain an auxetic material. Unlike most common materials, these structures broaden under mechanic stress, which makes them interesting for any specialized application of swollen hydrogels including movement or reoccurring forces. Current analytical methods to describe the swelling behavior of a hydrogel are mainly based on weight or volume analysis of hydrogels. For weight-based swelling ratios, these parameters can only be accurately estimated, when excess liquid is fully removed without withdrawing liquid from the hydrogel network and for liquids containing neglectable amounts of buffer substances, while volume-based swelling require a complex volume estimation especially challenging for complex hydrogel geometries. Furthermore, these methods do not provide an insight into the spatially resolved hydration of the inner hydrogel structure. Thus, magnetic resonance imaging, an analytical tool widely used for image-based medical diagnostics, will be applied as a spatially resolving, non-destructive methodology in a case study for the time-dependent wetting and swelling behavior of the 3D printed auxetic hydrogel structure previously developed as a function of the swelling medium used (Chapter 7).

2.2. Overview of publications and manuscripts

An overview of the manuscripts which were prepared within the scope of this thesis is given in the following paragraphs. Each manuscript addressed one or more of the research objectives described above Chapter 2.1. The respective research question of the study, the methods applied, the key results and the current publication status of the respective manuscript are thereby described.

Chapter 3: Purification of a hydrophobic elastin-like protein toward scale-suitable production of biomaterials

Sandra Haas, Monika Desombre, Frank Kirschhöfer, Matthias C. Huber, Stefan M. Schiller, Jürgen Hubbuch

Frontiers in Biotechnology and Bioengineering (2022), Volume 10, Article 878838

The scalability of the production process as well as the process performance are important factors for evaluating the potential production of new recombinant polymer constructs on an industrial scale. In this study, an artificially designed, hydrophobic elastin-like protein exhibiting low temperature transition behavior was assessed in terms of achieved purity, product yield, formulation salinity and nucleic acid contamination as a function of three different purification processes. Those were either based on an affinity chromatography, high salt precipitation, or a combination of high-salt precipitation and temperature-dependent centrifugation steps. In addition to the evaluation of the process performance, all process routes were discussed with respect to their scale-dependent economic costs.

Chapter 4: Changing mechanical properties of photopolymerized, dityrosine-crosslinked protein-based hydrogels

Sandra Haas, Saskia Körner, Laura Zintel, Jürgen Hubbuch

Frontiers in Biotechnology and Bioengineering (2022), Volume 10, Article 1006438

Protein-based hydrogels were prepared from bovine serum albumin and casein by visible light-induced photopolymerization, thereby crosslinking the naturally occurring tyrosine residues of the proteins. The influence of the buffer system composition and the storage medium on the mechanical properties of the hydrogels was investigated. The results of this study have shown that changes in the composition of the uncrosslinked precursor solution as well as the storage medium affect the mechanical properties of the resulting protein-based hydrogels for both proteins and are therefore crucial parameters for material development.

Chapter 5: Mechanical properties of protein-based hydrogels derived from binary protein mixtures – A feasibility study

Sandra Haas, Jürgen Hubbuch

Polymers (2023), Volume 15, Article 964

Casein, bovine serum albumin, α-amylase and a hydrophobic elastin-like protein were used to successfully crosslink proteins with distinct characteristics to form homopolymeric and copolymeric protein-based hydrogels. Hydrogels prepared with varying protein shares were prepared in two different buffer solutions. Analysis of the mechanical properties of the manufactured hydrogel was conducted to gain a better understanding of the influence of the proteins on the resulting hydrogel network. This may help to create the path to develop tailored protein-based hydrogels by dityrosine crosslinking.

Chapter 6: Bio-based material formulation for extrusion printing by dityrosine crosslinking of unmodified casein

Sandra Haas, Friederike Götz, Jürgen Hubbuch

Bioprinting (2022), Volume 28, Article e00245

This article describes the development of a photopolymerizable ink formulation based on the unmodified and naturally occurring protein casein. Different thickening agents were investigated for their suitability to extend the manufacturing window for extrusion-based 3D printing by increasing the viscosity of the ink formulation. Additionally, manufacturability was taken into account by optimizing the mixing protocol to dispense the highly viscous thickeners. Finally, an auxetic structure was successfully printed using an ink formulation blended with sodium alginate.

Chapter 7: Magnetic resonance imaging: Time-dependent wetting and swelling behavior of an auxetic hydrogel based on natural polymers

Sandra Haas, Barbara Schmieg, Paul Wendling, Gisela Guthausen, Jürgen Hubbuch

Polymers (2022), Volume 14, Article 5023

In this manuscript, magnetic resonance imaging was used as an analytical tool to study the wetting and swelling behavior of a previously dried auxetic hydrogel which was 3D printed using the ink formulation developed in Chapter 6. The developed analytical method offers the advantage of monitoring internal structural changes and overall changes in the area covered by the functionalized hydrogel non-destructively as a function of time and as a function of the immersing liquid characteristics.

3 Purification of a hydrophobic elastin-like protein toward scale-suitable production of biomaterials

Sandra Haas, Monika Desombre, Frank Kirschhöfer, Matthias C. Huber, Stefan M. Schiller, Jürgen Hubbuch

Frontiers in Biotechnology and Bioengineering (2022), Volume 10, Article 878838

Abstract

Elastin-like proteins (ELPs) are polypeptides with potential applications as renewable bio-based high-performance polymers which undergo a stimulus-responsive reversible phase transition. The ELP investigated in this manuscript – ELP[V2Y-45] – promises fascinating mechanical properties in biomaterial applications. Purification process scalability and purification performance are important factors for the evaluation of potential industrial scale production of ELPs. Salt-induced precipitation, inverse transition cycling (ITC) and immobilized metal ion affinity chromatography (IMAC) were assessed as purification protocols for a polyhistidine-tagged hydrophobic ELP showing low temperature transition behavior. IMAC achieved a purity of 86 % and the lowest nucleic acid contamination of all processes. Metal ion leakage did not propagate chemical modifications and could be successfully removed through size exclusion chromatography. The simplest approach using a high-salt precipitation resulted in a 60 % higher target molecule yield compared to both other approaches with the drawback of a lower purity of 60 % and higher nucleic acid contamination. An additional ITC purification led to the highest purity of 88% and high nucleic acid removal. However, expensive temperature dependent centrifugation steps are required and aggregation effects even at low temperatures have to be considered for the investigated ELP. Therefore, ITC and IMAC are promising downstream processes for biomedical applications with scale dependent economical costs to be considered, while salt-induced precipitation may be a fast and simple alternative for large scale bio-based polymer production.

3.1. Introduction

In the recent years, the demand for high-performance products based on biological and renewable resources has arisen[104,105]. Nevertheless, the lack of simple production processes with affordable production costs is the reason for the current low market share of microbial polymers[106]. Maturation of recombinant deoxyribonucleic acid (DNA) technologies allowed the development of engineered peptide-based polymers based on natural role models showing high resilience[107,108]. In this context, elastin-like proteins (ELP) are a class of genetically encoded biopolymers based on the repeating pentapeptide sequence Val-Pro-Gly-Xaa-Gly (VPGXG) found in the mammalian elastin with the guest residue Xaa representing any naturally occurring amino acid except proline[49,109]. These engineered biopolymers show comparable mechanical properties as natural elastin, which enables applications in the biomedical and high-performance material field[110]. Several applications for ELPs are proposed, including ELP sequences as purification tags for different types of biomacromolecules[50,111–115], ELPs as drug delivery systems, *de novo* organelles and vesicular protocells[116–122], as material for tissue repair or engineering[118,123] or in 3D printing[124–126]. ELPs with low transition temperature gained further interest as an interesting sub-group with potential future biomedical applications[127–129]. Although several studies regarding the biosynthesis of ELPs were conducted[130], limited knowledge on the downstream processing of hydrophobic ELPs with low transition temperatures is available and, to the best of our knowledge, no industrial scale production of any ELP exists.

Chromatography is a popular, scalable strategy for protein purification based on the interaction between ligands bound to a stationary phase and molecules in the mobile phase. In immobilized metal ion affinity chromatography (IMAC), this interaction is based on metal ions like nickel or cobalt which show an affinity for mainly histidine and cysteine in aqueous solutions. To enhance the affinity of engineered genetically modified proteins, mostly polyhistidine tags are implemented into their amino acid sequence. Due to its high biospecific affinity, a high separation efficiency is reached in a single step purification, even under denaturing conditions such as high urea concentrations.[131–133] Main drawbacks of IMAC are the need of a purification tag, hazardous consumables (typically, imidazole is used as competitive agent) and possible physiological and pathological effects of divalent cations on proteins[134,135].

To overcome these drawbacks, Meyer *et al.*[50] introduced inverse transition cycling (ITC) as non-chromatographic purification route for ELPs or proteins with fused ELP tags. Below their transition temperature Tt, ELPs are soluble monomers showing full hydration. With rising temperature, polypeptide hydrophobicity is increased, its hydration is decreased and molecular interactions between ELP chains are leading to aggregation of the now insoluble ELPs.[49,50,136,137] Other external stimuli, such as changes in ionic strength or pH, as well as protein concentration and protein characteristics such as molecular weight and the exact amino acid sequence may induce this reversible precipitation[136]. ELPs are most commonly expressed in *Escherichia coli (E.coli)* in order to obtain monodisperse polymers with precise control of their amino acid sequence. This allows transition temperature design with a precision of a few degrees Celsius, even when fused to another protein.[107,138–140]

As for microbial expression of ELPs in inclusion bodies - such as for the ELP construct used in this manuscript - these have to be solubilized before ITC purification. In general, IB solubilization is performed using high concentrations of chaotropic agents (e.g. guanidine

hydrochloride or urea) or strong anionic tensides. These solubilization methods force protein unfolding, making a refolding of functional proteins into native conformation to a crucial step towards their recovery for globular proteins.[141,142] Since ELPs are in a disordered state below Tt, no refolding step is required in the following. Still, the weakening of hydrophobic interaction by chaotropic agents increases Tt of the ELP[21,143]. To avoid high centrifugation temperatures in the ITC process, buffer exchange against an aqueous buffer system without urea is usually performed by a salt-induced precipitation with the aim of ELP precipitation and subsequent dissolution the desired buffer. This additionally proved to already reduce the amount of host-cell protein (HCP) contamination[144–146]

Purification by ITC starts with a sample containing soluble and insoluble impurities together with soluble ELPs and is based on repeating centrifugation steps below or above Tt. During the cold spin, the centrifugation step is performed at a temperature below Tt, separating insoluble contaminants from the soluble ELP. Vice versa the ELP remains in the centrifugation pellet and is separated from soluble contaminants during the hot spin. The combination of a hot and cold spin is referred to as one cycle of ITC.[50,144,145,147] As its main advantage, no specialized technical equipment or reagents are needed for an ITC purification[148]. However, available industrial scale centrifugation techniques are generally discontinuous, limiting the throughput and therefore hindering economic upscaling[149]. Also, centrifugation steps are of high energy consumption and therefore highly expensive, especially when heating or cooling steps are necessary[150,151].

To date, studies comparing the performance of purification processes of biomacromolecules tagged either an ELP or polyhistidine were performed, showing a comparable product yield[111,113,148]. Additionally, new purification processes such as microfiltration of ELP fusion proteins[152] and organic extractions[146,153] were introduced. Still, IMAC and ITC are common downstream processes for ELPs as purification target, which are possibly suitable for large-scale productions. However, these purification methods were not compared to each other using a hydrophobic, polyhistidine-tagged ELP with low transition temperature as target molecule, which excludes the influence of different expression rates related to the applied tag.

In this study, salt-induced precipitation, ITC and IMAC were assessed to purify a C-terminal hexahistidine-tagged ELP from fermentation broth in laboratory scale. The recently published hydrophobic construct ELP[V2Y-45][128] - the guest residues are valine and tyrosine in a 2:1 ratio and the pentapeptide structure is repeated 45 times – was therefore chosen as purification target. This construct promises distinct biomaterial properties towards its mechanical behavior and biocompatibility, yet, due its low temperature transition behavior it is more complex and difficult to purify.[128] Firstly, a simple non-chromatographic process based on a high salt precipitation (HSP) without further purification steps was performed. Secondly, one cycle of ITC was conducted after the salt-induced precipitation. Thirdly, IMAC was used to purify the ELP and leaked nickel ions were traced. All processes were performed with the same fermentation batch, formulated into the same target buffer and discussed with a view to their final yield, removal of nucleic acids and salinity of the final buffer system with regard to possible further applications and suitability for large-scale purification processes.

3.2. Materials and Methods

3.2.1. Materials, buffers and protein expression system

Solutions and buffers were prepared with ultrapure water (PURELAB Ultra, ELGA LabWater, Lane End, UK). All buffers were pH-adjusted with 4 M sodium hydroxide solution and filtered through a 0.45 µm cellulose acetate membrane (Pall Corporation, New York, US-NY) prior usage. All chemicals were purchased from Merck KGaA (Darmstadt, DE). The investigated ELP is referred to as ELP[V2Y-45] following the nomenclature introduced by Meyer *et al.* [111]. The guest residues are valine and tyrosine in a 2:1 ratio and the pentapeptide structure is repeated 45 times. The one-vector-toolbox-platform approach developed by Huber *et al.* [128] was used for plasmid generation. ELP[V2Y-45] with an expected molecular weight of 21.6 kDa due to its amino acid sequence (see Appendix B.1) was expressed in inclusion bodies in *E.coli* strain Tuner(DE3) through isopropyl-β-D-thiogalactoside induction (Figure 3.1, *Fermentation*).

3.2.2. Preparation of starting material

With the obtained fermentation harvest, cell lysis was performed in three homogenization cycles using the high-pressure homogenizer EmulsiFlex-C3 (Avestin Inc., Ottawa, CAN) with a pressure of 1000 to 1500 bar. The inclusion bodies (IB) were dissolved either (a) during homogenization using a 20 mM sodium phosphate buffer (SPB) pH 8 containing 4 M urea followed by a centrifugation (30 min, 25°C, 17000 g) or (b) by a separated IB dissolving step. Thereby, homogenization was performed in 20 mM SPB pH 8 and the cell lysate was centrifuged (30 min, 17000g) at 4 or 25°C. The resulting pellet was solved in 20 mM SPB pH 8 containing 4 M urea in a ratio of 5 ml/g for at least one hour following a second centrifugation step (30 min, 25 °C, 17000 g). The resulting supernatant of the cell lysate centrifugation at 25°C was stored in aliquots at - 20 °C until further processing and is referred to as starting material in the following (Figure 3.1, *Preparation of starting material*).

3.2.3. High salt precipitation (HSP)

Ammonium sulfate (up to 1 M) and sodium chloride (NaCl, up to 1.5 M) were used to precipitate ELP[V2Y-45] - initially purified with two cycles of inverse transition cycling - to determine the salt concentration needed for the precipitation of the target molecule. Therefore, protein concentration in the supernatant before and after centrifugation (20 min, 25 °C, 17.000 g) was determined.

In the following process steps, a final concentration of 0.4 M ammonium sulfate (AMS) was dissolved in the starting material (Figure 3.1, *High salt precipitation*). The solution was centrifuged (20 min, 25 °C, 17000 g) and the supernatant was separated from the pellet. For further analysis, the pellet of the HSP was resuspended in 7.5 ml/g 20 mM SPB pH 8 containing 4 M urea at room temperature (RT) followed by another round of centrifugation (20 min, 25 °C, 17000 g).

3.2.4. Inverse Transition Cycling (ITC)

A salt-induced precipitation of the starting material was performed as described above using 0.4 M AMS. The resulting centrifugation pellet after the HSP was suspended in 7.5 ml/g ultrapure water at 4 °C. The cold spin (4 °C, 17000 g) was performed for 2, 5, 10, 20 and

30 min. For the subsequent comparison of the purification routes a centrifugation time of 2 min was chosen. The resulting supernatant was separated from the pellet and incubated at RT for 30 min before hot spin execution (20 min, 25 °C, 17000 g). The target protein in the centrifugation pellet was suspended in 20 mM SPB pH 8 containing 4 M urea for further analysis (Figure 3.1, *Inverse Transition cycling*).

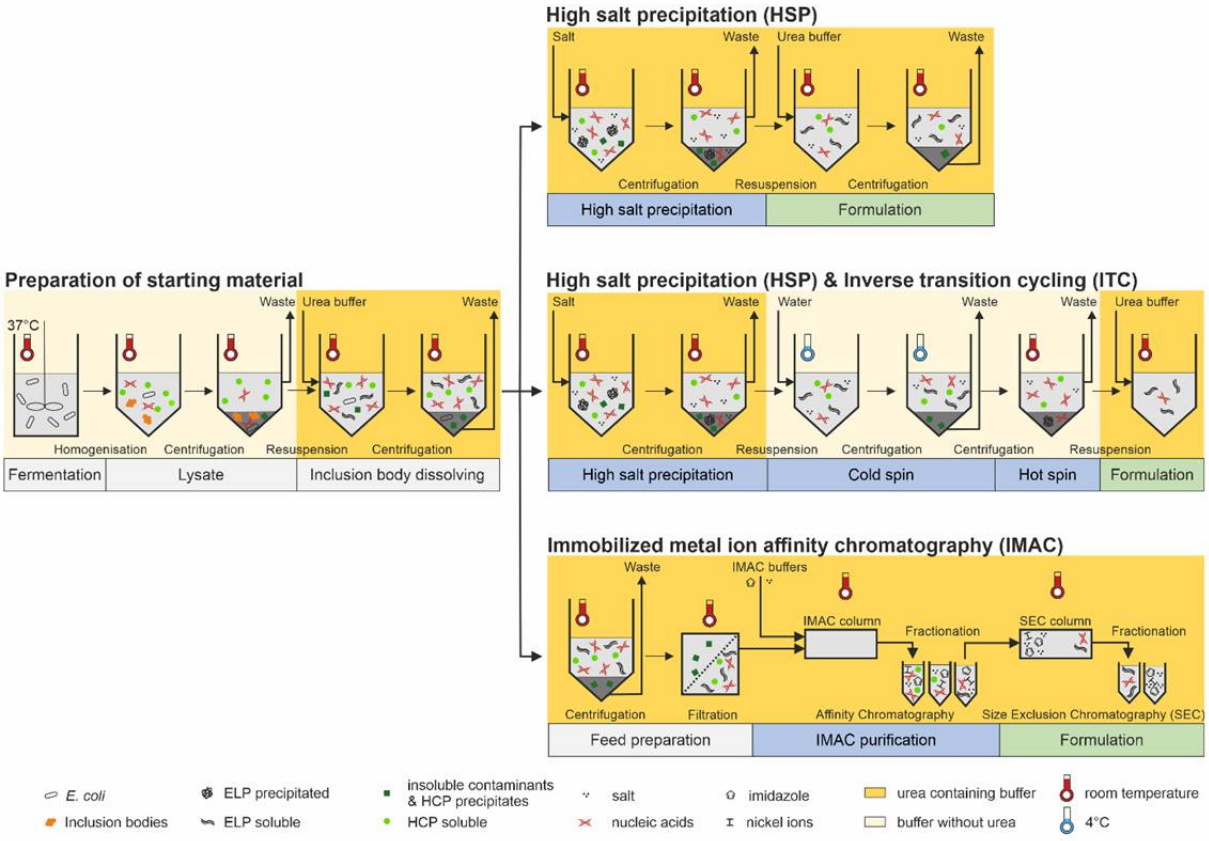

Figure 3.1 – Schematic overview of the processes investigated in this study. **Left:** Fermentation, cell lysis and inclusion body dissolving were performed in one batch for all following processes to prepare the same starting material. **Right-top:** A high salt precipitation and direct formulation by resuspension of the centrifugation pellet containing the target molecule in a urea-containing buffer system was performed as most simple purification approach. **Right-center:** After the high salt precipitation, one cycle of inverse transition cycling in a buffer system without urea was additionally performed starting with a cold spin below transition temperature of the target molecule in ultrapure water followed by a hot spin above its transition temperature. Formulation of the target molecule was performed by a resuspension of the hot spin centrifugation pellet in a urea-containing buffer system. **Right-bottom:** Immobilized metal ion affinity chromatography (IMAC) was used as an alternative purification approach. Prior purification the starting material was centrifuged and filtered to avoid column blockage. Formulation with the aim to reduce metal ion and salt ion contamination was carried out using a follow-up size exclusion chromatography step.

3.2.5. **Immobilized ion metal affinity chromatography (IMAC)**

The starting material was centrifuged (10 min, 25 °C, 17000 g) and the resulting supernatant was filtered with a 0.45 µm cellulose acetate membrane (Pall Corporation) prior chromatographic steps (Figure 3.1, *Immobilized ion metal affinity chromatography*). All preparative runs were conducted with an Äkta Pure 25 chromatography system controlled with Unicorn 6.4.1 SP2 (GE Healthcare, Chicago, US-IL). A HisTrap HP column (GE Healthcare) using nickel ions as binding sites was equilibrated with binding buffer (20 mM sodium phosphate, 4 M urea, 0.5 M NaCl, 20 mM imidazole, pH 7.4). The protein solution was applied using the sample pump. After a washing step of 10 column volume (CV) with binding buffer, a single-step elution with 5 CV elution buffer (20 mM sodium phosphate, 4 M urea, 0.5 M NaCl, 0.5 M imidazole, pH 7.4) was performed and fractionated. The elution fractions including target protein were pooled according to the measured absorption at 280 nm. A HiTrap Desalting column (GE Healthcare) was used as size exclusion chromatography (SEC) in flow through mode towards 20 mM SPB pH 8 containing 4 M urea for further analysis.

3.2.6. **Analytics**

Different quantitative analytical methods were assessed to determine the ELP[V2Y-45] concentration after each process step. Since the investigated ELP precipitated at RT in aqueous solutions, either cooling of the whole analytical process was inevitable or the Tt had to be raised, e.g. by addition of 4 M urea. However, these requirements did not allow the quantification of ELP[V2Y-45] containing process related impurities with the assessed methods (see Appendix B.2).

Purification analytics. Sodium dodecyl sulfate polyacrylamide gel electrophoresis (SDS-PAGE) was used to evaluate process step performance and the purity of the target molecule. Centriguation pellets were dissolved using the same buffer to pellet ratio as used for the corresponding process step. Samples were diluted by factor 100 (dissolved centrifugation pellets) or 65 (centrifugation supernatants) prior analytics. SDS-PAGE was run on a PowerEase 500 Power Supply using NuPAGE™ running buffer, LDS sample buffer and NuPAGE™ 4-12 % BisTris protein gels (all Invitrogen™, Carlsbad, US-CA) according to the manufacturer's manual. Gels were stained with a Coomassie® brilliant blue G-250 solution and scanned with a Bio-5000 VIS Gel Scanner (Serva Electrophoresis, Heidelberg, DE). The target protein's purity was determined by image processing of the SDS-PAGE gels using ImageJ V1.53e (NIH, Bethesda, US-MD). Thereby, the ratio of the background corrected integrated density of the target molecule band compared to the whole band was determined. The yield Y of a process was calculated by Equation (3.1)

$$Y = P_{ELP[V2Y-45]} * m_{protein,tot}, \qquad (3.1)$$

where $P_{ELP[V2Y-45]}$ is the purity of ELP[V2Y-45] determined by image processing of the SDS-PAGE gels as described and $m_{protein,tot}$ being the protein mass in the final formulation per ml starting material.

Protein quantification. Nucleic acid contamination evaluated by the ratio of absorbance at 260 to 280 nm (A260/A280 ratio) and protein concentration of purified samples was measured via 280 nm absorbance using the spectrophotometer Nanodrop 2000c (Thermo Fisher Scientific,

Waltham, US-MA). The molar extinction coefficient at 280 nm $\varepsilon_{ELP[V2Y-45],280nm}$ was determined to be 0.799 L/(g*cm) in a concentration range up to 10 mg/ml in 20 mM SPB containing 4 M urea (Appendix B.3). For this, ELP[V2Y-45] was initially purified with two cycles of ITC, formulated in ultrapure water and lyophilized for 72 hours at 0.66 mbar and -55 °C using the freeze-dryer Alpha1-4 LDplus (Martin Christ, Osterode am Harz, Germany). Conductivity measurements of formulated solutions with a concentration of 2 mg/ml ELP[V2Y-45] were performed to qualitatively compare the salinity of the final formulations using a conductivity meter CDM230 (Radiometer Analytical SAS, Lyon, FR).

Molecular weight analysis. Molecular weight of purified ELP[V2Y-45] was evaluated for all proposed downstream processes by matrix-assisted laser desorption ionization-time of flight mass spectrometry (MALDI-ToF-MS) with an UltraFlextreme™ MALDI-ToF-system controlled with the software FlexControl 3.4 (Bruker, Billerica, US-MA). Each crystallized sample was manually targeted with the Smartbeam™-Laser (Bruker) at 355 nm. Formulated ELP[V2Y-45] was mixed in a 1:5 ratio with sinapinic acid and spotted on the MALDI target. All measurements were performed in a 10 to 50 kDa mass range using the Random Walk modus without automatic matrix suppression.

Particle size analysis. Dynamic light scattering (DLS) measurements of the protein solutions were conducted with four replicates using the Zetasizer Nano ZSP (Malvern Panalytical, Malvern, UK). Each measurement was carried out with a sample volume of 50 µL in a quartz glass cuvette (ZEN 2112) and consisted of 20 acquisitions for 5 s per temperature step with a temperature ramp between 0 and 24 °C in steps of 2 °C. For these investigations, ELP[V2Y-45] was purified with two cycles of ITC, formulated in ultrapure water and lyophilized for 72 hours at 0.66 mbar and -55 °C. Prior measurement, ELP[V2Y-45] was dissolved in ultrapure water with a concentration of 2 mg/ml.

Quantification of leaked nickel ions. To quantify leaking metal ions at neutral pH in common buffer systems, an spectrometric assay using a UV/Vis spectrometer was used[154]. The assay was performed as described by Swaim *et al.* with the difference that a 6% w/v hydroxynaphthol blue (HNB) stock solution was prepared [155]. In short, the difference in the absorption spectra of the dye HNB and the formed HNB-metal complex at 647 nm is used to determine the metal ion concentration. A calibration line with nickel(II) chloride hexahydrate in a range from 0 to 4.5 µM in 0.45 µM steps was determined. The slope of the calibration was then used to calculate the nickel ion concentration in calibration range for non-turbid samples. After a strip and recharge of the column, six method runs without protein load were conducted and the elution fractions as well as ELP[V2Y-45] containing solutions after the formulation with SEC were analyzed.

3.3. Results

3.3.1. Preparation of starting material

All purification routes were assessed using the same starting material which was prepared in one batch to eliminate possible preprocessing variances. As shown in the resulting SDS-PAGE (Appendix B.4), several proteins in the size range of 3.5 to 97 kDa as well as the target molecule - with an estimated size of 26 kDa in SDS-PAGE analytics - are present in the cell lysate and the starting material. In order to get an impression of the nucleic acid content during the

purification process, A260/A280 ratios were determined to be 1.51 ± 0.01 for the cell lysate after homogenization, 1.53 ± 0.03 for the cell lysate pellet after centrifugation and 1.71 ± 0.01 in the starting material after solubilization of the IBs (Appendix B.4 – Table B.4). In order to ease handling during production, i.e. by centrifugation at room temperature, the influence of centrifugation temperature after the IB dissolving was assessed and evaluated by SDS-PAGE (Appendix B.5 - Figure B.5 A). Thereby, no difference in band intensities of a centrifugation temperature of 4°C compared to a centrifugation at 25°C could be observed by visual inspection. Additionally, direct dissolution of the inclusion bodies by performing cell lysis in a buffer system containing 4 M urea was conducted and evaluated by SDS-PAGE (Appendix B.5 - Figure B.5 B). In contrast to the previously described IB dissolution in a separated process step, the band intensity of the target molecule compared to the overall host cell protein band intensities is thereby less intense.

3.3.2. **High salt precipitation**

The starting material was prepared in a buffer containing urea, in which no temperature induced aggregation was observed up to 50 °C, without higher temperatures tested (data not shown). Salt-induced precipitation, aimed at precipitating ELP[V2Y-45] in the IB solubilization buffer, was used to exchange the buffer towards an aqueous buffer without urea to allow ITC purification at moderate temperatures. To determine the required salt concentration, previously via two cycles of ITC purified ELP[V2Y-45] was precipitated with up to 1 M AMS and up to 1.5 M NaCl (Figure 3.2 A). A concentration of 0.4 M AMS precipitated 95 ± 1.2 % of 1 mg/ml ELP[V2Y-45] and 1.5 M NaCl precipitated 92 ± 1.1 %. Lower salt concentrations tested precipitated less than 50 % of the target molecule for both salts. As for AMS, higher salt concentrations did not show to influence the precipitation ratio.

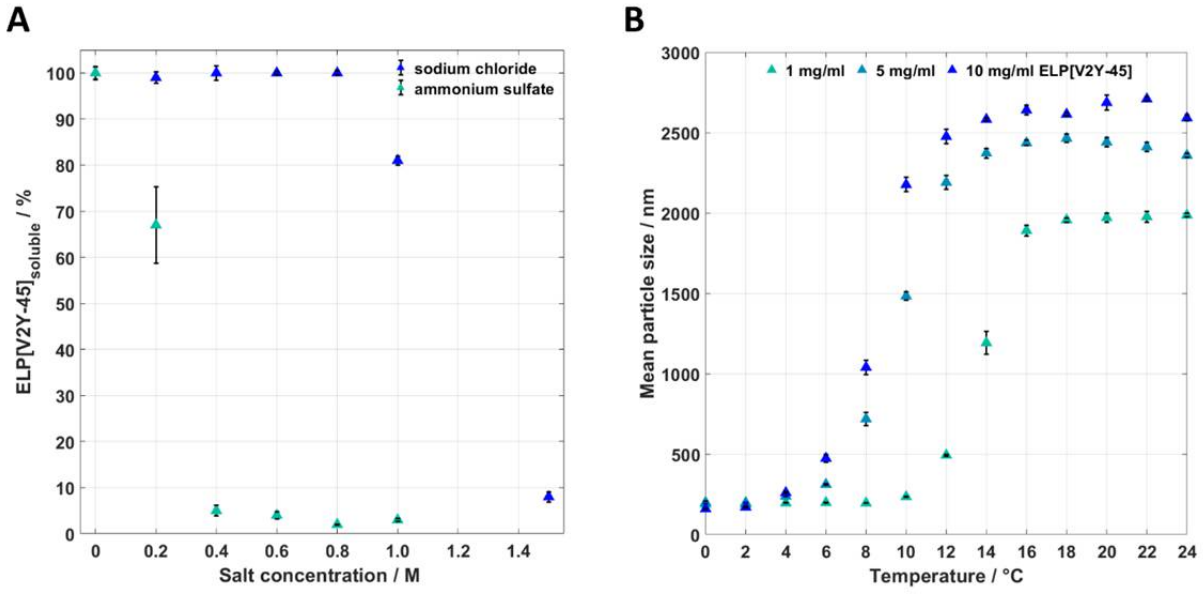

Figure 3.2 (A) Salt-induced precipitation of 1 mg/ml ELP[V2Y-45] in IB dissolving buffer containing 4 M urea at room temperature for sodium chloride (up to 1.5 M) and ammonium sulfate (up to 1 M) (n = 4). (B) Thermal dependency of the mean particle sizes for different concentrations of ELP[V2Y-45] in ultrapure water (n = 3).

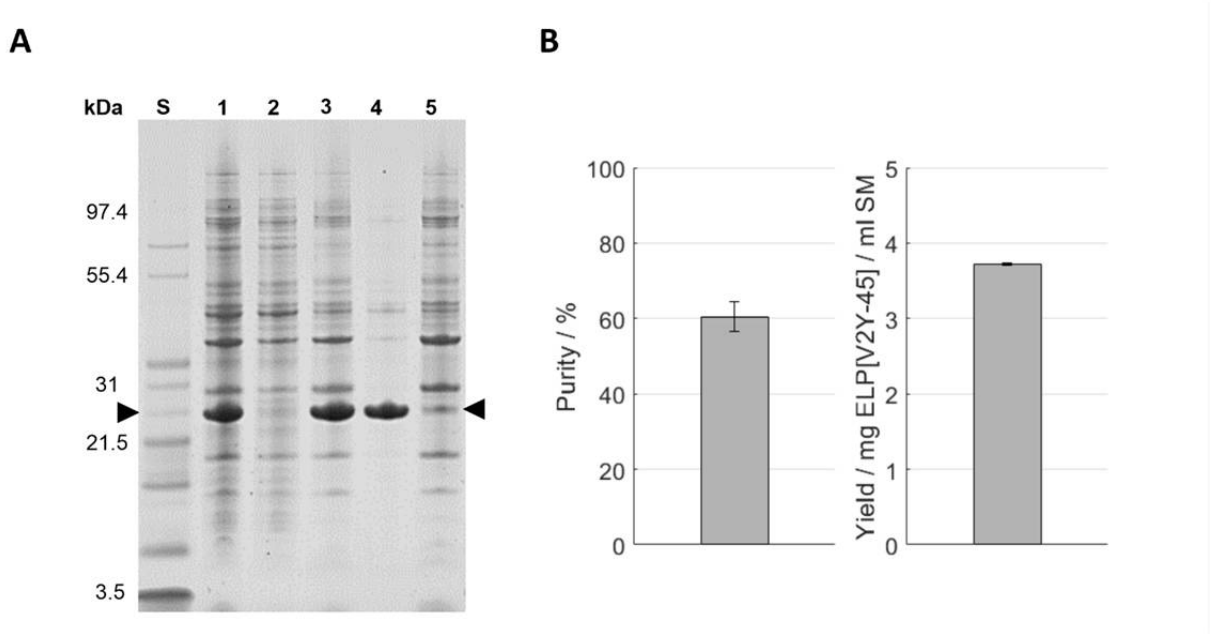

Figure 3.3 (A) SDS-PAGE analysis of the high salt precipitation. An Invitrogen™ Mark12™ Unstained Standard (lane S) was used and the target molecule is indicated by arrows. Molecular weights of selected proteins contained in the standard are shown on the left. The lanes are: starting material (lane 1); supernatant (lane 2) and pellet (lane 3) after the high salt precipitation; supernatant (lane 4) and pellet (lane 5) after the centrifugation of the dissolved precipitation pellet. (B) Purity and target molecule yield per ml starting material were evaluated using image analysis of the SDS-PAGE gel.

To verify whether both salts precipitated the target molecule in the presence of host cell proteins (HCPs), 1.5 M NaCl and 0.4 M AMS were added to the starting material. Both salts showed to precipitate the target molecule (see Appendix B.6), whereby 0.4 M AMS used for high salt purification and inverse transition cycling purification routes in the further stages of the study. As a first purification route, a high salt precipitation (HSP) was performed with a subsequent resuspension of the precipitation pellet in the formulation buffer and analysed via SDS-PAGE (Figure 3.3 A). An overview of the buffer compositions of the different process steps of all purification routes can be found in Appendix B.7. After the inclusion body dissolving, HSP with 0.4 M AMS was conducted. The resulting supernatant and pellet as well as the pellet of the final formulation contain proteins in the entire size range analyzed (3.5 to 200 kDa) in SDS-PAGE. The target molecule's band with a size of approximately 26 kDa (further indicated by arrows) is most prominent in the HSP pellet and consequently in the supernatant after centrifugation of the final formulation. In the final formulation - besides the target molecule - few protein bands with a size above 26 kDa are identifiable by visual inspection. Using this puification route, a yield of 3.72 ± 0.01 mg ELP[V2Y-45] per ml starting material with a molecular weight of 21594.2 ± 0.8 Da was achieved as shown by MALDI-ToF analysis (Table 3.3). As determined via image analysis, the purity of the target molecule was 60.5 ± 3.9 %

(Figure 3.3 B). The formulated solution showed a conductivity of 4.70 ± 0.04 mS/cm for a concentration of 2 mg/ml ELP[V2Y-45]. Nucleic acids remained predominantly in the HSP supernatant (A260/A280 = 1.94 ± 0.01), with the A260/A280 ratio of the HSP centrifugation pellet being 0.97 ± 0.04 and no further reduction during the formulation leading to a final A260/A280 ratio of 0.99 ± 0.01 (see Appendix B.8).

3.3.3. **Inverse Transition Cycling**

As a second purification route, one cycle of inverse transition cycling (ITC) in ultrapure water was assessed. To gain an understanding of critical process parameters of the ELP[V2Y-45] phase transition, thermal transition behavior of ELP[V2Y-45] was initially investigated. The particle size of ELP[V2Y-45] in water depends on the solution temperature and protein concentration as shown in Figure 3.2 B. For a protein concentration of 1 mg/ml the mean particle size is increasing above a temperature of 10 °C. Higher protein concentrations of 5 and 10 mg/ml already show an increase in mean particle size for temperatures greater than 4 °C. While the mean particle size increased, polydispersity was observed for all tested concentrations. This transition zone is smaller for 1 mg/ml which showed monodispersity above 16 °C compared to 14 °C for both higher concentrations. Aggregation, indicated by a stable mean particle size, was reached for temperatures below RT for all tested concentrations.
SDS-PAGE evaluation of one cycle of inverse transition cycling (ITC) in ultrapure water which was applied after a salt-induced precipitation with 0.4 M AMS is shown in Figure 3.4 A. The

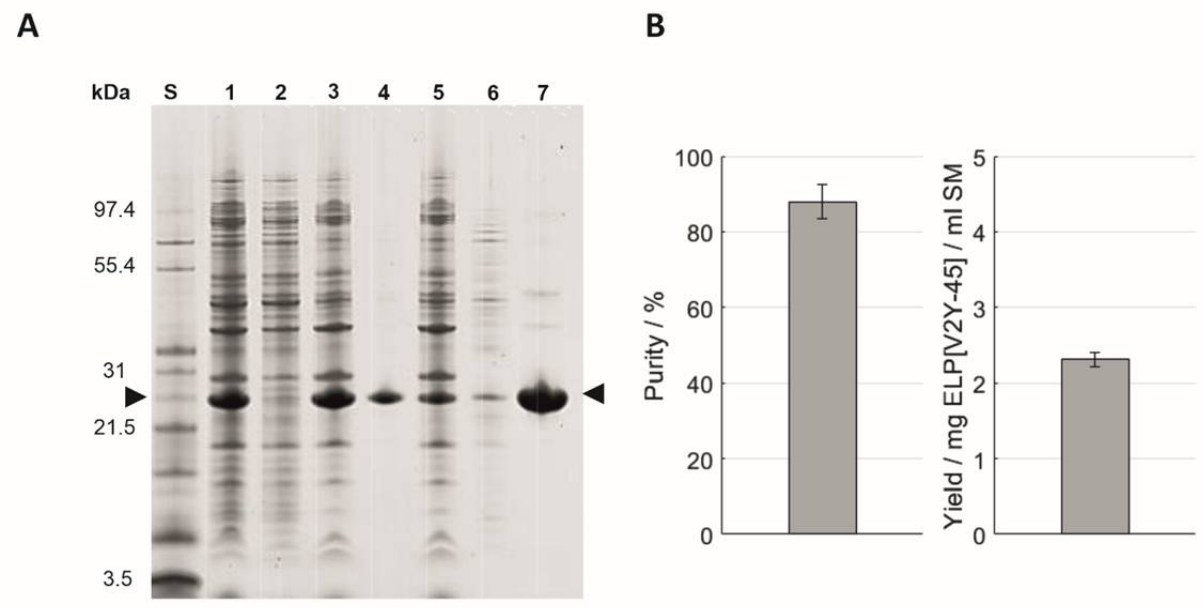

Figure 3.4 (A) SDS-PAGE analysis of the ITC purification. An Invitrogen™ Mark12™ Unstained Standard (lane S) was used and the target molecule is indicated by arrows. Molecular weights of selected proteins contained in the standard are shown on the left. The lanes are: starting material (lane 1); supernatant (lane 2) and pellet (lane 3) after the high salt precipitation; supernatant (lane 4) and pellet (lane 5) after the cold spin; supernatant (lane 6) and pellet (lane 7) after the high temperature centrifugation of the cold spin supernatant (hot spin). (B) Purity and target molecule yield per ml starting material were evaluated using image analysis of the SDS-PAGE gel.

indicated target molecule band at a size around 26 kDa is predominantly visible in the starting material and HSP pellet. In the following cold spin process, the target molecule's band shows a comparable intensity in the centrifugation pellet and supernatant being less intense than in the HSP pellet. All other proteins show comparable band intensities in the cold spin centrifugation pellet compared to the HSP while being barely identifiable in the cold spin supernatant. The cold spin supernatant showed with a A260/280 ratio of 1.85 ± 0.07 a higher nucleic acid content compared to the cold spin pellet (0.86 ± 0.02) or the starting material (1.71 ± 0.01) (see Appendix B.8). After the hot spin, protein bands throughout the analyzed size spectrum which are less intense than in the cold spin pellet are identifiable in the centrifugation supernatant. The A260/A280 ratio in the hot spin pellet was reduced to 0.52 ± 0.00, while being 2.15 ± 0.01 in the hot spin supernatant. In the hot spin pellet, two protein bands in the size range between 31 and 55.4 kDa are visible to the eye. Compared to the target molecule band, these have a low intensity resulting in a target molecule purity of 88.0 ± 4.4 % and a yield of the target molecule of 2.31 ± 0.09 mg ELP[V2Y-45] per ml starting material achieved as both determined by image analysis (Figure 3.4 B). The conductivity of the final formulation after dissolving of the hot spin centrifugation pellet was 3.62 mS/cm and the molecular weight determined to be 21589.7 ± 1.1 Da. As evaluated by image analysis of the ITC purification SDS-PAGE (Figure), a product loss of 17.05 ± 0.64 % occured during the cold spin centrifugation (Table 3.1). In order to maximize the yield of the target molecule, influencing process parameters such as centrifugation time, target molecule concentration and centrifugation temperature have been further evaluated. Longer centrifugation times of 30 min showed to double the target molecule's loss up to 34.06 ± 0.92 % as evaluated by image analysis of the resulting SDS-PAGE gel. A further decrease in centrifugation temperature to 2 °C did not show an improvement in target molecule yield (data not shown). Also, increasing the buffer-to-pellet ratio to 10 ml/g for the HSP pellet and thus reducing the target molecule concentration during cold spin did not reduce the target molecule loss that occurred (data not shown).

Table 3.1 Centrifugation times between 2 and 30 min were tested for the cold spin which was conducted at 4 °C. The purification performance of the cold spin was evaluated by the loss of the target molecule as determined via image analysis of SDS-PAGE gels. (n=3)

Centrifugation time	**Loss target molecule**
min	%
30	34.06 ± 0.92
20	28.89 ± 4.24
10	23.39 ± 0.66
5	19.93 ± 4.45
2	17.05 ± 0.64

3.3.4. **Immobilized metal affinity chromatography**

As a commonly applied purification method, immobilized metal affinity chromatography (IMAC) was performed for comparison. The chromatography feed was prepared by centrifugation and filtration of the thawed starting material. This led to a volume reduction of approximately 10 % and a loss of the target protein of around 6 % before sample loading on the column as evaluated by image analysis of the SDS-PAGE (Figure 3.5 A). Protein bands are present throughout the analyzed size range in the starting material (A260/A280 = 1.71 ± 0.01), as well as the IMAC feed (A260/A280 = 1.75 ± 0.05) and the centrifugation pellet. A comparable band intensity for most protein bands except for the band of a protein size around 26 kDa and proteins with a size above 31 kDa are observable in the IMAC flow through (A260/A280 = 1.82 ± 0.13). These bands are less intense in the flow through compared to the IMAC feed solution. In the IMAC wash (A260/A280 ratio = 1.51 ± 0.01) protein bands are present throughout the analyzed size spectrum. Compared to the bands recognizable above 31 kDa, bands of smaller proteins are less intense. Addition of 20 mM imidazole could be used to reduce the amount of eluted proteins during the column wash, as indicated by a lower UV280nm sum signal (Appendix B.9). In the IMAC eluate the protein band with a size around 26 kDa is predominant, with less intense bands for proteins with a higher molecular weight being visible. After the formulation via SEC, the same protein bands than in the IMAC eluate are present in the SDS-PAGE, while being less intense. In the SEC, two separated peaks for the UV280nm sum signal and conductivity signal were gained in the chromatogram which

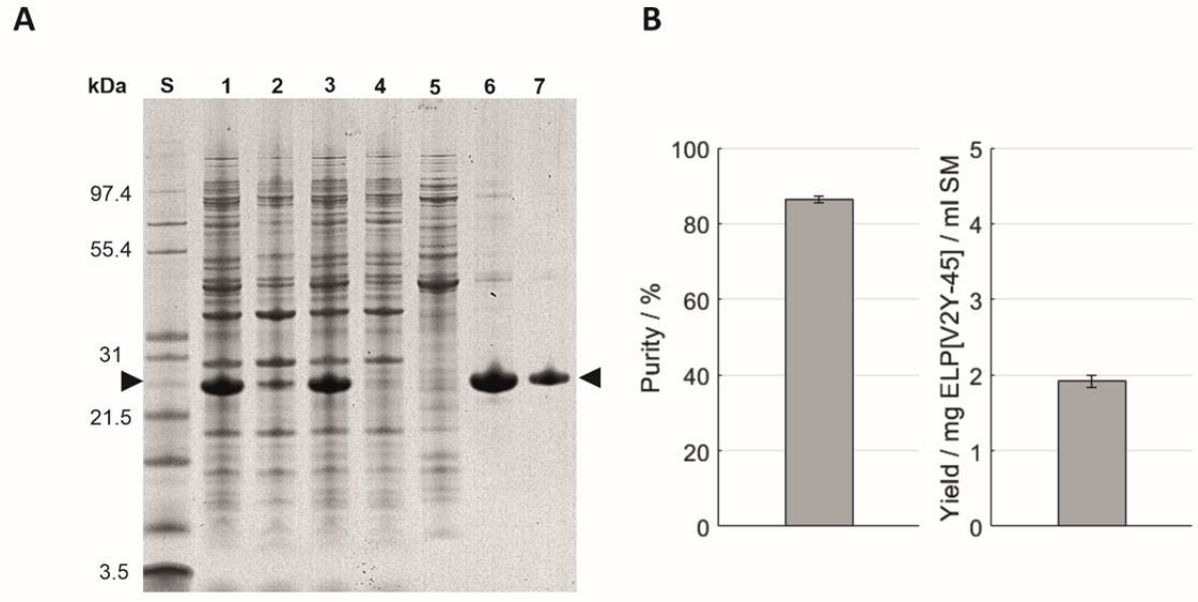

Figure 3.5 (A) SDS-PAGE analysis of the IMAC purification. An Invitrogen™ Mark12™ Unstained Standard (lane S) was used and the target molecule is indicated by arrows. Molecular weights of selected proteins contained in the standard are shown on the left. The lanes are: starting material (lane 1); IMAC feed (lane 3) and pellet (lane 2) after centrifugation; IMAC flow through (lane 4); IMAC wash (lane 5); IMAC eluate (lane 6); size-exclusion chromatography eluate (lane 7). (B) Purity and target molecule yield per ml starting material were evaluated using image analysis of the SDS-PAGE gel.

Table 3.2 Leaked nickel ion concentration depending on consecutive method runs without protein load after a strip and recharge of the IMAC column (n=3)

Method runs	Ni^{2+} concentration
-	µM
1	8.8 ± 1.6
2	8.0 ± 0.6
3	6.7 ± 0.2
4	5.3 ± 0.2
5	4.3 ± 0.2
6	4.2 ± 0.2

where experimentally separated by fractionation (Appendix B.10). The concentration of leaked nickel ions was determined using a photometric assay and was determined for consecutive chromatography method runs without protein load applied. In the first method run after a column strip and recharge, the elution fraction contained 8.8 ± 1.6 µM nickel ions, while constantly decreasing to 4.2 ± 0.2 µM for the sixth consecutive run Table 3.2). In the

Table 3.3 Formulated ELP[V2Y-45] solutions of the three downstream processes were analyzed regarding the target molecules molecular weight, its purity which was calculated from its band intensities in SDS-PAGE, the final target molecule yield, formulation buffer conductivity and nucleic acid contamination in the final formulation (n=3)

Process	Molecular weight	Purity	Yield	Conductivity	A260/A280
	Da	%	mg ELP[V2Y-45] / ml starting material	mS/cm	-
HSP	21594.2 ± 0.8	60.5 ± 3.9	3.72 ± 0.01	4.70 ± 0.04	0.99 ± 0.01
ITC	21589.7 ± 1.1	88.0 ± 4.4	2.31 ± 0.09	3.62 ± 0.01	0.52 ± 0.01
IMAC	21588.4 ± 0.1	86.5 ± 0.9	1.92 ± 0.08	3.59 ± 0.01	0.46 ± 0.00

simultaneous presence of ELP[V2Y-45] and imidazole, the nickel assay became turbid and therefore the IMAC elution with protein loading was not analyzable (Appendix B.11). In the final formulation after SEC, no nickel ions could be traced and molecular weight of the target molecule was 21588.4 ± 0.1 Da. A purity of 86.5 ± 0.9 % and a target molecule yield of 1.92 ± 0.08 mg per ml starting material was achieved (Figure 3.5 B) with a conductivity of the final formulation of 3.59 ± 0.01 mS/cm and a A260/A280 ratio of 0.46 ± 0.00 (Table 3.3).

3.4. Discussion

The aim of this study was to evaluate purification performance of three different processes with regard to their final yield, target molecule purity against HCPs and nucleic acids as well as occurring differences in their final formulation and suitability for large-scale purification. Based on its amino acid sequence, the expected molecular weight of the investigated ELP[V2Y-45] is 21.6 kDa. As for SDS-PAGE analysis, the estimated size of the target molecule was around 26 kDa, which corresponds to a commonly described size overestimation by 20 % on SDS-PAGE gels for other ELP constructs[140,147]. With direct IB solubilization during homogenization and homogenization in a non-solubilizing buffer system with a subsequent solubilization two different possibilities for IB solubilization were tested. Both approaches showed to dissolve IBs, while direct IB solubilization leads to a higher HCP contamination as indicated by SDS-PAGE analysis results. Therefore, a separation of homogenization and IB solubilization was performed for all processes discussed. Typical lab protocols for ELP purification use low temperature during cell lysate centrifugation[129,144,156]. Increasing centrifugation temperature of the cell lysate after IB dissolution to 25°C did not show to influence the starting material composition compared to a centrifugation at 4°C for the investigated hydrophobic ELP[V2Y-45], which allows the reduction of cooling steps and therefore overall processing costs. All purification routes were assessed with the same starting material with all process steps being carried out as one batch to avoid batch-to-batch variations.

3.4.1. High salt precipitation (HSP)

As typical for this class of genetically encoded proteins, ELP[V2Y-45] shows a transition behavior, which depends on the chemical composition and environmental stimuli. For efficient purification processes, profound knowledge of the temperature and salt induced phase transition are beneficial. In the IB dissolving buffer containing urea, phase transition could not be induced up to at least 50°C. Urea is a well-known denaturant for proteins which weakens hydrophobic interactions and therefore raises Tt without collapsing the ELP conformation[21,143]. In order to counteract this shift, the addition of salts lowers the transition temperature and therefore precipitate the target molecule even for high urea concentrations present at RT, which then can be diluted in the desired target buffer system[157]. Consistent with another study for ELPs, 1.5 M NaCl or concentrations greater than or equal 0.4 M AMS turned out to precipitate more than 90% of the target molecule[158]. Higher NaCl concentrations were not tested, since such salt concentrations are highly corrosive and therefore undesired in industrial scale. To reduce the overall salinity in the process, 0.4 M AMS were chosen for further experiments, albeit known to precipitate more contaminant protein than sodium chloride.[157,158]

The simple approach of an HSP followed by resuspension of the centrifugation pellet in the formulation buffer removed a major fraction of HCPs in a single step reaching a purity of

60.5 ± 3.9 %. This is in a comparable range with the purification yield of 57 ± 2 % shown for an ELP fusion protein before[146]. Fewer process steps and a less complex sample handling – the entire process after IB dissolution is carried out in the same vial – are possible explanations for an increase in target molecule yield of 60.7 % compared to ITC and 93.1 % compared to IMAC. Also, nucleic acid contamination was reduced as indicated by a decrease of the A260/A80 ratio from 1.71 ± 0.01 to 0.99 ± 0.01. Though, a slightly higher salinity is introduced into the final formulation as indicated by a higher conductivity compared to the more complex processes. Especially regarding possible applications which are sensitive to salt concentrations such as hydrogel fabrication, this has to be taken into account[146]. The main advantage of an HSP process is its simplicity, fast and efficient purification in a single step without temperature dependent centrifugation steps or toxic consumables. For applications where higher purities, full removal of nucleic acids or a control over the salinity is required, further processing would be necessary or other approaches should be preferred. Thus, for non-biomedical applications - such as applications in environmental engineering (e.g. removal of heavy metals)[159,160], bionanocomposite materials[161] or molecular sensors[162,163] - the salt-induced precipitation process may be the best solution towards an industrial process scale for biomaterial production because of its simplicity and high target molecule yield.

3.4.2. **Inverse transition cycling (ITC)**

For purification via ITC, the target molecule should be in a buffer system showing moderate transition temperatures, especially when working with ELP-tagged proteins which may denature otherwise[144]. For the hydrophobic ELP[V2Y-45], this requires a buffer exchange towards an aqueous buffer without high salinity or high concentrations of chaotropic agents by an HSP with resuspension of the centrifugation pellet in ultrapure water. As described in common protocols, the cold spin was performed at 4°C[144]. For the investigated ELP, a loss of target molecule occurred in a range from 17 % (2 min centrifugation time) up to 34 % (30 min centrifugation time) in a single step. Although turbidity could not be determined by visual inspection, first agglomeration effects in ultrapure water could already be observed at 4°C using DLS for concentrations of 5 mg/ml and above. DLS is a commonly used technique for the determination of particle size distributions of non-turbid solutions[164,165], using the hydrodynamic radius for spherical particles for the size analysis of proteins. As ELPs show a disordered structure in soluble state and turbidity for temperatures above Tt, the calculated mean particle size very likely does not correspond to its actual geometrical size. However, using the same measurement setup, it is possible to assess relative dependencies and trends. Since protein concentration during the centrifugation step was above 10 mg/ml, first agglomeration effects have to be considered which are further enhanced by longer processing times. Additionally, the centrifuge was heating up for long processing times at both tested centrifugation temperatures, which may have enhanced ELP[V2Y-45] precipitation. As higher protein concentration lead to a shift in the transition temperature towards a lower temperature[136,166], a higher buffer to pellet ratio for resuspension of the HSP pellet was used to reduce the target molecule concentration during the centrifugation step. This, however, did not lead to an increase of the target molecule yield. This said, an even further decrease in protein concentration may be beneficial. On the other hand, further dilution leads to larger centrifugation volumes, which are unwanted in a large production scale.

ITC purification is a simple approach to further purify ELPs without specialized equipment in lab scale[129,148]. During the hot spin, nucleic acid contamination could be further reduced compared to the HSP step and the highest purity (88.0 ± 4.4 %) of all methods applied was achieved. Nevertheless, nucleic acids could not be reduced as efficient as for IMAC and may require additional processing for ITC purified samples[50,153,167]. Still, highly efficient ITC purification is limited to ELPs without aggregation effects at low temperatures in relevant concentration ranges and buffer systems. An increase of the transition temperature by addition of chaotropic agents in the centrifugation buffer may increase the yield with possible simultaneous decrease in the target molecule's purity. In this manuscript, we focused on simple purification protocols with limited process steps to optimize the target molecule yield. However, more cycles would increase the purity at the cost of the overall yield. Still, the main drawback of this technique is the necessity of temperature dependent centrifugation steps. Especially for large volumes, heating and cooling steps are time consuming and expensive which may be a high barrier towards large-scale downstream processing using ITC.

3.4.3. **Immobilized metal ion affinity chromatography (IMAC)**

IMAC was used as a chromatographic approach for the purification of ELP[V2Y-45]. Elution of polyhistidine-tagged proteins is achieved using buffers that contain imidazole or other competing substances in addition to high salt concentrations. Using imidazole as eluant, to this study comparable leached metal ion concentrations below 10 µM Ni2+ were previously reported[154]. Although protein functionality can be affected due to conformation changes after contact with divalent metal ions[148], no evidence for chemical modification of ELP[V2Y-45] could be found in the molecular weight analysis. To reduce impurities from small molecules, such as metal or salt ions and imidazole, buffer exchange towards a target buffer system is required after IMAC. In this study, neither increased salinity compared to ITC nor metal ion contamination could be traced after subsequent preparative SEC. As described in literature, IMAC proved to be very efficient nucleic acid reduction[168] with 0.46 ± 0.00 the lowest A260/A280 ratio of all processes discussed. Since no process step could be identified as main cause for the loss of target molecule on the SDS-PAGE gels, we believe, the product loss occurs due to a more complex sample handling. The additional centrifugation and filtration step applied to avoid column blockage, as well as volume loss due to sample injection by sample pump, are possible sources for an overall material loss which was not optimized in this study. Alternatively, HSP could be conducted instead of centrifugation and filtration as preprocessing step before column loading. IMAC is a widely used process with a great wealth of experience in upscaling. A high purity after a single step purification could be achieved in combination with the highest nucleic acid removal rate and low salinity after SEC. Still, the main drawbacks are high investment costs for necessary equipment such as chromatography resins, more complex sample handling compared to the other processes discussed, concerns regarding in-vivo reactions due to the introduced tag and the usage of toxic consumables thereby.

3.5. **Conclusion**

With salt-induced precipitation, ITC and IMAC, three different processes were compared in regard to their purification performance for the hydrophobic ELP[V2Y-45] with low transition temperature. HSP without further processing leads to a 60 % higher yield of target molecule.

However, a lower purity of 60 %, higher contamination with nucleic acids and higher salinity have to be considered, which excludes, for instance, biomedical applications. When adding ITC to a HSP process, a purity of 88 % after one cycle could be achieved. In contrast to common ELP constructs, the overall yield would be decreased by 17 – 34% during the cold spin at 4°C. Of course, more cycles could be conducted to reach higher purities at the cost of overall product yield and therefore were not further assessed in this study. It could be shown, that affinity chromatography did not propagate molecular weight modifications of the target molecule. Further, metal and salt ions could be fully removed in a following SEC step. A comparable purity and a slightly lower yield compared to ITC were reached, which may be due to volume reduction related to a more complex sampling handling. The effect of different expression rates based on a purification tag seem to be neglectable, since comparable target molecule purities and yields were shown for ELP fusions before. Both, ITC and IMAC are therefore promising candidates for downstream processes with the aim of biomedical applications. However, further processing such as nuclease treatment or endotoxin removal might be necessary. A detailed consideration of processing costs for temperature dependent centrifugation steps for ITC in contrast to high resin investment costs for IMAC has to be made for large scale productions. For non-biomedical applications without the need of high purities or nucleic acid reduction, a simple and fast salt-induced precipitation process may be the simplest solution in the ease of scalability and target molecule yield.

4 Changing mechanical properties of photopolymerized, dityrosine-crosslinked protein-based hydrogels

Sandra Haas, Saskia Körner, Laura Zintel, Jürgen Hubbuch

Frontiers in Biotechnology and Bioengineering (2022), Volume 10, Article 1006438

Abstract

Hydrogels based on renewable resources are a promising class of materials for future applications in pharmaceutics, drug delivery and personalized medicine. Thus, optional adjustments of mechanical properties such as swelling behavior, elasticity and network strength are desired. In this context, hydrogels based on the biological raw materials bovine serum albumin and casein were prepared by dityrosine-crosslinking of their tyrosine residues through visible light-induced photopolymerization. Changing the tyrosine accessibility by urea addition before photopolymerization increased the storage modulus of the hydrogels by 650 % while simultaneously being more elastic. Furthermore, contributions of the buffer system composition, variation of protein concentration and storage medium towards mechanical properties of the hydrogel such as storage moduli, elasticity, fracture strain, compressive strength and relative weight swelling ratio are discussed. It could be shown, that changes in precursor solution and storage medium characteristics are crucial parameters towards tuning the mechanical properties of protein-based hydrogels.

4.1. Introduction

Hydrogels are three-dimensional (3D) polymer networks with the ability to expand their volume in aqueous solutions[169]. Since the first hydrogel formulation was published, the number of publications on hydrogel formulations and applications in the field of pharmaceutics and medicine steadily grew over the years[31,170–172]. In this context, renewable and naturally occurring resources like proteins and peptides, which show high biocompatibility and biodegradability, represent potential raw material sources for hydrogel formulations[33,173].
Hydrogel formulations can be classified by different properties, such as the crosslinking mechanism, physical properties, external stimuli behavior, and monomer or polymer chain source[30]. Protein- or peptide-based hydrogels can either self-aggregate after denaturation by heat, salt-, urea- or acid-induced gelation as described for hen egg white lysozyme[174], soy proteins[175,176], and whey proteins including β-lactoglobulin[177–179] and bovine serum albumin (BSA)[180]. Other than those, enzymatic crosslinking or chemical crosslinkers - with the drawback of the need of added functional groups for crosslinking or the use of potentially toxic initiators - are commonly applied to obtain hydrogels[27,172]. Recently, the potential of visible-light induced hydrogelation mediated by tris(2,2′-bipyridyl)dichlororuthenium(II) ($Ru(bpy)_3Cl_2$) in the development of 3D printable bio-based materials was shown[181]. Thereby, phenolic hydroxy groups – which are naturally present in tyrosine residues of proteins – are crosslinked to dityrosine finally inducing gelation[57,58].
Dityrosine crosslinks are found to be contributing to the elastic properties of natural materials such as resilin and elastin[182,183]. So far, studies focus on dityrosine crosslinking of different peptide sequences include elastin-like proteins[59,60,62,184], mussel adhesive proteins[59], unmodified proteins (e.g. gelatin, fibrinogen and maltose binding protein)[63,185] and unmodified proteins at different folding states (I27, Protein L, BSA, maltose binding protein)[6,64,65]. Recently, the influence of the reaction rate towards the viscoelasticity of folded protein hydrogels was further assessed[186]. However, there is a lack of knowledge on the influence of the type of protein and reaction conditions. Likewise, processing parameters, such as the formulation buffer and storage medium impact mechanical properties and storability of hydrogels before the actual application.
In this manuscript, we assessed dityrosine-crosslinked hydrogels - crosslinked by ruthenium-mediated photopolymerization - derived from two naturally occurring proteins, the globular BSA and a conjugated casein. To allow tailor-made development of intelligent materials, key processing parameters such as buffer composition and characteristics during precursor solution preparation, the presence of urea and protein concentration as well as different storage media were described towards their influence on mechanical properties.

4.2. Materials and Methods

4.2.1. Precursor solution formulation

Buffer stock solutions. If not stated otherwise, all chemicals were purchased from Merck KGaA (Darmstadt, DE). 20 mM sodium phosphate buffer (SPB) or a 25 mM multi-component buffer (MCB) containing different urea concentrations (0 to 4 M) were prepared with ultrapure water (PURELAB Ultra, ELGA LabWater, Lane End, UK), while Gibco® Dulbecco's phosphate-buffered saline (DPBS, Life Technologies Corporation, Grand Island, US-NY) was used as purchased. The MCB had a global capacity of 25 mM in the range of pH 6 to pH 9 and consisted of 47 mM N-[tris(hydroxymethyl)methyl]-3-aminopropanesulfonic acid (TAPS), 11 mM 3-morpholino-2-hydroxypropanesulfonic acid (MOPSO) and 38 mM sodium citrate. At a buffer temperature of 22 °C, the buffer was pH-adjusted using 4 M sodium hydroxide solution and filtered through a 0.45 µm cellulose acetate membrane (Pall Corporation, New York, US-NY).

Protein stock solutions. Protein stock solutions of bovine serum albumin (BSA) and casein (EMD Millipore Corporation, Billerica, US-MA) were prepared with a concentration of 120 mg/ml in the respective buffer solution using a dual asymmetric centrifuge (DAC) at 2500 rpm (SpeedMixer® DAC 150.1 FVZ-K, Hauschild GmbH & Co. KG, Hamm, DE). Protein concentrations were determined with a NanoDrop 2000c UV-Vis spectrophotometer (Thermo Fischer Scientific, Waltham, US-MA) using the extinction coefficients $\varepsilon_{BSA,280nm} = 0.67$ L/(g*cm)[187] and $\varepsilon_{Casein,280nm} = 0.73$ L/(g*cm) (experimentally determined).

Protein purification to reduce impurities (e.g. production buffer salts) was either performed by dialysis or ultrafiltration. Dialysis of protein stock solution was performed using SnakeSkin™ dialysis tubing (Thermo Fisher Scientific, Waltham, US-MA) with a 10 kDa molecular weight cut off (MWCO) and 100-fold buffer excess. Two buffer exchanges were performed, the first after > 2 hours, the second after > 2 more hours. Alternatively, Vivaspin® ultrafiltration units (Sartorius Stedim Biotech, Göttingen, DE) were used according to the manufacturer's recommendation for protein purification or subsequent dialysis to reach higher stock solution concentrations ($MWCO_{BSA}$ = 30 kDa; $MWCO_{Casein}$ = 10 kDa).

Photoinitiator and Co-Factor. The photoinitiator tris(2,2′-bipyridyl)dichlororuthenium(II) hexahydrate ($Ru(bpy)_3Cl_2 \cdot 6\ H2O$) was diluted in the corresponding buffer to a concentration of 5 mM and stored at 4 °C. The co-factor ammonium persulfate (APS, chemical formula: $(NH_4)_2S_2O_8$) was diluted with a concentration of 2 M in the corresponding buffer, stored as aliquots at -20 °C and thawed directly prior to usage.

Precursor solution. Formulation buffer, protein and photoinitiator stock solutions were mixed using the DAC (2500 rpm, 5 min). Afterwards, APS stock solution was added and mixed in a light-protected container (2500 rpm, 2 min) to generate a uncrosslinked precursor solution (Figure 4.1 *Formulation*). The concentration of $Ru(bpy)_3Cl_2$ (0.25 mM) and APS (100 mM) was kept constant, while protein source, protein concentration and formulation buffer composition were varied (Appendix C.1).

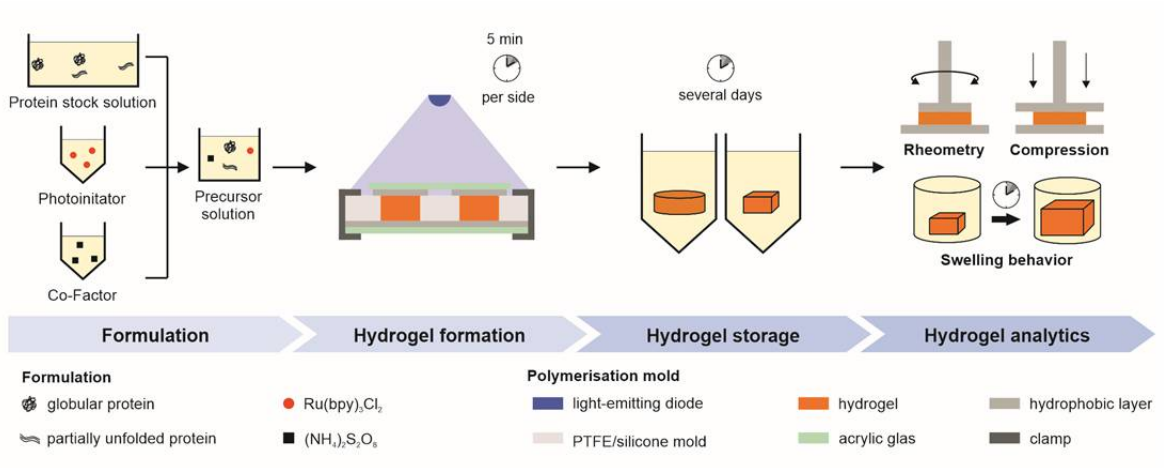

Figure 4.1 Schematic overview of the experimental workflow. Pre-processed protein, photoinitiator and co-factor stock solution were mixed to generate a precursor solution. Polymerization was achieved through illumination in a mold. Hydrogels were stored under different conditions and mechanical properties were determined either by oscillatory rheometry, swelling studies or uniaxial compression tests.

4.2.2. Hydrogel formation

The precursor solution was transferred into a dedicated mold (Figure 4.1 *Hydrogel formation*). We used the following molds: A cylindrical polytetrafluoroethylene (PTFE) mold (diameter 10mm, height 3mm), a cylindrical silicone mold (diameter 12.5 mm, height 3 mm) and a cuboidal silicone mold (side lengths 5 mm, height 3 mm). The mold was covered on top and bottom with transparent acrylic glass and a hydrophobic layer in between and irradiated for 5 min from atop and below using a blue emitter at 457 nm (LZ4-00B208, LED Engin Inc, San Jose, US-CA) with a radiant flux of 3.9 W in a distance of 7 cm.

4.2.3. Storage and analytics

Hydrogel storage. Before mechanical characterization, polymerized hydrogels were stored under different storage conditions as stated in Table C.1 in the Appendix C. Subsequently, rheometric analysis or uniaxial compression analysis were performed as analytical methods.

Oscillatory frequency sweeps. Oscillatory measurements were performed with hydrogel discs at 22 °C on a Physica MCR 301 plate rheometer (Anton Paar GmbH, Graz, AT) equipped with a plate-plate geometry (10 mm diameter). The linear viscoelastic region (LVR) was determined using amplitude sweeps for angular frequencies $\omega = 1$ and 25 rad·s^{-1} and shear stress τ between 5 and 10.000 Pa ($n = 2$). Frequency sweeps were performed within the LVR using $\tau = 10$ Pa and $\omega = 1$ to 25 rad·s^{-1} ($n = 3$).

Uniaxial compression analysis. Uniaxial compression tests were performed with hydrogel discs on a universal testing machine (zwickiLine Z0.5TN, ZwickRoell GmbH & Co. KG, Ulm, DE) equipped with a load cell Xforce HP 100 N and stainless-steel compression platens (30 mm diameter) at a uniform velocity of 2 mm/min until sample breakdown after a pre-force of 0.2 N was reached ($n = 3$). Two parameters were determined, the engineered stress $\sigma = F/A_{0,}$ where F is the force applied and A_0 is the original cross-sectional area and the engineered strain $\varepsilon = (L\text{-}L_0)/L_{0,}$ where L is the sample length and L_0 is the original sample length at the applied

pre-force. The fracture strain ε_{max} refers to the engineered strain at sample fracture. Accordingly, the compressive strength σ_{max} refers to the engineered stress at sample fracture.

Swelling studies. Swelling studies were performed with hydrogel cuboids which were stored in DPBS and MCB with the production pH without urea. The cuboids were weighed directly after polymerization and subsequently after 1, 2, 3, 7, 10, and 14 days. The relative weight swelling ratio m_{rel} of the hydrogels was calculated as $m_{rel} = m/m_o$, where m and m_o are the masses of the hydrogel specimen at time points t and t_0 respectively (n = 3). The storage medium was renewed after each measurement up to a final 60-fold buffer excess compared to the hydrogel volume.

Statistical analysis. All experiments were performed in triplicates and data have been given as mean ± standard deviation. Statistical analysis for oscillatory frequency sweeps was performed using the two-sided Wilcoxon ranksum test with a p-value below 0.05 being classified as statistically significant and marked with a single asterisk (*). Statistical analysis for uniaxial compression tests were compared using a paired Student's t-test with p-values less than 0.05 being considered significant and marked with a single asterisk (*). Beforehand, distribution normality was assessed with a Shapiro-Wilk test with a maximum significance level $\alpha = 0.05$.

4.3. Results and Discussion

4.3.1. Buffer Components

In order to evaluate potential factors influencing the mechanical properties of protein-based hydrogels, varying formulation buffer compositions, proteins and protein concentrations as well as storage condition were examined. Initially, hydrogels prepared by visible light-induced chemical crosslinking of 100 mg/ml BSA were polymerized in a sodium phosphate buffer (SPB) at pH 8 containing up to 3 M urea. When using the SPB at pH 8, the generation of the required protein stock solutions containing higher urea concentrations, was prevented by urea-induced gelation[27]. The influence of buffer pH was analyzed subsequently, applying a multi-component buffer system (MCB), which was used for all further experiments. Buffer components known to stabilize the native structure of BSA - here MOPSO and TAPS[188,189] - enabled the preparation of 100 mg/ml BSA gels at pH 7 and pH 8 and urea concentrations up to 4 M. The third buffer component, sodium citrate is known to increase the solubility of casein[190,191] which was used as a second protein.

4.3.2. Network density of BSA-based hydrogels

Network failure of polymerized BSA-based hydrogels was analyzed using stress-dependent oscillatory rheology. It is indicated by an increasing loss modulus (G'') until a sudden breakdown of the storage modulus (G') during amplitude sweeps (Figure 4.2 A). Network failure at strains above 88 Pa was observable as indicated by the linear viscoelastic region (LVR), whereby the hydrogel network prepared with 2 and 3 M urea present in the SPB were more stable compared to the one prepared without urea (Appendix C.2).

G', which is used as a measure for the network density, was determined by frequency sweeps. These were carried out at a constant shear stress of 10 Pa, being in the LVR for all hydrogels discussed in this manuscript. For all hydrogels tested, G' dominates G'' across the whole frequency range applied (1 - 25 $rad \cdot s^{-1}$) confirming gel-like behavior[192] as exemplarily depicted in Figure 4.2 B. For BSA-based hydrogels prepared in SPB, a significant increase in G' for increasing urea concentrations occurred for samples containing more than 1 M urea (Figure

4.2 C). In numbers, G' was increased by 650 % from 2.47 ± 0.18 kPa of the 0 M urea samples to 16.04 ± 0.72 kPa for 3 M urea, while G'' was increased by 313 % from 0.14 ± 0.03 kPa to 0.45 ± 0.14 kPa.

The addition of urea disrupts intramolecular hydrophobic interactions and the protein unfolds (partially). Intermolecular interaction, such as those leading to urea-induced gelation, therefore may increase, resulting in a higher network strength. In addition, due to their amphiphilic nature, tyrosines can be located both, on the protein surface or inaccessibly in the hydrophobic core of native proteins[193]. Thus, solvent accessibility for the tyrosine residues is altered upon addition of urea[26,194], potentially allowing the formation of different network strengths under otherwise constant polymerization conditions. Previously, weaker hydrogels for dityrosine-crosslinked BSA, I27 and protein L were reported for protein unfolding using 6 M guanidine hydrochloride[64], while increased entanglements resulted in a higher Young's modulus for a dityrosine-crosslinked ferredoxin-like globular protein which was previously unfolded with 7 M guanidine hydrochloride[195]. In contrast to the uncharged chaotropic agent urea, the salt guanidine hydrochloride ionizes in aqueous solutions masking electrostatic interactions[196]. This indicates, that the used protein and protein unfolding mechanism is crucial towards the resulting mechanical properties of dityrosine-crosslinked hydrogels.

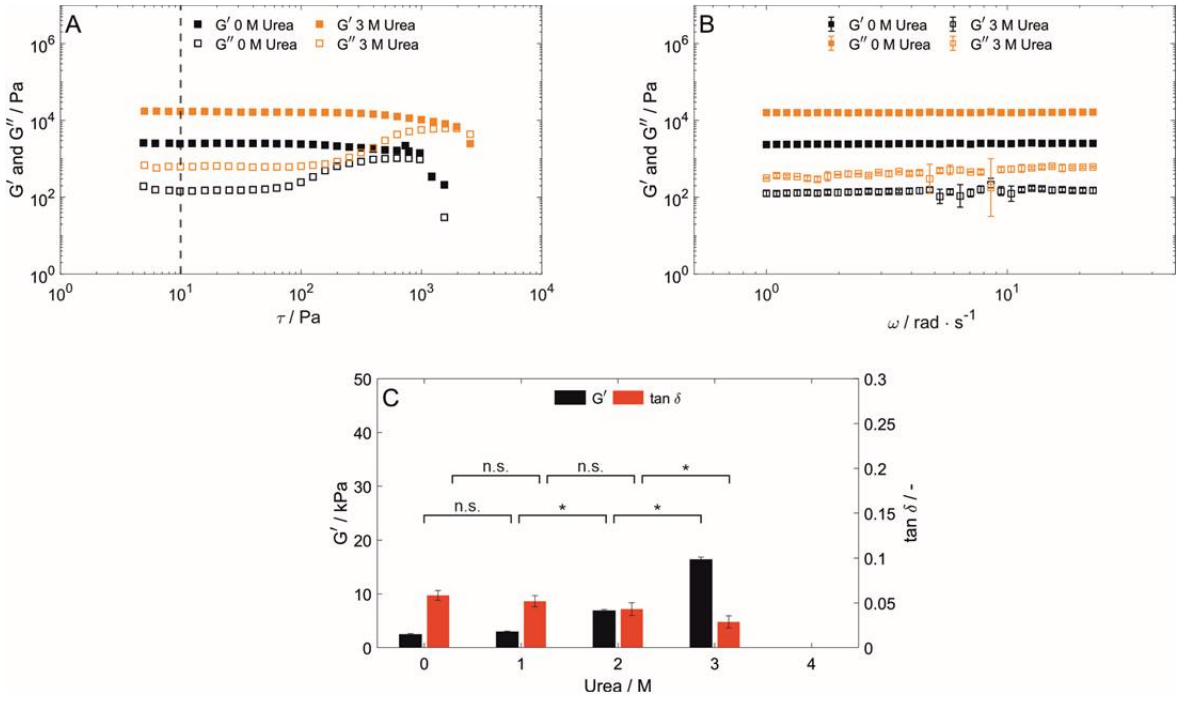

Figure 4.2 Characterization of hydrogels containing 100 mg/ml BSA prepared in SPB. (A) Shear stress dependent (ω = 25 rad·s-1, 22°C) and (B) frequency-dependent (τ = 10 Pa, highlighted by a vertical line in (A), 22°C) oscillatory shear test of hydrogels prepared and stored in a 20 mM SPB at pH 8 without urea and with 3 M urea present in the precursor solution and storage medium. (n=3) (C) Hydrogel storage modulus (G') and loss factor (tan δ) in dependency of the urea content in the precursor solution and storage medium. (n = 3) Abbreviations: n.s.: not significant, *: $p < 0.05$

As for the polymerization in SPB, hydrogel discs were stored in their preparation buffer (Figure 4.2) to exclude external stimuli effects by changes of the environmental conditions (e.g. urea concentration) during storage. Therefore, based on these results, it remained unclear whether an increase in dityrosine crosslinks, entanglements, urea-induced gelation reactions or storage medium characteristics are causing the increasing storage modulus.

4.3.3. **Elasticity of BSA-based hydrogels**

In addition, hydrogel elasticity was evaluated with regard to the loss factor ($\tan \delta = G'' / G'$) determined by a frequency sweep analysis (Figure 4.2 C), whereby a loss factor of 0 corresponds to ideal elastic behavior. Hydrogel elasticity significantly increased upon increasing concentration of urea being present in SPB. Since dityrosine crosslinks are known to contribute to the high elastic properties of structural proteins[182], this finding may point towards an increase of dityrosine crosslinks being created during hydrogel formation with an increasing urea content. However, no significant change could be observed for the addition of urea at lower concentrations. Several conceivable possibilities could explain this finding, for example protein unfolding altering the number of formed entanglements and/or intermolecular interactions during hydrogel formation or in the formed hydrogel, or the exposure of tyrosine residues being caused by protein unfolding may depend on a threshold concentration of urea. To gain a further understanding of the mechanical properties and the influence of urea, dityrosine quantification by taking advantage of its autofluorescence as reported by Elvin *et al.*[60] and advanced material characterization techniques such as protein structural analysis by circular dichroism spectroscopy or hydrogel structure analysis by small-angle scattering should be conducted prospectively.

4.3.4. **Effect of BSA Concentration on Rheological Properties**

In order to investigate the influence of the protein concentration on the resulting mechanical properties, hydrogels with varying BSA concentrations were prepared. Thereby, an optimized buffer system enabled photopolymerization of hydrogels containing between 20 to 100 mg/ml even with 4 M urea being present in MCB pH 7. Hydrogel discs which were stable in their shape could only be obtained for all concentrations above 40 mg/ml. By variation of the BSA and urea concentration in the precursor solution, the storage modulus G' of the generated hydrogels could be tuned in a range of 0.38 ± 0.02 kPa to 3.93 ± 0.29 kPa (0 M urea) and 0.99 ± 0.14 kPa to 30.05 ± 1.12 kPa (4 M urea) when stored in formulation buffer (see Figure 4.3 A).

As for BSA-hydrogels prepared in SPB, for all tested BSA concentrations, G' (Figure 4.3 A) and elasticity (Figure 4.3 B) were significantly increased when urea was added to the precursor and storage solution. With the exception of the step from 60 to 80 mg/ml prepared without urea ($p = 0.83$, $Z = 0.21$), an increase in BSA concentration increased G' significantly Figure 4.3 A). Interestingly, even though having the lowest network strength, hydrogels containing 40 mg/ml were the least elastic for both urea concentrations tested, while being most elastic for a BSA concentration of 60 mg/ml (Figure 4.3 B). The increase in molecules leads to simultaneous effects such as increasing intermolecular interactions, more surface available and therefore crosslinkable tyrosine residues, more possible chain entanglements - which all are expected to increase the network density – combined with a possibly introduced steric hinderance – all

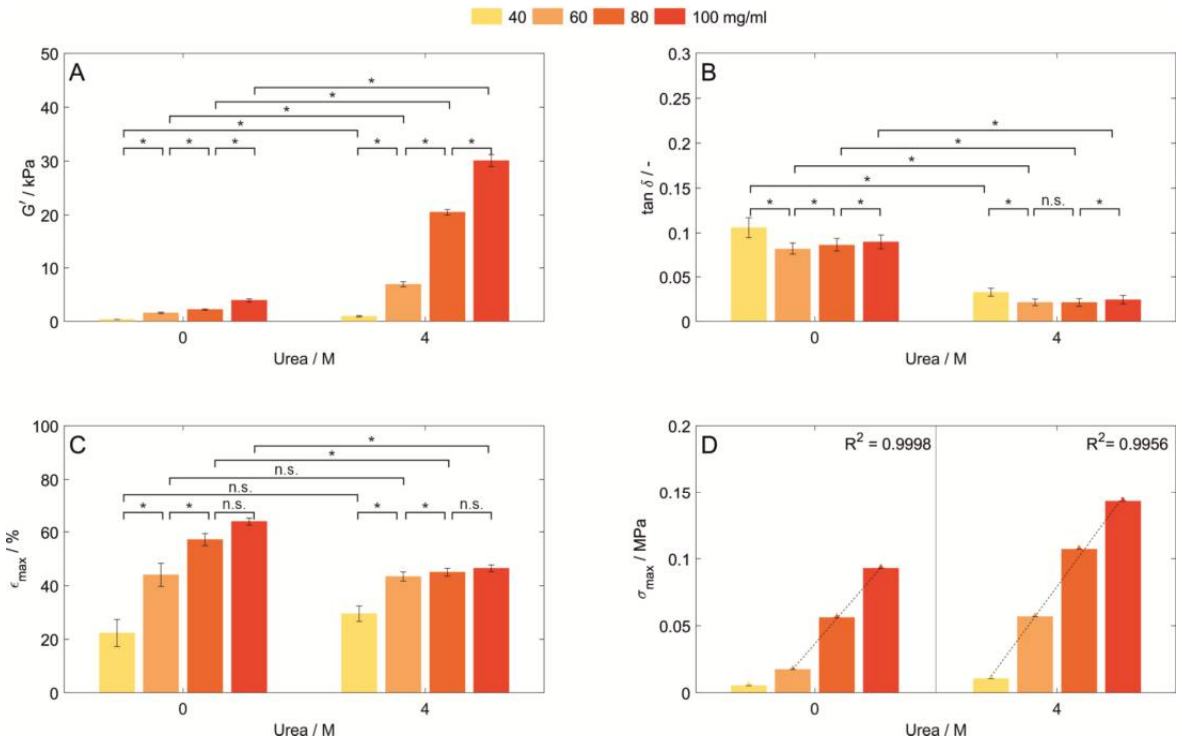

Figure 4.3 Characterization of hydrogels containing 40, 60, 80, and 100 mg/ml BSA prepared in MCB pH 7 with 0 or 4 M urea. All samples were stored in formulation buffer prior analysis. (A) Storage modulus (G') and (B) loss factor (tan δ) determined by frequency-dependent oscillatory shear rheology. (n =3) (C) Fracture strain (ε_{max}) and (D) compressive strength (σ_{max}) of those hydrogels determined by uniaxial compression tests. Abbreviations: n.s.: not significant, *: $p < 0.05$.

influencing the hydrogel elasticity. Prospective work in material characterization to understand the correlation between these effects has to be conducted to gain a further understanding of the formed hydrogel networks.

4.3.5. **Fracture strain and compressive strength of BSA-based hydrogels**

Fracture strain ε_{max} and compressive strength σ_{max} were determined by uniaxial compression until sample fracture for hydrogels prepared with varying BSA concentrations in MCB pH 7. The stress-strain curve thereby showed an unusual curve shape with multiple drops of the measured stress before increasing again (Appendix C.3). During compression, parts of the network are collapsing at lower stresses than the overall hydrogel fracture resulting in this unusual curve shape. However, rheological characteristics showed a high reproducibility of mechanical properties of the intact network structure. Since undirected photopolymerization is used as crosslinking mechanism without aimed crosslinking sites, the reason for the non-reproducible compression curves might be an inhomogeneous network.

The fracture strain increases significantly for both urea concentrations until a concentration of 80 mg/ml BSA without a further significant increase if the concentration is further raised (Figure 4.3 C). Thereby, at least two effects contribute to the fracture strain. Firstly, the increase in protein molecules enables more intermolecular interactions and chemical crosslinks, thus being able to withstand higher stress. Secondly, a large number of these intermolecular

interactions and chemical crosslinks reduces the mobility of amino acid chains and concentrates the stress on weak chains within the inhomogeneous network. While the first effect seems to be dominant up to a concentration of 80 mg/ml, the second seems to become more important with increasing protein concentration.

Hydrogels prepared without urea showed a significantly higher maximum strain up to 57.2 ± 2.3 % / 63.9 ± 1.3 % (80/100 mg/ml, 0 M urea) compared to the samples prepared in the presence of urea with 45.0 ± 1.4 % / 46.5 ± 1.3 % for 80 / 100 mg/ml (see Figure 4.3 C). By the addition of urea, no significant change in maximum strain could be observed for 40 mg/ml BSA ($p = 0.2303$). This might be attributed to synergistic effects of an increased crosslinking density and changes in the protein hydrophobicity affecting the surface charge of BSA and thus electrical repulsion between proteins – with the latter being reported as a method for strain-stiffening of protein-based hydrogels[197]. Since both conditions were stored without external stimuli in their formulation buffer, the influence of the presence of urea in the hydrogel network has to be further investigated.

Interestingly, the compressive strength of the hydrogels shows linear dependency with the protein concentrations for BSA-based hydrogels prepared without urea in the range from 60 to 100 mg/ml ($R^2 = 0.9998$) and the whole concentration range tested when urea was present in the precursor solution ($R^2 = 0.9956$ - Figure 4.3 D). The same trend was observed for the hydrogel toughness (see Appendix C.4). This linearity could not be seen for any other mechanical property assessed. Further enhancement of the compressive strength and toughness can be achieved by addition of 4 M urea in the precursor solution and storage medium, increasing the compressive strength between 154 % from 0.093 to 0.143 MPa (100 mg/ml) and 328 % from 0.017 to 0.057 MPa (60 mg/ml) and the toughness between 136 % from 4.1 to 5.5 kJ/m³ (100 mg/ml) and 239 % from 0.9 to 2.2 kJ/m³ (60 mg/ml). This indicates that the compressive strength and toughness can be modulated in a wide range depending on the specific conditions of hydrogel composition, urea content in the precursor solution and storage conditions.

4.3.6. **Influence of preparation and storage buffer**

To exclude effects caused by the presence of urea during storage, a buffer exchange to a dedicated storage buffer prior to storage and analysis was performed following hydrogel formation (Figure 4.4). DPBS was chosen as a frequently used physiological buffer for sample storage, which exerts a change in environmental conditions on the hydrogels through pH value, type and concentration of ions. For this evaluation, 100 mg/ml BSA- and casein-based hydrogels were produced in MCB containing 0, 2, and 4 M urea. All resulting BSA-based hydrogels showed higher storage moduli in a range from 17.29 ± 2.19 kPa to 63.39 ± 6.42 kPa (Figure 4.4 A) compared to those prepared and stored in SPB (Figure 4.2 A). Increasing urea concentrations in the precursor solution of the BSA-based hydrogels resulted in a significant increase of all storage moduli (302 % increase for the formulation buffer pH 8 and 232 % for pH 7, respectively, when gels prepared with 4 M urea are compared to urea-free gels). Since the increase in G' could be observed following a buffer exchange to a similar dedicated storage buffer prior to hydrogel storage, the increasing storage moduli seem not to be related to the different storage medium characteristics discussed before.

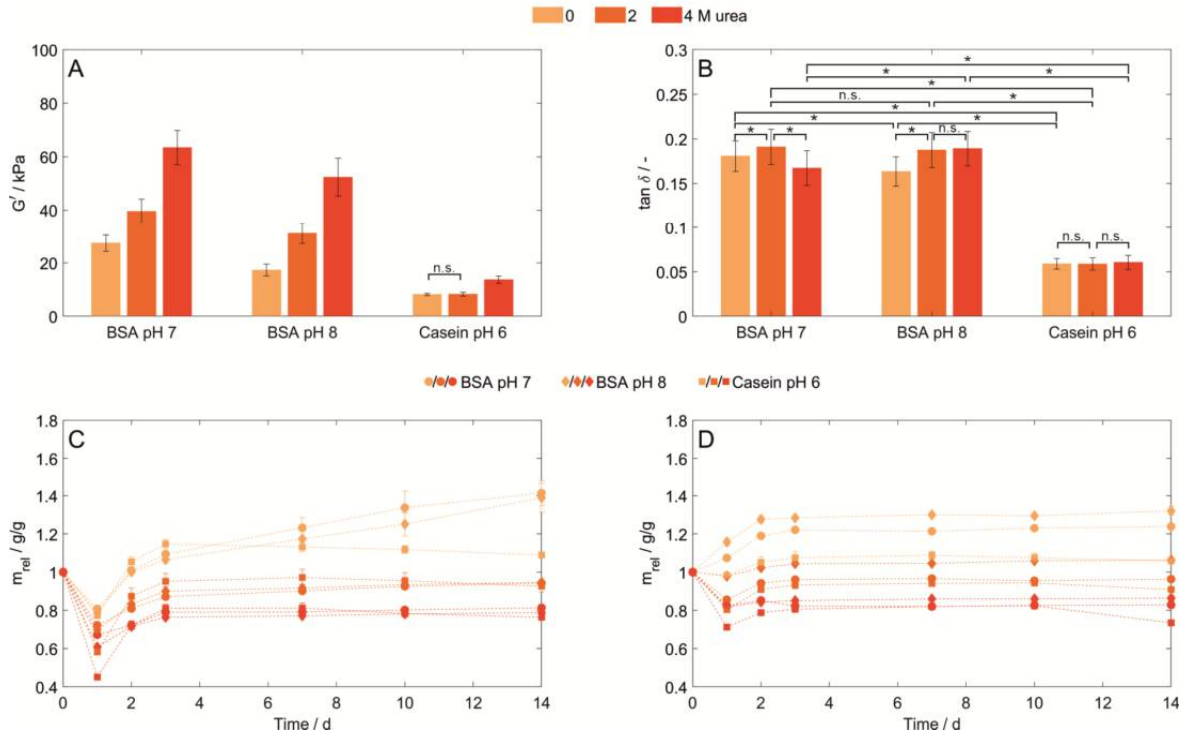

Figure 4.4 Characterization of hydrogels containing 100 mg/ml BSA (pH 7 and 8) or casein (pH 6) prepared in MCB containing 0, 2 or 4 M urea. (A) Storage modulus (G') and (B) loss factor (tan δ) as determined by frequency-dependent oscillatory shear rheology. All samples were stored in DPBS (n = 3) (C and D): Relative weight swelling ratio (m_{rel}) of BSA- and casein-based hydrogels stored in (C) DPBS or (D) MCB without urea at formulation buffer pH. (n = 3)

4.3.7. **Preparation pH of BSA-based hydrogels**

To vary the intermolecular interactions during hydrogel preparation in the presence and absence of urea, the protein surface charge was altered for hydrogels stored in DPBS. Therefore, BSA-based hydrogels were prepared at two different pH values known not to induce structural transitions to neglect changes in the amount of surface available tyrosines.

A significant higher network density - even in the presence of urea during formulation and hydrogel formation - was achieved when the hydrogels were polymerized closer to their pI, as being previously reported for albumin hydrogels produced by heat-induced denaturation[198] (Figure 4.4 A). The net surface charge of a protein mainly corresponds to the pH value of protein solutions and increases with an increasing distance to the isoelectric point (pI). Globular BSA with a pI around pH 5.0 to 5.2[199] and a theoretical pI based on its amino acid sequence of pH 5.82 (P02769, UniProtKB/Swiss-Prot), has a net surface charge of -30 (pH 7) and -46 (pH 8, both calculated using Prot pi and ProMoST as pKa database[200]). Thus, a lower protein-protein repulsion was expected at pH 7 compared to pH 8 in the formulation buffer and during hydrogel formation explaining the higher higher network density at pH 7 due to more intermolecular interactions.

For BSA-based hydrogels prepared at pH 7, elasticity was decreased comparing 0 and 2 M urea, while upon addition of 4 M urea a significant increase ($p = 6 \cdot 10^{-13}$, $Z = 7.19$) compared to 2 M urea could be shown (Figure 4.4 B). In comparison to the preparation at different pH values

for gels prepared without urea, elasticity increased significantly at pH 8 (tan δ = 0.163 ± 0.017) compared to pH 7 (tan δ = 0.181 ± 0.017, $p = 2 \cdot 10^{-10}$, Z = 6.34). As those gel specimens were produced with the same protein concentration, stored in the same buffer system and the dityrosine content was assumed to be similar, changes intermolecular interactions, here induced by formulation buffer pH, showed to significantly influence the hydrogel elasticity and network density.

4.3.8. **Casein-based hydrogels**

Besides the globular protein BSA, with casein a conjugated protein was introduced for hydrogel formation. Casein consists of four subunits without a stable secondary or tertiary structure[201]. In order to fulfill their biological function of calcium and phosphate transportation, these subunits are forming micelles, whose detailed structure and organization are still under investigation[41]. Casein-based hydrogels prepared at pH 7 and 8 showed sample shrinking and macroscale ruptures directly after polymerization (not shown).

Possibly, the chain rearrangements after the introduction of a constrained structure into the typically less structured casein subunits in combination with possible entanglements of chains within these structures lead to tensions with the ability to disrupt the entire hydrogel structure, however this was not further assessed. For casein-based hydrogels prepared in MCB at pH 6, these macroscale fractures were not observed and mechanical properties after storage in DPBS were determined. Consistent with the results discussed for BSA, an increasing storage modulus could be observed for increasing urea concentrations in the precursor solution - with the difference that significant changes could only be observed for 4 M urea being present in the precursor solution while elasticity seems to be independent of the urea concentration (Figure 4.4 B). Protein unfolding as discussed for BSA cannot be a suitable explanation since casein subunits do not have a stable secondary or tertiary structure. Though, by the addition of urea micelle integrity will be disrupted, while even at concentrations of 6 M urea, particles in the original micelle size can be traced[25]. To evaluate whether the disruption of casein micelles enabled the formation of more dityrosine crosslinks due to an enhanced surface accessibility of tyrosine residues or whether other increased inter- or intramolecular interaction are causing the increased network density, dityrosine quantification and structural analysis of casein and the resulting hydrogels should be conducted prospectively.

4.3.9. **Swelling behavior of casein- and BSA-based hydrogels**

Hydrogel swelling behavior is influenced by the competition between the Donnan osmotic pressure and the elasticity of the hydrogel network[202]. In general, a swelling medium without added urea was chosen, as the presence of urea is known to lead to a collapse of hydrogel structures[203]. The latter was confirmed during initial experiments where hydrogels were stored in DPBS (Figure 4.4 C). All hydrogels lost weight after preparation and storage for the first 24 hours compared to their initial weight at t = 0 to which the liquid volume and buffer substances dissolved in it also contribute in addition to the actual hydrogel network. While hydrogel formation in the absence of urea resulted in a weight loss between 19 % (BSA pH 7, 0 M urea) and 23 % (Casein pH 6, 0 M urea) of their weight, adding urea enhanced this effect up to a weight decrease of 55 % (Casein pH 6, 4 M urea). After the first (t = 24 h) and second (t = 48 h) buffer exchange, all hydrogels are gaining weight. For hydrogels formulated and prepared

without urea, the preparation weight is reached or surpassed at the second day up to a weight increase of 41 % (BSA pH 7), 39 % (BSA pH 8) and 9 % (Casein pH 6) after 14 days. All other conditions do not reach their starting weight in the considered time period. The weight loss after 14 days for 2 M urea is in a range of 5 % (BSA pH 8) to 7 % (Casein pH 6), while being with 19 % (BSA pH 7) to 24 % (Casein pH 6) higher for 4 M urea. Thus, the swelling behavior of hydrogels formed in the presence of urea (preparation stage) correlates with the urea concentration used during network formation.

As all hydrogels were stored in a dedicated storage buffer system with a change in ionic strength (from 96 mM salts in the MCB to 150 mM in DPBS), pH (pH 6,7 or 8 in MCB to pH 7 to 7.3 in DPBS) and urea concentration, multiple external stimuli were applied independently or simultaneously. To exclude the influence of changing salt concentrations when altering the pH – normally associated with common buffer systems - the corresponding hydrogel was stored at different pH values was tested in MCB without urea for all conditions (Figure 4.4 D). Thereby, BSA-based hydrogels stored in their formulation buffer directly swelled by 7 % (pH 7) to 16 % (pH 8), while the casein-based hydrogel still lost 2% of its weight. Hydrogels prepared with urea being present showed a urea concentration-dependent weight loss during storage, high urea concentrations (c = 4 M) resulted in a shrinkage of up to 29 % for casein and 18 % for both BSA-based hydrogels. From day 2 on, all hydrogels showed a swelling behavior, while the swelling degree until the second day was urea-dependent (3-8 % for hydrogels prepared at 4 M urea compared to a swelling degree of 11-12 % for hydrogels prepared without urea).

In summary, four findings concerning the swelling behavior can be highlighted. Firstly, an increasing ionic strength decreases the Donnan osmotic pressure due to more ionic interactions between mobile ions and fixed charges inside the hydrogel network[202], resulting in shrinking or lower swelling by pushing liquid out of the hydrogel network as seen for DPBS. Secondly, as for the hydrogels prepared in the presence of urea - which makes up as much as 20 % of the initial hydrogel weight -, urea diffuses out of the hydrogel leading to a weight decrease and simultaneously to an increase in hydrophobic interactions in the hydrogel network, explaining the overall shrinking and weight loss of these hydrogels. Thirdly, all hydrogels subject to any external stimulus showed a shrinking behavior following the first buffer exchange and then started to swell again. Thereby, the urge of the hydrogel to swell indicated by an increasing weight is opposed to shrinking effects and weight loss due to the decreasing urea content and/or increasing salt concentration inside the hydrogel network, as discussed before. As for the first day, the shrinking effect seems to be dominant, indicating that either the diffusion of urea out of/salts into the hydrogel network takes more time or the osmotic pressure not being sufficiently due to a too small buffer excess. Fourthly, the protein and formulation buffer pH influence the relative swelling ratio to a certain degree. This may be related to different protein characteristics such as surface charge distribution which is also known to affect swelling ratio in heat-induced BSA-hydrogels[198]. As discussed before, these properties are also responsible for the hydrogel network density requiring further experiments to gain a deeper understanding on the swelling behavior of protein-based hydrogels.

Overall, the protein-based hydrogels presented in this manuscript showed stimuli-responsive swelling behavior. Thereby, hydrogel and buffer characteristics showed to be influencing the relative weight swelling behavior with the more pronounced the differences between swelling medium and formulation buffer, the more shrinking was observed independent of formulation buffer pH or protein.

4.3.10. **Predictability of the mechanical properties**

The two proteins used in this manuscript show several different characteristics. Just to name some, their amino acid composition, molecular structures and molecular weight differ. For example, 17 disulfide bonds - which are not affected by urea – are stabilizing the molecular structure of the BSA backbone, while there a none in casein. While BSA has a total of 20 tyrosine residues, which corresponds to a tyrosine content of 3.4 % (P02769, UniProtKB/Swiss-Prot), the overall tyrosine content in casein is expected to be between 3.9 and 4.2 % depending on the exact proportion of its subunits[201,204,205]. Due to the loose structure and a higher tyrosine content, a higher surface availability of tyrosine and therefore dityrosine crosslinks content compared to BSA would thus be expected. In contrast, just looking at the adiabatic compressibility, native BSA is with $10.5 \cdot 10^{-11}$ Pa^{-1} more compressible than the prevalent casein subunit α-casein with $5.68 \cdot 10^{-11}$ Pa^{-1}, suggesting more elastic hydrogels being derived from BSA[206].

Thus, the resulting mechanical properties of photopolymerized, dityrosine-crosslinked hydrogels derived from proteins are difficult to be foreseen as multiple factors such as the protein characteristics, as well as its folding state and formulation dependent intermolecular interactions during hydrogel formation showed to be crucial process parameters. To compare different proteins with the aim to tune or predict these hydrogel properties, a much deeper understanding of the underlying hydrogel network and its formation will be necessary prospectively.

4.4. Conclusion

BSA and casein were crosslinked through visible light-induced photopolymerization mediated by a ruthenium-based photoinitiator in the presence of urea concentrations up to 4 M. Even though their different protein characteristics, protein-based hydrogels were obtained with significantly different rheological properties, showing the potential of more peptide-constructs or unmodified proteins as prospective material source for hydrogel formation. Depending on the protein, protein concentration, formulation buffer and storage conditions, storage moduli were varied in a range between 0.4 to 63 kDa. The chaotropic agent urea, which is known to weaken hydrophobic interactions, was used as a tool for changing the hydrogel properties. Possibly, urea-induced gelation reactions, an enhanced surface accessibility of tyrosines or an increasing number of chain entanglements by unfolding BSA and disrupting casein micelles result in higher network densities with simultaneous increase in hydrogel elasticity. As the choice of formulation buffer pH and buffer components are influencing protein characteristics, such as the surface net charge, the individual parameters of the formulation buffer composition as well as the used storage medium have to be chosen carefully in accordance to the desired mechanical properties of polymerized hydrogels.

For the design of bio-based hydrogels or materials for a specific application, characterization of the hydrogel network structure, e.g. by determination of dityrosine content in polymerized hydrogels or small-angle scattering has to be conducted to gain a further understanding of the parameters influencing the mechanical properties. Using this reaction mechanism, naturally occurring, unmodified proteins may be used in future as bio-based materials with potential for biomedical applications, potentially including 3D-printing for the custom design of scaffolds for personalized medicine.

5 Mechanical properties of protein-based hydrogels derived from binary protein mixtures – A feasibility study

Sandra Haas, Jürgen Hubbuch

Polymers (2023), Volume 15, Article 964

Abstract

Hydrogels based on natural polymers such as proteins are considered to be biocompatible and therefore represent an interesting class of materials for applications in the field of biomedicine and high-performance materials. However, there is a lack of understanding on the proteins which are able to form hydrogel networks by photoinduced dityrosine crosslinking as well as a profound knowledge on the formed network itself and the mechanisms which are responsible for the resulting mechanical properties of such protein-based hydrogels. In this study, casein, bovine serum albumin, α-amylase, and a hydrophobic elastin-like protein were used to prepare binary protein mixtures with defined concentration ratios. After polymerization, the mechanical properties determined with rheological methods of the resulting homopolymeric and copolymeric hydrogels were dependent on the protein shares used. In additional uniaxial compression tests, the fracture strain was shown to be independent of the protein shares, while hydrogel toughness and compressive strength were increased for protein-based hydrogels containing casein.

5.1. Introduction

Protein-based hydrogels may help to meet the increasing need of non-petroleum-based specialized materials, as they are based on biological, renewable resources, have a good cyto-/biocompatibility and show a high extend of biodegradability[104,173]. Additionally, since some proteins can be expressed as recombinant polymers with high monodispersity and with precise control and adaptability of their amino acid sequence, they can be customized to the needs of their potential specific application[207]. Since proteins can undergo stimulus-dependent conformational changes, biomaterials with increasingly complex functions and improved functional properties can be designed[208]. In addition to naturally occurring proteins, artificially designed proteins such as elastin-like proteins (ELPs) can be used as a raw material source for hydrogels proposed for applications in drug delivery[138], in tissue engineering[118,209] or in three-dimensional (3D) printing[124,126]. This class of proteins is based on the repetitive core amino acid sequence Val-Pro-Gly-Xaa-Gly of mammalian tropoelastin – Xaa being any amino acid besides proline – with mechanical properties comparable to natural elastin[48–50,110].

Each type of protein, whether it is a naturally occurring or engineered protein, has particular characteristics in terms of its structure due to specific inter- and intramolecular interactions. Protein-based hydrogels can be prepared either by physical or chemical crosslinking approaches or by a combination of both[210]. One of these hydrogelation methods is based on the crosslinking of phenolic hydroxy groups which are naturally present in tyrosine to form dityrosines under mild reaction conditions. This processing pathway is mediated by a ruthenium-containing photoinitiator which is induced by visible light[57,58] and has been applied to several proteins, including bovine serum albumin (BSA), casein, tyrosine-enriched gelatin, maltose-binding protein, I27, protein L, anegen, ELPs and silk[6,60,62,64,65,185,186,211–215]. However, the main challenge in the development of protein-based hydrogels remains the insufficient understanding of the protein characteristics and polymerization conditions in relation to the resulting mechanical properties of the hydrogels, the limited material availability of artificial protein constructs, and the drawback of many influencing factors on the resulting mechanical properties of the hydrogels hindering the design of hydrogels with specific desired mechanical properties. To shed some light into this question, we conducted the following feasibility study. We propose the formation of copolymeric hydrogels by using binary protein mixtures for crosslinking with the aim of combining the mechanical properties of different homopolymeric protein-based hydrogels. For this purpose, copolymeric hydrogels are made from binary mixtures of three different commercially available proteins (the globular protein BSA, the enzyme α-amylase, and the conjugated casein) and a hydrophobic elastin-like protein construct that was artificially designed. The resulting mechanical properties of the homo- and copolymeric protein-based hydrogel were evaluated in terms of its structural strength, elasticity, compressive fracture strain, compressive strength, and toughness.

5.2. Materials and Methods

5.2.1. Buffer preparation

The formulation buffer solutions were (1) a 20 mM sodium phosphate buffer (SPB) with 4 M urea and (2) a 96 mM multi-component buffer (MCB) consisting of 47 mM N-[tris(hydroxymethyl)methyl]-3-aminopropanesulfonic acid (TAPS), 11 mM 3-morpholino-2-hydroxypropanesulfonic acid (MOPSO), 38 mM sodium citrate and 4 M urea. All buffers were prepared with ultrapure water (PURELAB Ultra, ELGA LabWater, LaneEnd, UK) and were pH-adjusted to pH 8 using a 4 M sodium hydroxide solution. The buffers were filtered through an 0.45 µm cellulose acetate membrane (Pall Corporation, New York, US-NY) before use.

5.2.2. Photoinitiator and Co-Factor

The photoinitiator tris(2,2′-bipyridyl)dichlororuthenium(II) hexahydrate ($Ru(bpy)_3Cl_2 \cdot 6\ H2O$) was prepared in the corresponding buffer to a concentration of 5 mM and stored at 4 °C. The electron acceptor ammonium persulfate (APS, chemical formula: $(NH_4)_2S_2O_8$) was prepared with a concentration of 2 M in the corresponding buffer, stored as aliquots at -20 °C and thawed directly prior to usage.

5.2.3. Elastin-like protein production

Following the nomenclature introduced by Meyer *et al.*[111], the used hydrophobic ELP is referred to as ELP[V2Y-45] with the guest residues valine and tyrosine in a 2:1 ratio and with a total of 45 repetitions of the pentapeptide sequence. Fermentation and purification was performed using the inverse transition cycling (ITC) process previously described[216]. Briefly, the homogenized and subsequently centrifuged *Escherichia coli* lysate was resuspended in a buffer containing 4 M urea to dissolve inclusion bodies containing the ELP construct. Insoluble contaminants were removed by another round of centrifugation before the addition of 0.4 M ammonium sulfate to precipitate ELP[V2Y-45] which was separated from soluble contaminants by a subsequent centrifugation. Subsequently, the pellet of the high salt precipitation was resuspended in ultrapure water. As the hydrophobic ELP[V2Y-45] reversibly aggregates in water at room temperature, two temperature-dependent centrifugation steps were applied in water to remove contaminants (referred to as one cycle of ITC) and the pellet of the hot spin centrifugation finally formulated into 20 mM SPB containing 4 M urea by its resuspension.

5.2.4. Preparation of the protein stock solutions

Four different proteins were used in this manuscript, a hydrophobic ELP construct, casein, bovine serum albumin (BSA), and α-amylase**.** Casein (EMD Millipore Corporation, Billerica, US-MA) was dissolved in the respective buffer at a concentration of 130 mg/ml using a dual asymmetric centrifuge (DAC, SpeedMixer® DAC 150.1 FVZ-K, Hauschild GmbH & Co. KG, Hamm, DE) at 2500 rpm, while α-amylase (*Bacillus sp.,* A4862, Merck KGaA, Darmstadt, DE) was purchased as a liquid formulation. Dialysis was performed for rebuffering of α-amylase and for purification of casein (e.g. by removing production buffer salts) using SnakeSkin™ dialysis tubing (Thermo Fisher Scientific, Waltham, US-MA) with a 10 kDa molecular weight cut-off and a 100-fold buffer excess. Two buffer exchanges were performed, the first after

> 2 hours, the second after > 2 more hours. BSA was prepared in the respective buffer solution in the DAC at 2500 rpm directly prior use.
If necessary, Vivaspin® ultrafiltration units (Sartorius Stedim Biotech, Göttingen, DE) with a molecular weight cut-off of 10 kDa were used according to the manufacturer's recommendation to reach higher stock solution concentrations. Protein concentrations were determined with a NanoDrop 2000c UV-Vis spectrophotometer (Thermo Fischer Scientific, Waltham, US-MA) using the extinction coefficients $\varepsilon_{BSA,280nm} = 0.67$ L/(g*cm)[187], $\varepsilon_{\alpha\text{-Amylase},280nm} = 2.60$ L/(g*cm)[217], $\varepsilon_{ELP[V2Y\text{-}45],280nm} = 0.799$ L/(g*cm)[216], and $\varepsilon_{Casein,280nm} = 0.73$ L/(g*cm)[213].

5.2.5. **Hydrogel formation**

Hydrogels with a total protein concentration of 80 mg/ml composed of a single protein (homopolymeric hydrogels) or a binary protein mixture (copolymeric hydrogels), 0.25 mM $Ru(bpy)_3Cl_2$ and 100 mM APS were prepared as previously described[213]. Briefly, formulation buffer, protein and photoinitiator stock solutions were mixed following another round of mixing in the DAC after the addition of the APS stock solution. The precursor solution was transferred into a cylindrical mold (diameter 10 mm, height 3 mm) and irradiated for 5 minutes from atop and below using a blue emitter (LZ4-00B208, LED Engin Inc, San Jose, US-CA). Polymerized hydrogels were then stored in their formulation buffer for 7 d prior analytics with a 100-fold liquid excess to monitor the swollen state.

5.2.6. **Oscillatory rheometry**

The linear viscoelastic region (LVR) of polymerized hydrogels was determined by amplitude sweeps (angular frequency $\omega = 1$ and 25 rad·s^{-1}, shear stress $\tau = 5$-10.000 Pa, number of replicates n = 2), followed by frequency sweeps within the LVR ($\tau = 10$ Pa, $\omega = 1$-25 rad·s^{-1}, n = 3) on a Physica MCR 301 plate rheometer equipped with the plate-plate geometry PP10 (all Anton Paar GmbH, Graz, AT) to obtain the mean plateau value of the storage modulus G' and loss factor tan δ.

5.2.7. **Uniaxial compression tests**

Uniaxial compression tests were performed on a universal testing machine (zwickiLine Z0.5TN, ZwickRoell GmbH & Co. KG, Ulm, DE) equipped with a stainless-steel compression platen and the Xforce HP 100 N load cell (both ZwickRoell GmbH & Co. KG). Swollen hydrogel discs were compressed with a uniform velocity of 2 mm/min until sample breakdown to determine the fracture strain $\varepsilon_{max} = (L\text{-}L_0)/L_0$, with the sample length L_0 being the sample length at a pre-force of 0.2 N and L being the sample length at sample fracture, the compressive strength $\sigma_{max} = F/A_0$, with F being the applied force at sample fracture and A_0 being the unstressed cross-sectional area, and the hydrogel toughness by integrating the stress-strain curves until sample failure in relation to the uncompressed hydrogel volume.

5.3. Results

5.3.1. Homopolymeric protein-based hydrogels

In order to evaluate their suitability to form homopolymeric protein-based hydrogels, four different proteins with distinct characteristics (see Table 5.1) were crosslinked and the resulting mechanical properties of the hydrogels such as their structural strength and elasticity were determined. Technically, as casein consists of four different subunits, casein-based hydrogels would be referred to as copolymers, however for the ease of simplification with regard to the subsequent use of binary protein mixtures, we consider the obtained casein-based as a homopolmyeric network within this manuscript. The homopolymeric hydrogels were polymerized by visible light-induced crosslinking of a precursor solution containing 80 mg/ml of only one type of protein per formulation. Each protein was prepared in two buffer systems – with the exception of ELP[V2Y-45] which was prepared in SPB only due to limited material availability. The structural strength of the hydrogels was evaluated in terms of storage modulus G' (Figure 5.1 A), while elasticity was evaluated on the basis of loss factor (tan δ = G"/G') with a loss factor of 0 corresponding to ideal elastic behavior (Figure 5.1 B). Both parameters were determined using frequency sweeps, with a shear stress selected within the linear viscoelastic range. For all protein stock solutions and buffers, gel-like behavior of the previously photopolymerized hydrogel networks was confirmed by G' being greater than G'' over the whole amplitude range applied. In contrast to the hydrogels prepared from the other proteins investigated, casein hydrogels prepared in SPB developed visible cracks not impeding the overall disc integrity during or shortly after polymerization before being transferred to the storage solution. The structural strength of casein hydrogels increased by 27 % when being prepared in MCB instead of SPB, while for BSA and α-amylase hydrogels, it was decreased by 54 % (BSA) and 49 % (α-amylase). In the same context, elasticity was increased for casein hydrogels by 14 %, while there was an opposite trend for hydrogels prepared of BSA (- 33 %) or α-amylase (- 13 %).

When prepared in SPB, α-amylase, BSA and ELP hydrogels had a storage modulus between 6.4 ± 0.8 kPa (α-amylase) and 10.9 ± 0.6 kPa (BSA), while hydrogels from the conjugated protein casein had the highest storage modulus (24.8 ± 1.2 kPa) and thus structural strength of all protein-based hydrogels tested. Regarding elasticity, BSA hydrogels were the least elastic (tan δ = 0.017 ± 0.004), while hydrogels obtained from casein (tan δ = 0.011 ± 0.002) and α-amylase (tan δ = 0.012 ± 0.002) had a comparable elasticity, and the hydrogel prepared of the artificially designed elastin-like protein exhibited the highest elasticity with tan δ = 0.004 ± 0.002. Additional information about the mechanical properties of the protein hydrogels was obtained by uniaxial compression tests. For these analyses, we focused on SPB as the more common buffer system. With regard to the fracture strain (all in the range between 32 ± 7 and 44 ± 3 %), compressive strength (all in the range between 0.028 ± 0.010 and 0.052 ± 0.016 MPa) and hydrogel toughness (all in the range between 1.25 ± 0.66 and 2.16 ± 0.62 kJ/m³), taking the standard deviations into account, no differences were obtained for the investigated proteins (Figure 5.1 C-E). More profound statements about statistical significance would need an increased number of replicates per condition.

Table 5.1 Selected protein characteristics potentially influencing the mechanical properties of the resulting hydrogel network

Protein	**Casein**	**BSA**	**α-Amylase**	**ELP[V2Y-45]**
Type	Heteroprotein (consisting of mainly 4 subunits, ≈ 38% α_{s1}-, ≈ 10% α_{s2}-, ≈ 36 % β-, ≈ 13 % κ-casein)[a)]	Globular protein	Enzyme	Modified protein
Origin	Bovine milk	Bovine blood serum	*Bacillus species*	Recombinant production in *Escherichia coli*
Structural arrangement	No well-defined secondary and tertiary structure of subunits which are forming micelles [a)]	Ordered Tertiary structure	Ordered Tertiary structure	Intrinsically disordered protein
Size / kDa	Subunits: ≈ 19 – 25 [b)] Micelles: 250-500 [c)]	66.0	52.9 [d)]	21.6
Tyrosines / %	≈ 3.9 – 4.2 [b), c)]	3.6 [e)]	4.2 [d)]	6.1
pI (native structure) / -	≈ 4.6 [c)]	≈ 5.0 - 5.2 [f)]	unknown	unknown
Theoretical pI [g)] / -	5.0 [h)] 5.3 [i)]	6.2 [e)]	5.3 [d)]	6.8
Theoretical Charge at pH 8 [g)] / -	-12.6 [h)] -8.4 [i)]	-20.9 [e)]	-15.1 [d)]	-2.0
Adiabatic compressibility (native structure) [j)] / Pa^{-1}	$5.68 \cdot 10^{-11}$ [k)]	$10.5 \cdot 10^{-11}$	$5.12 \cdot 10^{-11}$	unknown
Disulfide bonds / -	Rare, inter- rather than intra-molecular cystine bridges [l)]	15[e)]	0 [d)]	0

a) Bhat *et al.*, 2016
b) Swaisgood, 2003
c) Fox, 2003
d) *α-Amylase, C8AWK4, UniProtKB/Swiss-Prot*
e) *BSA, A0A3Q1LNN7, UniProtKB/Swiss-Prot*
f) Brown *et al.*, 2004
g) *Prot pi and ProMoST as pKa database*[200]
h) *α_{s1}-Casein, P02662, UniProtKB/Swiss-Prot*
i) *β-Casein, P02666, UniProtKB/Swiss-Prot*
j) Gekko and Hasegawa, 1986
k) *α_s-Caseins*
l) De Kruif and Holt, 2003

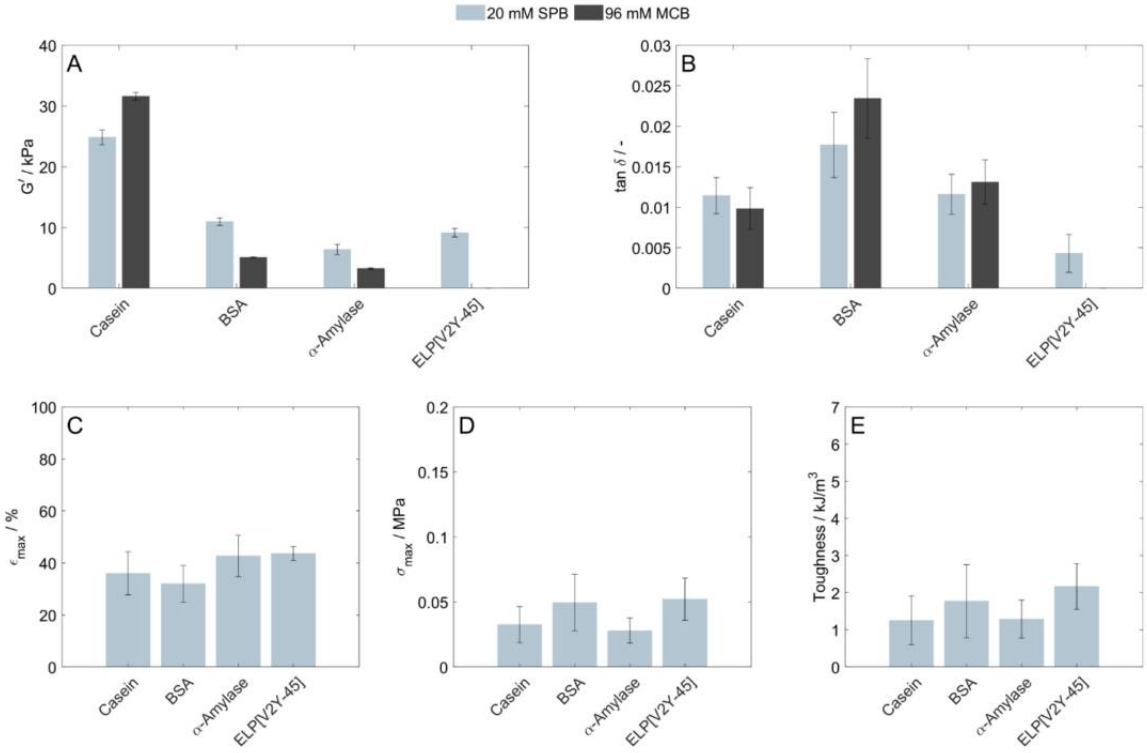

Figure 5.1 Characterization of protein-based hydrogels consisting of 80 mg/ml of a single protein prepared in 20 mM SPB (light blue) or 96 mM MCB (black). (A) Hydrogel storage modulus (G') and (B) loss factor (tan δ) related to the used protein and buffer (n = 3), as determined by rheometric measurements. Uniaxial compression tests were performed with hydrogels prepared in 20 mM SPB to determine their (C) fracture strain, (D) compressive strength and (E) toughness. for up to 3 layers of those auxetic structures (C) Structures consisting of up to 30 layers and hydrogelated by layer-wise photopolymerization.

5.3.2. **Rheological properties of copolymeric hydrogels**

To investigate the resulting mechanical properties of copolymeric protein-based hydrogels as a function of the different protein shares, binary mixtures of the proteins were polymerized and analyzed. Hydrogels prepared with 100 % casein in SPB developed visible cracks during or shortly after polymerization which were lower in extent and number for mixtures containing 25 % of a second protein and were not found by visual inspection for mixtures containing 50 % casein or less. Three findings can be highlighted regarding the structural strength of copolymeric hydrogels prepared from binary mixtures (Figure 5.2 A & B). First, the storage modulus and thus the structural strength of copolymeric hydrogels consisting of mixtures of BSA and α-amylase remained in a comparable range, a trend which was found for both buffer conditions tested. Second, for two proteins which had higher deviations in their structural strength when prepared as homopolymeric hydrogels – in this case the combination of casein and another of the proteins studied – a linear correlation (coefficient of determination $R^2 > 0.97$) of their structural strength as a function of protein share was found, when the 100% casein condition was excluded for samples prepared in SPB. Third, G' of a hydrogel made from 75% casein and either 25 % BSA or ELP[V2Y-45] decreased by 22 % compared to a hydrogel made of 100 % casein, when being prepared in SPB. When comparing it to a hydrogel prepared

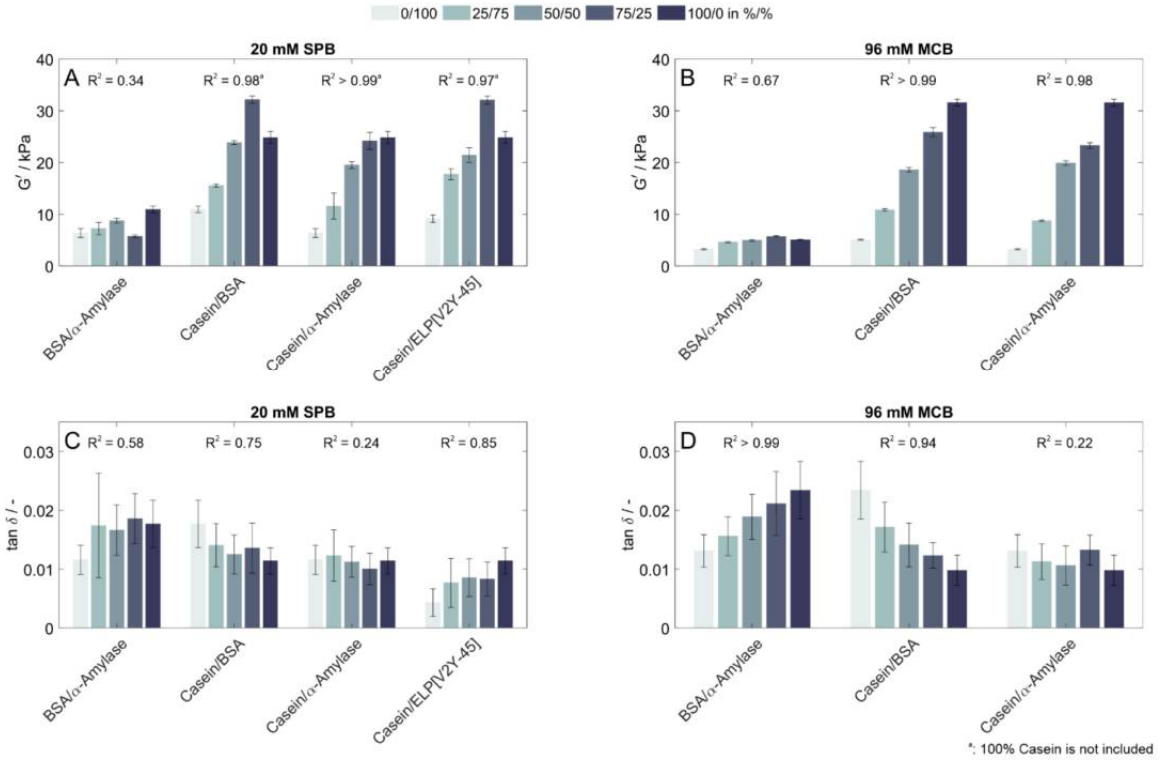

Figure 5.2 Rheological characterization of hydrogels containing different protein shares as binary mixtures. (A) Storage modulus (G') and (C) loss factor (tan δ) of hydrogels prepared and stored in 20 mM SPB, and (B) G' and (D) tan δ of hydrogels prepared and stored in 96 mM MCB determined by frequency-dependent oscillatory shear rheology (n =3).

with 25 % α-amylase and 75 % casein, G' of the 100 % casein hydrogel still slightly increased by 3%. However, in all cases this was not following the linear increase of G' observed for the increasing amount of casein until then. Interestingly, when these same protein combinations were prepared in a different solution (MCB), G' linearly increased with increasing casein content up to 100 % casein.

In terms of elasticity (Figure 5.2 C & D), as mentioned earlier, BSA was the least elastic single protein formulation in both buffer conditions, especially when prepared and stored in MCB. Although most sample values were within standard deviations of the tan δ values, copolymers prepared with BSA in combination with either casein or α-amylase showed a fair correlation in SPB (R^2 = 0.58 (BSA/α-amylase) - 0.74 (BSA/casein)) but a strong correlation between their elasticity when being prepared in MCB ($R^2 > 0.94$). For copolymers consisting of ELP[V2Y-45] – the protein with the most elastic of all analyzed homopolymeric networks - and casein, a similar correlation was found (R^2 = 0.85). For copolymers obtained from mixtures of casein and α-amylase with comparable elasticity of their homopolymers, a low correlation was found ($R^2 < 0.24$) in both buffer conditions investigated.

5.3.3. **Uniaxial compression of copolymeric hydrogels**

In order to obtain more information about the resulting hydrogels, uniaxial compression was performed for all protein combinations prepared and stored in SPB to evaluate additional mechanical properties. For all tested conditions, the fracture strain was between 32 ± 7 %

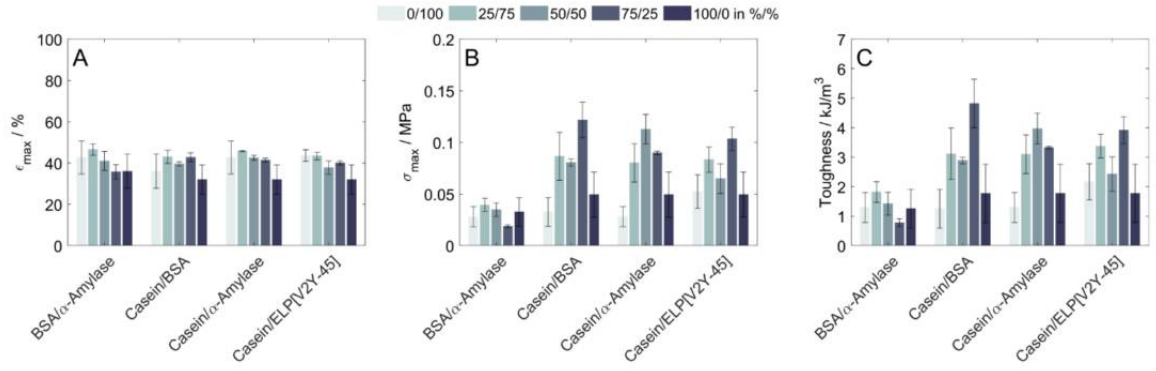

Figure 5.3 Mechanical characterization of hydrogels containing different protein shares as binary mixtures determined by uniaxial compression. (A) Fracture strain, (B) compressive strength and (C) toughness were determined for hydrogels prepared and stored in 20 mM SPB (n =3).

(100 % casein) and 47 ± 3 % (25 % BSA/75 % α-amylase), with no clear trend in the data sets (Figure 5.3A). At the same time, compressive strength and toughness were found to be dependent on the used protein shares (Figure 5.3 B & C). While for BSA/α-amylase, the compressive strength and toughness of all mixtures deviated within their standard deviations for both properties, these properties were increased for hydrogels being prepared as copolymers from a mixture of casein and any other of the investigated proteins compared to the respective homopolymers. In numbers, the maximum increase was observed for mixtures of casein and BSA, having a compressive strength increased by 166 % and toughness increased by 149 % (75 % casein/25 % BSA compared to 100 % BSA), respectively by 75 % and 76 % (compressive strength and toughness of 75 % casein/25 % BSA compared to 100 % casein).

5.4. Discussion

5.4.1. Buffer components

In order to analyze the potential influence of different buffer mediums on the protein-based hydrogels, in addition to a simple standard phosphate buffer for protein solutions (SPB), we also used a more complex MCB formulation. The buffer components MOPSO and TAPS used in the MCB are known to stabilize the native structure of BSA[188,189] – and thus possibly stabilizing the second protein investigated with an ordered tertiary structure (α-amylase) as well. This may result in a lower crosslinking density due to a lower degree of protein unfolding which was previously shown to be critical for the structural strength [213]. The third buffer component, sodium citrate, is known to increase the solubility of casein[190,191], which may increase the surface availability of potential crosslinking sites. As previously described[213], the visible crack formation directly after polymerization for hydrogels containing a casein share ≥ 75 % may thus be related to the non-stabilizing buffer formulation conditions, which may also explain the lower structural strength of homopolymeric casein hydrogels prepared in SPB compared to the copolymers formed with a 75 % casein share in SPB. In addition to the different buffer components, the MCB formulation has a higher ionic strength, as evidenced by the fact that a total of 96 mM salts are used instead of 20 mM in the case of the SPB. This affects the swelling behavior and thus mechanical properties of the hydrogels, as a higher ionic strength

leads to more ionic interactions between mobile ions and fixed charges inside the hydrogels[202]. Based on the design of this study, it remains unclear, whether the different buffers are responsible for altering the type and number of formed crosslinks during the crosslinking process (e.g. by influencing the number of formed dityrosine crosslinks or the occurring entanglements) or whether storage medium characteristics are causing the differences in the rheological properties by influencing the occurring intra- and intermolecular interactions.
To maintain the hydrophobic ELP construct in a disaggregated state at room temperature[216] and to allow comparable conditions for all samples, both buffer solutions contain 4 M urea, which causes (partial) protein unfolding for globular proteins and reduces casein micelle formation by disrupting intra- and intermolecular hydrophobic interactions[25,26]. Thus, two effects may occur due to the non-native protein structure, which may be additionally influenced by the different buffer components. First, the altered protein confirmation may affect the degree of entanglements, as has been reported for dityrosine-crosslinked ferredoxin-like globular protein[195]. Second, the solvent accessibility of tyrosine residues, and thus the number of dityrosine crosslinks formed, may be altered by the addition of urea[26]. Thus, the addition of urea affects the uncrosslinked proteins either by increasing the solubility of the structurally more disordered casein and the ELP construct used, or by inducing protein unfolding of the proteins with an ordered tertiary structure – in this study BSA, which still has a partly stabilized backbone due to the presence of disulfide bridges, and α-amylase. This further influences the hydrogel network formed and the hydrophobic interactions in the resulting hydrogel network. Furthermore, it should be taken into account that high urea concentrations are known to damage cells[218,219], so that resulting hydrogels should be washed with physiological buffers to allow applications which require high biocompatibility, such as tissue engineering or drug delivery systems. In conclusion, the formulation buffer has to be chosen carefully depending on the proteins used and the desired mechanical properties.

5.4.2. **Influence of protein characteristics**

In this study, we used four different proteins that differ in several characteristics such as their structural arrangement, charge at the pH used, molecular weight, tyrosine content, and more (see Table 5.1). The successful preparation of hydrogels from all four investigated proteins demonstrates, that the applied crosslinking method can be used for a wide variety of proteins to generate protein-based hydrogels and could be applied to more protein constructs. Since both buffer solutions were prepared with 4 M urea, all proteins were used in a non-native state. Due to the high amount of potentially influencing factors and variables which differ for complex protein molecules, no sound statement about the specific influence of the individual properties listed in Table 5.1 can be made by the presented data. Furthermore, a detailed discussion of the mechanisms responsible for the resulting mechanical properties would require a much deeper understanding of the hydrogel network formed, so this is not addressed in this manuscript. Thus, this manuscript aims to highlight the potential in modulating mechanical properties of copolymeric hydrogels derived from binary protein mixtures from a more phenomenological point of view.
In the copolymeric hydrogels, the structural strength (G') was dependent on the interplay of the two proteins used in the binary mixture, without one or the other protein dominating in terms of rheological properties. In this manuscript, we used weight-dependent concentrations of the proteins in mg/ml instead of molar ratios. Thus, the number of protein molecules and their ratio

are different for all mixtures. However, this unit was chosen because it allows the assumption, that the total sum of amino acids per ml of precursor solution is comparable. The resulting trend in the rheological properties seems to be related to the type of amino acids, which is further evidenced since the homopolymers derived from different proteins showed different storage moduli.

Considering the elasticity of the hydrogels, the resolution of the analytical method performed does not seem to be sufficient to evaluate the influence of different protein species, as most of the tan δ values obtained were within the standard deviations of another mixture. However, the general trend suggests a correlation and thus an interplay between proteins, as seen for the structural strength, but this needs to be demonstrated by more sophisticated analytical methods such as nanoindentation or atomic force microscopy. If this correlation will be verified in further experiments, this would provide a facile way to tune the rheological properties of protein-based hydrogels based on a low quantity of necessary experimental data.

While there was no discernible effect of the protein shares on the fracture strain, the compressive strength and hydrogel toughness for binary mixtures were increased compared to the homopolymeric hydrogels for all tested conditions with the exception of BSA/α-amylase. Furthermore, the structural strength of the homopolymeric hydrogel prepared of casein was even enhanced by replacing a certain amount of the protein with another protein, which could either be related to inaccurate measurements or a stressed network due to the observed visible cracks in the polymerized hydrogels. Common methods for increasing the toughness of hydrogels include creating more homogeneous hydrogels, introducing an energy dissipation mechanism to limit the propagation of macrocracks (e.g. by interpenetrating polymer networks, fiber-reinforced composite hydrogels or nanocomposite hydrogels) or combining these two mechanisms[220]. Based on the data presented in this study, it remains unclear which toughening mechanism is responsible for the increased toughness in hydrogel mixtures, as both proteins are crosslinked with the same crosslinking mechanism to copolymers. Thus, to gain an understanding of this effect, it should be analyzed prospectively by advanced characterization techniques such as a profound protein structural analysis before crosslinking depending on the buffer conditions by circular dichroism spectroscopy or Fourier-transform infrared spectroscopy and subsequent hydrogel structure analysis, e.g. by small-angle scattering and dityrosine quantification.

5.5. Conclusion

We have demonstrated the mechanical tunability of protein-based hydrogels by employing binary mixtures of four different protein constructs, either derived from natural sources or recombinantly expressed. The hydrogels were prepared by polymerizing the protein mixtures using visible light-induced dityrosine crosslinking. Furthermore, we have shown that the rheological properties such as the structural strength and elasticity can be modified by the use of binary protein mixtures to prepare copolymeric hydrogels, where the resulting mechanical properties of the hydrogels have been found to rely on an interplay between the two proteins used. The copolymeric protein-based hydrogels containing casein exhibited higher toughness upon uniaxial compression than their corresponding homopolymers, with the synergistic effects which are responsible for this effect should be further investigated. Overall, the work highlights the feasibility to modulate mechanical properties by simply mixing different proteins with

known properties of their formed dityrosine-crosslinked hydrogel network, thus providing a facile way to tailor the properties of protein-based hydrogels to the needs of their specific applications.

6 Bio-based material formulation for extrusion printing by dityrosine crosslinking of unmodified casein

Sandra Haas, Friederike Götz, Jürgen Hubbuch

Bioprinting (2022), Volume 28, Article e00245,
https://doi.org/10.1016/j.bprint.2022.e00245

Abstract

In the development of new functional bio-based materials in the field of three-dimensional (3D) printing, visible light-induced dityrosine crosslinking gains increasing interest. In this context, most current bio-based materials and ink formulations rely on previously modified chemical substances with increased tyrosine availability. In contrast, we developed and characterized a photopolymerizable ink formulation for extrusion printing based on the unmodified and naturally occurring protein casein. Manufacturability of formulations containing protein, photoinitiating system, buffer and a thickening agent turned out to be a key factor for the ink development. In total, eight different thickening agents were assessed regarding their suitability to increase the viscosity of the ink formulation to expand the fabrication window for extrusion-based 3D printing. The mechanical properties of the ink formulation and hydrogel in presence of sodium alginate were further characterized and the macroscopic fabrication of auxetic structures consisting of up to 30 layers was achieved by applying extrusion-based printing.

6.1. Introduction

Three-dimensional (3D) printing is an additive manufacturing process which allows rapid prototyping and the development of customized structures[86]. In this context, protein-based inks gained interest for future applications as structured biomaterials or in biomedical applications due to their expected high biocompatibility, biodegradability and stimuli-responsiveness[173]. Consequently, formulations of polymeric networks consisting of proteins as buildings blocks with the ability to absorb water – so-called protein-based hydrogels – were developed[210]. Additional functionalization by macroscopic structuring for example as auxetic structures with a negative Poisson's ratio, is a promising approach for further material enhancement enabling potential applications in the field of smart filters, sensors and medical devices [221]. Auxetics can improve mechanical properties such as shear resistance, fracture toughness and resilience compared to unstructured samples of the same material[77,222] and the use of auxetics to generate more robust hydrogel scaffolds has already been investigated[223].

In the development of functional biomaterials, dityrosine crosslinking of phenolic hydroxy groups achieved by enzymatic, fenton-like or photoinitiated reactions showed to be a promising approach for hydrogelation[183]. Dityrosines were found contributing to the highly elastic properties of structural proteins[182]. A common dityrosine crosslinking photoinitiator for 3D printing processes is the visible light-induced metal complex tris(2,2′-bipyridyl)dichlororuthenium(II) ($Ru(bpy)_3Cl_2$)[224–227]. Alternatives such as riboflavin and Rose Bengal show slower crosslinking rates[225,228,229] and the need of ultraviolet light makes them unfavorable in cell-laden bioinks or tissues due to its mutagenicity and phototoxicity[230–232].

Typical protein sources for protein-based inks in 3D printing are gelatin, collagen, fibrin, fibrinogen, keratin, and silk[84,233]. Current 3D printing processes using $Ru(bpy)_3Cl_2$ focus on methacrylated gelatin (GelMA) blended with clay minerals, synthetic materials, nanoparticles or ionically crosslinked alginate[234–237], silk hydrogels polymerized within a sacrificial template structure[238], previously modified alginate with enriched phenolic hydroxy groups[181], methacrylated bovine serum albumin[239] and decellularized extracellular matrix[225]. However, phenolic hydroxy groups are naturally present in tyrosine residues of proteins even inducing hydrogelation by dityrosine photocrosslinking of unmodified protein constructs[57,58]. Nevertheless, to the best of our knowledge, no extrudable material based on a dityrosine-crosslinked, unmodified protein had yet been reported. The reasoning behind this lack might me due to challenging requirements regarding hydrogel formulations when used for 3D printing, as printing quality and resolution is largely dependent on the rheological properties of the ink and the used hydrogelation mechanism[86,240,241]. This often induces the need of thickeners, functional additives used to increase the yield stress and therefore structural integrity and printability of ink formulations aimed for extrusion printing[86]. Despite the desired modification of rheological ink properties, the addition of a thickening agent might influence the mechanical properties of the hydrogel[242] and may introduce challenges during in the ink manufacturing, as foams may be stabilized[243].

In this study, we developed an extrudable bio-based ink based on dityrosine-crosslinking of the unmodified, naturally occurring protein casein. To enhance the fabrication window of the low viscosity protein precursor solution, blends with various thickening agents were prepared and evaluated. In total, we assessed eight commonly used thickening agents in terms of their suitability for the employment in extrusion-based printing in combination with ruthenium-

mediated dityrosine crosslinking of biomacromolecules. Due to the ease of manufacturability, extrudability and photopolymerizability of the formulation, sodium alginate (SA) was selected as thickening agent for the following 3D printing process. The influence of the addition of SA to the ink formulation was evaluated with regard to the rheological properties of the inks and the mechanical properties of the polymerized hydrogel. Finally, auxetic structures with a total of 30 layers were 3D-printed using a casein-SA ink formulation and future applications of this formulation were discussed.

6.2. Materials and Methods

6.2.1. Evaluation and selection of bio-based ink formulations for extrusion-based 3D printing

Buffer and stock solutions. 20 mM sodium phosphate buffer containing 4 M urea (both Merck KGaA, Darmstadt, DE) was prepared with ultrapure water (PURELAB Ultra, ELGA LabWater, Lane End, UK). At a buffer temperature of 22 °C, the pH was adjusted using a 4 M sodium hydroxide solution (Merck KGaA) and the buffer was filtered through an 0.45 µm membrane (Pall Corporation, New York, US-NY). For the preparation of the ink formulations, stock solutions of the photoinitiator and oxidant were prepared. The photoinitiator tris(2,2′-bipyridyl)dichlororuthenium(II) hexahydrate ($Ru(bpy)_3Cl_2 \cdot 6\ H_2O$, Merck KGaA) was diluted in the buffer with a concentration of 5 mM and stored at 4 °C. A 2 M stock solution of the oxidant ammonium persulfate (APS, chemical formula: $(NH_4)_2S_2O_8$, Merck KGaA) was prepared in the buffer, stored as aliquots at -20 °C and thawed directly prior to usage.

Manufacturability. Eight thickening agents were tested for their ability to increase the viscosity of the solution with homogeneous dissolution of all components. Therefore, these thickening agents were mixed into the basic ink formulation consisting of 10 wt% casein dissolved in the buffer containing 4 M urea and 0.25 mM photoinitiator. The compositions were prepared on the assumption of a volume increase by 1 ml per gram protein or thickening agent. Different mass fractions of thickening agents were introduced to the formulation using different mixing protocols (see Table 6.1). The tested thickening agents were:

- xanthan gum (Deuteron XG, Deuteron GmbH, Achim, DE) – a natural high molecular weight polysaccharide with a broad range of applications from the food industry to oil drilling[244].
- Deuteron VT 819 (DVT, Deuteron GmbH, Achim, DE) - a modified xanthan gum with a glyoxal-modified surface[245].
- Laponite RD (LRD, BYK-Chemie GmbH, Wesel, DE) - a synthetic hectorite clay consisting of plate-like particles with negatively charged faces and less negatively or positively charged edges in aqueous solutions. Electrostatic attractions between oppositely charged faces and edges in combination with van der Waals forces between the particles are responsible for formation of a three-dimensional network increasing solution viscosity.[246]
- FLOCARE™ PSD 100 (SNF SAS, Andrézieux, FR) - a thickener on basis of sodium polyacrylate which is known to be soluble in presence of up to 6 M urea[247].
- Rheovis® PU 1191 (BASF SE, Ludwigshafen, DE) - an associative thickener based on hydrophobically modified ethoxylated urethane dispensed in water[248].

- guar gum (Merck KGaA)- a plant-derived gel-forming galactomannan which forms hydrogen bonds with water molecules and thus is commonly used as a thickening agent in food, pharmaceuticals and other industrial applications[249].
- methyl cellulose (MC, Merck KGaA) - a cellulose derivative which is commonly blended with other polymers in 3D printing to enhance their printability[250]. It is obtained by partial substitution of hydrophilic hydroxyl groups with hydrophobic methoxy groups which makes methylcellulose undergo a temperature-induced sol-gel transition due to increasing hydrophobic interactions[251].
- alginic acid sodium salt (SA, Merck KGaA) - a linear and highly charged polysaccharide with a gelation mechanism based on ionic crosslinking in the presence of calcium ions or in acid solutions[252].

For all tested thickening agents, different mixing protocols were assessed with the workflow schematically shown in Figure 6.1. In protocol A, all components were mixed simultanesously into the buffer and photoinitiator solution using a dual asymmetric centrifuge (DAC, SpeedMixer® DAC 150.1 FVZ-K, Hauschild GmbH & Co. KG, Hamm, DE) at 2500 rpm until complete dissolution (Figure 6.1 A). In the second approach tested (protocol B – Figure 6.1 B), the thickening agent was dissolved in 60 % of the total buffer volume using the DAC at 2500 rpm. After its complete dissolution, the remaining buffer solution, casein powder and photoinitiator stock solution were added and mixed again in the DAC (2500 rpm, 5 min). In mixing protocol C (Figure 6.1 C), casein was dissolved in the entire buffer volume and photoinitiator stock solution by mixing in the DAC (2500 rpm, until dissolution), the thickening

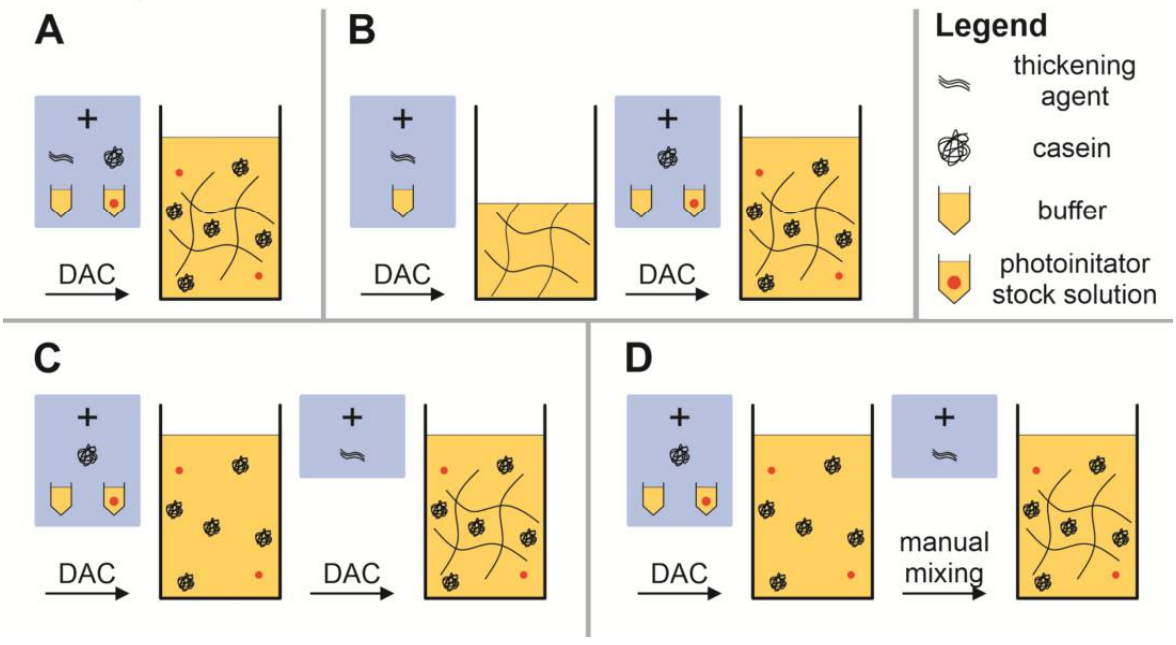

Figure 6.1 Mixing protocols to obtain formulations of buffer, photoinitiator, 10 wt% casein and the used thickening agent. (A) All components were dissolved simultaneously. (B) The thickening agent was dissolved in 60 % of the total buffer volume before addition of all other components. (C+D) Casein was dissolved in the whole buffer volume and the thickening agent was added either using the DAC (C) or manually (D). DAC = Dual asymmetric centrifuge

Table 6.1 Thickening agents and their concentration ranges tested with different mixing protocols for their suitability as thickening agent for an ink formulation with buffer, 10 wt% casein and photoinitiator. For ink formulations with a high mixing quality, subsequent hydrogel polymerization was tested by addition of APS with the mixing protocol and concentration stated. Elsewise, observations by visual inspection indicating a poor mixing quality were stated and these thickening agents not further assessed for hydrogel polymerization

Thickening agent	**Concentration range tested / wt%**	**Applied mixing protocol for hydrogel polymerization / -**	**Concentration for hydrogel polymerization / wt%**
Alginic acid sodium salt	2 - 4	B	3.5
Guar gum	0.5 - 2	D	2
Laponite RD	1 - 2.5	A	2
Methylcellulose	5 – 7.5	C	5
Modified xanthan gum	0.25 – 1.5	D	0.4 & 0.5
FLOCARE™ PSD 100	0.25 - 1	- (clumping)	
Rheovis® PU 1191	5 – 20	- (phase separation)	
Xanthan gum	0.5 – 0.75	- (stable foam)	

agent was then added in a second step and mixed again in the DAC (2500 rpm, 5min). The last approach tested (protocol D – Figure 6.1 D) was similar to mixing protocol C with the difference of the thickening agent being dissolved by manual stirring. All formulations were stored for several days to evaluate their storage stability by visual inspection.

Polymerization studies by tube inversion. To evaluate the ability to form stable hydrogels after photopolymerization, formulations containing either 2 wt% LRD, 5 wt% MC, 2 wt% guar gum, 0.5 wt% DVT or 3.5 wt% SA – all prepared with a corresponding mixing protocol stated in Table 6.1 – were assessed. APS stock solution – which is added as the last component to initiate the photopolymerization reaction - was added to the formulation with a final concentration in the formulation of 75 mM and mixed in the DAC (2500 rpm, 5 min) in a transparent container to generate a precursor solution. Hydrogelation was assessed by tube inversion after 24 h storage under ambient conditions.

Hydrogel disc polymerization. The formulations containing either 5 wt% MC, 2 wt% guar gum, 0.4 wt% DVT or 3.5 wt% SA were prepared as described with the differences of a light-protected container being used. After the addition of APS, the precursor solution was transferred into a cylindrical polytetrafluoroethylene (PTFE) mold (diameter 10mm, height 3mm) which was covered on top and bottom with transparent acrylic glass and a hydrophobic layer to avoid contact between sample and the glass surface. The precursor solution was irradiated for 8 min from the top using a blue light emitting diode (LED) at 457 nm (LZ4-00B208, LED Engin Inc, San Jose, US-CA) with a radiant flux of 3.9 W in a distance of 7.5 cm to initiate the photopolymerization of hydrogel discs. The discs were released from the mold

and evaluated visually towards their shape fidelity and possible irregularities (e.g. by entrapped gas).

Manually extrudability. To assess shape fidelity of extruded strands, a precursor solution prepared without APS was transferred into a syringe. The ink formulation was manually extruded through a nozzle (inner diameter 0.4 mm) on a glass plate and its extrudability assessed by visual inspection by the means of their shape fidelity and ink irregularities.

6.2.2. Characterization of the selected bio-based ink formulation

Shear viscosity measurements. Shear rate-dependent viscosity of unpolymerized formulations with 2, 3, 3.5 and 4 wt% SA was assessed by rotational measurements at 22 °C on a Physica MCR 301 plate rheometer (Anton Paar GmbH, Graz, AT) equipped with a cone-plate geometry (CP60-0.5, diameter 60 mm, angle 0.5°, Anton Paar GmbH). After a resting time of 5 min, each solution was recorded under rotation at a shear rate between 0.01 and 10000 s^{-1} (n = 3).

Oscillatory frequency sweeps. Polymerized hydrogel discs without and with 3.5 wt% SA were stored for seven days in 100-fold buffer excess and were assessed by oscillatory measurements at 22 °C on a Physica MCR 301 plate rheometer equipped with a plate-plate geometry (PP10, diameter 10 mm). The linear viscoelastic region (LVR) was determined using amplitude sweeps for angular frequencies $\omega = 1$ and 25 $rad \cdot s^{-1}$ and a shear stress τ between 5 and 10.000 Pa (n = 2). Frequency sweeps were performed within the LVR using $\tau = 10$ Pa and $\omega = 1$ to 25 $rad \cdot s^{-1}$ (n = 3).

Uniaxial compression tests. Polymerized hydrogel discs were prepared without and with 3.5 wt% SA and were stored for seven days in 100-fold buffer excess. Uniaxial compression tests of these hydrogel discs were performed on a universal testing machine (zwickiLine Z0.5TN, ZwickRoell GmbH & Co. KG, Ulm, DE) equipped with a 100 N load cell (Xforce HP 100 N) and stainless-steel compression platen (diameter 30 mm). After a pre-force of 0.2 N was reached, a uniform velocity of 2 mm/min was applied until sample fracture. The compressive strength σ_{max} refers to the engineered stress σ at sample fracture, with the applied force F and the unstressed cross-sectional are A_0 (Equation (6.1)).

$$\sigma = \frac{F}{A_0}, \tag{6.1}$$

Accordingly, the fracture strain ε_{max} refers to the engineered strain ε at sample fracture, with L being the sample length at the applied force and L_0 being the sample length at pre-force (Equation (6.2)).

$$\varepsilon = \frac{L - L_0}{L_0} \tag{6.2}$$

6.2.3. Extrusion printing of the selected bio-based ink formulation

Extrusion printing. 3D Printing of the selected ink formulation with 3.5 wt% SA was performed using a BioScaffolder 3.1 (GeSiM mbH, Radeberg, DE) equipped with a pneumatic cartridge dispenser (GeSiM mbH) and a blue LED pen (SST-10-B-B90, Luminus, Brussels, BE). For all experiments, light-blocking cartridges (10 ml, Nordson Corporation, Westlake, US-OH) and conic ultraviolet light-blocking nozzles with an inner diameter of 0.41 mm

(VIEWEG GmbH, Kranzberg, DE) were used. Printing parameters were kept uniform for all printing experiments and were set to a velocity of 1.6 mm/s, strand height of 0.1 mm, start pause of 0.3 s, end pause of 0.1 s and vertical tear off with an applied pressure of 19 kPa. The pressure was manually adapted during the print of multiple layers when necessary.

Printability assessment by image analysis of 3D printed lines. The line width of one layer of extruded single strands with a length of 30 mm on a glass slide was analyzed by image analysis to assess whether additional illumination is needed to induce photopolymerization. The strands were either not additionally illuminated or photopolymerization was additionally induced using the blue LED pen for 10 s by a centered illumination above each strand from a distance of 6.5 cm.

Images of printed lines consisting of single strands were taken 5 min after extrusion using a monochrome area scan camera (Genie Nano-M2420, Teledyne DALSA, Waterloo, CA). The glass slides were placed on a black background and illuminated by a white LED ring light (HPR2-150 SW, CCS Inc., Woburn, US-MA). Image analysis was performed in MATLAB 2020b (The MathWorks Ink., Natick, US-MA) based on a method introduced by Strauß *et al.*[253]. Briefly, the original image was imported, binarized, small objects such as dust particles removed and the line vertically aligned.

Variations of the line width caused by unsteady ink flow at the beginning and end of the extrusion process were excluded from the analysis by cutting of the initial and terminal 10 % of the total line length. In order to obtain the line width in mm, the number of columns containing white pixels were multiplied with the camera-dependent conversion factor from pixel (n = 10). To compare the median values of the line width of the printed lines which were illuminated using the LED pen and the non-illuminated printed lines, a statistical analysis was performed using the two-sided Wilcoxon ranksum test with a p-value below 0.05 being classified as statistically significant.

Auxetic structures. As a first structure, a non-curved, axially symmetric re-entrant honeycomb structure with the inner angle $\Theta = 70$ ° comprising of four unit cells was designed. The second auxetic structure consisted of nine point-symmetrically arranged re-entrant honeycomb unit cells with curved edges. For printability assessment, three layers of these structures were extruded without additional illumination and 30 layers were printed by an induced photopolymerization using the blue LED pen for 10 s and a centered illumination above the object from a distance of 6.5 cm.

6.3. Results and Discussion

6.3.1. Evaluation and selection of bio-based ink formulations for extrusion-based 3D printing

Basic ink formulation. As the aim of this manuscript was to develop a protein-based ink suitable for extrusion-based 3D-printing, the extrusion behavior of the precursor solution containing 10 wt% casein without added thickening agents was tested in a first step by manually extruding the material using a syringe. To achieve a protein concentrations of 10 wt% in the precursor solution, casein solubility was increased by addition of 4 M urea which disrupts casein micelle integrity[41]. Upon manual extrusion, the basic formulation showed the behavior of a liquid and formed droplets that did not remain in shape after deposition on the glass plate (see Figure 6.2, bottom left). The observed behavior demonstrated the unsuitability of the basic

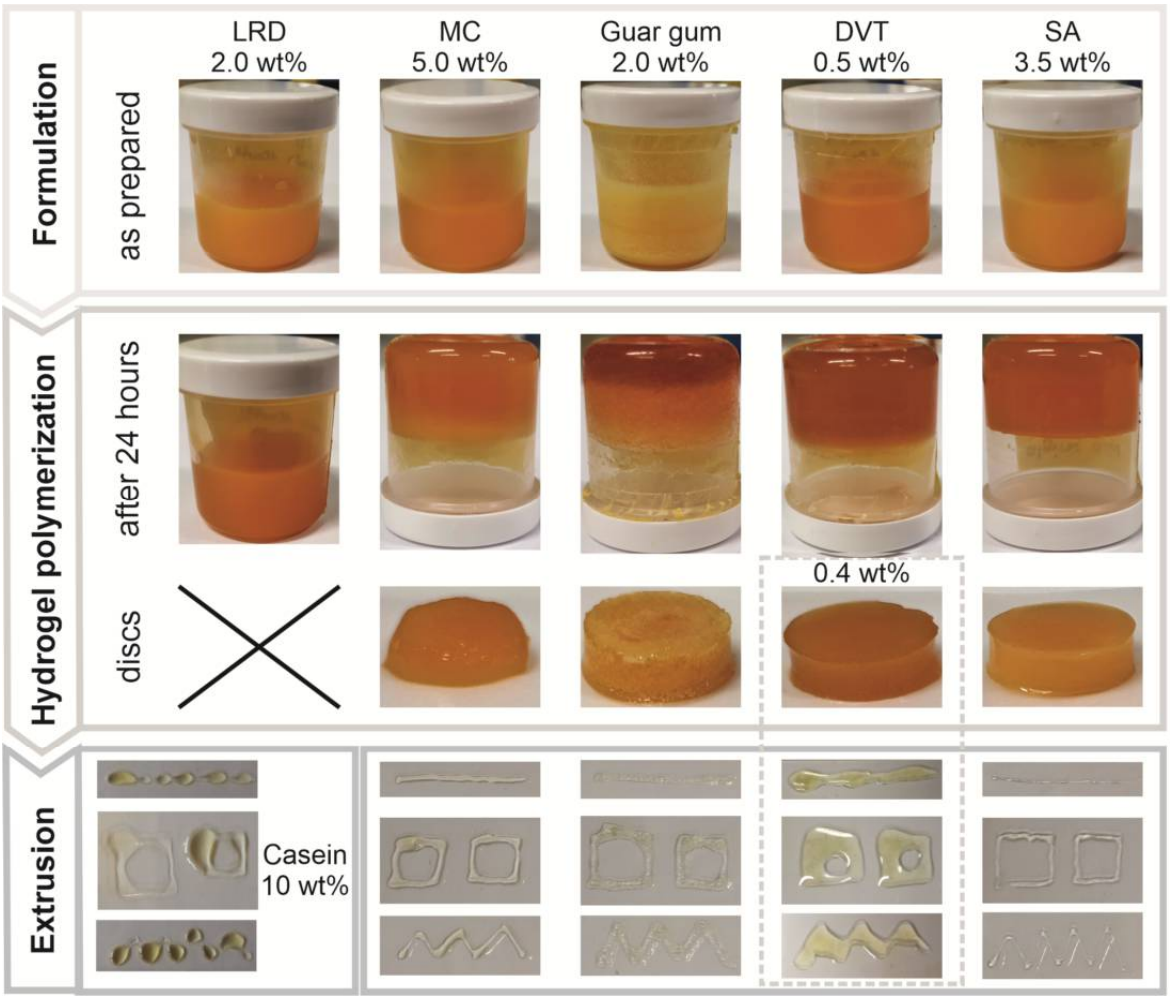

Figure 6.2 Assessment of the manufacturability, polymerizability and extrudability of ink formulations containing different thickener agents for viscosity increase. Top: Ink formulations directly after mixing in the DAC after addition of the electron acceptor starting the photoreaction. Middle: Gelation was assessed by turning the container upside-down after 24 h reaction time and by polymerizing hydrogel discs in a mold. Bottom: Printability was assessed by manual extrusion of a casein solution without thickener (left) and the corresponding formulations through a nozzle with 0.4 mm inner diameter.

formulation for extrusion-based printing and the need of further enhancing the formulation to achieve favorable rheological properties.

Manufacturability. Eight substances were analyzed towards their suitability as thickening agent to enhance the extrudability and shape fidelity of the protein-based hydrogel precursor solution consisting of protein, buffer salts, photoinitiator and urea by an increased ink viscosity. These thickening agents were chosen according to different chemical mechanisms which are responsible for the viscosity increase. The high concentrations of a hydrophobic protein and the chaotropic agent urea, which is known for a reduction of inter- and intramolecular hydrophobic interactions may interfere with the thickening agent. It should be mentioned that the formulation therefore is not suitable for cell-laden inks as high urea concentrations are known to damage cells and the formulation is not designed in a physiological buffer system[218,219]. For all chemical substances, different mixing protocols were assessed to dissolve or suspend the thickening

agent and protein in the buffer solution, as these effect the ability to dissolve all components or influence unwanted effects such as mixture foaming. Exemplary, the obtained formulations of 3.5 wt% SA and 10 wt% casein together with buffer and photoinitiator solution immediately after mixing and after a storage time of 24 h are shown in Figure 6.3. Here, for protocols A and C, either the protein or the thickener was not completely dissolved after the mixing process. In all cases, the obtained mixture was foamy. In contrast to protocols B and C, the formulation prepared according to mixing protocol A still had visible air bubbles entrapped after a 24 h storage time. Since not all components were completely dissolved after mixing in the DAC, mixing protocol B was used for further ink development. Depending on the applied mixing protocol, homogeneous mixtures without APS included were obtained upon addition of the other five thickening agents LRD, MC, guar gum, DVT and SA which were therefore used for further evaluations of the photopolymerizability of the ink formulation (see Table 6.1).

For three thickening agents, the addition to the protein-buffer formulation resulted in the formation of inhomogeneous mixtures or stable foams: xanthan gum, Flocare™ PSD 100 and Rheovis® PU 1191. Firstly, the addition of the xanthan gum lead to irreversible foaming of casein for all mixing protocols tested. As reported, the combination of xanthan gum and proteins is used to generate protein-based foams[254] and casein was found to stabilize foams of skimmed milk[255], but to our knowledge, no experiments have been performed in the presence of 4 M urea or with the centrifugal mixing method used. However, foaming was not inhibited in any of the mixing protocols tested, and the protein foam was found to be stable over a storage period of several days without visible changes, precluding the use of xanthan gum in an extrudable ink formulation. Secondly, after addition of Flocare™ PSD 100, a gel clump was formed in the highly viscous solution containing casein. Recently, sodium polyacrylate was introduced to form aqueous two phase systems together with polyethylene glycol, where hydrophobic proteins usually tend to be in the polyethylene glycol-rich phase[256,257]. Thus, the hydrophobic protein casein even in the presence of urea may explain the agglomeration into a gel clump. Thirdly, casein formulations prepared with Rheovis® PU 1191 showed phase separation after

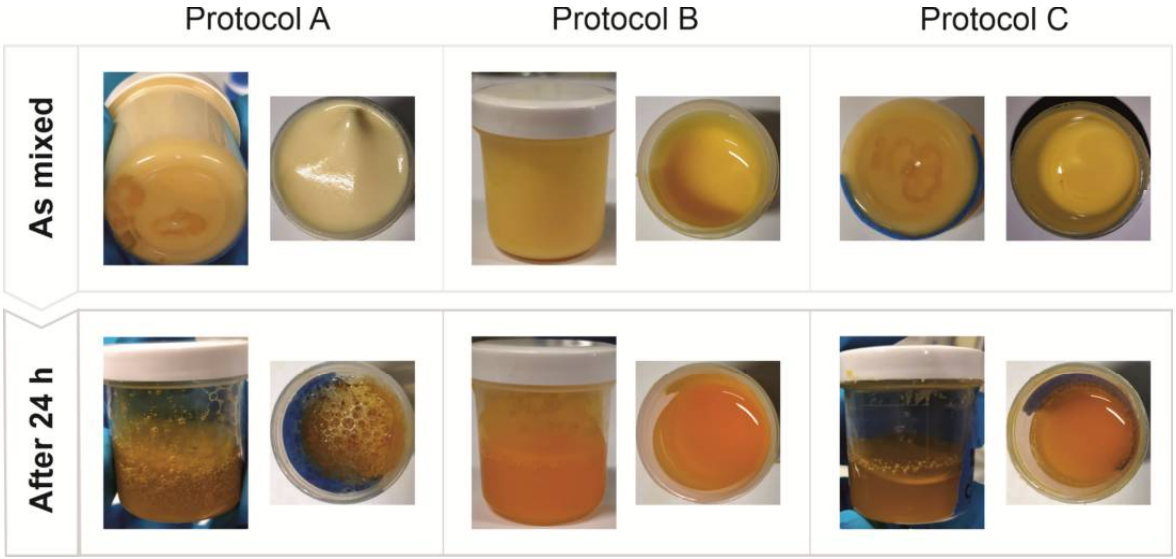

Figure 6.3 Comparison of the obtained mixed ink formulation in dependency of the applied mixing protocol immediately after the mixing process and after 24 h for formulations of 3.5 wt% SA, 10 wt% casein, buffer and photoinitiator.

three days of storage. In ternary systems, such as in this manuscript, consisting of the thickener, aqueous buffer solution with urea and protein, these polyurethane systems are known for possible phase separations[258,259] which also occurred in the tested formulations. Therefore, the three mentioned thickening agents were not further assessed.

Hydrogel polymerization. To ensure, that dityrosine-crosslinking of casein is not inhibited due to the underlying viscosity increasing mechanism, hydrogelation was assessed in a subsequent study**.** Based on the results of the manufacturability, five ink formulations with a corresponding mixing protocol were assessed regarding their ability to form photocrosslinked hydrogels (Table 6.1). The oxidant APS was added to the formulations containing the thickening agent, photoinitiator and protein to initiate the photopolymerization reaction Figure 6.2, top). The formulations containing 2.0 wt% LRD, 5 wt% MC and 3.5 wt% SA were homogenously mixed with APS with only some air bubbles being present on the formulation surface. In contrast, the formulations containing 0.5 wt% DVT and 2.0 wt% guar gum turned into foamy solutions after mixing with APS. After a storage period of 24 h under ambient lab room conditions, gelation was obtained for all formulation except for the one prepared with LRD, as determined by tube inversion method (Figure 6.2, mid).

The ink formulation containing 2 wt% LRD did not polymerize after 24 h under ambient room conditions, even though successful ruthenium-mediated photopolymerization of GelMA blended with up to 3 wt% Laponite was previously shown [234]. Besides possible sterical hinderance by the formed network of LRD particles, intermolecular interactions (e.g. between the charged surfaces of the laponite plate and surface charges of caseins reducing casein mobility) may be responsible for the inhibition of hydrogelation.

To obtain a better comparability of the polymerization behavior, new batches of each polymerizable formulation were deliberately prepared in light-protected containers and a defined volume of each polymerizable formulation was polymerized into defined cylindrical hydrogel discs (Figure 6.2, mid). Hydrogel discs polymerized with MC could not be removed maintaining a cylindrical structure and therefore appeared to be mechanically instable. This might be attributed to a sterical hinderance and possible interactions between MC and the hydrophobic protein casein preventing effective crosslinking of the casein tyrosines.

The formulation prepared with 2 wt% guar gum was polymerized under ambient conditions in a transparent container. Two polymerization zones were identified, one without entrapped air bubbles located on the container bottom and one foam-like polymerization zone on top. As xanthan gum, guar gum is used to stabilize protein foams[260], possibly enhancing the foaming during the mixing process. The foam layer was reduced during storage, albeit the whole formulation again thoroughly foamed after mixing with APS. With the polymerization being faster than the defoaming process, the described polymerization zones could be observed. When polymerized into hydrogels discs, these showed to be stable in their shape, but entrapped air bubbles resulted in a partially porous hydrogel structure.

In contrast, DVT seems to reduce foaming compared to unmodified xanthan gum and the foam is reduced during overnight storage and therefore seems less stable. In order to further reduce foaming during the ink preparation, the amount of DVT was reduced from 0.5 to 0.4 wt% for the polymerization of hydrogel discs, and homogenous hydrogel discs with high shape fidelity and without visible entrapped air bubbles were obtained.

The formulation containing 3.5 wt% SA could be homogenously mixed with APS with only few air bubbles being visible on the formulation surface. Hydrogel discs with a high shape

fidelity could be prepared for this formulation. SA is widely applied in ink formulations for 3D printing[261] and was previously shown not to interfere with covalent photocrosslinking of GelMA and a synthetic polymer when formulated as a material blend[262]. This finding was transferable to the ruthenium-mediated dityrosine crosslinking used in this manuscript, even in the presence of high urea concentrations.
Overall, four out of the five formulations tested enabled casein hydrogelation, with 0.4 wt% DVT and 3.5 wt% SA being the most promising candidates for a biomacromolecule ink, as these also allowed the formation of a defined cylindrical structure with high shape fidelity and without visible entrapped air bubbles.
Manual extrudability. As initial assessment of the suitability of the ink for extrusion-based printing, the ability to form strands with high shape fidelity upon manual extrusion and was evaluated by visual inspection Figure 6.2, bottom). For the addition of 3.5 wt% SA and 5 wt% MC, strands with high shape fidelity were manually extruded. In contrast, entrapped air bubbles were observed in the extruded strands of the formulation containing guar gum and the extruded strands were spreading for formulation prepared with DVT. With regard to the suitability to increase the formulation viscosity while still enabling photopolymerization, the ink formulation containing 3.5 wt% SA was selected for further characterization and extrusion-based 3D printing.

6.3.2. Characterization and extrusion printing of the selected bio-based ink formulation

Shear viscosity measurements. Unpolymerized casein-SA-ink formulations prior crosslinking were rheologically characterized to assess their suitability for the use in extrusion-based printing. The viscosity of protein-containing ink formulations prepared with mass fractions of SA between 2 and 4 wt% in dependency of the applied shear rate is shown in Figure 6.4 A. All formulations show a Newtonian plateau, but with increasing shear rate, the viscosity of all tested formulations decreased, showing non-Newtonian, shear-thinning behavior, which is often favored in extrusion-based printing[263,264]. The shear-thinning properties of SA are a consequence of the combination of long polymer chains - which start to align in a more parallel way at higher shear rates - and the stiffness of the hydrated molecules[265]. As ions are shielding the charge of the SA molecule resulting in a less rigid molecule[265], the presence of charged buffer salts and proteins further affects this behavior compared to pure SA solutions. As the casein was used as-delivered in Hammarsten grade without further purification, calcium ions are expected impurities[266] which may induce a certain degree of gelation of the SA solution[267]. Overall, by addition of different mass fractions of SA to the 10 wt% casein formulation, the viscosity at a shear rate of 0.1 s^{-1}, representing an estimate of the viscosity at rest, could be tuned within a range between 4.06 ± 0.09 Pas (2 wt% SA) and 25.5 ± 0.17 Pas (4 wt% SA). Although 4 wt% SA had the highest viscosity, the manufacturability was more complicated because more air bubbles could not escape during storage due to the increased viscosity, so 3.5 wt% SA was chosen for 3D printing experiments.
Mechanical properties of photopolymerized hydrogels. To determine whether the addition of the thickening agent SA affects the mechanical properties of the resulting hydrogels, ink formulations with and without 3.5 wt% SA were produced and polymerized into discs which were analyzed by oscillatory rheometry and with uniaxial compression tests (Table 6.2). The addition of SA to the formulation may have effects on the mechanical properties of the

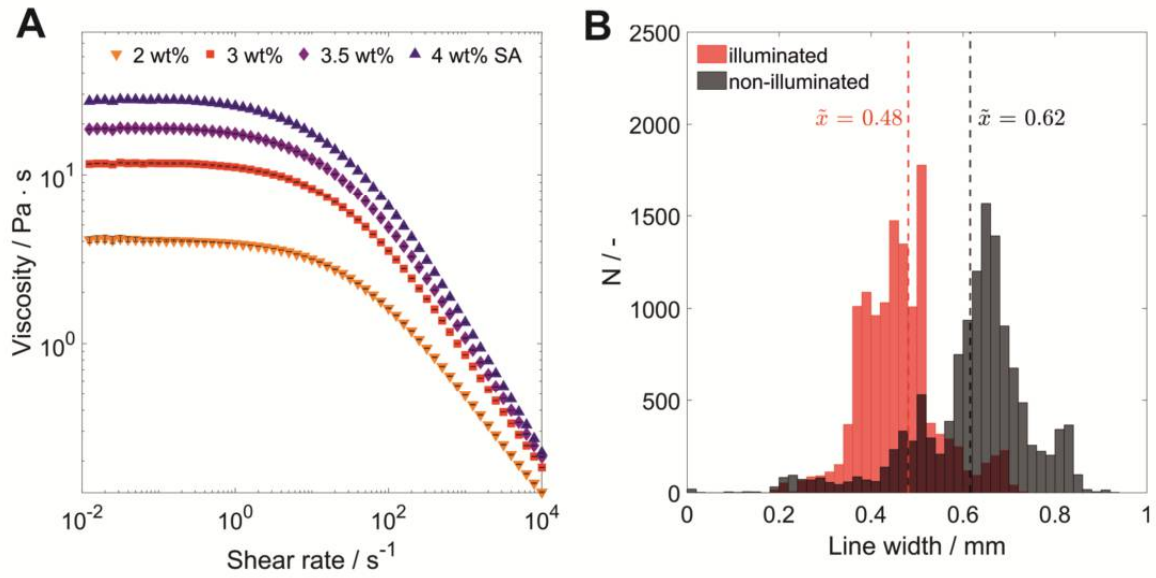

Figure 6.4 Characterization of the printability of the casein-SA ink. (A) Viscosity curve of ink formulations in 20 mM sodium phosphate buffer containing 4 M urea with 10 wt% casein and 25 mM photoinitiator containing different concentrations of SA. (n = 3) (B) Histogram of line width distribution for lines printed without additional illumination (black) and lines printed with illumination for 10 s after extrusion using the LED pen (red).

dityrosine-crosslinked hydrogels due to several reasons. Firstly, the viscosity of the ink formulation was increased resulting in lower mobility of the protein. Secondly, sterical hinderance may prevent the formation of covalent crosslinks. Thirdly, possible interactions between SA and the protein have to be considered.

Both polymerized formulations showed gel-like behavior as indicated by the storage modulus dominating the loss modulus in the whole frequency range applied resulting in a loss factor tan δ < 1. The storage modulus G' is used as a measure for the hydrogel network density and was determined by frequency sweeps at a constant shear stress of 10 Pa, which was in the LVR for both hydrogel formulations. Hydrogels prepared without SA showed a higher crosslinking density (G' = 29.9 ± 0.7 kPa) and compressive strength (σ_{max} = 0.082 ± 0.005 MPa) compared to hydrogels prepared with SA (G' = 25.1 ± 2.1 kPa, σ_{max} = 0.045 ± 0.005 MPa). Also, the addition of SA decreased the hydrogel elasticity, as indicated by an increase in the loss factor (tan δ = G''/G') from 0.010 ± 0.003 (without SA) to 0.020 ± 0.013 (3.5 wt% SA) and decreasing maximum strain from 39.9 ± 0.7 % (without SA) to 35.2 ± 3.2 % (3.5 wt% SA).

Table 6.2 Oscillatory frequency sweep measurements comparing the storage modulus and loss factor as well as maximum strain and compressive strength determined in uniaxial compression tests of hydrogels prepared with and without sodium alginate in their formulation (n=3).

Sodium alginate / wt %	**G' / kPa**	**tan δ / -**	**ε_{max} / %**	**σ_{max} / MPa**
0	29.9 ± 0.7	0.010 ± 0.003	39.9 ± 0.7	0.082 ± 0.005
3.5	25.1 ± 2.1	0.020 ± 0.013	35.2 ± 3.2	0.045 ± 0.005

This observation may be related to less dityrosine bonds present in the hydrogels which are found to be responsible for high elastic properties of structural proteins[182]. This hypothesis would have to be verified in subsequent studies by dityrosine quantification, for example based on the method introduced by Elvin *et al.*[60]. The results presented in this study indicate effects on the mechanical properties of the hydrogels in the presence of SA, such as a decreased elasticity and crosslinking and therefore has to be considered when designing mechanical properties of a printed hydrogel.

Printability assessment of the casein-SA ink formulation. Despite the ability to form extruded strands which remain in shape, photocrosslinking of casein in these strands has to be ensured. Therefore - prior to printing of complex structures - the necessity of additional illumination using an LED after strand extrusion was evaluated, as the employed photoinitiating system is initiated by visible light present under ambient room conditions. This was evaluated by image analysis of the line width of single strands which were printed on a glass slide without additional illumination or with illumination for 10 s using the LED pen. The median width of lines extruded without illumination ($\tilde{x}_{\text{non-illuminated}}$ = 0.62 mm) was significantly higher than for illuminated lines ($\tilde{x}_{\text{illuminated}}$ = 0.48 mm, Z = -99.59, $p < 0.001$, Figure 6.4 B). Further, the 3D printing of multiple layers of a two re-entrant honeycomb scaffold structure (Figure 6.5 A) was assessed by extruding three layers without LED illumination (Figure 6.5 B). The strand width increased with the number of layers as determined by visual inspection, indicating that the extruded highly viscous solutions did not maintain their shape but exhibited a certain degree of spreading.

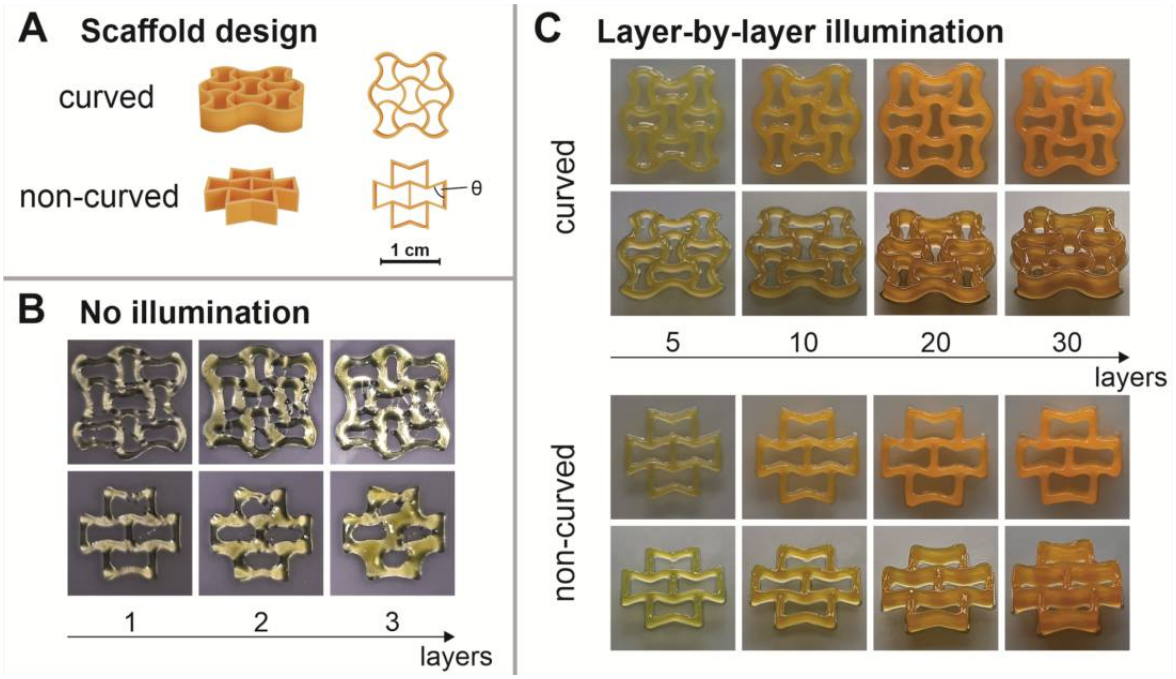

Figure 6.5 Multi-layer printing depending on the light exposure. (A) Scaffold design of a non-curved, axially symmetric and a curved, point symmetric macroscopically structured auxetics. (B) Ambient light-induced photopolymerization without further illumination for up to 3 layers of those auxetic structures (C) Structures consisting of up to 30 layers and hydrogelated by layer-wise photopolymerization.

This indicates, that the polymerization induced by ambient light is not fast enough to achieve sufficient stability of the hydrogel without an additional illumination using blue light. Additionally, even though the extruded strands exhibit a high shape fidelity compared to the other thickeners tested before, the addition of 3.5 wt% SA does not sufficiently stabilize the formulation to enable multiple layer printing.

3D printing of multiple layer using the casein-SA ink. In order to show the capability of the developed casein-SA ink as an extrudable bio-based material, this manuscript focuses on printing a macroscopically structured auxetic material based on re-entrant honeycomb structures. As printing of structures with sharp angles is known to result in overlapping extrusion paths and therefore increasing print irregularities[268], two re-entrant honeycomb scaffold structures were printed accompanied by a layer-by-layer photopolymerization approach to assess the printability of the selected ink formulation. In both cases, a macroscopic auxetic could be printed successfully by using the casein-SA-ink up to a height of 3 mm which corresponds to a total of 30 layers (Figure 6.5 C). Thus, we demonstrated that the developed material based on the commercially available casein can be macrostructured by extrusion printing into a promising metamaterial.

6.4. Conclusion

In this manuscript, we present a photocrosslinkable, extrudable ink formulation based on the naturally occurring, unmodified protein casein. Due to its liquid behavior, the protein solution could not be extruded in strands without prior viscosity enhancement by the addition of a thickening agent. To assess the influence and possible interferences of the thickening agent on the manufacturability, polymerizability and printability, extensive experiments were conducted to screen for interferences between the chemical components of the ink formulation – such as buffer salts and proteins, the photoinitiating system, thickening agents and others. Except SA, the other thickening agents assessed showed to lead to phase separation, foaming, incomplete or inhomogeneous dissolution of all components, inhibited hydrogelation, or extruded strands which were not stable in their shape. In contrast, SA enhanced the extrudability of the protein solution while still allowing a homogenous ink formulation which can be hydrogelated by ruthenium-mediated dityrosine crosslinking of casein. Further, the addition of SA was shown to influence the resulting mechanical properties of photocrosslinked hydrogels which was attributed to a decreased network density and lower elasticity, which has to be considered for the development of hydrogels with desired mechanical properties. Finally, two re-entrant honeycomb structure were successfully printed using the formulation containing 3.5 wt% SA with up to 30 layers in height with the presented printer setup and photopolymerization of each deposited layer. Overall, the established photocrosslinkable and extrudable casein-SA-based ink formulation demonstrates the applicability of new protein-based inks based on cheap and commercially available proteins which are currently not considered in bio-based printing.

7 Magnetic resonance imaging: Time-dependent wetting and swelling behavior of an auxetic hydrogel based on natural polymers

Sandra Haas, Barbara Schmieg, Paul Wendling, Gisela Guthausen, Jürgen Hubbuch

Polymers (2022), Volume 14, Article 5023

Abstract

A time-dependent understanding of swelling characteristics and external stimuli behavior is crucial for the development and understanding of functional hydrogels. Magnetic resonance imaging (MRI) offers the opportunity to study three-dimensional (3D) soft materials nondestructively. This technique is already widely used as image-based medical diagnostic tool and is applied here to evaluate complex structures of a hydrogel – a double network of chemically crosslinked casein enhanced with alginate – fabricated by 3D printing. When hydrogel disks immersed in four different liquid systems were analyzed, the material exhibited distinct system-dependent behavior characterized by rheological and mechanical measurements. Further material functionalization was achieved by macroscopic structuring of the hydrogel as an auxetic material based on a re-entrant honeycomb structure. MRI offers the advantage of monitoring overall changes in the area of the analyzed specimen and internal structural changes simultaneously. To assess the behavior of this complex structure, a series of short MRI measurements, each lasting 1.7 min, captured liquid diffusion and thus structural swelling behavior. A clear dependence of external and internal structural changes as a function of liquid properties causing these changes was observed. In conclusion, this approach might pave the way for prospective applications to monitor liquid diffusion into (e.g. vascularization) and swelling behavior of functional hydrogels.

7.1. Introduction

Three-dimensional (3D) polymeric structures with their swelling agent being water are known as hydrogels and are commonly used for biomedical applications such as targeted drug delivery, tissue engineering, smart biosensors, as well as in 3D and four-dimensional (4D) printing[68,169,269]. Such applications introduce sensitive components such as cells, or the need of complex material shapes. Macroscopic structuring, e.g. by an auxetic structure, can add a further dimension of functionalization to a material. Auxetic structures exhibit a negative Poisson's ratio, and thus, for example, react with construction in certain spatial directions upon the application of mechanical stress. In comparison to unstructured objects of the same material, the introduction of an auxetic structure can improve mechanical properties such as shear resistance, fracture toughness, and resilience.[75,77,221,222]

In general, hydrogels can be produced by physical or chemical crosslinking of a monomer source[31]. As one possibility, unmodified proteins can be used to obtain dityrosine- crosslinked hydrogels by crosslinking phenolic hydroxy groups via enzymatic, fenton-like, or photoinitiated reactions [183]. In the field of 3D printing, a common photoinitiator for dityrosine crosslinking is tris(2,2′-bipyridyl)dichlororuthenium(II) ($Ru(bpy)_3Cl_2$) which is induced by visible light in the presence of an electron acceptor such as ammonium or sodium persulfate[224–227]. Using this approach, stimuli-responsive hydrogels can be obtained[61,213]. In detail, these hydrogels change their structural and volume phase transition as a response to external stimuli[270]. To enhance the fabrication window in extrusion 3D printing, thickeners such as the linear and highly charged polysaccharide sodium alginate are widely used to increase the structural integrity of ink formulations[86,261]. Due to its high biocompatibility and ease of handling, alginate is also widely applied as an extrudable bioink hydrogel material itself[271], as in the presence of multivalent metal cations or in acid solutions, hydrogelation of sodium alginate is propagated by ionic crosslinking[252]. Thus, with additional crosslinking of sodium alginate, a so-called double-network hydrogel can be obtained.

Since water is an integral part of hydrogels, an improved understanding of swelling degree and mechanical stability should be obtained[272]. Current approaches to determine the swelling degree and water uptake mainly focus on weight or volume analysis of dried or as-prepared hydrogels in comparison to soaked hydrogel samples. Hereby, weight measurements can easily be executed, while estimating the volume of the complex geometries is not always feasible. Thus, weight-based swelling ratios are usually reported in the literature.[220,272] However, these methods do not provide insight into the time-dependent, spatially resolved hydration of the inner hydrogel structure and require the full removal of excess liquids without withdrawing liquid from the hydrogel network.

Therefore, an easy transferable, site-resolving, nondestructive 3D analytical method is desired for material development. Magnetic resonance imaging (MRI) is a 3D imaging technique which is used in medical diagnostics, material sciences and food research[273]. The image contrast thereby often relies on the nuclear magnetic resonance (NMR) relaxation properties and spin density differences in a material[97,98,274]. Recently, it was shown to be applicable to the investigation of complex 3D objects obtained by 3D printing[275] and of different common bioink materials[102]. Besides the high initial costs and complexity of operation, the main advantage of MRI is its independency from the analyzed material and from optical transparency, enabling volumetric time and spatially resolved longitudinal studies on the same object[273,276].

Initially, traditional material characterization of the hydrogel material – based on sodium alginate and dityrosine-crosslinked casein[277] – was performed by swelling studies as well as rheometric analysis and uniaxial compression of casted discs using four different liquid systems. Following this, macroscopic auxetic structuring introduced by 3D printing was used for further functionalization of the protein-based hydrogel. In order to assess the now complex structure of the hydrogel, we applied MRI assessing time-dependent external and internal stimuli behavior. As a proof of principle, the two-dimensional (2D)-crosssections of an auxetic geometry were analyzed with regard to their changes in the twodimensional plane. Monitoring included the observation of visual structural changes of the lattice network as well as the estimation of area ratios of the hydrogel crosssections by using image analysis.

7.2. Materials and Methods

7.2.1. Buffer and stock solutions

The formulation buffer for material fabrication consisted of 20 mM sodium phosphate buffer (SPB) pH 8 containing 4 M urea. All liquid systems were prepared with ultrapure water (PURELAB Ultra, ELGA LabWater, Lane End, UK). At a temperature of 22 °C, the pH was adjusted using a 4 M sodium hydroxide solution and the buffer filtered through an 0.45 µm membrane (Pall Corporation, New York, US-NY). The photoinitiator tris(2,2′-bipyridyl)dichlororuthenium(II) hexahydrate ($Ru(bpy)_3Cl_2 \cdot 6\ H_2O$) was diluted in the formulation buffer with a concentration of 5 mM and stored at 4 °C as a stock solution. A 2 M stock solution of the oxidant ammonium persulfate (APS, chemical formula: $(NH_4)_2S_2O_8$) was prepared in the formulation buffer, stored as aliquots at -20 °C, and thawed directly prior to usage.

To examine swelling or the effect of external stimuli in different systems, four different liquid systems for immersion of the dried hydrogel were prepared. These liquids were:

- System 1: ultrapure water,
- System 2: ultrapure water + 0.1 M $CaCl_2$,
- System 3: ultrapure water + 0.1 M $CaCl_2$ + 4 M urea,
- System 4: ultrapure water + 20 mM SPB + 4 M urea.

For all liquids, pH (pH Meter HI 3220-2, Hanna Instruments, Woonsocket, US-RI equipped with the pH electrode Sentix® 62, Xylem Inc., US-NY) and conductivity using a conductivity meter CDM230 (Radiometer Analytica SAS, Lyon, FR) were determined (see Appendix D.1). All chemicals reported in this manuscript were purchased from Merck KGaA (Darmstadt, DE).

7.2.2. Ink preparation

The ink formulation consisted of 10 wt% casein, 0.25 mM $Ru(bpy)_3Cl_2$, 75 mM APS, and 3.5 wt% sodium alginate (SA) and the formulation buffer described above. Therefore, SA was dissolved in 60 % of the total buffer volume in a dual asymmetric centrifuge (DAC, SpeedMixer® DAC 150.1 FVZ-K, Hauschild GmbH & Co. KG, Hamm, DE) at 2500 rpm. Subsequently, the remaining formulation buffer, casein powder and photoinitiator stock solution were added and mixed in the DAC (2500 rpm, 5 min). To enable the induction of the photopolymerization reaction, the precursor solution of the ink was finalized by addition of the APS stock solution directly prior to polymerization using the DAC (2500 rpm, 2 min).

7.2.3. **Disc polymerization**

After the addition of APS, the precursor solution of the ink was transferred into a cylindrical polytetrafluoroethylene mold (diameter 10mm, height 3mm) which was covered on top and bottom with a transparent hydrophobic layer and acrylic glass. The precursor solution was irradiated for 5 min from above and below using a blue light emitting diode (LZ4-00B208, LED Engin Inc, San Jose, US-CA) with a radiant flux of 3.9 W at a distance of 7.5 cm. The discs were released from the mold and dried for 72 h at 40 °C (T6120, Heraeus Holding GmbH, Hanau, DE).

7.2.4. **Extrusion printing**

An auxetic structure was 3D-printed using a BioScaffolder 3.1 (GeSiM mbH, Radeberg, DE) after adding the APS stock solution. The scaffold design consisted of nine point-symmetrically arranged re-entrant honeycomb unit cells with curved edges and had a total height of 3 mm (see Appendix D.2). The printer was equipped with a pneumatic cartridge dispenser (GeSiM mbH), light-blocking cartridges (10 ml, Nordson Corporation, Westlake, US-OH), and conic ultraviolet light-blocking nozzles (0.41 mm inner diameter, VIEWEG GmbH, Kranzberg, DE). A velocity of 1.6 mm/s, strand height of 0.1 mm, start pause of 0.3 s, end pause of 0.1 s, and vertical tear off with an applied pressure of 19 kPa were set as printing parameters. Photopolymerization was initiated after each layer by 60 s illumination using the blue light-emitting diode as described in Chapter 7.2.3.

7.2.5. **Magnetic resonance imaging (MRI)**

The 3D-printed auxetic structures were dried for 72 h at 40 °C and the time-dependent swelling behavior characterized by MRI using an Avance HD III SWB 200 MHz tomograph (Bruker BioSpin MRI GmbH, Ettlingen, DE) applying fast low-angle shot (FLASH) pulse sequence (experiment parameters are summarized in Appendix D.3). To speed up the measurement time for a meaningful time resolution, a compromise between resolution and measurement time was found by measuring a stack of 2D measurements (referred to as 2.5D MRI). FLASH was chosen as a fast and reliable pulse sequence which allows contrast generation mainly along T1 and T2*. The image contrast was found to be adequate for the purpose of the manuscript after optimization of the MRI-parameters for the investigated samples.

A total number of 10 slices along the z-axis without a distance between the cross sections were simultaneously imaged. Each slice summarizes the signal of a z-axial distance of 0.6 mm. In all cases, the hydrogel specimens were placed in a flat bottom glass vial (25 mm diameter) containing 3 ml of the respective liquid system. Subsequently, the glass vial was manually positioned into the magnet, and correct sample positioning was tested by an initial measurement (< 10s). The measurement sequence ($t_0 - t_{17}$) was initiated 60 - 120 s after liquid addition with the first measurement being referred to as t_0. The time series consisted of 18 measurements with a time interval of 1.7 min each.

To optimize the liquid-to-hydrogel contrast, hydrogel specimens immersed in 0.1 M $CaCl_2$ within the magnet were additionally measured by applying rapid acquisition with relaxation enhancement (RARE) pulse sequences with the same time interval (experimental parameters are summarized in Appendix D.4) in the images. Due to the slightly different chemical composition, this step was essential for being able to apply the subsequent data analysis steps

with high enough reliability. The chosen MRI parameters provide in this case a combined weighting by T1 and T2, while the T1 weighting is reduced compared to the FLASH parameters. For the numerical details we refer to the Tables in Appendices D.3 and D.4. In all cases, the ^{1}H spin signal of all 10 slices was transferred into a grayscale representation for visualization purposes.

7.2.6. **Image analysis**

MRI data of the fifth slice in z-direction were processed in MATLAB® R2021b (The MathWorks, Natick, US-MA). An overview of the image processing is shown in Figure 7.1. All pixel intensities were normalized to the maximum intensity in the slice. The image resolution was aligned to the highest resolution measured in the data set (function "imresize", bilinear method) to minimize statistical errors during the following edge detection and overall pixel counting. Due to the small liquid-to-hydrogel contrast in some images, two edge detection methods were performed for each file (function "edge", methods "canny" and "zerocross"). An overlay of the resulting images was used to generate and fill structures. If necessary, non-continuous edges were manually connected to generate an enclosed area. In the following postprocessing, small objects (< 2000 px) were removed, small holes (< 150 px) in the structure were filled, and the structure edges were smoothed. Finally, the area of the lattice and interstices were determined by counting the pixels of interest multiplied with the image resolution. The obtained area ratio (AR) is defined by Equation (7.1) as:

$$AR_{System,t} = \frac{Area_{System,t}}{Area_{System,t_0}}, \tag{7.1}$$

where $Area_{System,t}$ describes the area of either the hydrogel lattice, interstices, or the overall hydrogel area being a combination of the area determined for lattice and interstices (see Figure 7.1, *Data Evaluation*) depending on the four liquid phases (System 1 to System 4) at distinctive time points t and t_0 respectively (number of replicates (n) = 2).

Distances (marked in Figure 7.5 in the results section) were estimated with ImageJ V1.53k (NIH, Bethesda, US-MD) of distinct measurements, and their length ratios (LR) are defined as follows (Equation (7.2)):

$$LR_{System,t} = \frac{Distance_{System,t}}{Distance_{System,t_0}}, \tag{7.2}$$

where $Distance_{System,t}$ refers to the length of longitudinal and transverse cross section of the overall structure or the inner unit cell depending on the four liquid systems at distinctive time points t and t_0 (n = 2).

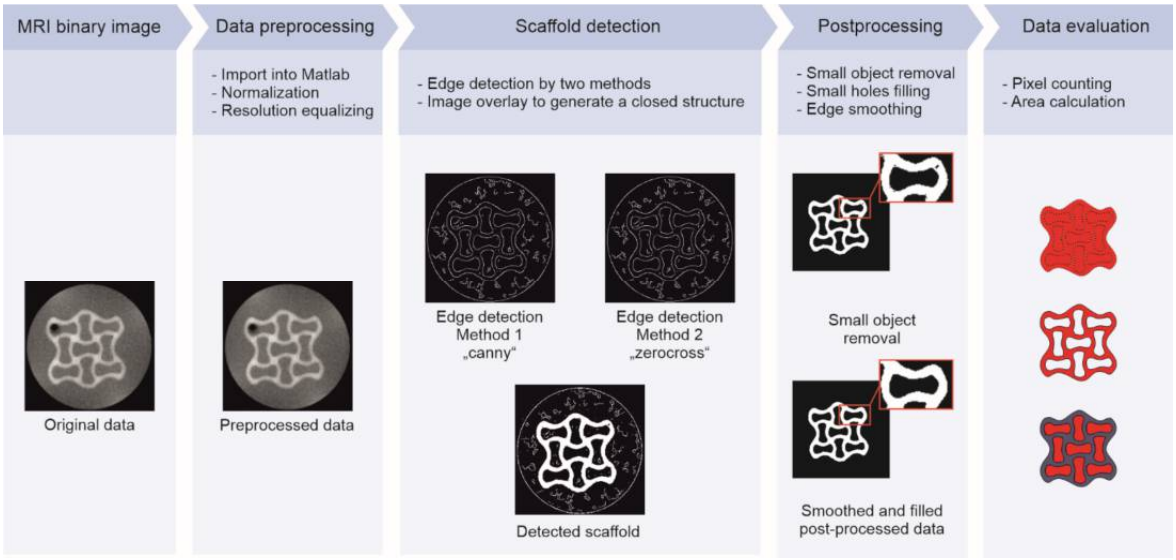

Figure 7.1 Overview of the image processing. After import into MATLAB®, raw image files were preprocessed by normalization and resolution equalization. The scaffold was detected for the fifth slice in the z-direction in each data set, whereas small objects were removed during image postprocessing. Scaffold defects were filled and edges smoothed to determine the hydrogel lattice and interstitial area in the measured slice.

7.2.7. **Additional hydrogel characterization methods**

Weight-based swelling studies. The hydrogel discs were weighted as-prepared (m_0), after being dried for 72 h (m_{dry0}), soaked in liquid (m_1) and being dried again for 72 h (m_{dry1}). These weights were used to determine the swelling ratio $m_{rel} = m_1/m_0$ as well as the dry-weight ratio $m_{dry,rel} = m_{dry1}/m_{dry0}$ (n = 3).

Oscillatory rheometry. Prior to analytics, previously dried hydrogel discs (preparation see Chapter 7.2.3) were stored for 7 d in each of the four liquid systems (see Chapter 7.2.1) with a 100-fold liquid excess for monitoring of the swollen state. Amplitude sweeps (angular frequency $\omega = 1$ and 25 rad·s^{-1}, shear stress $\tau = 5$ - 10.000 Pa, n = 2) and frequency sweeps ($\tau = 10$ Pa and $\omega = 1$ - 25 rad·s^{-1}, n = 3) were performed on a Physica MCR 301 plate rheometer equipped with a plate-plate geometry (PP10, diameter 10 mm, all Anton Paar GmbH, Graz, AT) at 22°C. To reduce the influence of potential outliers, the storage modulus G' and the loss factor tan δ (= G''/G' with G'' being the loss modulus) of a hydrogel were determined by averaging all data points obtained by the frequency sweep measurements after excluding outliers which were identified by a difference of three scaled median absolute deviations from the median.

Uniaxial compression tests. Sample preparation for uniaxial compression tests was executed along the lines of the rheometry tests (see Chapter 7.2.7, Oscillatory rheometry). Accordingly, hydrogel discs were dried and stored in each liquid system for 7 d prior to analysis of the swollen state. Uniaxial compression tests were performed either on a universal testing machine (zwickiLine Z0.5TN or Z2.5) equipped with either a Xforce HP 100 N (all ZwickRoell GmbH

& Co. KG, Ulm, DE) for forces ≤ 100 Nor a KAP-Z 1kN (Angewandte System Technik GmbH, Dresden, DE) load cell and stainless-steel compression platen (diameter 30 mm, ZwickRoell GmbH & Co. KG, Ulm, DE) for forces > 100 N. Initial hydrogel length was determined at a pre-force of 0.2 N, with a uniform velocity of 2 mm/min being applied until sample fracture to determine the compressive strength σ_{max} and the fracture strain ε_{max} (n = 5).

7.3. Results

7.3.1. Hydrogel characterization

Initially, commonly applied analytical methods for hydrogel characterization such as weight-based swelling studies, rheometric analysis, and uniaxial compression were performed. The results are given in Table 7.1. The weight-based swelling ratio m_{rel} was found to be dependent on the external stimuli of the different liquid systems applied. Comparable results were obtained for the swelling ratio of the same hydrogel specimens in their dried state $m_{dry,rel}$. The network density which is correlated to the storage modulus G', as well as the loss factor tan δ (= G''/G' with G'' being the loss modulus) to describe the elasticity were determined by rheometric analysis. The network density was the lowest (32 kPa) for equilibration in formulation buffer (System 4), increasing to 75 kPa for ultrapure water (System 1) and reaching an increased network density of 100 kPa (System 2) and 104 kPa (System 3) for liquids containing $CaCl_2$. The elasticity was the highest in formulation buffer as stated by the lowest tan δ, while decreasing upon $CaCl_2$ addition, and a further decrease when urea was removed or even more when only water was used as liquid. The specimen equilibrated in formulation buffer was the least stable with a fracture strain of 44 ± 9 % and a compressive strength of 0.06 MPa. Upon addition of $CaCl_2$, these were increased to 73 % elongation and 0.78 MPa. The uniaxial compression analysis could not be evaluated with the used analytical setup for liquids without urea as only partial sample rupture occurred without a clear break point in the stress-strain curve.

7.3.2. Magnetic resonance imaging (MRI)

To study the immersion of different liquids in a previously 3D-printed and subsequently dried auxetic hydrogel, time- and spatially resolved MRI was performed. Therefore, the measurement sequence of FLASH pulses was set to a time span of 1.7 min between two measurements. Figure 7.2 A-D display four image series highlighting four exemplary points in time (t_0 = 1.7 min; t_4 = 8.5 min; t_8 = 15.3 min; t_{17} = 30.6 min) within a measurement sequence for each condition.

Table 7.1 Swelling ratios and mechanical properties obtained in the swelling studies, by oscillatory rheometry and uniaxial compression of hydrogel discs. All measurements were performed at room temperature (22°C).

Liquid phase	m_{rel} %	m_dry_{rel} %	G' kPa	tan δ -	ε_{max} %	σ_{max} MPa
System 1	31.2 ± 1.4	32.9 ± 0.1	75 ± 13	0.22 ± 0.01	-[a]	-[a]
System 2	36.0 ± 1.3	36.9 ± 0.3	100 ± 13	0.13 ± 0.01	-[a]	-[a]
System 3	59.3 ± 1.4	71.0 ± 0.8	104 ± 18	0.06 ± 0.00	73 ± 5	0.78 ± 0.15
System 4	137.8 ± 2.0	122.3 ± 1.2	32 ± 4	0.02 ± 0.00	44 ± 9	0.06 ± 0.02

[a] not analyzable

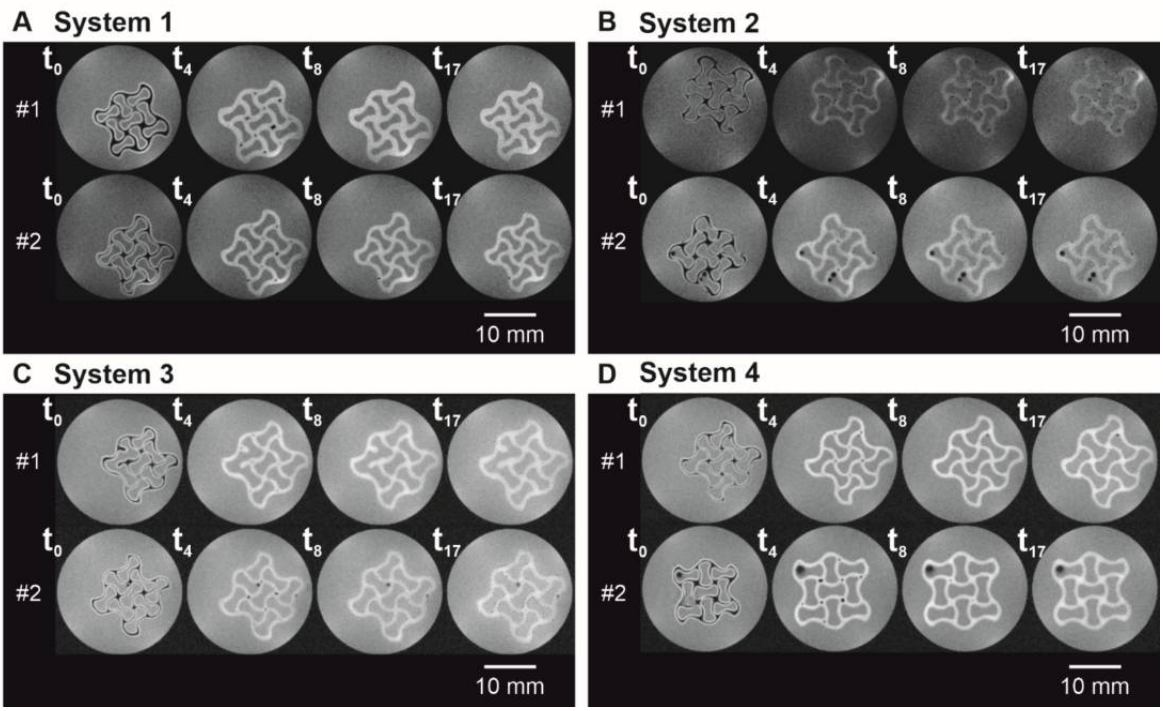

Figure 7.2 Auxetic structures in different liquid phases in MRI grayscale images with a field of view of 25 x 25 mm² at distinct time points. The liquid phase was (A) System 1, (B) System 2, (C) System 3, and (D) System 4 (n = 2).

For all conditions, the measurements at t_0 showed liquid penetration in the outer edges of the hydrogel species (white color), while the inner core of the structure was still dry (black color, Figure 7.2 A-D, t_0). With ongoing time, the white area within the hydrogel lattices increased, visualizing the wetting and subsequent swelling of the scaffold. While the liquid immersed into the hydrogel and was present throughout the strands at t_4 = 8.5 min, there were still dry spots at the nodal points of the hydrogel network observable. Except for two little black spots (Figure D, sample #2, t_8), the liquid had penetrated the hydrogel networks completely for t_8 = 15.3 min. When looking (visual inspection) at the experimental data for hydrogel specimens immersed in formulation buffer (Figure 7.2 D) and ultrapure water (Figure Figure 7.2 A), a stimuli-dependent behavior can be seen in the different lattice thicknesses and overall hydrogel dimensions. As such clear changes could not be perceived in systems 2 and 3, an image analysis was made in the following to quantify and visualize changes in the hydrogel dimensions more reliably. The low liquid-to-hydrogel contrast for samples immersed in 0.1 M $CaCl_2$ samples (Figure 7.2 B) hindered a meaningful image analysis, therefore an application-optimized MRI measurement (Figure 7.3) by RARE pulse sequences was performed. For visualization purposes, the colors in these images were swapped, meaning that black corresponds to a high signal and white to a lower signal. Due to movement of the sample within the liquid, the first image of the second replicate showed blurring as the image generation in MRI integrates the signals over the measurement time, here 1 min 42 s. Artefacts – most likely air bubbles adhering to the hydrogel scaffold - in the interstices of the structure are found in two time series (sample #2 in Figure D and Figure 7.2 B).

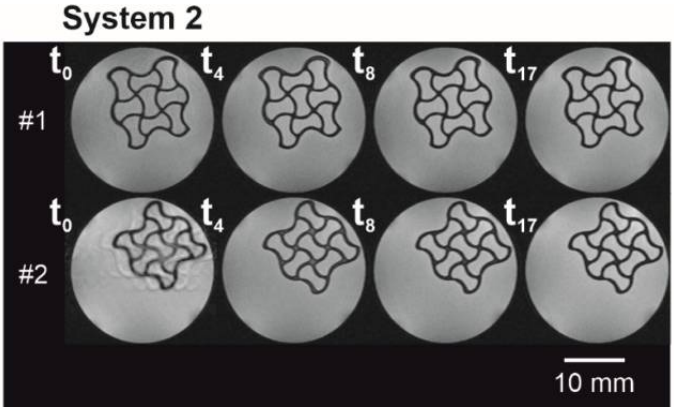

Figure 7.3 Auxetic structures in System 2 in MRI grayscale images with a field of view of 25 x 25 mm² at distinct time points. The MRI measurements' settings were optimized towards an increased buffer-to-hydrogel contrast (n = 2).

7.3.3. **Swelling behavior – Area ratios**

To quantify the swelling behavior as a function of the liquid used, the hydrogel lattice and the interstices, as well as the area covered by the hydrogel construct were determined by image analysis (Figure 7.4 A-C). The MRI images of the fifth layer in z-direction were chosen to ensure comparable image quality. As the overall sample size may vary due to imperfect structures (e.g. by variation during sample processing or printing defects), the area obtained for different time points was normalized to the area obtained at t_0. Previously dried hydrogel specimens placed in urea containing liquid phases (System 3, System 4) showed an overall increase in their area by about 27 %, while hydrogel specimens placed in liquid phases without urea (System 1, System 2) started to increase their area by 17 % (System 1) or 7 % (System 2) and were then shrinking approximately covering the initial area again. The course of the area ratio according to Equation (7.1) is shown in Figure 7.4 A.

Having a closer look at the composition of the overall hydrogel dimension, one has to distinguish the covered area by the hydrogel lattice and the enclosed interstices filled with the liquid phase. In contrast to the overall dimension, a different time-dependent trend is found for the lattices: The lattice area decreased by 12 ± 4 % (System 4) at t_5 and 16 ± 2 % (System 3) at t_4 for urea-containing liquids (Figure 7.4 B). Subsequently, there was a steady increase over the time period considered, almost reaching the initial area for these two conditions. For both liquids without urea (Systems 1 and 2), the area increased for the second time point and is then steadily decreasing. Systems 2 – 4 containing salt or salt and urea leveled approximately at the same area ratio of 0.96 ± 0.05 (System 4) to 0.98 ± 0.02 (System 3), while the area ratio of System 1 decreased to 0.88 ± 0.04.

When analyzing the interstices for urea-containing solutions (System 3; System 4), the covered area steadily increased for the first eight time points t_0 – t_8 and reached a constant area of approximately twice the area compared to the beginning. For System 2, the interstitial area increased considerably lower, with a maximum of 12 ± 10 % at t_4, and a slight decrease in interstitial area thereafter. Hydrogel specimens in ultrapure water (System 1) exhibited the smallest geometry changes. Initially, swelling to a maximum area of 109 ± 21 % at t_4 followed by a constant decrease without reaching a plateau at t_{17} was documented.

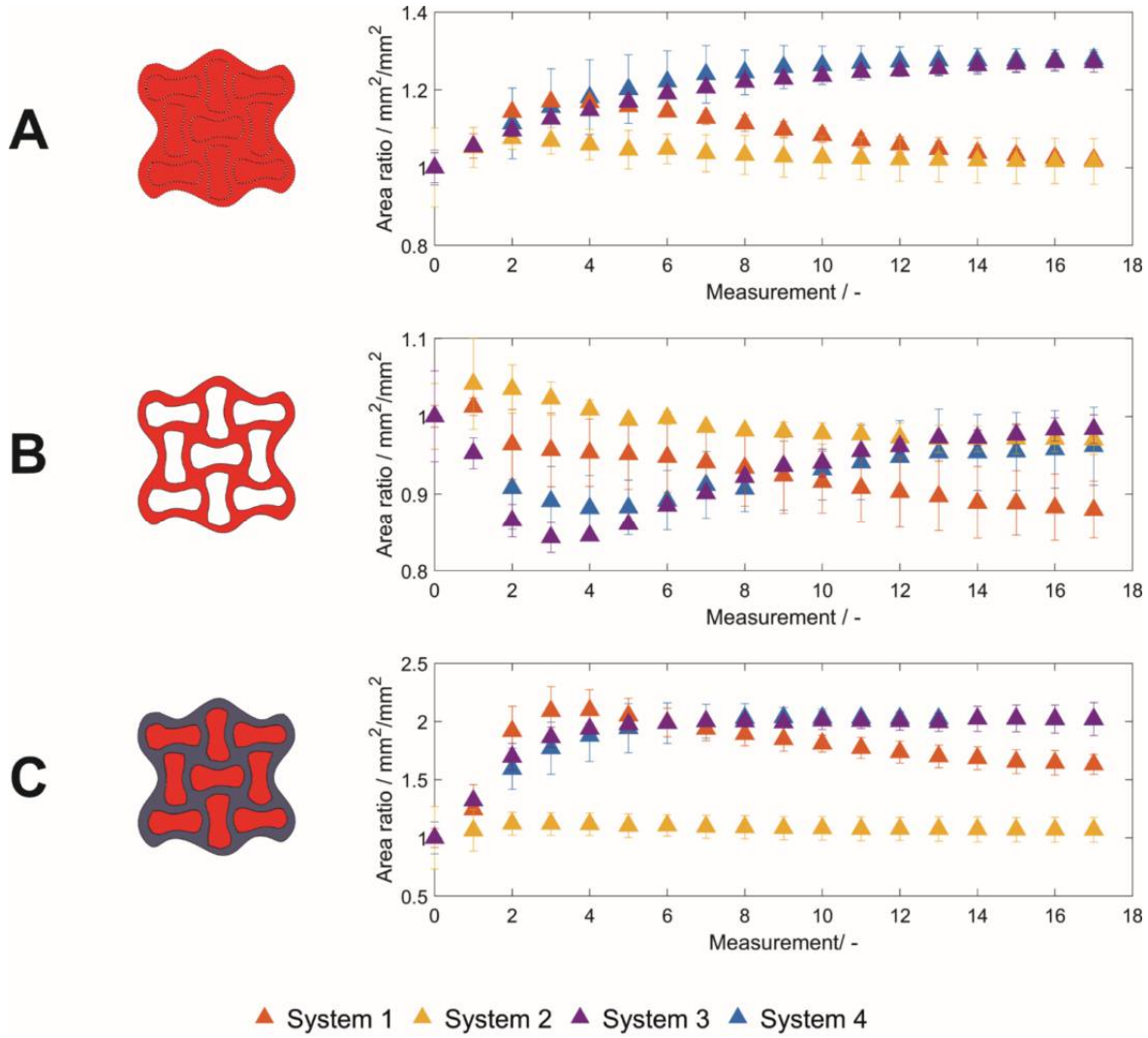

Figure 7.4 Areas of (A) the hydrogel specimen, (B) lattice, and (C) interstices relative to t_0 depending on the liquid phase as a function of time. The evaluated area is highlighted in the corresponding exemplary structure. Data is expressed as the mean ± empirical standard deviation of two hydrogel specimens per condition.

7.3.4. **Swelling behavior – Distances**

Auxetic structures are applied in technical settings because of their characteristic anisotropic elongation and shortening under stress. By MRI, this can be measured by observing the time-dependent geometric changes of distances within the nine point-symmetrically arranged re-entrant honeycomb structures. The geometry of the cells of the honeycomb, which can be separated in longitudinal and transverse unit cells, was investigated by comparing the length ratio between longitudinal and transverse unit cells (Equation (7.2)). As displayed in Figure 7.5, the x-direction of the outer rows consists of two longitudinal (marked in red) and one transverse (marked in turquoise) unit cell (Figure 7.5 A). In y-direction, one longitudinal and two transverse cells can be found. Comparing Figure 7.5 A and B, the length ratio was steadily increasing for urea containing liquids to a maximum of 1.22 (System 4) and 1.23 (System 3) at t_{17}, while the length ratio increased and decreased again to values similar to the starting value for non-urea-containing liquids (System 1; System 2) for both orientations. Considering the eight monitored hydrogel samples stored in different liquids (n = 2), a general trend for a higher

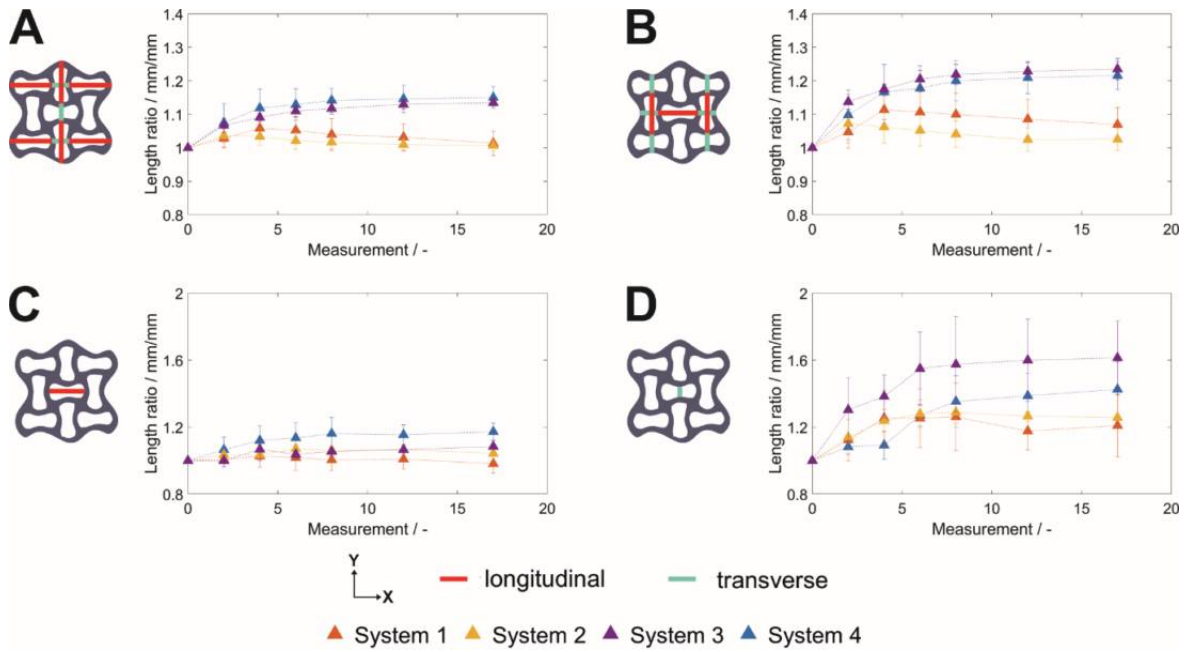

Figure 7.5 Time-dependent length of structural elements of the auxetic lattice consisting of nine point-symmetrically arranged unit cells. (A) Two longitudinal unit cells and one transverse unit cell, (B) one longitudinal and two transverse unit cells and the (C) longitudinal as well as (D) transverse dimension of the center unit cell. The distances are highlighted in the corresponding exemplary structure. Data is expressed as the mean ± empirical standard deviation of two hydrogel specimens relative to the value at t_0 with one (C + D) or three lines per sample (A + B) with two samples per condition.

value of the length ratio could be observed for the target distances with a higher percentage of transverse cells contributing to the respective elongation.
In the center unit of the hydrogel lattice (C+D), the geometry changes might only be influenced by the outer cells as the liquid diffusion into the dried lattice is possible from all outer edges and no anisotropic external stress was applied. Again, the elongation of the transverse cell was more pronounced than the elongation of the longitudinal central cell when compared to distances measured at t_0. However, influenced by the unfavorable resolution for the longitudinal central cell in Figure 7.5 D, the deviation increases. Based on that, the differences between the urea-containing liquid systems (System 3, System 4) might be caused by the low number of samples and may be enhanced by further optimization of the parameters of the MRI for a more detailed evaluation.

7.4. Discussion

7.4.1. Magnetic resonance imaging for hydrogel characterization

Buffer substances such as urea or salts in general can account for more than half of the as-prepared hydrogel dry weight. By using different liquid phases with special characteristics with and without salts and urea being present, commonly applied weight-based swelling ratios are thus inapplicable as diffusion of buffer substances into or out of the hydrogel network cannot be neglected. In addition, weight-based swelling ratios are mostly determined using simple geometric structures such as cylinders or cubes. Thus, the analysis of a more complex auxetic

structure with interstices filled with liquid causes difficulties in reproducible removal of excess water.

To overcome these disadvantages, MRI was applied as a new tool to describe the time-dependent stimuli and thus swelling behavior caused by liquid diffusion into an auxetic, protein-based hydrogel network. Using this approach, both, the liquid front development as such but also the swelling behavior of outer and inner structures could be traced in a time- and spatially resolved way. Please be aware, that potential scaffold defects, such as small holes within the structure, are smoothed during image processing, which can lead to misinterpretations of the liquid penetration time and swelling behavior. This is especially important for production processes which tend to lead to many structural defects. Since no printing defects were observed during visual inspection of the printed hydrogels (see exemplarily Appendix D.2) – apart from the still visible incomplete strands in Sample #1 illustrated in Figure 7.2 C and thus different hydrogel to liquid ratio of this sample – this effect was not further considered in the context of this manuscript. Within the scope of this manuscript, it was possible to trace three different liquids with one analysis method as shown by a high liquid-to-hydrogel contrast in Figure 7.2 for liquid systems 1, 3, and 4. By changing the MRI pulse sequence, an optimized liquid-to-hydrogel contrast (Figure 7.3) allowed the monitoring of hydrogel specimens placed in a fourth liquid (System 2) that could not be previously analyzed using the proposed image analysis method. Overall, these results are an indicative for a good transferability of the approach used for the screening of new materials. Further, we can envision the adaption of this method to study short-time diffusional effects of core-shell microcapsules, hydrogel shells which exemplarily encapsulate a liquid core containing bioactive molecules. In the area of tissue engineering, the concept could be suitable for the long-term monitoring of hydrogels containing cells[278] or for liquid diffusion monitoring (e.g. vascularization) and swelling behavior of functional hydrogels.

7.4.2. **Stimuli responsiveness of the used protein-based hydrogel formulation**

In order to discuss the stimuli responsiveness of the hydrogel formulations used, several effects which are responsible for the formation and expansion of a hydrogel network have to be considered, taking into account a more detailed study of the influencing parameters during hydrogel formation published previously[213]. The network formation is caused by the chemical crosslinking of casein by the induced photoreaction, so the main proportion of casein is expected to be incorporated into the hydrogel network. In contrast, the used thickening agent sodium alginate is soluble in aqueous solutions and thus may diffuse out of the hydrogel network. However, it can be physically crosslinked by ionic interactions in the presence of divalent cations such as those introduced by 0.1 M $CaCl_2$ in the liquid phase. This double crosslinking was verified by an increasing storage modulus in the rheometric analysis while elasticity decreased upon $CaCl_2$ addition, and was even further decreasing for liquids without urea with an opposite effect for the compressive strength and maximum elongation.

In addition to the formation of the hydrogel network by chemical crosslinking or a combination of the chemical dityrosine crosslinking of casein and physical ionic crosslinking of sodium alginate, interactions inside the hydrogel network are responsible for its expansions and mechanical properties. These interactions are based on a complicated interplay between the crosslinked protein (and sodium alginate), the formulation buffer components which remain in the (dried) hydrogel specimen, as well as the composition of the immersion liquid system.

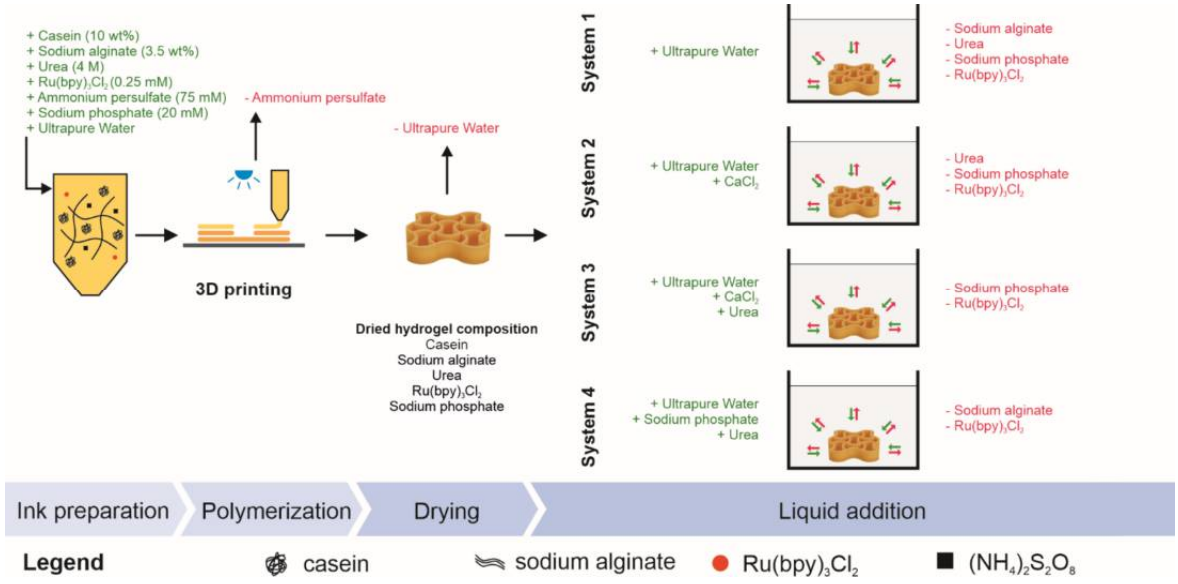

Figure 7.6 Overview of the chemical substances present in the hydrogel specimens during sample preparation and as a function of the immersion liquid system. Components added to the system (as part of the ink formulation or the different liquid systems used to re-hydrate the auxetic structure) are marked in green, while components which might be diluted out of the hydrogel specimens are marked in red.

Concentration differences in the liquid systems and within the hydrogel result in diffusion of the various components into or out of the hydrogel. Figure 7.6 illustrates the uptake and decrease of chemical substances in the hydrogel specimens, which are either incorporated in the hydrogel network or present in the liquid phase depending on the immersing liquid. Since the spatially resolved concentration and thus contribution of the individual components to the swelling behavior of the hydrogel were not in the focus of this study and thus not analyzed on a molecular basis, the course of the time-dependent swelling will not be discussed in detail.
In general, an overall volume increase is explained by the liquid immersion into a dry hydrogel network causing an association of the polymer molecules with water, explaining the initial increase in the overall area for all liquid systems. Thus, intermolecular effects are gaining importance with increasing liquid content affecting the hydrogel characteristics. The chaotropic agent urea – which is part of the formulation buffer since it enhances the solubility of the hydrophobic protein casein - decreases hydrophobic interactions[41]. Upon drying, together with sodium phosphate as the other formulation buffer substance, it will remain in the hydrogel structure. Therefore, just looking at the urea content in the hydrogel specimens, if no urea is present in the immersing liquid, urea may slowly diffuse out of the hydrogel network. This leads to increasing intermolecular interactions and thus an overall decrease in lattice area and the overall network dimensions. Additionally, due to the presence of salts such as sodium phosphate and $CaCl_2$, the ionic strength is altered depending on the liquid system. The higher the ionic strength, which is correlated with the solution's conductivity, the more ionic interactions cause a volume decrease in hydrogels. Moreover, the pH and thus the surface net charge of the protein depends on the used liquid system. For micellar casein with a pI around pH 4.6[279], a lower protein repulsion is expected in the urea-containing liquid systems (≈ pH 8) compared to the non-urea-containing liquids (< pH 7). The combination of these effects results

in a complex time and stimuli-dependent behavior of the overall area covered by hydrogel dimension, as well as the lattice and interstitial area. However, to address the exact reason for the observed time-dependent behavior, the hydrogel structure and its reaction to each stimulus applied should be further understood, e.g. by using advanced material characterization techniques.

7.4.3. **Macroscopic auxetic structuring**

Besides of the induction of stimuli-dependent behavior on a micromolecular level, the protein-based hydrogel was functionalized by macroscopic auxetic structuring. This geometric pattern enables site-directed macromolecular responses. Auxetic structures exhibit a negative Poisson's ratio, meaning that upon an external force in a uniaxial, longitudinal direction (stretching), their perpendicular cross section increases[222], which is opposite to most of the material structures known. As the liquid uptake into a dried structure exhibits a non-uniaxial force, one would not inevitably expect an auxetic behavior upon liquid immersion. However, this was observed upon liquid uptake from the outside, and the cross section as well as the overall dimension increased further for the center unit cell (Figure 7.5). Dominating re-entrant parts compared to the longitudinal dimension bend the 3D printed object in one direction. Using extrusion-based 3D printing as a fabrication method generated an auxetic architecture with higher strand widths at the nodes compared to the strands as the material is merging within a printed layer before light-induced crosslinking. The resulting longer diffusion paths at the nodes and the delayed wetting compared to the strands could be visualized in a site-dependent way by MRI. As the directed stretching is more pronounced at the center unit cell of the auxetic structure, which is influenced by diffusion as well as the directed stretching and swelling of the neighboring units, these effects may be contributing to and enhance the overall auxetic behavior during liquid uptake.

7.5. **Conclusion**

We used MRI as a non-destructive tool to investigate the time-dependent and site-resolved liquid immersion into hydrogel as well as their swelling behavior – both depending on the impact of external stimuli. This is especially helpful for the development of functionalized materials with complex geometry, e.g. hydrogels functionalized by macroscopic auxetic structuring through 3D printing, as 4D changes could be monitored within one measurement series. To enhance process understanding of the swelling which is connected to geometric changes, this method should be applied to different hydrogel constructs as well as more simplified and 3D structures with more replicates per condition to prove statistical relevance of our findings. Within the scope of this manuscript, changes in hydrogel dimension either related to its area or uniaxial length were quantified by image analysis. Edge detection and filtering options allowed to distinguish the interstices filled with liquid and the immersing liquid front during the liquid uptake thus capturing the auxetic behavior, which could exemplarily be shown for the core unit cell. As the method is nondestructive, differences in the swelling and deswelling during a time interval of 30 minutes could be observed for four different liquid compositions, which may also be a favorable material property in some applications. The fast measurement time of MRI allows a site-resolved insight into the hydrogel during liquid uptake. For 3D-printed hydrogels, this strategy could facilitate nondestructive tests and enhanced process understanding in more complex scenarios than the presented study. One potential

application could be the site-directed diffusion of small molecules into 3D printed objects, which plays an important role to supply embedded enzymes or cells[280,281]. In material sciences, a detailed data basis regarding time-dependent and stimuli-dependent swelling effects could be obtained even for liquids with high content of salts or other buffer substances which are prone to misinterpretation when solely looking at weight-based swelling ratios. Therefore, we assume MRI to pave the path to enhanced process understanding for determination of the swelling characteristics of hydrogels and especially functionalized hydrogels in materials sciences.

8 Conclusion and Outlook

The present work had the aim to advance in the field of protein-based hydrogels including an increased knowledge of purification processes for an hydrophobic elastin-like protein, a more profound knowledge on the influencing formulation factors towards the mechanical properties of protein-based hydrogels derived by dityrosine crosslinking of different proteins, the provision an ink formulation for three-dimensional (3D) printing processing and the development of an suitable analytical technique for complex hydrogel formulations and geometries.

In a first study (Chapter 3), a chromatographic and two non-chromatographic purification processes for a hydrophobic elastin-like protein exhibiting low temperature transition were performed. Subsequently, these processing routes were evaluated by the means of critical process performance parameters such as the yield and purity of the target molecule, as well as the salinity and nucleic acid content of the final formulation and method scalability. While the non-chromatographic inverse transition cycling (ITC) had a facile handling in laboratory scale and reached the highest purity in this study, nucleic acid reduction was better for the affinity chromatography-based approach. The main drawback of the ITC is the possibly economically challenging scalability, as high centrifugation volumes with a precise temperature control are necessary, in combination with an overall yield decrease of > 17 % within one centrifugation step for this specific protein construct due to its lower critical solution temperature below room temperature in water. As only one specific ELP construct was analyzed within this thesis, this number should be increased for a more sophisticated prediction of the most economic processing. Also, further optimization of the process conditions may further increase the process performances, which would also needed to be extended by nuclease treatments or endotoxin removal for potential biomedical applications.

In a second and third study, the thesis aimed at investigating different formulation parameters towards the resulting mechanical properties of photoinduced dityrosine crosslinked protein-based hydrogels. Several parameters in the protein solution formulation before crosslinking were examined, proving an influence of protein content, protein species, protein confirmation and protein surface net charge, as well as the used storage solution influencing the intra- and intermolecular interactions within the formed hydrogel network (Chapter 4). Subsequently, copolymeric hydrogels were prepared. Using binary combinations of four proteins with different individual characteristics, the suitability of various proteins as material source for dityrosine crosslinked protein-based hydrogels was proven (Chapter 5). Additionally, mechanical properties of the hydrogels were influenced depending on the used protein shares. This offered a simple approach to tailor protein-based hydrogels depending on the specific application by simply mixing proteins with known homopolymeric network properties. Still, the 3D arrangement of the proteins in the formed networks as well as the share of different interactions on the mechanical properties of such hydrogels remains unknown and should be addressed in prospective research.

To enlarge the toolbox for the processing of dityrosine crosslinked hydrogels based on proteins, extrusion-based 3D printing was investigated as a manufacturing method to obtain 3D objects with complex shapes. Therefore, an ink formulation based on the photoinduced crosslinking of casein blended with the bio-based material was developed (Chapter 6). Thereby, the mixing procedure as well as choice of thickening agent showed to be crucial to obtain an extrudable strand with high shape fidelity still enabling photopolymerization of the casein. Within this thesis, as a proof of concept, an auxetic structure based on a 30-layer re-entrant honeycomb structure was successfully printed by extrusion-based 3D printing. While this proof of concept showed the general applicability, several challenges for understanding the molecular processes within the ink formulation and the hydrogel network remain. First, the ink production has to be further improved taken the scalability of the ink mixing process depending on the desired batch size into account. Second, this manuscript could describe the influence of the thickening agent as well as its concentration and different applied mixing protocols phenomenologically. Considering a fast and facile development of further protein-based ink formulations, a more profound understanding of the interactions on a molecular level of the protein and thickening agent is necessary to predict the suitability of different chemical substances. Third, within the complex mixture of proteins, buffer components, additives, and photoinitiating system, co-dependencies and effects may take place. With regard to the development of possible future ink formulations, understanding the processes during hydrogel formation stays a challenge.

The development of functionalized hydrogel with complex geometrical structures and ink formulations showed the need of a suitable analytical tool to monitor the wetting and swelling behavior of such hydrogels with more sophisticated tools (Chapter 7). This was exemplarily demonstrated by introducing magnetic resonance imaging for the time-dependent monitoring of the swelling behavior of a previously 3D printed and dried hydrogel scaffold being immersed in four different liquids. To gain a further insight into the swelling behavior of different hydrogels, this approach should be transferred to more simplified hydrogel geometries and an increased number of complex hydrogel geometries, extended for a meaningful 3D analysis of the swelling behavior and for the generation of digital twins, as well as the application to different hydrogel materials.

Overall, the present work provides the basis to generate a toolbox for the development of protein-based hydrogels derived by visible light-induced dityrosine crosslinking by a more profound description of the influencing parameters during the hydrogel formulation. The more profound understanding of production process of a hydrophobic elastin-like protein will help to develop more efficient and economically meaningful productions for this class of proteins. The feasibility to print these hydrogels into functionalized hydrogels by macrostructuring enables the creation of even more complex constructs with adapted mechanical properties. As the manufacturing of complex geometries also increases the need for sophisticated methods (in micro- and macroscale, in 3D, etc.), MRI was adapted for the online observation of localized swelling effects within the hydrogel, which may be suitable during the development of more complex artificial hydrogels.

Bibliography

(1) Silva, N. H. C. S.; Vilela, C.; Marrucho, I. M.; Freire, C. S. R.; Pascoal Neto, C.; Silvestre, A. J. D. Protein-Based Materials: From Sources to Innovative Sustainable Materials for Biomedical Applications. *J. Mater. Chem. B* **2014**, *2* (24), 3715–3740. https://doi.org/10.1039/c4tb00168k.

(2) Agnieray, H.; Glasson, J. L.; Chen, Q.; Kaur, M.; Domigan, L. J. Recent Developments in Sustainably Sourced Protein-Based Biomaterials. *Biochem. Soc. Trans.* **2021**, *49* (2), 953–964. https://doi.org/10.1042/BST20200896.

(3) Rajeshkumar, G.; Arvindh Seshadri, S.; Devnani, G. L.; Sanjay, M. R.; Siengchin, S.; Prakash Maran, J.; Al-Dhabi, N. A.; Karuppiah, P.; Mariadhas, V. A.; Sivarajasekar, N.; Ronaldo Anuf, A. Environment Friendly, Renewable and Sustainable Poly Lactic Acid (PLA) Based Natural Fiber Reinforced Composites – A Comprehensive Review. *J. Clean. Prod.* **2021**, *310*, 127483. https://doi.org/10.1016/J.JCLEPRO.2021.127483.

(4) Anastassiadis, S.; Morgunov, I.; Kamzolova, S.; Finogenova, T. Citric Acid Production Patent Review. *Recent Pat. Biotechnol.* **2008**, *2* (2), 107–123. https://doi.org/10.2174/187220808784619757.

(5) Leuchtenberger, W.; Huthmacher, K.; Drauz, K. Biotechnological Production of Amino Acids and Derivatives: Current Status and Prospects. *Appl. Microbiol. Biotechnol.* **2005**, *69* (1), 1–8. https://doi.org/10.1007/S00253-005-0155-Y/FIGURES/14.

(6) Hughes, M. D. G.; Cussons, S.; Mahmoudi, N.; Brockwell, D. J.; Dougan, L. Tuning Protein Hydrogel Mechanics through Modulation of Nanoscale Unfolding and Entanglement in Postgelation Relaxation. *ACS Nano* **2022**. https://doi.org/10.1021/ACSNANO.2C02369.

(7) Hughes, M. D. G.; Hanson, B. S.; Cussons, S.; Mahmoudi, N.; Brockwell, D. J.; Dougan, L. Control of Nanoscale in Situ Protein Unfolding Defines Network Architecture and Mechanics of Protein Hydrogels. *ACS Nano* **2021**, *15* (7), 11296–11308. https://doi.org/10.1021/ACSNANO.1C00353/ASSET/IMAGES/MEDIUM/NN1C00353_M008.GIF.

(8) Taylor, W. R. The Classification of Amino Acid Conservation. *J. Theor. Biol.* **1986**, *119* (2), 205–218. https://doi.org/10.1016/S0022-5193(86)80075-3.

(9) Moss, G. P.; Smith, P. A. S.; Tavernier, D. Glossary of Class Names of Organic Compounds and Reactive Intermediates Based on Structure (IUPAC Recommendations 1995). *Pure Appl. Chem.* **1995**, *67* (8–9), 1307–1375. https://doi.org/10.1351/PAC199567081307/MACHINEREADABLECITATION/RIS.

(10) Moss, G. P. Basic Terminology of Stereochemistry (IUPAC Recommendations 1996). *Pure Appl. Chem.* **1996**, *68* (12), 2193–2222. https://doi.org/10.1351/PAC199668122193/PDF.

(11) Parker, N.; Schneegurt, M.; Tu, A.--Hue T.; Forster, B. M.; Lister, P.; OpenStax College; Open Textbook Library; OpenStax (Nonprofit organization). *Microbiology*; 2016.

(12) Uversky, V. N. Introduction to Intrinsically Disordered Proteins (IDPs). *Chem. Rev.* **2014**, *114* (13), 6557–6560. https://doi.org/10.1021/CR500288Y/ASSET/IMAGES/LARGE/CR-2014-00288Y_0002.JPEG.

(13) Dunker, A. K.; Babu, M. M.; Barbar, E.; Blackledge, M.; Bondos, S. E.; Dosztányi, Z.; Dyson, H. J.; Forman-Kay, J.; Fuxreiter, M.; Gsponer, J.; Han, K.-H.; Jones, D. T.; Longhi, S.; Metallo, S. J.; Nishikawa, K.; Nussinov, R.; Obradovic, Z.; Pappu, R. V.; Rost, B.; Selenko, P.; Subramaniam, V.; Sussman, J. L.; Tompa, P.; Uversky, V. N. What's in a Name? Why These Proteins Are Intrinsically Disordered. *http://dx.doi.org/10.4161/idp.24157* **2013**, *1* (1), e24157. https://doi.org/10.4161/IDP.24157.

(14) Manning, M. C.; Chou, D. K.; Murphy, B. M.; Payne, R. W.; Katayama, D. S. Stability of Protein Pharmaceuticals: An Update. *Pharm. Res.* **2010**, *27* (4), 544–575. https://doi.org/10.1007/S11095-009-0045-6/FIGURES/4.

(15) Cromwell, M. E. M.; Hilario, E.; Jacobson, F. Protein Aggregation and Bioprocessing. *AAPS J.* **2006**, *8* (3). https://doi.org/10.1208/AAPSJ080366.

(16) Mahler, H. C.; Friess, W.; Grauschopf, U.; Kiese, S. Protein Aggregation: Pathways, Induction Factors and Analysis. *J. Pharm. Sci.* **2009**, *98* (9), 2909–2934. https://doi.org/10.1002/JPS.21566.

(17) Chi, E. Y.; Krishnan, S.; Randolph, T. W.; Carpenter, J. F. Physical Stability of Proteins in Aqueous Solution: Mechanism and Driving Forces in Nonnative Protein Aggregation. *Pharm. Res.* **2003**, *20* (9), 1325–1336. https://doi.org/10.1023/A:1025771421906/METRICS.

(18) Wang, W.; Nema, S.; Teagarden, D. Protein Aggregation—Pathways and Influencing Factors. *Int. J. Pharm.* **2010**, *390* (2), 89–99. https://doi.org/10.1016/J.IJPHARM.2010.02.025.

(19) Zhang, Y.; Cremer, P. S. Interactions between Macromolecules and Ions: The Hofmeister Series. *Curr. Opin. Chem. Biol.* **2006**, *10* (6), 658–663. https://doi.org/10.1016/J.CBPA.2006.09.020.

(20) Timson, D. J. The Roles and Applications of Chaotropes and Kosmotropes in Industrial Fermentation Processes. *World J. Microbiol. Biotechnol. 2020 366* **2020**, *36* (6), 1–13. https://doi.org/10.1007/S11274-020-02865-8.

(21) Zangi, R.; Zhou, R.; Berne, B. J. Urea's Action on Hydrophobic Interactions. *J. Am. Chem. Soc.* **2009**, *131* (4), 1535–1541. https://doi.org/10.1021/ja807887g.

(22) Stumpe, M. C.; Grubmüller, H. Urea Impedes the Hydrophobic Collapse of Partially Unfolded Proteins. *Biophys. J.* **2009**, *96* (9), 3744–3752. https://doi.org/10.1016/J.BPJ.2009.01.051.

(23) Garcia, A.; Canchi, D. R.; García, A. E. Cosolvent Effects on Protein Stability Unusual Structures in DNA Repeats View Project DNA Structures and Polymorphism View Project Deepak R Canchi Rensselaer Polytechnic Institute 4 PUBLICATIONS 907 CITATIONS SEE PROFILE Cosolvent Effects on Protein Stability. *Artic. Annu. Rev. Phys. Chem.* **2013**. https://doi.org/10.1146/annurev-physchem-040412-110156.

(24) Van Der Vegt, N. F. A.; Nayar, D. The Hydrophobic Effect and the Role of Cosolvents. *J. Phys. Chem. B* **2017**, *121* (43), 9986–9998. https://doi.org/10.1021/acs.jpcb.7b06453.

(25) De Kruif, C. G.; Holt, C. Casein Micelle Structure, Functions and Interactions. In *Advanced Dairy Chemistry---1 Proteins: Part A / Part B*; Fox, P. F., McSweeney, P. L. H., Eds.; Springer US: Boston, MA, 2003; pp 233–276. https://doi.org/10.1007/978-1-4419-8602-3_5.

(26) Moinpour, M.; Barker, N. K.; Guzman, L. E.; Jewett, J. C.; Langlais, P. R.; Schwartz, J. C. Discriminating Changes in Protein Structure Using Tyrosine Conjugation. *Protein Sci.* **2020**, *29* (8), 1784–1793. https://doi.org/10.1002/pro.3897.

(27) Totosaus, A.; Montejano, J. G.; Salazar, J. A.; Guerrero, I. A Review of Physical and Chemical Protein-Gel Induction. *Int. J. Food Sci. Technol.* **2002**, *37* (6), 589–601. https://doi.org/10.1046/j.1365-2621.2002.00623.x.

(28) Xiong, Y. L.; Kinsella, J. E. Mechanism of Urea-Induced Whey Protein Gelation. *J. Agric. Food Chem.* **1990**, *38* (10), 1887–1891. https://doi.org/10.1021/jf00100a001.

(29) Ahmed, E. M. Hydrogel: Preparation, Characterization, and Applications: A Review. *J. Adv. Res.* **2015**, *6* (2), 105–121. https://doi.org/10.1016/J.JARE.2013.07.006.

(30) Khan, S.; Ullah, A.; Ullah, K.; Rehman, N. U. Insight into Hydrogels. *Designed Monomers and Polymers*. Taylor and Francis Ltd. July 3, 2016, pp 456–478. https://doi.org/10.1080/15685551.2016.1169380.

(31) Ullah, F.; Othman, M. B. H.; Javed, F.; Ahmad, Z.; Akil, H. M. Classification, Processing and Application of Hydrogels: A Review. *Mater. Sci. Eng. C* **2015**, *57*, 414–433. https://doi.org/10.1016/j.msec.2015.07.053.

(32) Kapoor, S.; Kundu, S. C. Silk Protein-Based Hydrogels: Promising Advanced Materials for Biomedical Applications. *Acta Biomaterialia*. 2016. https://doi.org/10.1016/j.actbio.2015.11.034.

(33) Abaee, A.; Mohammadian, M.; Jafari, S. M. Whey and Soy Protein-Based Hydrogels and Nano-Hydrogels as Bioactive Delivery Systems. *Trends in Food Science and Technology*. Elsevier Ltd December 1, 2017, pp 69–81. https://doi.org/10.1016/j.tifs.2017.10.011.

(34) Lagrange, V.; Whitsett, D.; Burris, C. Global Market for Dairy Proteins. *J. Food Sci.* **2015**, *80* (S1), A16–A22. https://doi.org/10.1111/1750-3841.12801.

(35) Buchacher, A.; Iberer, G. Purification of Intravenous Immunoglobulin G from Human Plasma - Aspects of Yield and Virus Safety. *Biotechnol. J.* **2006**, *1* (2), 148–163. https://doi.org/10.1002/BIOT.200500037.

(36) Tripathi, N. K.; Shrivastava, A. Recent Developments in Bioprocessing of Recombinant Proteins: Expression Hosts and Process Development. *Front. Bioeng. Biotechnol.* **2019**, *7*, 420. https://doi.org/10.3389/FBIOE.2019.00420/BIBTEX.

(37) Kent, S. B. H. Total Chemical Synthesis of Proteins. *Chem. Soc. Rev.* **2009**, *38* (2), 338–351. https://doi.org/10.1039/B700141J.

(38) Desombre, M. Development, Evaluation and Optimization of the Purification of an Artifical, Recombinant Elastomeric Biopolymer, Master's thesis at the Department of Chemical and Process Engineering, Karlsruhe Institute of Technology, 2020.

(39) Wusigale; Liang, L.; Luo, Y. Casein and Pectin: Structures, Interactions, and Applications. *Trends Food Sci. Technol.* **2020**, *97*, 391–403. https://doi.org/10.1016/J.TIFS.2020.01.027.

(40) Horne, D. S. A Balanced View of Casein Interactions. *Curr. Opin. Colloid Interface Sci.* **2017**, *28*, 74–86. https://doi.org/10.1016/J.COCIS.2017.03.009.

(41) De Kruif, C. G.; Huppertz, T.; Urban, V. S.; Petukhov, A. V. Casein Micelles and Their Internal Structure. *Advances in Colloid and Interface Science*. Elsevier March 1, 2012, pp 36–52. https://doi.org/10.1016/j.cis.2012.01.002.

(42) Holt, C.; Carver, J. A.; Ecroyd, H.; Thorn, D. C. Invited Review: Caseins and the Casein Micelle: Their Biological Functions, Structures, and Behavior in Foods. *J. Dairy Sci.* **2013**, *96* (10), 6127–6146. https://doi.org/10.3168/JDS.2013-6831.

(43) Bhat, M. Y.; Dar, T. A.; Singh, L. R. Casein Proteins: Structural and Functional Aspects. In *Milk Proteins - From Structure to Biological Properties and Health Aspects*; InTech, 2016. https://doi.org/10.5772/64187.

(44) Topală, T.; Bodoki, A.; Oprean, L.; Oprean, R. Bovine Serum Albumin Interactions with Metal Complexes. *Clujul Med.* **2014**, *87* (4), 215. https://doi.org/10.15386/CJMED-357.

(45) Majorek, K. A.; Porebski, P. J.; Dayal, A.; Zimmerman, M. D.; Jablonska, K.; Stewart, A. J.; Chruszcz, M.; Minor, W. Structural and Immunologic Characterization of Bovine, Horse, and Rabbit Serum Albumins. *Mol. Immunol.* **2012**, *52* (3–4), 174–182. https://doi.org/10.1016/J.MOLIMM.2012.05.011.

(46) Pujadas, G.; Palau, J. Evolution of α-Amylases: Architectural Features and Key Residues in the Stabilization of the (β/α)8 Scaffold. *Mol. Biol. Evol.* **2001**, *18* (1), 38–54. https://doi.org/10.1093/OXFORDJOURNALS.MOLBEV.A003718.

(47) Consortium, T. U.; Bateman, A.; Martin, M.-J.; Orchard, S.; Magrane, M.; Ahmad, S.; Alpi, E.; Bowler-Barnett, E. H.; Britto, R.; Bye-A-Jee, H.; Cukura, A.; Denny, P.; Dogan, T.; Ebenezer, T.; Fan, J.; Garmiri, P.; da Costa Gonzales, L. J.; Hatton-Ellis, E.; Hussein, A.; Ignatchenko, A.; Insana, G.; Ishtiaq, R.; Joshi, V.; Jyothi, D.; Kandasaamy, S.; Lock, A.; Luciani, A.; Lugaric, M.; Luo, J.; Lussi, Y.; MacDougall, A.; Madeira, F.; Mahmoudy, M.; Mishra, A.; Moulang, K.; Nightingale, A.; Pundir, S.; Qi, G.; Raj, S.; Raposo, P.; Rice, D. L.; Saidi, R.; Santos, R.; Speretta, E.; Stephenson, J.; Totoo, P.; Turner, E.; Tyagi, N.; Vasudev, P.; Warner, K.; Watkins, X.; Zaru, R.; Zellner, H.; Bridge, A. J.; Aimo, L.; Argoud-Puy, G.; Auchincloss, A. H.; Axelsen, K. B.; Bansal, P.; Baratin, D.; Batista Neto, T. M.; Blatter, M.-C.; Bolleman, J. T.; Boutet, E.; Breuza, L.; Gil, B. C.; Casals-Casas, C.; Echioukh, K. C.; Coudert, E.; Cuche, B.; de Castro, E.; Estreicher, A.; Famiglietti, M. L.; Feuermann, M.; Gasteiger, E.; Gaudet, P.; Gehant, S.; Gerritsen, V.; Gos, A.; Gruaz, N.; Hulo, C.; Hyka-Nouspikel, N.; Jungo, F.; Kerhornou, A.; Le Mercier, P.; Lieberherr, D.; Masson, P.; Morgat, A.; Muthukrishnan, V.; Paesano, S.; Pedruzzi, I.; Pilbout, S.; Pourcel, L.; Poux, S.; Pozzato, M.; Pruess, M.; Redaschi, N.; Rivoire, C.; Sigrist, C. J. A.; Sonesson, K.; Sundaram, S.; Wu, C. H.; Arighi, C. N.; Arminski, L.; Chen, C.; Chen, Y.; Huang, H.; Laiho, K.; McGarvey, P.; Natale, D. A.; Ross, K.; Vinayaka, C. R.; Wang, Q.; Wang, Y.; Zhang, J. UniProt: The Universal Protein Knowledgebase in 2023. *Nucleic Acids Res.* **2013**, *1* (1256879), 13–14. https://doi.org/10.1093/NAR/GKAC1052.

(48) Foster, J. A.; Bruenger, E.; Gray, W. R.; Sandberg, L. B. Isolation and Amino Acid Sequences of Tropoelastin Peptides. *J. Biol. Chem.* **1973**, *248* (8), 2876–2879. https://doi.org/10.1016/S0021-9258(19)44088-X.

(49) Urry, D. W. Free Energy Transduction in Polypeptides and Proteins Based on Inverse Temperature Transitions. *Prog. Biophys. Mol. Biol.* **1992**, *57* (1), 23–57. https://doi.org/10.1016/0079-6107(92)90003-O.

(50) Meyer, D. E.; Chilkoti, A. Purification of Recombinant Proteins by Fusion with Thermally-Responsive Polypeptides. *Nat. Biotechnol.* **1999**, *17* (11), 1112–1115. https://doi.org/10.1038/15100.

(51) Roberts, S.; Dzuricky, M.; Chilkoti, A. Elastin-like Polypeptides as Models of Intrinsically Disordered Proteins. *FEBS Lett.* **2015**, *589* (19), 2477–2486. https://doi.org/10.1016/J.FEBSLET.2015.08.029.

(52) Wise, S. G.; Weiss, A. S. Tropoelastin. *Int. J. Biochem. Cell Biol.* **2009**, *41* (3), 494–497. https://doi.org/10.1016/J.BIOCEL.2008.03.017.

(53) Huang, J.; Turner, S. R. Recent Advances in Alternating Copolymers: The Synthesis, Modification, and Applications of Precision Polymers. *Polymer (Guildf).* **2017**, *116*, 572–586. https://doi.org/10.1016/J.POLYMER.2017.01.020.

(54) Bae, Y. H.; Kim, S. W. Hydrogel Delivery Systems Based on Polymer Blends, Block Co-Polymers or Interpenetrating Networks. *Adv. Drug Deliv. Rev.* **1993**, *11* (1–2), 109–135. https://doi.org/10.1016/0169-409X(93)90029-4.

(55) Guisan, J. M.; Zuorro, A.; Jayachandran, B.; Parvin, T. N.; Alam, M. M.; Chanda, K.; Mm, B. Insights on Chemical Crosslinking Strategies for Proteins. *Mol. 2022, Vol. 27, Page 8124* **2022**, *27* (23), 8124. https://doi.org/10.3390/MOLECULES27238124.

(56) Oryan, A.; Kamali, A.; Moshiri, A.; Baharvand, H.; Daemi, H. Chemical Crosslinking of Biopolymeric Scaffolds: Current Knowledge and Future Directions of Crosslinked Engineered Bone Scaffolds. *Int. J. Biol. Macromol.* **2018**, *107* (PartA), 678–688. https://doi.org/10.1016/J.IJBIOMAC.2017.08.184.

(57) Fancy, D. A.; Denison, C.; Kim, K.; Xie, Y.; Holdeman, T.; Amini, F.; Kodadek, T. Scope, Limitations and Mechanistic Aspects of the Photo-Induced Cross-Linking of Proteins by Water-Soluble Metal Complexes. *Chem. Biol.* **2000**, *7* (9), 697–708. https://doi.org/10.1016/S1074-5521(00)00020-X.

(58) Fancy, D. A.; Kodadek, T. Chemistry for the Analysis of Protein-Protein Interactions: Rapid and Efficient Cross-Linking Triggered by Long Wavelength Light. *Proc. Natl. Acad. Sci. U. S. A.* **1999**, *96* (11), 6020–6024. https://doi.org/10.1073/pnas.96.11.6020.

(59) Jeon, E. Y.; Hwang, B. H.; Yang, Y. J.; Kim, B. J.; Choi, B. H.; Jung, G. Y.; Cha, H. J. Rapidly Light-Activated Surgical Protein Glue Inspired by Mussel Adhesion and Insect Structural Crosslinking. *Biomaterials* **2015**, *67*, 11–19. https://doi.org/10.1016/j.biomaterials.2015.07.014.

(60) Elvin, C. M.; Carr, A. G.; Huson, M. G.; Maxwell, J. M.; Pearson, R. D.; Vuocolo, T.; Liyou, N. E.; Wong, D. C. C.; Merritt, D. J.; Dixon, N. E. Synthesis and Properties of Crosslinked Recombinant Pro-Resilin. *Nature* **2005**, *437* (7061), 999–1002. https://doi.org/10.1038/nature04085.

(61) Ding, Y.; Li, Y.; Qin, M.; Cao, Y.; Wang, W. Photo-Cross-Linking Approach to Engineering Small Tyrosine-Containing Peptide Hydrogels with Enhanced Mechanical Stability. *Langmuir* **2013**, *29* (43), 13299–13306. https://doi.org/10.1021/la4029639.

(62) Camp, C. P.; Peterson, I. L.; Knoff, D. S.; Melcher, L. G.; Maxwell, C. J.; Cohen, A. T.; Wertheimer, A. M.; Kim, M. Non-Cytotoxic Dityrosine Photocrosslinked Polymeric Materials With Targeted Elastic Moduli. *Front. Chem.* **2020**, *8*, 173. https://doi.org/10.3389/fchem.2020.00173.

(63) Hughes, M. D. G.; Cussons, S.; Mahmoudi, N.; Brockwell, D. J.; Dougan, L. Single Molecule Protein Stabilisation Translates to Macromolecular Mechanics of a Protein Network. *Soft Matter* **2020**, *16* (27), 6389–6399. https://doi.org/10.1039/C9SM02484K.

(64) Da Silva, M. A.; Lenton, S.; Hughes, M.; Brockwell, D. J.; Dougan, L. Assessing the Potential of Folded Globular Polyproteins As Hydrogel Building Blocks. *Biomacromolecules* **2017**, *18* (2), 636–646. https://doi.org/10.1021/acs.biomac.6b01877.

(65) Khoury, L. R.; Nowitzke, J.; Shmilovich, K.; Popa, I. Study of Biomechanical Properties of Protein-Based Hydrogels Using Force-Clamp Rheometry. *Macromolecules* **2018**, *51* (4), 1441–1452. https://doi.org/10.1021/ACS.MACROMOL.7B02160/SUPPL_FILE/MA7B02160_SI_001.PDF.

(66) Khanmohammadi, M.; Nemati, S.; Ai, J.; Khademi, F. Multipotency Expression of Human Adipose Stem Cells in Filament-like Alginate and Gelatin Derivative Hydrogel Fabricated through Visible Light-Initiated Crosslinking. *Mater. Sci. Eng. C* **2019**, *103*, 109808. https://doi.org/10.1016/J.MSEC.2019.109808.

(67) Lim, K. S.; Schon, B. S.; Mekhileri, N. V.; Brown, G. C. J.; Chia, C. M.; Prabakar, S.; Hooper, G. J.; Woodfield, T. B. F. New Visible-Light Photoinitiating System for Improved Print Fidelity in Gelatin-Based Bioinks. *ACS Biomater. Sci. Eng.* **2016**, *2* (10), 1752–1762. https://doi.org/10.1021/acsbiomaterials.6b00149.

(68) El-Husseiny, H. M.; Mady, E. A.; Hamabe, L.; Abugomaa, A.; Shimada, K.; Yoshida, T.; Tanaka, T.; Yokoi, A.; Elbadawy, M.; Tanaka, R. Smart/Stimuli-Responsive Hydrogels: Cutting-Edge Platforms for Tissue Engineering and Other Biomedical Applications. *Mater. Today Bio* **2022**, *13*, 100186. https://doi.org/10.1016/J.MTBIO.2021.100186.

(69) Vázquez-González, M.; Willner, I. Stimuli-Responsive Biomolecule-Based Hydrogels and Their Applications. *Angew. Chemie Int. Ed.* **2020**, *59* (36), 15342–15377. https://doi.org/10.1002/ANIE.201907670.

(70) Annabi, N.; Mithieux, S. M.; Zorlutuna, P.; Camci-Unal, G.; Weiss, A. S.; Khademhosseini, A. Engineered Cell-Laden Human Protein-Based Elastomer. *Biomaterials* **2013**, *34* (22), 5496–5505. https://doi.org/10.1016/J.BIOMATERIALS.2013.03.076.

(71) Bealer, E. J.; Onissema-Karimu, S.; Rivera-Galletti, A.; Francis, M.; Wilkowski, J.; de la Cruz, D. S.; Hu, X. Protein–Polysaccharide Composite Materials: Fabrication and Applications. *Polym. 2020, Vol. 12, Page 464* **2020**, *12* (2), 464. https://doi.org/10.3390/POLYM12020464.

(72) Wang, Z.; Kang, S.; Cao, S.; Krecker, M.; Tsukruk, V. V.; Singamaneni, S. Protein-Based Functional Nanocomposites. *MRS Bull.* **2020**, *45* (12), 1017–1026. https://doi.org/10.1557/MRS.2020.302.

(73) Lee, J.-H.; Singer, J. P.; Thomas, E. L.; Thomas, E. L.; Lee, J.-H.; Singer, J. P. Micro-/Nanostructured Mechanical Metamaterials. *Adv. Mater.* **2012**, *24* (36), 4782–4810. https://doi.org/10.1002/ADMA.201201644.

(74) Kolken, H. M. A.; Zadpoor, A. A. Auxetic Mechanical Metamaterials. *RSC Adv.* **2017**, *7* (9), 5111–5129. https://doi.org/10.1039/C6RA27333E.

(75) Schwarz, A.; Lichti, T.; Wenz, F.; Scheuring, B. M.; Hübner, C.; Eberl, C.; Elsner, P. Development of a Scalable Fabrication Concept for Sustainable, Programmable Shape-Morphing Metamaterials. *Adv. Eng. Mater.* **2022**, 2200386. https://doi.org/10.1002/ADEM.202200386.

(76) Ge, Q.; Dunn, C. K.; Qi, H. J.; Dunn, M. L. Active Origami by 4D Printing. *Smart Mater. Struct.* **2014**, *23* (9), 094007. https://doi.org/10.1088/0964-1726/23/9/094007.

(77) Alderson, A.; Alderson, K. L. Auxetic Materials. *Proc. Inst. Mech. Eng. Part G J. Aerosp. Eng.* **2007**, *221* (4), 565–575. https://doi.org/10.1243/09544100JAERO185.

(78) Gebhardt, A. Understanding Additive Manufacturing. *Underst. Addit. Manuf.* **2011**. https://doi.org/10.3139/9783446431621.FM.

(79) Huang, S. H.; Liu, P.; Mokasdar, A.; Hou, L. Additive Manufacturing and Its Societal Impact: A Literature Review. *Int. J. Adv. Manuf. Technol.* **2013**, *67* (5–8), 1191–1203. https://doi.org/10.1007/s00170-012-4558-5.

(80) Ligon, S. C.; Liska, R.; Stampfl, J.; Gurr, M.; Mülhaupt, R. Polymers for 3D Printing and Customized Additive Manufacturing. *Chemical Reviews*. American Chemical Society August 9, 2017, pp 10212–10290. https://doi.org/10.1021/acs.chemrev.7b00074.

(81) Zhao, C.; Lv, Q.; Wu, W. Application and Prospects of Hydrogel Additive Manufacturing. *Gels* **2022**, *8* (5). https://doi.org/10.3390/GELS8050297.

(82) Hölzl, K.; Lin, S.; Tytgat, L.; Van Vlierberghe, S.; Gu, L.; Ovsianikov, A. Bioink Properties before, during and after 3D Bioprinting. *Biofabrication* **2016**, *8* (3), 032002. https://doi.org/10.1088/1758-5090/8/3/032002.

(83) Ravanbakhsh, H.; Karamzadeh, V.; Bao, G.; Mongeau, L.; Juncker, D.; Zhang, Y. S.; Ravanbakhsh, H.; Zhang, Y. S.; Bao, G.; Mongeau, L.; Karamzadeh, V.; Juncker, D. Emerging Technologies in Multi-Material Bioprinting. *Adv. Mater.* **2021**, *33* (49), 2104730. https://doi.org/10.1002/ADMA.202104730.

(84) Malda, J.; Visser, J.; Melchels, F. P.; Jüngst, T.; Hennink, W. E.; Dhert, W. J. A.; Groll, J.; Hutmacher, D. W. 25th Anniversary Article: Engineering Hydrogels for Biofabrication. *Adv. Mater.* **2013**, *25* (36), 5011–5028. https://doi.org/10.1002/adma.201302042.

(85) Bagheri, A.; Jin, J. Photopolymerization in 3D Printing. *ACS Appl. Polym. Mater.* **2019**, *1* (4), 593–611. https://doi.org/10.1021/acsapm.8b00165.

(86) Mu, X.; Agostinacchio, F.; Xiang, N.; Pei, Y.; Khan, Y.; Guo, C.; Cebe, P.; Motta, A.; Kaplan, D. L. Recent Advances in 3D Printing with Protein-Based Inks. *Prog. Polym.*

Sci. **2021**, *115*, 101375. https://doi.org/10.1016/J.PROGPOLYMSCI.2021.101375.

(87) Ning, L.; Chen, X. A Brief Review of Extrusion-Based Tissue Scaffold Bio-Printing. *Biotechnol. J.* **2017**, *12* (8), 1600671. https://doi.org/10.1002/BIOT.201600671.

(88) Wenger, L.; Radtke, C. P.; Gerisch, E.; Kollmann, M.; Niemeyer, C. M.; Rabe, K. S.; Hubbuch, J. Systematic Evaluation of Agarose- and Agar-Based Bioinks for Extrusion-Based Bioprinting of Enzymatically Active Hydrogels. *Front. Bioeng. Biotechnol.* **2022**, *10*, 2182. https://doi.org/10.3389/FBIOE.2022.928878/BIBTEX.

(89) Renn, D. W. Agar and Agarose: Indispensable Partners in Biotechnology. *Ind. Eng. Chem. Prod. Res. Dev.* **1984**, *23* (1), 17–21. https://doi.org/10.1021/I300013A004/ASSET/I300013A004.FP.PNG_V03.

(90) Wu, W.; Deconinck, A.; Lewis, J. A. Omnidirectional Printing of 3D Microvascular Networks. *Adv. Mater.* **2011**, *23* (24), H178–H183. https://doi.org/10.1002/ADMA.201004625.

(91) Zhou, K.; Sun, Y.; Yang, J.; Mao, H.; Gu, Z. Hydrogels for 3D Embedded Bioprinting: A Focused Review on Bioinks and Support Baths. *J. Mater. Chem. B* **2022**, *10* (12), 1897–1907. https://doi.org/10.1039/D1TB02554F.

(92) Sears, N. A.; Wilems, T. S.; Gold, K. A.; Lan, Z.; Cereceres, S. N.; Dhavalikar, P. S.; Foudazi, R.; Cosgriff-Hernandez, E. M. Hydrocolloid Inks for 3D Printing of Porous Hydrogels. *Adv. Mater. Technol.* **2019**, *4* (2). https://doi.org/10.1002/admt.201800343.

(93) Pekar, J. J. A Brief Introduction to Functional MRI. *IEEE Eng. Med. Biol. Mag.* **2006**, *25* (2), 24–26. https://doi.org/10.1109/MEMB.2006.1607665.

(94) Gallagher, F. A. An Introduction to Functional and Molecular Imaging with MRI. *Clin. Radiol.* **2010**, *65* (7), 557–566. https://doi.org/10.1016/J.CRAD.2010.04.006.

(95) Britton, M. M. MRI of Chemical Reactions and Processes. *Prog. Nucl. Magn. Reson. Spectrosc.* **2017**, *101*, 51–70. https://doi.org/10.1016/J.PNMRS.2017.03.001.

(96) Van Geuns, R. J. M.; Wielopolski, P. A.; De Bruin, H. G.; Rensing, B. J.; Van Ooijen, P. M. A.; Hulshoff, M.; Oudkerk, M.; De Feyter, P. J. Basic Principles of Magnetic Resonance Imaging. *Prog. Cardiovasc. Dis.* **1999**, *42* (2), 149–156. https://doi.org/10.1016/S0033-0620(99)70014-9.

(97) Callaghan, P. T. *Principles of Nuclear Magnetic Resonance Microscopy*; Oxford University Press: New York, New York, USA, 1991.

(98) Kimmich, R. *NMR*; Springer Verlag: Berlin, 1997. https://doi.org/10.1007/978-3-642-60582-6.

(99) Berger, A. How Does It Work?: Magnetic Resonance Imaging. *BMJ Br. Med. J.* **2002**, *324* (7328), 35. https://doi.org/10.1136/BMJ.324.7328.35.

(100) Prior-Cabanillas, A.; Barrales-Rienda, J. M.; Frutos, G.; Quijada-Garrido, I. Swelling Behaviour of Hydrogels from Methacrylic Acid and Poly(Ethylene Glycol) Side Chains by Magnetic Resonance Imaging. *Polym. Int.* **2007**, *56* (4), 506–511. https://doi.org/10.1002/PI.2144.

(101) Richardson, J. C.; Bowtell, R. W.; Mäder, K.; Melia, C. D. Pharmaceutical Applications of Magnetic Resonance Imaging (MRI). *Adv. Drug Deliv. Rev.* **2005**, *57* (8), 1191–1209. https://doi.org/10.1016/J.ADDR.2005.01.024.

(102) Schmieg, B.; Gretzinger, S.; Schuhmann, S.; Guthausen, G.; Hubbuch, J. Magnetic Resonance Imaging as a Tool for Quality Control in Extrusion-Based Bioprinting. *Biotechnol. J.* **2022**, *17* (5), 2100336. https://doi.org/10.1002/BIOT.202100336.

(103) Archer, B. J.; Uberruck, T.; Mack, J. J.; Youssef, K.; Jarenwattananon, N. N.; Rall, D.; Wypysek, D.; Wiese, M.; Blumich, B.; Wessling, M.; Iruela-Arispe, M. L.; Bouchard, L. S. Noninvasive Quantification of Cell Density in Three-Dimensional Gels by MRI. *IEEE Trans. Biomed. Eng.* **2019**, *66* (3), 821–830. https://doi.org/10.1109/TBME.2018.2857443.

(104) Muñoz-Bonilla, A.; Echeverria, C.; Sonseca, Á.; Arrieta, M. P.; Fernández-García, M. Bio-Based Polymers with Antimicrobial Properties towards Sustainable Development. *Materials*. MDPI AG February 20, 2019, p 641. https://doi.org/10.3390/ma12040641.

(105) *Functional Biopolymers*; Thakur, V. K., Thakur, M. K., Eds.; Springer Series on Polymer and Composite Materials; Springer International Publishing: Cham, 2018. https://doi.org/10.1007/978-3-319-66417-0.

(106) Kreyenschulte, D.; Krull, R.; Margaritis, A. Recent Advances in Microbial Biopolymer Production and Purification. *Crit. Rev. Biotechnol.* **2014**, *34* (1), 1–15. https://doi.org/10.3109/07388551.2012.743501.

(107) Chow, D.; Nunalee, M. L.; Lim, D. W.; Simnick, A. J.; Chilkoti, A. Peptide-Based Biopolymers in Biomedicine and Biotechnology. *Mater. Sci. Eng. R Reports* **2008**, *62* (4), 125–155. https://doi.org/10.1016/J.MSER.2008.04.004.

(108) Balu, R.; Whittaker, J.; Dutta, N. K.; Elvin, C. M.; Choudhury, N. R. Multi-Responsive Biomaterials and Nanobioconjugates from Resilin-like Protein Polymers. *J. Mater. Chem. B* **2014**, *2* (36), 5936–5947. https://doi.org/10.1039/C4TB00726C.

(109) Rodríguez-Cabello, J. C.; Reguera, J.; Girotti, A.; Alonso, M.; Testera, A. M. Developing Functionality in Elastin-like Polymers by Increasing Their Molecular Complexity: The Power of the Genetic Engineering Approach. *Progress in Polymer Science (Oxford)*. Elsevier Ltd November 1, 2005, pp 1119–1145. https://doi.org/10.1016/j.progpolymsci.2005.07.004.

(110) Zhang, Y.-N.; Avery, R. K.; Vallmajo-Martin, Q.; Assmann, A.; Vegh, A.; Memic, A.; Olsen, B. D.; Annabi, N.; Khademhosseini, A. A Highly Elastic and Rapidly Crosslinkable Elastin-Like Polypeptide-Based Hydrogel for Biomedical Applications. *Adv. Funct. Mater.* **2015**, *25* (30), 4814–4826. https://doi.org/10.1002/adfm.201501489.

(111) Meyer, D. E.; Trabbic-Carlson, K.; Chilkoti, A. Protein Purification by Fusion with an Environmentally Responsive Elastin-like Polypeptide: Effect of Polypeptide Length on the Purification of Thioredoxin. *Biotechnol. Prog.* **2001**, *17* (4), 720–728. https://doi.org/10.1021/bp010049o.

(112) Kim, D. H.; Smith, J. T.; Chilkoti, A.; Reichert, W. M. The Effect of Covalently Immobilized RhIL-1ra-ELP Fusion Protein on the Inflammatory Profile of LPS-Stimulated Human Monocytes. *Biomaterials* **2007**, *28* (23), 3369–3377. https://doi.org/10.1016/j.biomaterials.2007.04.010.

(113) Hu, F.; Ke, T.; Li, X.; Mao, P. H.; Jin, X.; Hui, F. L.; Ma, X. D.; Ma, L. X. Expression and Purification of an Antimicrobial Peptide by Fusion with Elastin-like Polypeptides in Escherichia Coli. *Appl. Biochem. Biotechnol.* **2010**, *160* (8), 2377–2387. https://doi.org/10.1007/s12010-009-8850-2.

(114) Madan, B.; Chaudhary, G.; Cramer, S. M.; Chen, W. ELP-z and ELP-Zz Capturing Scaffolds for the Purification of Immunoglobulins by Affinity Precipitation. *J. Biotechnol.* **2013**, *163* (1), 10–16. https://doi.org/10.1016/j.jbiotec.2012.10.007.

(115) Yeboah, A.; Cohen, R. I.; Rabolli, C.; Yarmush, M. L.; Berthiaume, F. Elastin-like Polypeptides: A Strategic Fusion Partner for Biologics. *Biotechnol. Bioeng.* **2016**, *113* (8), 1617–1627. https://doi.org/10.1002/bit.25998.

(116) Rodríguez-Cabello, J. C.; Arias, F. J.; Rodrigo, M. A.; Girotti, A. Elastin-like Polypeptides in Drug Delivery. *Advanced Drug Delivery Reviews*. Elsevier B.V. February 1, 2016, pp 85–100. https://doi.org/10.1016/j.addr.2015.12.007.

(117) Simnick, A. J.; Amiram, M.; Liu, W.; Hanna, G.; Dewhirst, M. W.; Kontos, C. D.; Chilkoti, A. In Vivo Tumor Targeting by a NGR-Decorated Micelle of a Recombinant Diblock Copolypeptide. In *Journal of Controlled Release*; Elsevier, 2011; Vol. 155, pp 144–151. https://doi.org/10.1016/j.jconrel.2011.06.044.

(118) Varanko, A. K.; Su, J. C.; Chilkoti, A. Elastin-Like Polypeptides for Biomedical Applications. *Annu. Rev. Biomed. Eng.* **2020**, *22* (1), 343–369. https://doi.org/10.1146/annurev-bioeng-092419-061127.

(119) Huber, M. C.; Schreiber, A.; von Olshausen, P.; Varga, B. R.; Kretz, O.; Joch, B.; Barnert, S.; Schubert, R.; Eimer, S.; Kele, P.; Schiller, S. M. Designer Amphiphilic Proteins as Building Blocks for the Intracellular Formation of Organelle-like Compartments. *Nat. Mater.* **2015**, *14* (1), 125–132. https://doi.org/10.1038/nmat4118.

(120) Schreiber, A.; Huber, M. C.; Schiller, S. M. Prebiotic Protocell Model Based on Dynamic Protein Membranes Accommodating Anabolic Reactions. *Langmuir* **2019**, *35* (29),

9593–9610. https://doi.org/10.1021/acs.langmuir.9b00445.

(121) Schreiber, A.; Stühn, L. G.; Huber, M. C.; Geissinger, S. E.; Rao, A.; Schiller, S. M. Self-Assembly Toolbox of Tailored Supramolecular Architectures Based on an Amphiphilic Protein Library. *Small* **2019**, *15* (30), 1900163. https://doi.org/10.1002/smll.201900163.

(122) Huber, M. C.; Schreiber, A.; Schiller, S. M. Minimalist Protocell Design: A Molecular System Based Solely on Proteins That Form Dynamic Vesicular Membranes Embedding Enzymatic Functions. *ChemBioChem* **2019**, *20* (20), 2618–2632. https://doi.org/10.1002/cbic.201900283.

(123) Caves, J. M.; Cui, W.; Wen, J.; Kumar, V. A.; Haller, C. A.; Chaikof, E. L. Elastin-like Protein Matrix Reinforced with Collagen Microfibers for Soft Tissue Repair. *Biomaterials* **2011**, *32* (23), 5371–5379. https://doi.org/10.1016/j.biomaterials.2011.04.009.

(124) Salinas-Fernández, S.; Santos, M.; Alonso, M.; Quintanilla, L.; Rodríguez-Cabello, J. C. Genetically Engineered Elastin-like Recombinamers with Sequence-Based Molecular Stabilization as Advanced Bioinks for 3D Bioprinting. *Appl. Mater. Today* **2020**, *18*, 100500. https://doi.org/10.1016/j.apmt.2019.100500.

(125) Lin, R.; Yan, X.; Hao, H.; Gao, W.; Liu, R. Introducing Temperature-Controlled Phase Transition Elastin-like Polypeptides to Transient Electronics: Realization of Proactive Biotriggered Electronics with Local Transience. *ACS Appl. Mater. Interfaces* **2019**, *11* (50), 46490–46496. https://doi.org/10.1021/acsami.9b14798.

(126) Duarte Campos, D. F.; Lindsay, C. D.; Roth, J. G.; LeSavage, B. L.; Seymour, A. J.; Krajina, B. A.; Ribeiro, R.; Costa, P. F.; Blaeser, A.; Heilshorn, S. C. Bioprinting Cell- and Spheroid-Laden Protein-Engineered Hydrogels as Tissue-on-Chip Platforms. *Front. Bioeng. Biotechnol.* **2020**, *8*, 374. https://doi.org/10.3389/fbioe.2020.00374.

(127) Bataille, L.; Dieryck, W.; Hocquellet, A.; Cabanne, C.; Bathany, K.; Lecommandoux, S.; Garbay, B.; Garanger, E. Recombinant Production and Purification of Short Hydrophobic Elastin-like Polypeptides with Low Transition Temperatures. *Protein Expr. Purif.* **2016**, *121*, 81–87. https://doi.org/10.1016/J.PEP.2016.01.010.

(128) Huber, M. C.; Schreiber, A.; Wild, W.; Benz, K.; Schiller, S. M. Introducing a Combinatorial DNA-Toolbox Platform Constituting Defined Protein-Based Biohybrid-Materials. *Biomaterials* **2014**, *35* (31), 8767–8779. https://doi.org/10.1016/j.biomaterials.2014.06.048.

(129) MacEwan, S. R.; Chilkoti, A. Applications of Elastin-like Polypeptides in Drug Delivery. *Journal of Controlled Release*. Elsevier B.V. September 28, 2014, pp 314–330. https://doi.org/10.1016/j.jconrel.2014.06.028.

(130) Girotti, A.; Fernández-Colino, A.; López, I. M.; Rodríguez-Cabello, J. C.; Arias, F. J. Elastin-like Recombinamers: Biosynthetic Strategies and Biotechnological

Applications. *Biotechnol. J.* **2011**, *6* (10), 1174–1186. https://doi.org/10.1002/biot.201100116.

(131) Porath, J. Immobilized Metal Ion Affinity Chromatography. *Protein Expression and Purification*. Academic Press August 1, 1992, pp 263–281. https://doi.org/10.1016/1046-5928(92)90001-D.

(132) Bornhorst, J. A.; Falke, J. J. Purification of Proteins Using Polyhistidine Affinity Tags. *Methods in Enzymology*. Academic Press Inc. January 1, 2000, pp 245–254. https://doi.org/10.1016/s0076-6879(00)26058-8.

(133) Gaberc-Porekar, V.; Menart, V. Perspectives of Immobilized-Metal Affinity Chromatography. *Journal of Biochemical and Biophysical Methods*. Elsevier October 30, 2001, pp 335–360. https://doi.org/10.1016/S0165-022X(01)00207-X.

(134) Gutiérrez, R.; Martín del Valle, E. M.; Galán, M. A. Immobilized Metal-Ion Affinity Chromatography: Status and Trends. *Sep. Purif. Rev.* **2007**, *36* (1), 71–111. https://doi.org/10.1080/15422110601166007.

(135) Tamás, M.; Sharma, S.; Ibstedt, S.; Jacobson, T.; Christen, P. Heavy Metals and Metalloids As a Cause for Protein Misfolding and Aggregation. *Biomolecules* **2014**, *4* (1), 252–267. https://doi.org/10.3390/biom4010252.

(136) Urry, D. W. Physical Chemistry of Biological Free Energy Transduction as Demonstrated by Elastic Protein-Based Polymers. *Journal of Physical Chemistry B*. American Chemical Society December 18, 1997, pp 11007–11028. https://doi.org/10.1021/jp972167t.

(137) Li, N. K.; Quiroz, F. G.; Hall, C. K.; Chilkoti, A.; Yingling, Y. G. Molecular Description of the Lcst Behavior of an Elastin-like Polypeptide. *Biomacromolecules* **2014**, *15* (10), 3522–3530. https://doi.org/10.1021/BM500658W/SUPPL_FILE/BM500658W_SI_001.PDF.

(138) Simnick, A. J.; Lim, D. W.; Chow, D.; Chilkoti, A. Biomedical and Biotechnological Applications of Elastin-Like Polypeptides. *Polym. Rev.* **2007**, *47* (1), 121–154. https://doi.org/10.1080/15583720601109594.

(139) Guda, C.; Zhang, X.; McPherson, D. T.; Xu, J.; Cherry, J. H.; Urry, D. W.; Daniell, H. Hyper Expression of an Environmentally Friendly Synthetic Polymer Gene. *Biotechnol. Lett.* **1995**, *17* (7), 745–750. https://doi.org/10.1007/BF00130362.

(140) Meyer, D. E.; Chilkoti, A. Genetically Encoded Synthesis of Protein-Based Polymers with Precisely Specified Molecular Weight and Sequence by Recursive Directional Ligation: Examples from the the Elastin-like Polypeptide System. *Biomacromolecules* **2002**, *3* (2), 357–367. https://doi.org/10.1021/bm015630n.

(141) Singh, A.; Upadhyay, V.; Upadhyay, A. K.; Singh, S. M.; Panda, A. K. Protein Recovery from Inclusion Bodies of Escherichia Coli Using Mild Solubilization Process. *Microbial*

Cell Factories. BioMed Central Ltd. March 25, 2015, p 41. https://doi.org/10.1186/s12934-015-0222-8.

(142) Burgess, R. R. Chapter 17 Refolding Solubilized Inclusion Body Proteins. In *Methods in Enzymology*; Academic Press Inc., 2009; Vol. 463, pp 259–282. https://doi.org/10.1016/S0076-6879(09)63017-2.

(143) Zhao, Y.; Singh, M. K.; Kremer, K.; Cortes-Huerto, R.; Mukherji, D. Why Do Elastin-Like Polypeptides Possibly Have Different Solvation Behaviors in Water-Ethanol and Water-Urea Mixtures? *Macromolecules* **2020**, *53* (6), 2101–2110. https://doi.org/10.1021/acs.macromol.9b02123.

(144) Hassouneh, W.; Christensen, T.; Chilkoti, A. Elastin-Like Polypeptides as a Purification Tag for Recombinant Proteins. In *Current Protocols in Protein Science*; John Wiley & Sons, Inc.: Hoboken, NJ, USA, 2010; Vol. 61, pp 6.11.1-6.11.16. https://doi.org/10.1002/0471140864.ps0611s61.

(145) MacEwan, S. R.; Hassouneh, W.; Chilkoti, A. Non-Chromatographic Purification of Recombinant Elastin-like Polypeptides and Their Fusions with Peptides and Proteins from Escherichia Coli. *J. Vis. Exp.* **2014**, No. 88. https://doi.org/10.3791/51583.

(146) Mills, C. E.; Ding, E.; Olsen, B. Protein Purification by Ethanol-Induced Phase Transitions of the Elastin-like Polypeptide (ELP). *Ind. Eng. Chem. Res.* **2019**, *58* (27), 11698–11709. https://doi.org/10.1021/acs.iecr.9b00769.

(147) McPherson, D. T.; Xu, J.; Urry, D. W. Product Purification by Reversible Phase Transition Following Escherichia Coli Expression of Genes Encoding up to 251 Repeats of the Elastomeric Pentapeptide GVGVP. *Protein Expr. Purif.* **1996**, *7* (1), 51–57. https://doi.org/10.1006/prep.1996.0008.

(148) Trabbic-Carlson, K.; Liu, L.; Kim, B.; Chilkoti, A. Expression and Purification of Recombinant Proteins from Escherichia Coli: Comparison of an Elastin-like Polypeptide Fusion with an Oligohistidine Fusion. *Protein Sci.* **2004**, *13* (12), 3274–3284. https://doi.org/10.1110/PS.04931604.

(149) Kohsakowski, S.; Seiser, F.; Wiederrecht, J. P.; Reichenberger, S.; Vinnay, T.; Barcikowski, S.; Marzun, G. Effective Size Separation of Laser-Generated, Surfactant-Free Nanoparticles by Continuous Centrifugation. *Nanotechnology* **2020**, *31* (9), 095603. https://doi.org/10.1088/1361-6528/ab55bd.

(150) Nagarajan, S.; Chou, S. K.; Cao, S.; Wu, C.; Zhou, Z. An Updated Comprehensive Techno-Economic Analysis of Algae Biodiesel. *Bioresour. Technol.* **2013**, *145*, 150–156. https://doi.org/10.1016/j.biortech.2012.11.108.

(151) Kwan, T. H.; Hu, Y.; Lin, C. S. K. Techno-Economic Analysis of a Food Waste Valorisation Process for Lactic Acid, Lactide and Poly(Lactic Acid) Production. *J. Clean. Prod.* **2018**, *181*, 72–87. https://doi.org/10.1016/j.jclepro.2018.01.179.

(152) Ge, X.; Trabbic-Carlson, K.; Chilkoti, A.; Filipe, C. D. M. Purification of an Elastin-like Fusion Protein by Microfiltration. *Biotechnol. Bioeng.* **2006**, *95* (3), 424–432. https://doi.org/10.1002/bit.21046.

(153) Verheul, R.; Sweet, C.; Thompson, D. H. Rapid and Simple Purification of Elastin-like Polypeptides Directly from Whole Cells and Cell Lysates by Organic Solvent Extraction. *Biomater. Sci.* **2018**, *6* (4), 863–876. https://doi.org/10.1039/c8bm00124c.

(154) Kokhan, O.; Marzolf, D. R. Detection and Quantification of Transition Metal Leaching in Metal Affinity Chromatography with Hydroxynaphthol Blue. *Anal. Biochem.* **2019**, *582* (March), 113347. https://doi.org/10.1016/j.ab.2019.113347.

(155) Swaim, C. M.; Brittain, T. J.; Marzolf, D. R.; Kokhan, O. Quantification of Metal Leaching in Immobilized Metal Affinity Chromatography. *J. Vis. Exp.* **2019**, *2020* (155), 1–7. https://doi.org/10.3791/60690.

(156) Fong, B. A.; Wood, D. W. Expression and Purification of ELP-Intein-Tagged Target Proteins in High Cell Density E. Coli Fermentation. *Microb. Cell Fact.* **2010**, *9* (1), 1–11. https://doi.org/10.1186/1475-2859-9-77/TABLES/4.

(157) Floss, D. M.; Schallau, K.; Rose-John, S.; Conrad, U.; Scheller, J. Elastin-like Polypeptides Revolutionize Recombinant Protein Expression and Their Biomedical Application. *Trends in Biotechnology*. Elsevier Current Trends January 1, 2010, pp 37–45. https://doi.org/10.1016/j.tibtech.2009.10.004.

(158) Fong, B. A.; Wu, W. Y.; Wood, D. W. Optimization of ELP-Intein Mediated Protein Purification by Salt Substitution. *Protein Expr. Purif.* **2009**, *66* (2), 198–202. https://doi.org/10.1016/j.pep.2009.03.009.

(159) Kostal, J.; Mulchandani, A.; Gropp, K. E.; Chen, W. A Temperature Responsive Biopolymer for Mercury Remediation. *Environ. Sci. Technol.* **2003**, *37* (19), 4457–4462. https://doi.org/10.1021/ES034210Y/ASSET/IMAGES/LARGE/ES034210YF00005.JPEG.

(160) Prabhukumar, G.; Matsumoto, M.; Mulchandani, A.; Chen, W. Cadmium Removal from Contaminated Soil by Tunable Biopolymers. *Environ. Sci. Technol.* **2004**, *38* (11), 3148–3152. https://doi.org/10.1021/ES035150Z.

(161) Wang, E.; Lee, S. H.; Lee, S. W. Elastin-like Polypeptide Based Hydroxyapatite Bionanocomposites. *Biomacromolecules* **2011**, *12* (3), 672–680. https://doi.org/10.1021/BM101322M/SUPPL_FILE/BM101322M_SI_002.AVI.

(162) Dhandhukia, J.; Weitzhandler, I.; Wang, W.; MacKay, J. A. Switchable Elastin-like Polypeptides That Respond to Chemical Inducers of Dimerization. *Biomacromolecules* **2013**, *14* (4), 976–985. https://doi.org/10.1021/BM301558Q/SUPPL_FILE/BM301558Q_SI_001.PDF.

(163) Hassouneh, W.; Nunalee, M. L.; Shelton, M. C.; Chilkoti, A. Calcium Binding Peptide Motifs from Calmodulin Confer Divalent Ion Selectivity to Elastin-like Polypeptides. *Biomacromolecules* **2013**, *14* (7), 2347–2353. https://doi.org/10.1021/BM400464S/SUPPL_FILE/BM400464S_SI_001.PDF.

(164) Ross Hallett, F. Particle Size Analysis by Dynamic Light Scattering. *Food Res. Int.* **1994**, *27* (2), 195–198. https://doi.org/10.1016/0963-9969(94)90162-7.

(165) Hiroi, T.; Shibayama, M. Measurement of Particle Size Distribution in Turbid Solutions by Dynamic Light Scattering Microscopy. *J. Vis. Exp.* **2017**, *2017* (119). https://doi.org/10.3791/54885.

(166) Despanie, J.; Dhandhukia, J. P.; Hamm-Alvarez, S. F.; MacKay, J. A. Elastin-like Polypeptides: Therapeutic Applications for an Emerging Class of Nanomedicines. *J. Control. Release* **2016**, *240*, 93–108. https://doi.org/10.1016/j.jconrel.2015.11.010.

(167) Dong Woo Lim; Kimberly Trabbic-Carlson; J. Andrew MacKay, A.; Chilkoti*, A. Improved Non-Chromatographic Purification of a Recombinant Protein by Cationic Elastin-like Polypeptides. **2007**. https://doi.org/10.1021/BM060849T.

(168) Murphy, J. C.; Jewell, D. L.; White, K. I.; Fox, G. E.; Willson, R. C. Nucleic Acid Separations Utilizing Immobilized Metal Affinity Chromatography. *Biotechnol. Prog.* **2003**, *19* (3), 982–986. https://doi.org/10.1021/bp025563o.

(169) Alemán, J.; Chadwick, A. V.; He, J.; Hess, M.; Horie, K.; Jones, R. G.; Kratochvíl, P.; Meisel, I.; Mita, I.; Moad, G.; Penczek, S.; Stepto, R. F. T. Definitions of Terms Relating to the Structure and Processing of Sols, Gels, Networks, and Inorganic-Organic Hybrid Materials (IUPAC Recommendations 2007). *Pure Appl. Chem.* **2007**, *79* (10), 1801–1829. https://doi.org/10.1351/pac200779101801.

(170) Wichterle, O.; Lím, D. Hydrophilic Gels for Biological Use. *Nature* **1960**, *185* (4706), 117–118. https://doi.org/10.1038/185117a0.

(171) Van Vlierberghe, S.; Dubruel, P.; Schacht, E. Biopolymer-Based Hydrogels as Scaffolds for Tissue Engineering Applications: A Review. *Biomacromolecules*. American Chemical Society May 9, 2011, pp 1387–1408. https://doi.org/10.1021/bm200083n.

(172) Elzoghby, A. O.; Abo El-Fotoh, W. S.; Elgindy, N. A. Casein-Based Formulations as Promising Controlled Release Drug Delivery Systems. *Journal of Controlled Release*. 2011. https://doi.org/10.1016/j.jconrel.2011.02.010.

(173) Jonker, A. M.; Löwik, D. W. P. M.; van Hest, J. C. M. Peptide- and Protein-Based Hydrogels. *Chem. Mater.* **2012**, *24* (5), 759–773. https://doi.org/10.1021/cm202640w.

(174) Yan, H.; Saiani, A.; Gough, J. E.; Miller, A. F. Thermoreversible Protein Hydrogel as Cell Scaffold. *Biomacromolecules* **2006**, *7* (10), 2776–2782. https://doi.org/10.1021/bm0605560.

(175) Chien, K. B.; Chung, E. J.; Shah, R. N. Investigation of Soy Protein Hydrogels for Biomedical Applications: Materials Characterization, Drug Release, and Biocompatibility. *J. Biomater. Appl.* **2014**, *28* (7), 1085–1096. https://doi.org/10.1177/0885328213497413.

(176) Maltais, A.; Remondetto, G. E.; Subirade, M. Soy Protein Cold-Set Hydrogels as Controlled Delivery Devices for Nutraceutical Compounds. *Food Hydrocoll.* **2009**, *23* (7), 1647–1653. https://doi.org/10.1016/j.foodhyd.2008.12.006.

(177) Akkermans, C.; Venema, P.; van der Goot, A. J.; Gruppen, H.; Bakx, E. J.; Boom, R. M.; van der Linden, E. Peptides Are Building Blocks of Heat-Induced Fibrillar Protein Aggregates of β-Lactoglobulin Formed at PH 2. *Biomacromolecules* **2008**, *9* (5), 1474–1479. https://doi.org/10.1021/bm7014224.

(178) Gosal, W. S.; Clark, A. H.; Ross-Murphy, S. B. Fibrillar β-Lactoglobulin Gels: Part 1. Fibril Formation and Structure. *Biomacromolecules* **2004**, *5* (6), 2408–2419. https://doi.org/10.1021/bm049659d.

(179) Remondetto, G. E.; Paquin, P.; Subirade, M. Cold Gelation of β-Lactoglobulin in the Presence of Iron. *J. Food Sci.* **2002**, *67* (2), 586–595. https://doi.org/10.1111/j.1365-2621.2002.tb10643.x.

(180) Lu, S.; Zhu, L.; Wang, Q.; Liu, Z.; Tang, C.; Sun, H.; Yang, J.; Qin, G.; Sun, G.; Chen, Q. High-Strength Albumin Hydrogels With Hybrid Cross-Linking. *Front. Chem.* **2020**, *8*, 106. https://doi.org/10.3389/fchem.2020.00106.

(181) Sakai, S.; Kamei, H.; Mori, T.; Hotta, T.; Ohi, H.; Nakahata, M.; Taya, M. Visible Light-Induced Hydrogelation of an Alginate Derivative and Application to Stereolithographic Bioprinting Using a Visible Light Projector and Acid Red. *Biomacromolecules* **2018**, *19* (2), 672–679. https://doi.org/10.1021/acs.biomac.7b01827.

(182) Andersen, S. O. The Cross-Links in Resilin Identified as Dityrosine and Trityrosine. *BBA - Gen. Subj.* **1964**, *93* (1), 213–215. https://doi.org/10.1016/0304-4165(64)90289-2.

(183) Partlow, B. P.; Applegate, M. B.; Omenetto, F. G.; Kaplan, D. L. Dityrosine Cross-Linking in Designing Biomaterials. *ACS Biomater. Sci. Eng.* **2016**, *2* (12), 2108–2121. https://doi.org/10.1021/acsbiomaterials.6b00454.

(184) Ding, Y.; Li, Y.; Qin, M.; Cao, Y.; Wang, W. Photo-Cross-Linking Approach to Engineering Small Tyrosine-Containing Peptide Hydrogels with Enhanced Mechanical Stability. *Langmuir* **2013**, *29* (43), 13299–13306. https://doi.org/10.1021/la4029639.

(185) Elvin, C. M.; Vuocolo, T.; Brownlee, A. G.; Sando, L.; Huson, M. G.; Liyou, N. E.; Stockwell, P. R.; Lyons, R. E.; Kim, M.; Edwards, G. A.; Johnson, G.; McFarland, G. A.; Ramshaw, J. A. M.; Werkmeister, J. A. A Highly Elastic Tissue Sealant Based on Photopolymerised Gelatin. *Biomaterials* **2010**, *31* (32), 8323–8331. https://doi.org/10.1016/j.biomaterials.2010.07.032.

(186) Aufderhorst-Roberts, A.; Hughes, M. D. G.; Hare, A.; Head, D. A.; Kapur, N.; Brockwell, D. J.; Dougan, L. Reaction Rate Governs the Viscoelasticity and Nanostructure of Folded Protein Hydrogels. *Biomacromolecules* **2020**, *21* (10), 4253–4260. https://doi.org/10.1021/acs.biomac.0c01044.

(187) Amrhein, S.; Bauer, K. C.; Galm, L.; Hubbuch, J. Non-Invasive High Throughput Approach for Protein Hydrophobicity Determination Based on Surface Tension. *Biotechnol. Bioeng.* **2015**, *112* (12), 2485–2494. https://doi.org/10.1002/bit.25677.

(188) Taha, M.; Gupta, B. S.; Khoiroh, I.; Lee, M. J. Interactions of Biological Buffers with Macromolecules: The Ubiquitous "Smart" Polymer PNIPAM and the Biological Buffers MES, MOPS, and MOPSO. *Macromolecules* **2011**, *44* (21), 8575–8589. https://doi.org/10.1021/ma201790c.

(189) Gupta, B. S.; Taha, M.; Lee, M. J. Interactions of Bovine Serum Albumin with Biological Buffers, TES, TAPS, and TAPSO in Aqueous Solutions. *Process Biochem.* **2013**, *48* (11), 1686–1696. https://doi.org/10.1016/j.procbio.2013.08.018.

(190) Udabage, P.; McKinnon, I. R.; Augustin, M. A. Mineral and Casein Equilibria in Milk: Effects of Added Salts and Calcium-Chelating Agents. *J. Dairy Res.* **2000**, *67* (3), 361–370. https://doi.org/10.1017/S0022029900004271.

(191) Haller, H. S.; Pallansch, M. J. The Solubility in Aqueous Urea Solutions of the Micellar Caseinates of Milk and Milk Products Subjected to Various Sterilizing Heat Treatments. *J. Dairy Sci.* **1960**, *43* (10), 1407–1413. https://doi.org/10.3168/JDS.S0022-0302(60)90342-8.

(192) Almdal, K.; Dyre, J.; Hvidt, S.; Kramer, O. Towards a Phenomenological Definition of the Term "Gel." *Polym. Gels Networks* **1993**, *1* (1), 5–17. https://doi.org/10.1016/0966-7822(93)90020-I.

(193) Joshi, N. S.; Whitaker, L. R.; Francis, M. B. A Three-Component Mannich-Type Reaction for Selective Tyrosine Bioconjugation. *J. Am. Chem. Soc.* **2004**, *126* (49), 15942–15943. https://doi.org/10.1021/ja0439017.

(194) Nnyigide, O. S.; Lee, S. G.; Hyun, K. Exploring the Differences and Similarities between Urea and Thermally Driven Denaturation of Bovine Serum Albumin: Intermolecular Forces and Solvation Preferences. *J. Mol. Model.* **2018**, *24* (3), 1–15. https://doi.org/10.1007/s00894-018-3622-y.

(195) Fu, L.; Li, L.; Xue, B.; Jin, J.; Cao, Y.; Jiang, Q.; Li, H. Converting Muscle-Mimetic Biomaterials to Cartilage-like Materials. *bioRxiv* **2021**, 2021.05.18.444710. https://doi.org/10.1101/2021.05.18.444710.

(196) Monera, O. D.; Kay, C. M.; Hodges, R. S. Protein Denaturation with Guanidine Hydrochloride or Urea Provides a Different Estimate of Stability Depending on the Contributions of Electrostatic Interactions. *Protein Sci.* **1994**, *3* (11), 1984. https://doi.org/10.1002/PRO.5560031110.

(197) Gu, J.; Guo, Y.; Li, Y.; Wang, J.; Wang, W.; Cao, Y.; Xue, B. Tuning Strain Stiffening of Protein Hydrogels by Charge Modification. *Int. J. Mol. Sci.* **2022**, *23* (6), 3032. https://doi.org/10.3390/IJMS23063032.

(198) Park, H. Y.; Song, I. H.; Kim, J. H.; Kim, W. S. Preparation of Thermally Denatured Albumin Gel and Its PH-Sensitive Swelling. *Int. J. Pharm.* **1998**, *175* (2), 231–236. https://doi.org/10.1016/S0378-5173(98)00289-0.

(199) Brown, P. R.; Grushka, E.; Lunte, S. *Advances in Chromatography*; 2004; Vol. 43. https://doi.org/10.1201/9780203996959.

(200) Josuran, R. Prot pi https://www.protpi.ch/Calculator/ProteinTool.

(201) Fox, P. F. Milk Proteins: General and Historical Aspects. In *Advanced Dairy Chemistry---1 Proteins: Part A / Part B*; Fox, P. F., McSweeney, P. L. H., Eds.; Springer US: Boston, MA, 2003; pp 1–48. https://doi.org/10.1007/978-1-4419-8602-3_1.

(202) Chang, C.; He, M.; Zhou, J.; Zhang, L. Swelling Behaviors of PH- and Salt-Responsive Cellulose-Based Hydrogels. *Macromolecules* **2011**, *44* (6), 1642–1648. https://doi.org/10.1021/ma102801f.

(203) Goh, K. B.; Li, H.; Lam, K. Y. Development of a Multiphysics Model to Characterize the Responsive Behavior of Urea-Sensitive Hydrogel as Biosensor. *Biosens. Bioelectron.* **2017**, *91*, 673–679. https://doi.org/10.1016/j.bios.2017.01.023.

(204) Swaisgood, H. E. Chemistry of the Caseins. In *Advanced Dairy Chemistry---1 Proteins: Part A / Part B*; Fox, P. F., McSweeney, P. L. H., Eds.; Springer US: Boston, MA, 2003; pp 139–201. https://doi.org/10.1007/978-1-4419-8602-3_3.

(205) Kunz, C.; Lönnerdal, B. Casein and Casein Subunits in Preterm Milk, Colostrum, and Mature Human Milk. *J. Pediatr. Gastroenterol. Nutr.* **1990**, *10* (4), 454–461. https://doi.org/10.1097/00005176-199005000-00007.

(206) Gekko, K.; Hasegawa, Y. Compressibility-Structure Relationship of Globular Proteins. *Biochemistry* **1986**, *25* (21), 6563–6571. https://doi.org/10.1021/BI00369A034/ASSET/BI00369A034.FP.PNG_V03.

(207) Frandsen, J. L.; Ghandehari, H. Recombinant Protein-Based Polymers for Advanced Drug Delivery. *Chem. Soc. Rev.* **2012**, *41* (7), 2696–2706. https://doi.org/10.1039/C2CS15303C.

(208) Wang, Y.; Katyal, P.; Montclare, J. K. Protein-Engineered Functional Materials. *Adv. Healthc. Mater.* **2019**, *8* (11), 1801374. https://doi.org/10.1002/ADHM.201801374.

(209) Acosta, S.; Quintanilla-Sierra, L.; Mbundi, L.; Reboto, V.; Rodríguez-Cabello, J. C. Elastin-Like Recombinamers: Deconstructing and Recapitulating the Functionality of Extracellular Matrix Proteins Using Recombinant Protein Polymers. *Adv. Funct. Mater.* **2020**, *30* (44), 1909050. https://doi.org/10.1002/ADFM.201909050.

(210) Katyal, P.; Mahmoudinobar, F.; Montclare, J. K. Recent Trends in Peptide and Protein-Based Hydrogels. *Curr. Opin. Struct. Biol.* **2020**, *63*, 97–105. https://doi.org/10.1016/J.SBI.2020.04.007.

(211) Huber, M. C.; Jonas, U.; Schiller, S. M. An Autonomous Chemically Fueled Artificial Protein Muscle. *Adv. Intell. Syst.* **2022**, *4* (4), 2100189. https://doi.org/10.1002/AISY.202100189.

(212) Duan, T.; Li, H. In Situ Phase Transition of Elastin-Like Polypeptide Chains Regulates Thermoresponsive Properties of Elastomeric Protein-Based Hydrogels. *Biomacromolecules* **2020**, *21* (6), 2258–2267. https://doi.org/10.1021/ACS.BIOMAC.0C00206/ASSET/IMAGES/LARGE/BM0C00206_0005.JPEG.

(213) Haas, S.; Körner, S.; Zintel, L.; Hubbuch, J. Changing Mechanical Properties of Photopolymerized, Dityrosine-Crosslinked Protein-Based Hydrogels. *Front. Bioeng. Biotechnol.* **2022**, *0*, 1716. https://doi.org/10.3389/FBIOE.2022.1006438.

(214) Zhang, D.; Peng, H.; Sun, B.; Lyu, S. High Water Content Silk Protein-Based Hydrogels with Tunable Elasticity Fabricated via a Ru(II) Mediated Photochemical Cross-Linking Method. *Fibers Polym.* **2017**, *18* (10), 1831–1840. https://doi.org/10.1007/S12221-017-7463-6.

(215) Yang, Y. J.; Choi, Y. S.; Cha, H. J. Bioinspired Load-Bearing Hydrogel Based on Engineered Sea Anemone Skin-Derived Collagen-Like Protein. *Biotechnol. J.* **2018**, *13* (12), 1800086. https://doi.org/10.1002/BIOT.201800086.

(216) Haas, S.; Desombre, M.; Kirschhöfer, F.; Huber, M. C.; Schiller, S. M.; Hubbuch, J. Purification of a Hydrophobic Elastin-Like Protein Toward Scale-Suitable Production of Biomaterials. *Front. Bioeng. Biotechnol.* **2022**, *0*, 902. https://doi.org/10.3389/FBIOE.2022.878838.

(217) Nazmi, A. R.; Reinisch, T.; Hinz, H. J. Ca-Binding to Bacillus Licheniformis α-Amylase (BLA). *Arch. Biochem. Biophys.* **2006**, *453* (1), 18–25. https://doi.org/10.1016/J.ABB.2006.04.004.

(218) Zhang, Z.; Dmitrieva, N. I.; Park, J. H.; Levine, R. L.; Burg, M. B. High Urea and NaCl Carbonylate in Renal Cells in Culture and in Vivo, and High Urea Causes 8-Oxoguanine Lesions in Their DNA. *Proc. Natl. Acad. Sci. U. S. A.* **2004**, *101* (25), 9491–9496. https://doi.org/10.1073/PNAS.0402961101.

(219) Michea, L.; Ferguson, D. R.; Peters, E. M.; Andrews, P. M.; Kirby, M. R.; Burg, M. B. Cell Cycle Delay and Apoptosis Are Induced by High Salt and Urea in Renal Medullary Cells. *Am. J. Physiol. - Ren. Physiol.* **2000**, *278* (2 47-2). https://doi.org/10.1152/AJPRENAL.2000.278.2.F209/ASSET/IMAGES/LARGE/AFLU20201007W.JPEG.

(220) Oveissi, F.; Fletcher, D. F.; Dehghani, F.; Naficy, S. Tough Hydrogels for Soft Artificial

Muscles. *Mater. Des.* **2021**, *203*, 109609. https://doi.org/10.1016/J.MATDES.2021.109609.

(221) Ren, X.; Das, R.; Tran, P.; Ngo, T. D.; Xie, Y. M. Auxetic Metamaterials and Structures: A Review. *Smart Mater. Struct.* **2018**, *27* (2), 023001. https://doi.org/10.1088/1361-665X/AAA61C.

(222) Prawoto, Y. Seeing Auxetic Materials from the Mechanics Point of View: A Structural Review on the Negative Poisson's Ratio. *Comput. Mater. Sci.* **2012**, *58*, 140–153. https://doi.org/10.1016/J.COMMATSCI.2012.02.012.

(223) Warner, J. J.; Gillies, A. R.; Hwang, H. H.; Zhang, H.; Lieber, R. L.; Chen, S. 3D-Printed Biomaterials with Regional Auxetic Properties. *J. Mech. Behav. Biomed. Mater.* **2017**, *76*, 145–152. https://doi.org/10.1016/J.JMBBM.2017.05.016.

(224) Bertlein, S.; Brown, G.; Lim, K. S.; Jungst, T.; Boeck, T.; Blunk, T.; Tessmar, J.; Hooper, G. J.; F Woodfield, T. B.; Groll, J.; Bertlein, S.; Jungst, T.; Boeck, T.; Tessmar, J.; Groll, J.; Brown, G.; Lim, K. S.; Hooper, G. J.; F Woodfield, T. B.; Blunk, T. Thiol–Ene Clickable Gelatin: A Platform Bioink for Multiple 3D Biofabrication Technologies. *Adv. Mater.* **2017**, *29* (44), 1703404. https://doi.org/10.1002/ADMA.201703404.

(225) Kim, H.; Kang, B.; Cui, X.; Lee, S. H.; Lee, K.; Cho, D. W.; Hwang, W.; Woodfield, T. B. F.; Lim, K. S.; Jang, J. Light-Activated Decellularized Extracellular Matrix-Based Bioinks for Volumetric Tissue Analogs at the Centimeter Scale. *Adv. Funct. Mater.* **2021**, *31* (32), 2011252. https://doi.org/10.1002/ADFM.202011252.

(226) Dorishetty, P.; Balu, R.; Athukoralalage, S. S.; Greaves, T. L.; Mata, J.; De Campo, L.; Saha, N.; Zannettino, A. C. W.; Dutta, N. K.; Choudhury, N. R. Tunable Biomimetic Hydrogels from Silk Fibroin and Nanocellulose. *ACS Sustain. Chem. Eng.* **2020**, *8* (6), 2375–2389. https://doi.org/10.1021/ACSSUSCHEMENG.9B05317/ASSET/IMAGES/LARGE/SC9B05317_0009.JPEG.

(227) Dorishetty, P.; Balu, R.; Gelmi, A.; Mata, J. P.; Dutta, N. K.; Choudhury, N. R. 3D Printable Soy/Silk Hybrid Hydrogels for Tissue Engineering Applications. *Biomacromolecules* **2021**, *22* (9), 3668–3678. https://doi.org/10.1021/ACS.BIOMAC.1C00250/ASSET/IMAGES/LARGE/BM1C00250_0010.JPEG.

(228) Spikes, J. D.; Shen, H. R.; Kopečková, P.; Kopeček, J. Photodynamic Crosslinking of Proteins. III. Kinetics of the FMN- and Rose Bengal-Sensitized Photooxidation and Intermolecular Crosslinking of Model Tyrosine-Containing N-(2-Hydroxypropyl)Methacrylamide Copolymers. *Photochem. Photobiol.* **1999**, *70* (2), 130–137. https://doi.org/10.1111/J.1751-1097.1999.TB07980.X.

(229) Donnelly, P. E.; Chen, T.; Finch, A.; Brial, C.; Maher, S. A.; Torzilli, P. A. Photocrosslinked Tyramine-Substituted Hyaluronate Hydrogels with Tunable Mechanical Properties Improve Immediate Tissue-Hydrogel Interfacial Strength in Articular Cartilage. *J. Biomater. Sci. Polym. Ed.* **2017**, *28* (6), 582–600.

https://doi.org/10.1080/09205063.2017.1289035/SUPPL_FILE/TBSP_A_1289035_SM7800.DOCX.

(230) Lavker, R.; Kaidbey, K. The Spectral Dependence for UVA-Induced Cumulative Damage in Human Skin. *J. Invest. Dermatol.* **1997**, *108* (1), 17–21. https://doi.org/10.1111/1523-1747.EP12285613.

(231) Urushibara, A.; Kodama, S.; Yokoya, A. Induction of Genetic Instability by Transfer of a UV-A-Irradiated Chromosome. *Mutat. Res. Toxicol. Environ. Mutagen.* **2014**, *766*, 29–34. https://doi.org/10.1016/J.MRGENTOX.2014.02.005.

(232) Rapuano, P. B.; Scanameo, A. H.; Amponin, D. E.; Paulose, S. A.; Zyablitskaya, M.; Takaoka, A.; Suh, L. H.; Nagasaki, T.; Trokel, S. L.; Paik, D. C. Antimicrobial Studies Using the Therapeutic Tissue Cross-Linking Agent, Sodium Hydroxymethylglycinate: Implication for Treating Infectious Keratitis. *Invest. Ophthalmol. Vis. Sci.* **2018**, *59* (1), 332–337. https://doi.org/10.1167/IOVS.17-23111.

(233) Mobaraki, M.; Ghaffari, M.; Yazdanpanah, A.; Luo, Y.; Mills, D. K. Bioinks and Bioprinting: A Focused Review. *Bioprinting*. Elsevier B.V. June 1, 2020, p e00080. https://doi.org/10.1016/j.bprint.2020.e00080.

(234) Cidonio, G.; Alcala-Orozco, C. R.; Lim, K. S.; Glinka, M.; Mutreja, I.; Kim, Y. H.; Dawson, J. I.; Woodfield, T. B. F.; Oreffo, R. O. C. Osteogenic and Angiogenic Tissue Formation in High Fidelity Nanocomposite Laponite-Gelatin Bioinks. *Biofabrication* **2019**, *11* (3), 035027. https://doi.org/10.1088/1758-5090/AB19FD.

(235) Colosi, C.; Shin, S. R.; Manoharan, V.; Massa, S.; Costantini, M.; Barbetta, A.; Dokmeci, R.; Dentini, M.; Khademhosseini, A.; Khademhosseini, A.; Khademhosseini, H. A.-; Colosi, C.; Costantini, M.; Barbetta, A.; Dentini, M.; Shin, S. R.; Dokmeci, M. R.; Massa, S. Microfluidic Bioprinting of Heterogeneous 3D Tissue Constructs Using Low-Viscosity Bioink. *Adv. Mater.* **2016**, *28* (4), 677–684. https://doi.org/10.1002/ADMA.201503310.

(236) Lim, K. S.; Levato, R.; Costa, P. F.; Castilho, M. D.; Alcala-Orozco, C. R.; Van Dorenmalen, K. M. A.; Melchels, F. P. W.; Gawlitta, D.; Hooper, G. J.; Malda, J.; Woodfield, T. B. F. Bio-Resin for High Resolution Lithography-Based Biofabrication of Complex Cell-Laden Constructs. *Biofabrication* **2018**, *10* (3), 034101. https://doi.org/10.1088/1758-5090/AAC00C.

(237) Alcala-Orozco, C. R.; Mutreja, I.; Cui, X.; Kumar, D.; Hooper, G. J.; Lim, K. S.; Woodfield, T. B. F. Design and Characterisation of Multi-Functional Strontium-Gelatin Nanocomposite Bioinks with Improved Print Fidelity and Osteogenic Capacity. *Bioprinting* **2020**, *18*, e00073. https://doi.org/10.1016/J.BPRINT.2019.E00073.

(238) Cui, X.; Soliman, B. G.; Alcala-Orozco, C. R.; Li, J.; Vis, M. A. M.; Santos, M.; Wise, S. G.; Levato, R.; Malda, J.; Woodfield, T. B. F.; Rnjak-Kovacina, J.; Lim, K. S. Rapid Photocrosslinking of Silk Hydrogels with High Cell Density and Enhanced Shape Fidelity. *Adv. Healthc. Mater.* **2020**, *9* (4), 1901667. https://doi.org/10.1002/ADHM.201901667.

(239) Smith, P. T.; Narupai, B.; Tsui, J. H.; Millik, S. C.; Shafranek, R. T.; Kim, D. H.; Nelson, A. Additive Manufacturing of Bovine Serum Albumin-Based Hydrogels and Bioplastics. *Biomacromolecules* **2020**, *21* (2), 484–492. https://doi.org/10.1021/acs.biomac.9b01236.

(240) Chen, Z.; Zhao, D.; Liu, B.; Nian, G.; Li, X.; Yin, J.; Qu, S.; Yang, W. 3D Printing of Multifunctional Hydrogels. *Adv. Funct. Mater.* **2019**, *29* (20), 1900971. https://doi.org/10.1002/adfm.201900971.

(241) Schmieg, B.; Schimek, A.; Franzreb, M. Development and Performance of a 3D-Printable Poly(Ethylene Glycol) Diacrylate Hydrogel Suitable for Enzyme Entrapment and Long-Term Biocatalytic Applications. *Eng. Life Sci.* **2018**, *18* (9), 659–667. https://doi.org/10.1002/elsc.201800030.

(242) Zhang, Y.; Sun, M.; Liu, T.; Hou, M.; Yang, H. Effect of Different Additives on the Mechanical Properties of Gelatin Methacryloyl Hydrogel: A Meta-Analysis. *ACS Omega* **2021**, *6* (13), 9112–9128. https://doi.org/10.1021/ACSOMEGA.1C00244/ASSET/IMAGES/LARGE/AO1C00244_0023.JPEG.

(243) Carp, D. J.; Bartholomai, G. B.; Relkin, P.; Pilosofl, A. M. R. Effects of Denaturation on Soy Protein–Xanthan Interactions: Comparison of a Whipping–Rheological and a Bubbling Method. *Colloids Surfaces B Biointerfaces* **2001**, *21* (1–3), 163–171. https://doi.org/10.1016/S0927-7765(01)00169-2.

(244) Katzbauer, B. Properties and Applications of Xanthan Gum. *Polym. Degrad. Stab.* **1998**, *59* (1–3), 81–84. https://doi.org/10.1016/S0141-3910(97)00180-8.

(245) Deuteron GmbH. Deuteron VT 819 https://deuteron.com/wp-content/uploads/pdf-tech/Deuteron-VT-819-UK.pdf.

(246) Willenbacher, N. Unusual Thixotropic Properties of Aqueous Dispersions of Laponite RD. *J. Colloid Interface Sci.* **1996**, *182* (2), 501–510. https://doi.org/10.1006/JCIS.1996.0494.

(247) Mukerjee, P.; Ghosh, A. K. THE EFFECT OF UREA ON METHYLENE BLUE, ITS SELF-ASSOCIATION, AND INTERACTION WITH POLYELECTROLYTES IN AQUEOUS SOLUTION. *J. Phys. Chem.* **2002**, *67* (1), 193–197. https://doi.org/10.1021/J100795A047.

(248) BASF SE. Product selection guide - Additives https://dispersions-resins-products.basf.us/files/brochures/BASF-Catalog_North-America_02_letter_SP.pdf.

(249) Mudgil, D.; Barak, S.; Khatkar, B. S. Guar Gum: Processing, Properties and Food Applications - A Review. *J. Food Sci. Technol.* **2014**, *51* (3), 409–418. https://doi.org/10.1007/S13197-011-0522-X/TABLES/3.

(250) Contessi Negrini, N.; Bonetti, L.; Contili, L.; Farè, S. 3D Printing of Methylcellulose-Based Hydrogels. *Bioprinting* **2018**, *10*, e00024. https://doi.org/10.1016/J.BPRINT.2018.E00024.

(251) Sannino, A.; Demitri, C.; Madaghiele, M. Biodegradable Cellulose-Based Hydrogels: Design and Applications. *Materials (Basel).* **2009**, *2* (2), 353–373. https://doi.org/10.3390/MA2020353.

(252) Draget, K. I.; Skjåk-Bræk, G.; Stokke, B. T. Similarities and Differences between Alginic Acid Gels and Ionically Crosslinked Alginate Gels. *Food Hydrocoll.* **2006**, *20* (2–3), 170–175. https://doi.org/10.1016/J.FOODHYD.2004.03.009.

(253) Strauß, S.; Meutelet, R.; Radosevic, L.; Gretzinger, S.; Hubbuch, J. Image Analysis as PAT-Tool for Use in Extrusion-Based Bioprinting. *Bioprinting* **2020**, *21* (November 2020), e00112. https://doi.org/10.1016/j.bprint.2020.e00112.

(254) Mohanan, A.; Nickerson, M. T.; Ghosh, S. Utilization of Pulse Protein-Xanthan Gum Complexes for Foam Stabilization: The Effect of Protein Concentrate and Isolate at Various PH. *Food Chem.* **2020**, *316*, 126282. https://doi.org/10.1016/J.FOODCHEM.2020.126282.

(255) Borcherding, K.; Lorenzen, P. C. H. R.; Hoffmann, W. Effect of Protein Content, Casein–Whey Protein Ratio and PH Value on the Foaming Properties of Skimmed Milk. *Int. J. Dairy Technol.* **2009**, *62* (2), 161–169. https://doi.org/10.1111/J.1471-0307.2009.00472.X.

(256) Alcântara, L. A. P.; Amaral, I. V.; Bonomo, R. C. F.; Da Silva, L. H. M.; Do Carmo Hespanhol Da Silva, M.; Minim, V. P. R.; Minim, L. A. Partitioning of α-Lactalbumin and β-Lactoglobulin from Cheese Whey in Aqueous Two-Phase Systems Containing Poly (Ethylene Glycol) and Sodium Polyacrylate. *Food Bioprod. Process.* **2014**, *92* (4), 409–415. https://doi.org/10.1016/J.FBP.2013.09.006.

(257) Johansson, H. O.; Magaldi, F. M.; Feitosa, E.; Pessoa, A. Protein Partitioning in Poly(Ethylene Glycol)/Sodium Polyacrylate Aqueous Two-Phase Systems. *J. Chromatogr. A* **2008**, *1178* (1–2), 145–153. https://doi.org/10.1016/J.CHROMA.2007.11.071.

(258) Ibrahim, M. S.; Rogers, S.; Mahmoudy, N.; Murray, M.; Szczygiel, A.; Green, B.; Alexander, B. D.; Griffiths, P. C. Surfactant Modulated Interaction of Hydrophobically Modified Ethoxylated Urethane (HEUR) Polymers with Impenetrable Surfaces. *J. Colloid Interface Sci.* **2019**, *539*, 126–134. https://doi.org/10.1016/J.JCIS.2018.12.059.

(259) Kostansek, E. Using Dispersion/Flocculation Phase Diagrams to Visualize Interactions of Associative Polymers, Latexes, and Surfactants. *J. Coatings Technol. 2003 75940* **2003**, *75* (940), 1–8. https://doi.org/10.1007/BF02720511.

(260) Kabziński, M.; Neupauer, K.; Nowak, M.; Kruk, J.; Kaczmarczyk, K. The Impact of Addition of Xanthan Gum and Guar Gum on Rheological Properties of Foams Produced

by Continuous Method. *Polimery* **2019**, *64* (7–8), 538–541. https://doi.org/10.14314/POLIMERY.2019.7.11.

(261) Gopinathan, J.; Noh, I. Recent Trends in Bioinks for 3D Printing. *Biomater. Res. 2018 221* **2018**, *22* (1), 1–15. https://doi.org/10.1186/S40824-018-0122-1.

(262) Jia, W.; Gungor-Ozkerim, P. S.; Zhang, Y. S.; Yue, K.; Zhu, K.; Liu, W.; Pi, Q.; Byambaa, B.; Dokmeci, M. R.; Shin, S. R.; Khademhosseini, A. Direct 3D Bioprinting of Perfusable Vascular Constructs Using a Blend Bioink. *Biomaterials* **2016**, *106*, 58–68. https://doi.org/10.1016/J.BIOMATERIALS.2016.07.038.

(263) Smith, P. T.; Basu, A.; Saha, A.; Nelson, A. Chemical Modification and Printability of Shear-Thinning Hydrogel Inks for Direct-Write 3D Printing. *Polymer (Guildf).* **2018**, *152*, 42–50. https://doi.org/10.1016/J.POLYMER.2018.01.070.

(264) Pack, R. C.; Compton, B. G. Material Extrusion Additive Manufacturing of Metal Powder-Based Inks Enabled by Carrageenan Rheology Modifier. *Adv. Eng. Mater.* **2021**, *23* (2), 2000880. https://doi.org/10.1002/ADEM.202000880.

(265) Helgerud, T.; Gåserød, O.; Fjæreide, T.; Andersen, P. O.; Larsen, C. K. Alginates. *Food Stabilisers, Thick. Gelling Agents* **2009**, 50–72. https://doi.org/10.1002/9781444314724.CH4.

(266) Romero, M. J. R. H.; Nakashima, S.; Nikaido, T.; Ichinose, S.; Sadr, A.; Tagami, J. Inhibition of Hydroxyapatite Growth by Casein, a Potential Salivary Phosphoprotein Homologue. *Eur. J. Oral Sci.* **2015**, *123* (4), 288–296. https://doi.org/10.1111/EOS.12196.

(267) Cao, L.; Lu, W.; Mata, A.; Nishinari, K.; Fang, Y. Egg-Box Model-Based Gelation of Alginate and Pectin: A Review. *Carbohydr. Polym.* **2020**, *242*, 116389. https://doi.org/10.1016/J.CARBPOL.2020.116389.

(268) He, Y.; Yang, F.; Zhao, H.; Gao, Q.; Xia, B.; Fu, J. Research on the Printability of Hydrogels in 3D Bioprinting. *Sci. Rep.* **2016**, *6* (1), 29977. https://doi.org/10.1038/srep29977.

(269) Sydney Gladman, A.; Matsumoto, E. A.; Nuzzo, R. G.; Mahadevan, L.; Lewis, J. A. Biomimetic 4D Printing. *Nat. Mater.* **2016**, *15* (4), 413–418. https://doi.org/10.1038/NMAT4544.

(270) Samal, S. K.; Dash, M.; Dubruel, P.; Van Vlierberghe, S. Smart Polymer Hydrogels: Properties, Synthesis and Applications. *Smart Polym. their Appl.* **2014**, 237–270. https://doi.org/10.1533/9780857097026.1.237.

(271) Rastogi, P.; Kandasubramanian, B. Review of Alginate-Based Hydrogel Bioprinting for Application in Tissue Engineering. *Biofabrication* **2019**, *11* (4), 042001. https://doi.org/10.1088/1758-5090/AB331E.

(272) Karoyo, A. H.; Wilson, L. D. A Review on the Design and Hydration Properties of Natural Polymer-Based Hydrogels. *Mater. 2021, Vol. 14, Page 1095* **2021**, *14* (5), 1095. https://doi.org/10.3390/MA14051095.

(273) Groß, D.; Zick, K.; Guthausen, G. Recent MRI and Diffusion Studies of Food Structures. *Annu. Reports NMR Spectrosc.* **2017**, *90*, 145–197. https://doi.org/10.1016/BS.ARNMR.2016.09.001.

(274) Arndt, F.; Schuhmann, S.; Guthausen, G.; Schütz, S.; Nirschl, H. In Situ MRI of Alginate Fouling and Flow in Ceramic Hollow Fiber Membranes. *J. Memb. Sci.* **2017**, *524*, 691–699. https://doi.org/10.1016/J.MEMSCI.2016.11.079.

(275) Wiese, M.; Benders, S.; Blümich, B.; Wessling, M. 3D MRI Velocimetry of Non-Transparent 3D-Printed Staggered Herringbone Mixers. *Chem. Eng. J.* **2018**, *343*, 54–60. https://doi.org/10.1016/J.CEJ.2018.02.096.

(276) Busato, A.; Fumene Feruglio, P.; Parnigotto, P. P.; Marzola, P.; Sbarbati, A. In Vivo Imaging Techniques: A New Era for Histochemical Analysis. *Eur. J. Histochem.* **2016**, *60* (4). https://doi.org/10.4081/ejh.2016.2725.

(277) Haas, S.; Götz, F.; Hubbuch, J. Bio-Based Material Formulation for Extrusion Printing by Dityrosine Crosslinking of Unmodified Casein. *Bioprinting* **2022**, e00245. https://doi.org/10.1016/J.BPRINT.2022.E00245.

(278) Ladeira, B. M.; Custódio, C. A.; Mano, J. F. Core–Shell Microcapsules: Biofabrication and Potential Applications in Tissue Engineering and Regenerative Medicine. *Biomater. Sci.* **2022**, *10* (9), 2122–2153. https://doi.org/10.1039/D1BM01974K.

(279) Post, A. E.; Arnold, B.; Weiss, J.; Hinrichs, J. Effect of Temperature and PH on the Solubility of Caseins: Environmental Influences on the Dissociation of α S- and β-Casein. *J. Dairy Sci.* **2012**, *95* (4), 1603–1616. https://doi.org/10.3168/jds.2011-4641.

(280) Culla, A. C.; Vater, C.; Tian, X.; Bolte, J.; Ahlfeld, T.; Bretschneider, H.; Pape, A.; Goodman, S. B.; Gelinsky, M.; Zwingenberger, S. Treatment of Critical Size Femoral Bone Defects with Biomimetic Hybrid Scaffolds of 3D Plotted Calcium Phosphate Cement and Mineralized Collagen Matrix. *Int. J. Mol. Sci.* **2022**, *23* (6), 3400. https://doi.org/10.3390/IJMS23063400.

(281) Steier, A.; Schmieg, B.; Irtel von Brenndorff, Y.; Meier, M.; Nirschl, H.; Franzreb, M.; Lahann, J.; Steier, A.; Schmieg, B.; Irtel von Brenndorff, Y.; Franzreb, M.; Lahann, J.; Meier, M.; Nirschl, H. Enzyme Scaffolds with Hierarchically Defined Properties via 3D Jet Writing. *Macromol. Biosci.* **2020**, *20* (9), 2000154. https://doi.org/10.1002/MABI.202000154.

Appendix

A. Abbreviations and Symbols

Abbreviations

2D	two-dimensional
3D	three-dimensional
4D	four-dimensional
A260/A280 ratio	absorbance ratio 260 nm to 280 nm
AMS	ammonium sulfate
APS	ammonium persulfate
AR	area ratio
BSA	bovine serum albumin
CV	column volume
DAC	dual asymmetric centrifuge
DLS	dynamic light scattering
DNA	deoxyribonucleic acid
DPBS	Dulbecco's phosphate-buffered saline
DVT	Deuteron VT 819
ELP	elastin-like protein
FLASH	fast low-angle shot
GelMA	methacrylated gelatin
HCP	host cell protein
HNB	hydroxynaphthol blue
HSP	high salt precipitation
IB	inclusion body
IDP	intrinsically disordered protein
IDPR	intrinsically disordered protein region
IMAC	immobilized metal ion affinity chromatography
IPN	interpenetrating polymeric network
ITC	inverse transition cycling
LCST	lower critical solution temperature
LED	light emitting diode
LF	Larmor frequency
LR	length ratio
LRD	Laponite RD
LVR	linear viscoelastic region
MALDI-ToF-MS	matrix-assisted laser desorption ionization-time of flight mass spectrometry
MC	methyl cellulose
MCB	multi-component buffer
MOPSO	3-Morpholino-2-hydroxypropanesulfonic acid
MRI	magnetic resonance imaging
MWCO	molecular weight cut off
NaCl	sodium chloride

NMR	nuclear magnetic resonance
pI	isoelectric point
PLA	polylactic acid
PTFE	polytetrafluoroethylene
RARE	rapid acquisition with relaxation enhancement
RT	room temperature
SA	sodium alginate
SEC	size exclusion chromatography
SDS-PAGE	sodium dodecyl sulfate polyacrylamide gel electrophoresis
SPB	sodium phosphate buffer
TAPS	N-[Tris(hydroxymethyl)methyl]-3-aminopropanesulfonic acid

Symbols – Greek letters

α	significance level of Shapiro-Wilk-Normality test
γ	gyromagnetic ratio of a nucleus
tan δ	loss factor
ε	engineered strain in %
ε_{max}	engineered strain at sample fracture in %
$\varepsilon_{i,280\ nm}$	molar extinction coefficient of the protein i at 280 nm
Θ	interior angle of the non-curved, axially symmetric auxetic structure
σ	engineered stress in Pa
σ_{max}	engineered stress at sample fracture in Pa
τ	shear stress in Pa
ω	angular frequency in rad·s^{-1}

Symbols – Latin letters

A_0	original cross section area before compression in m²
B_0	external magnetic field in T
c	concentration
F	force in Pa
G’	storage modulus in kPa
G’’	loss modulus in kPa
L	sample length at applied force in m
L_0	hydrogel length at applied pre-force during compression in m
L_{max}	hydrogel length at maximum load during compression in m
m_0	hydrogel weight as-prepared in g
m_{dry0}	dried hydrogel weight as-prepared in g
m_{dryl}	dried hydrogel weight after being soaked in liquid and dried again in g
$m_{dry,rel}$	dried weight ratio in %
$m_{protein,tot}$	mass of all proteins in the target buffer solution in g
m_{rel}	relative weight swelling ratio in g/g or %

m_t	hydrogel weight after t days in g
n	number of replicates
P_i	purity of the target molecule i
R^2	coefficient of determination
T1	longitudinal relaxation time in ms
T2	transverse relaxation time in ms
t_i	measurement at time interval i
Tt	transition temperature in °C
Y	process yield of the target molecule in %

B. Supplementary Material for Chapter 3

B.1 Amino acid sequence of ELP[V2Y-45]

```
1         10        20        30        40        50
|         |         |         |         |         |
MDPMSSSGVPGVGVPGVGVPGYGVPGVGVPGVGVPGYGVPGVGVPGVGVP
GYGVPGVGVPGVGVPGYGVPGVGVPGVGVPGYGVPGVGVPGVGVPGYGVP
GVGVPGVGVPGYGVPGVGVPGVGVPGYGVPGVGVPGVGVPGYGVPGVGVP
GVGVPGYGVPGVGVPGVGVPGYGVPGVGVPGVGVPGYGVPGVGVPGVGVP
GYGVPGVGVPGVGVPGYGVPGVGVPGVGVPGYGGREASSHHHHHH
```

B.2 Quantitative analytical methods tested

Cation exchange chromatography

Analytical cation exchange chromatography was conducted on a Vanquish Flex - R2L UHPLC System (Thermo Fisher Scientific) equipped with a TSKgel Q-STAT column (Tosoh Bioscience, Tokyo, JP). The column was equilibrated for 2 min with low salt buffer (10 mM citrate containing 4 M urea, pH 3) before a 10 µl sample injection. A column wash for one more minute with low salt buffer was performed before a 6 min linear gradient from 0 to 100 % with high salt buffer (10 mM citrate containing 4 M urea and 0.75 M sodium chloride, pH 3), which was hold for 4 minutes. Finally, the column was re-equilibrated with a 2 min wash using low salt buffer. All samples were prior filtered through 0.45 µm cellulose acetate filter (Pall Corporation, New York, US-NY). An initially via two cycles of ITC purified sample was applied to determine the ELP[V2Y-45] retention time, before process solution of the IMAC feed was loaded onto the column.
In order to evaluate the purity of the ELP[V2Y-45] elution peak, it was fractionated and prepared for matrix-assisted laser desorption ionization-time of flight mass spectrometry (MALDI-ToF-MS). Therefore, Vivaspin® ultrafiltration units (Sartorius Stedim Biotech, Göttingen, DE) with a molecular weight cut off of 10 kDa were used to reach a final concentration of at least 2 mg/ml total protein concentration. Meanwhile, a buffer exchange towards 10 mM ammonium bicarbonate was performed by three centrifugation cycles. Molecular weight analysis was performed as described in the main text.
Besides ELP[V2Y-45], three more proteins with a size below 16 kDa could be traced in the elution peak (see Figure B.2). Therefore, no quantitative analysis of the target molecule could be reached by this analytical method.

Size Exclusion chromatography

Size exclusion chromatography can be conducted using urea containing buffer systems. Here, initially via two cycles of ITC purified ELP[V2Y-45] as well as two model proteins BSA (Merck KGaA) and lysozyme from chicken egg white (Hampton Research, Aliso Viejo, US-CA) were used as references for host-cell protein (HCP) contamination. All proteins were separately prepared with a concentration of 2 mg/ml in a 20 mM Tris (Tris(hydroxymethyl)aminomethane, Merck KGaA) buffer pH 8 containing 4 M urea, which was also used as running buffer in the SEC method. A constant flow rate of 0.3 ml/min was applied to a Zenix SEC-300 column (Sepax Technologies, Newark, US-DE) which was implemented in a Vanquish Flex – R2L UHPLC system. Thereby, two peaks could be observed

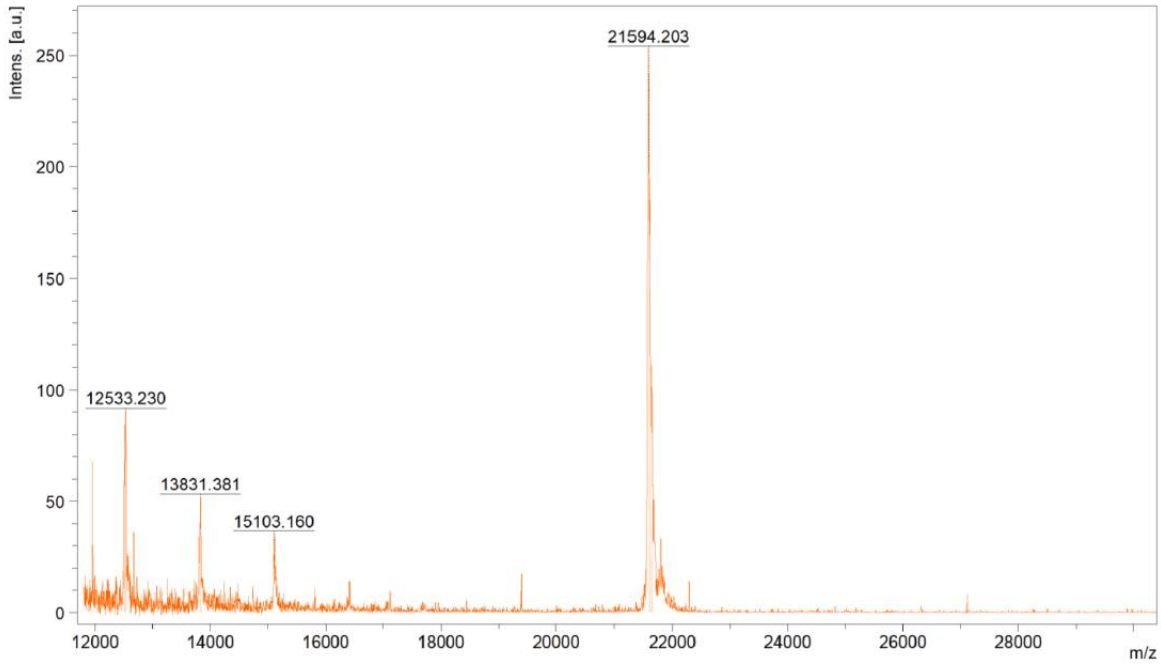

Figure B.2 Intensities of the mass to charge ratio (m/z) of the fractionated, concentrated and rebuffered elution of the UHPLC elution peak containing ELP[V2Y-45]. Four peaks were identified by the spectrometer, three in a range below 16000 m/z and a main peak at 21594.203 m/z corresponding to ELP[V2Y-45].

for ELP[V2Y-45]. The main peak after a retention time of 4.9 minutes covered 97.9 % of total area with a peak shoulder. A smaller peak (2.1 % of the total peak area) could be traced after 2.9 minutes. As one model protein, BSA showed multiple peak behavior and its signal overlapped with the ELP main peak. The second model protein lysozyme showed a pronounced peak tailing. Due to the unsharp ELP peak and difficult model protein behavior, this approach was not further assessed with process solution.

Reversed-phase chromatography (RP)

In preliminary experiments, ELP[V2Y-45] was dissolved with a concentration of 1 mg/ml in common RP running buffers. Thereby, it showed to be insoluble in isopropanol, hexane and acetonitrile without further addition of urea. Since RP separation is based on hydrophobicity and the presence of urea affects hydrophobic interactions no further tests were conducted.

Capillary electrophoresis

Capillary electrophoresis was conducted on a Caliper LabChip®GX II device (PerkinElmer, Waltham, US-MA) according to manufacturer`s protocol. Since ELP[V2Y-45] precipitated during sample preparation and no results could be obtained, sample preparation was adapted by dissolution of the analyzed sample in 20 mM Tris buffer pH 8 containing 4 M urea. As verification that this adaption does not influence analytical quality, lysozyme was used as a protein standard, which showed similar results for both sample preparation methods. However, for ELP[V2Y-45] which was previously purified via two cycles of ITC, estimated protein size was above 52 kDa and no defined single peak could be identified. For an HCP containing

sample, HCP signal overlayed the fluorescence signal of the ELP[V2Y-45]. Therefore, this method was not applicable for quantitative or qualitative analysis.

B.3 Extinction coefficient ELP[V2Y-45]

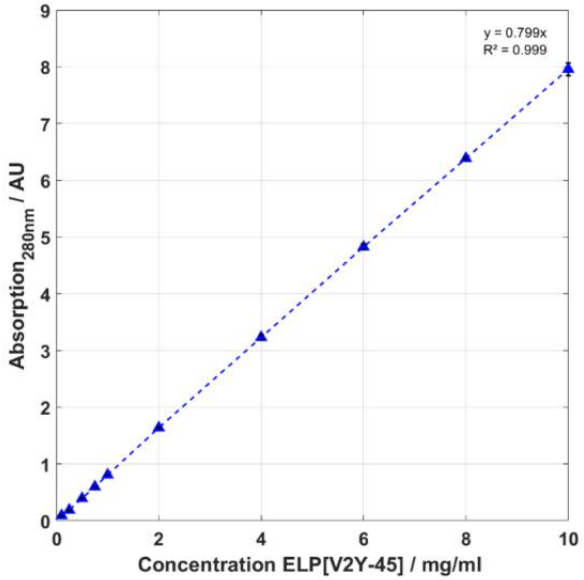

Figure B.3 The extinction coefficient was determined performing an absorption measurement at 280nm using the NanoDrop2000c (Thermo Fisher Scientific, Waltham, US-MA) UV-Vis spectrophotometer. A dilution series between 0.1 to 10 mg/ml of lyophilized ELP[V2Y-45] was prepared in an aqueous buffer system containing 4 M Urea. According to Lambert-Beer law $\varepsilon_{ELP[V2Y-45],280nm}$ = 0.799 L/(g*cm) in the linear absorption range up to at least 10mg/ml. (n = 3)

B.4 Preparation of starting material

Several proteins in the 3.5 to 97 kDa size range are present in the cell lysate. Beside other protein bands, a clearly pronounced band at approximately 26 kDa is observable in the lysate centrifugation pellet, while this band does not stand out in the lysate centrifugation supernatant. The addition of a buffer containing 4 M Urea to the resulting pellet solubilized the inclusion bodies containing the target molecule. After a following centrifugation, the band at 26 kDa in the supernatant is more clearly pronounced than in the centrifugation pellet, while other HCP bands are more pronounced in the pellet compared to the supernatant.

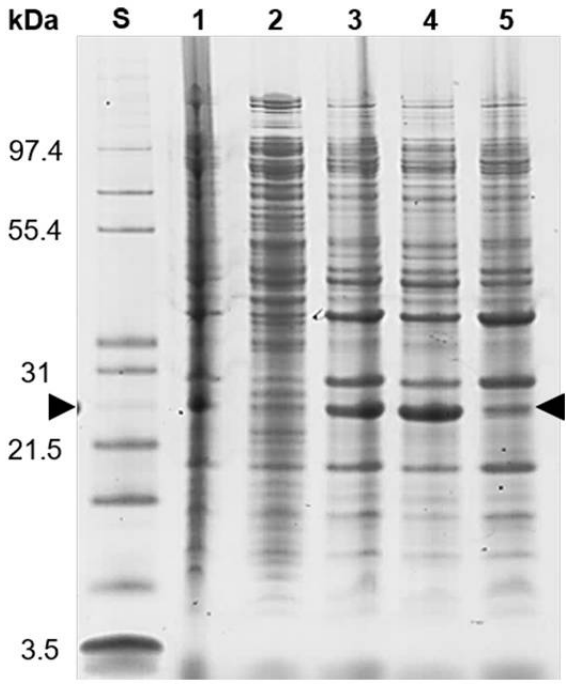

Figure B.4 SDS-PAGE analysis of the start material generation. An Invitrogen™ Mark12™ Unstained Standard (lane S) was used and the target molecule is indicated by arrows. Molecular weights of selected proteins contained in the standard are shown on the left. The lanes are: cell lysate (lane 1); supernatant (lane 2) and pellet (lane 3) after the lysate centrifugation; the generated start material (lane 4) and centrifugation pellet (lane 5) after the inclusion body dissolving.

Table B.4 A260/A280 ratios during the preparation of the start material for all following process steps. The lysate in an aqueous buffer without urea was measured before and after centrifugation. The lysate pellet was resuspended in a buffer system containing 4 M urea for inclusion body dissolution and got centrifuged again (n = 3).

Sample	**A260/A280** -
Lysate - before centrifugation	1.51 ± 0.01
Lysate - centrifugation supernatant	1.66 ± 0.11
Lysate – centrifugation pellet	1.53 ± 0.03
Inclusion body dissolving – centrifugation pellet	1.32 ± 0.01
Inclusion body dissolving – centrifugation supernatant	1.71 ± 0.01

B.5 Homogenization with and without urea

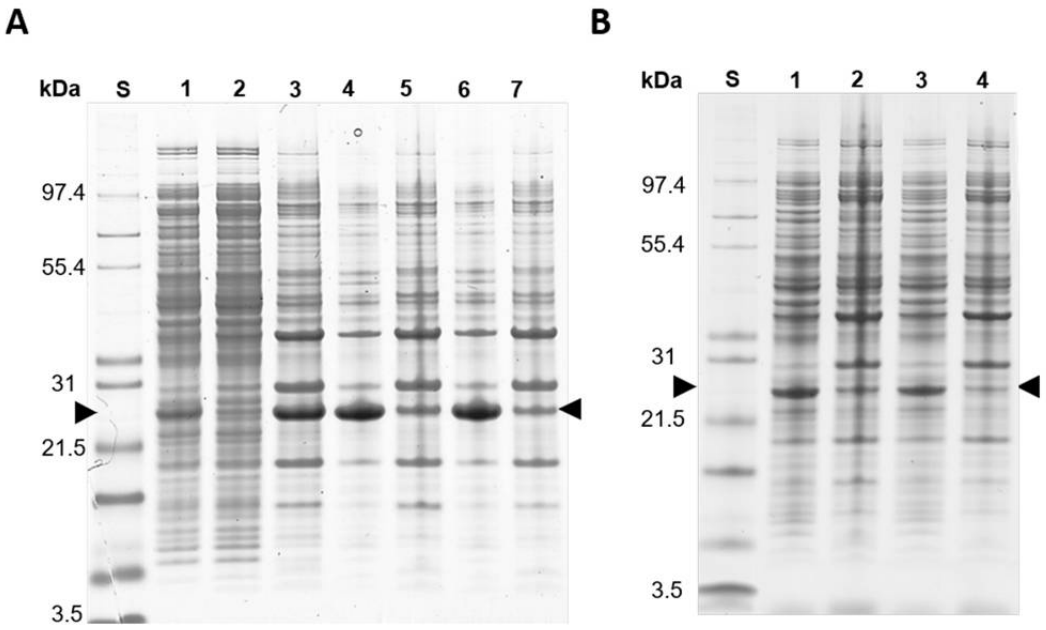

Figure B.5 - SDS-PAGE analysis of the homogenization without urea present during homogenization (A) and with urea present during homogenization (B). The lanes are: (A) cell lysate (lane 1); supernatant (lane 2) and pellet (lane 3) after the lysate centrifugation at 25°C; supernatant (lane 4) and pellet (lane 5) after centrifugation at 25°C of the dissoluted lysate pellet in urea-containing buffer; supernatant (lane 6) and pellet (lane 7) after centrifugation at 4°C of the dissoluted lysate pellet in urea-containing buffer; (B) supernatant (lane 1) and pellet (lane 2) after the lysate centrifugation at 25°C; supernatant (lane 3) and pellet (lane 4) after the lysate centrifugation at 4°C. An Invitrogen™ Mark12™ Unstained Standard (lane S) was used and the target molecule is indicated by arrows. Molecular weights of selected proteins contained in the standard are shown on the left.

B.6 Salt-induced precipitation of start-material

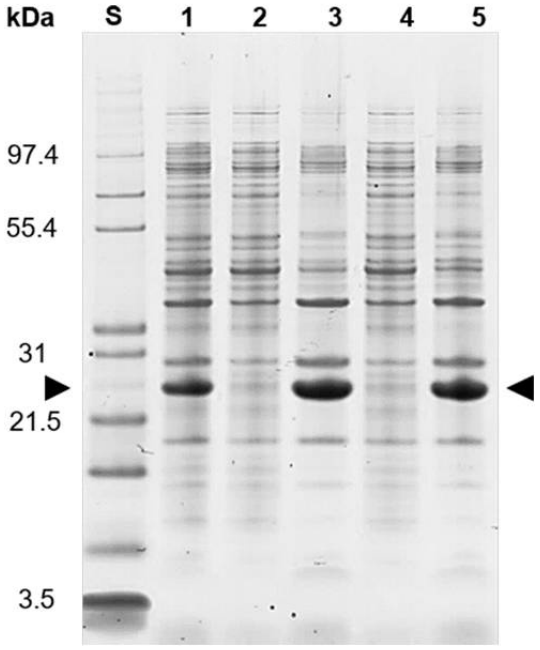

Figure B.6 - Application of 0.4 M ammonium sulfate and 1.5 M sodium chloride on the generated start material containing the target molecule and host cell proteins. An Invitrogen™ Mark12™ Unstained Standard (lane S) was used and the target molecule is indicated by arrows. Molecular weights of selected proteins contained in the standard are shown on the left. The lanes are: start material (lane 1); supernatant (lane 2) and pellet (lane 3) of 0.4M ammonium sulfate precipitation after centrifugation; supernatant (lane 4) and pellet (lane 5) of 1.5M sodium chloride precipitation after centrifugation.

B.7 Buffer compositions and processing temperature of the different purification routes

Table B.7 – Summary of the buffer compositions at different processing steps of the performed purification routes regarding their buffer substances, urea content, pH and temperature

Sample	Salts/Buffer	Urea	pH	T
	-	M	-	°C
Lysate	20mM SPB	0	8	22
Inclusion body dissolving	20mM SPB	4	8	22
High-salt precipitation	20mM SPB + 0.4M AMS	4	8	25
ITC – Cold spin	-	0	Neutral	4
ITC – Hot spin	-	0	Neutral	25
IMAC – Affinity chromatography	20mM SPB + 0.5 M NaCl + 0.5M imidazole	4	7.4	22
All processes - Formulation	20mM SPB	4	8	22

B.8 Nucleic acid content in the different purification routes

Table B.8 - A260/A280 ratios during the performed purification routes. For the high-salt precipitation, the pellet and supernatant were analyzed as well as the final formulation. As the ITC process starts after the HSP only measurements for the cold and hot spin are listed. IMAC feed before application on the chromatography column was compared to the different fractions of the chromatogram (n = 3).

Start material	**1.71 ± 0.01**				
HSP		**ITC**		**IMAC**	
HSP - Supernatant	1.94 ± 0.01	Cold spin - Supernatant	1.85 ± 0.07	IMAC - Feed	1.75 ± 0.05
HSP - Pellet	0.97 ± 0.04	Cold spin - Pellet	0.86 ± 0.02	IMAC - Flow Through	1.82 ± 0.13
Formulation - Pellet	0.89 ± 0.02	Hot spin - Supernatant	0.52 ± 0.00	IMAC - Column Wash	1.51 ± 0.01
Formulation - Supernatant	0.99 ± 0.01	Hot spin - Pellet	2.15 ± 0.01	IMAC - Eluate	0.46 ± 0.00

B.9 Sample load with and without imidazole

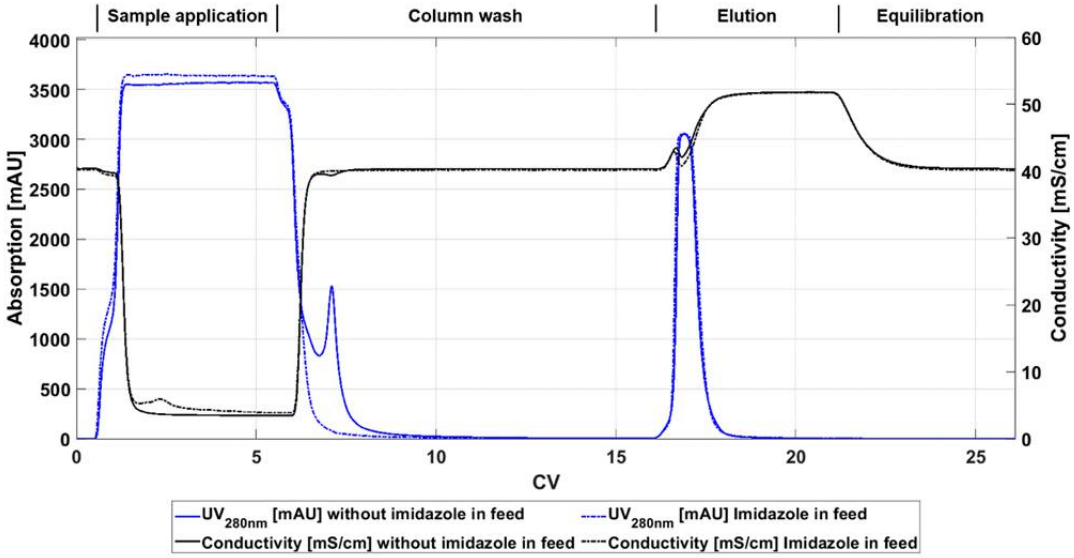

Figure B.9 - Chromatogram of IMAC purification of feed solutions with (line) and without (dashed line) 20mM imidazole. Sample application was performed with a sample pump. Method sections are shown above the graph.

B.10 Size exclusion chromatography

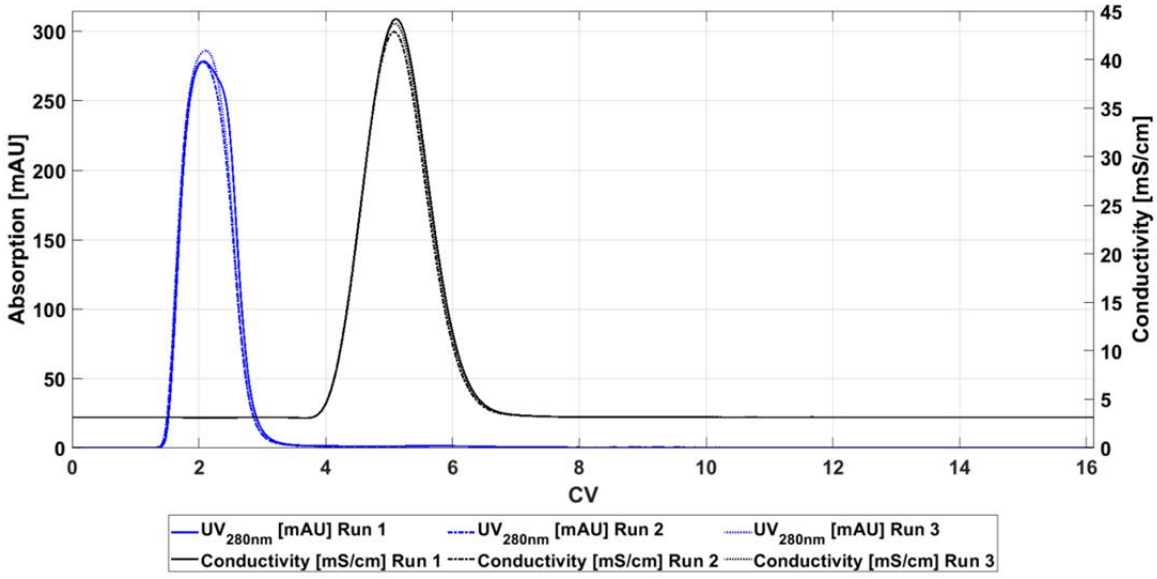

Figure B.10 - Chromatogram of size exclusion chromatography after IMAC purification. Absorbance at 280 nm (blue) indicates a full separation from ions which are correlated to the solution conductivity (black)

B.11 Nickel assay for ELP[V2Y-45]

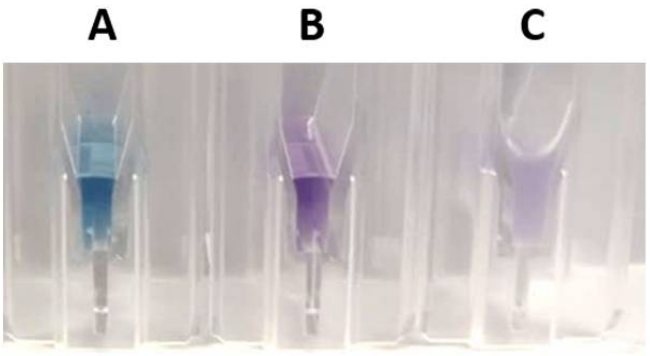

Figure B.11 - Three examples for Ni^{2+} determination. (A) Assay solution without Ni^{2+}, the blue color is caused by HNB. (B) An IMAC elution fraction without protein load is added to the assay solution, the HNB - Ni^{2+} complex shows purple color. (C) IMAC eluate containing [ELPV2Y-45] was used to perform the Ni^{2+} assay. The combination of HNB and imidazole seems to trigger the phase transition of ELP[V2Y-45], resulting in an increase in turbidity.

C. Supplementary Material for Chapter 4

C.1 Hydrogel formulations

Table C.2 - Summary of hydrogel compositions used to investigate the influence of precursor solution composition and storage conditions on the mechanical properties of dityrosine-crosslinked hydrogels

Sample	Precursor solution					Storage			
	Protein	Protein concentration	Urea	Buffer	pH	Urea	Buffer	pH	Excess
#	-	mg/ml	M	-	-	M	-	-	fold
1	BSA	100	0	SPB	8	0	SPB	8	100
2	BSA	100	1	SPB	8	1	SPB	8	100
3	BSA	100	2	SPB	8	2	SPB	8	100
4	BSA	100	3	SPB	8	3	SPB	8	100
5	BSA	100	4	SPB	8	-	-	-	-
6	BSA	100	0	MCB	7	0	DPBS	7.0 - 7.3	25[a)]
7	BSA	100	0	MCB	7	0	MCB	7	25[a)]
8	BSA	100	2	MCB	7	0	DPBS	7.0 - 7.3	25[a)]
9	BSA	100	2	MCB	7	0	MCB	7	25[a)]
10	BSA	100	4	MCB	7	0	DPBS	7.0 - 7.3	25[a)]
11	BSA	100	4	MCB	7	0	MCB	7	25[a)]
12	BSA	100	0	MCB	8	0	DPBS	7.0 - 7.3	25[a)]
13	BSA	100	0	MCB	8	0	MCB	8	25[a)]
14	BSA	100	2	MCB	8	0	DPBS	7.0 - 7.3	25[a)]
15	BSA	100	2	MCB	8	0	MCB	8	25[a)]
16	BSA	100	4	MCB	8	0	DPBS	7.0 - 7.3	25[a)]
17	BSA	100	4	MCB	8	0	MCB	8	25[a)]
18	Casein	100	0	MCB	6	0	DPBS	7.0 - 7.3	25[a)]
19	Casein	100	0	MCB	6	0	MCB	6	25[a)]
20	Casein	100	2	MCB	6	0	DPBS	7.0 - 7.3	25[a)]
21	Casein	100	2	MCB	6	0	MCB	6	25[a)]
22	Casein	100	4	MCB	6	0	DPBS	7.0 - 7.3	25[a)]
23	Casein	100	4	MCB	6	0	MCB	6	25[a)]
24	BSA	20	0	MCB	7	-	-	-	-
25	BSA	40	0	MCB	7	0	MCB	7	32.5[b)]
26	BSA	60	0	MCB	7	0	MCB	7	32.5[b)]
27	BSA	80	0	MCB	7	0	MCB	7	32.5[b)]
28	BSA	100	0	MCB	7	0	MCB	7	32.5 [b)]
29	BSA	20	4	MCB	7	-	-	-	-
30	BSA	40	4	MCB	7	4	MCB	7	32.5[b)]
31	BSA	60	4	MCB	7	4	MCB	7	32.5[b)]
32	BSA	80	4	MCB	7	4	MCB	7	32.5[b)]
33	BSA	100	4	MCB	7	4	MCB	7	32.5[b)]

a) total buffer excess, buffer was exchanged two times (after 24 and 48 hours), total storage time 72 hours

b) total buffer excess, buffer was exchanged three times (after 24, 48, and 72 hours), total storage time 96 hours

C.2 Linear viscoelastic region of BSA-based hydrogels

The linear viscoelastic region (LVR) was determined using amplitude sweeps (n = 2) for angular frequencies ω = 1 and 25 s^{-1} and shear stress τ between 5 and 10.000 Pa. In order to avoid inaccuracies due to large deviations in the measured values at low frequencies, the first 10 measured values were averaged to gain an initial value. The shear rate τ corresponding to a decrease (G ') or increase (G' ') by 10% measured from the initial value was determined as the LVR. Besides a significant increase in the storage modulus for 2 and 3 M urea present during polymerization and storage, LVR increased as well for these conditions compared to 0 M urea. Further, no difference between 0 and 1 M urea could be seen. As the LVR is a measure for the ability of the network to withstand shear forces, this indicates an increasing network strength.

Table C.2 – Linear viscoelastic region depending on urea content in preparation and storage buffer

Urea content / M	Frequency / s^{-1}	Linear viscoelastic region / Pa
0	1	99 ± 23
	25	142 ± 16
1	1	88 ± 10
	25	90 ± 10
2	1	136 ± 15
	25	282 ± 31
3	1	244 ± 5
	25	324 ± 73

C.3 Protein concentration dependent stress-strain curves

Raw data of the uniaxial compression tests is shown in Figure C.3. Comparing the two groups of hydrogels prepared with/without urea, the force increased slower for hydrogels prepared without urea (Figure C.3 A) and reached higher fracture strain compared to samples prepared with urea (Figure C.3 B). Multiple cracks before network fracture can be seen in the stress strain curves of hydrogels, here exemplary shown for BSA-based hydrogels prepared without urea with a concentration of 60 mg/ml (Figure C.3 C) and BSA-based hydrogels prepared with urea with a concentration of 100 mg/ml (Figure C.3 D). This indicates network inhomogeneities and collapsing of weaker connections before a sudden fracture of the entire hydrogel network.

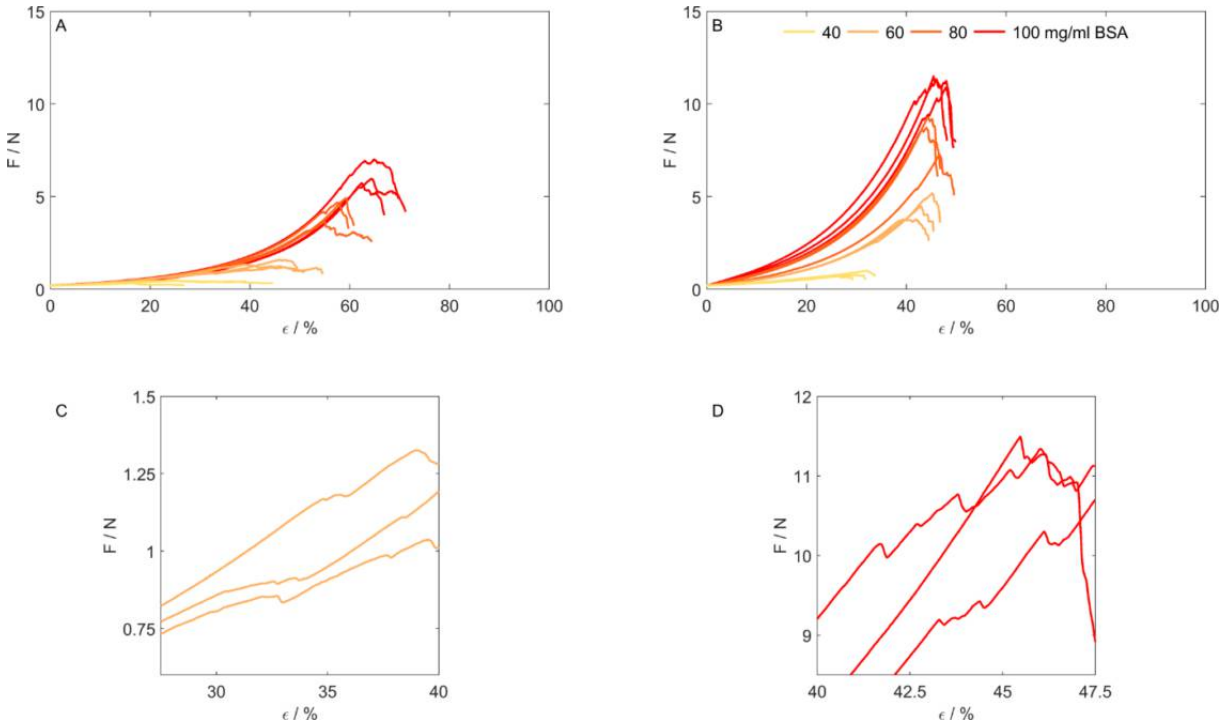

Figure C.3 – Stress-strain curves of the uniaxial compression tests performed with BSA-based hydrogels without (A and C) and with (B and D) 4 M urea present during polymerization and storage in a multi-component buffer. A protein concentration of 40 (yellow), 60 (light orange), 80 (orange) and 100 mg/ml (red) BSA was crosslinked. C and D show details of the triplicate measurements: The measured stress showed multiple drops long before sample failure for the two enlarged conditions 60 mg/ml without urea (C) and 100mg/ml with 4 M urea (D). Each line thereby corresponds to one hydrogel sample.

C.4 Protein concentration dependent hydrogel toughness

Table C.4 – Hydrogel toughness in dependency of the protein concentration for BSA-based hydrogels prepared in MCB without and with 4 M urea in the preparation and storage buffer. Toughness was determined by integrating the stress-strain curves until sample failure and the determination coefficient of a linear fit through 60 – 100 mg/ml (0 M urea) and all data points (4 M urea) is given.

Urea content / M	Protein concentration / mg/ml	Toughness / kJ/m³	R^2 of linear fit / -
0	40	0.2 ± 0.1	Not included in the fit
	60	0.9 ± 0.1	0.9993
	80	2.4 ± 0.3	
	100	4.1 ± 0.7	
4	40	0.4 ± 0.1	0.9998
	60	2.2 ± 0.3	
	80	3.9 ± 0.4	
	100	5.6 ± 0.4	

D. Supplementary Material for Chapter 7

D.1 Liquid characteristics

Table D.1 - Conductivity and pH of the liquids used for sample hydration (n = 2)

Buffer	Conductivity / mS/cm	pH / -
System 1	$< 1 \cdot 10^{-3}$	6.41 ± 0.32
System 2	18.4 ± 0.2	6.45 ± 0.47
System 3	14.9 ± 0.2	8.04 ± 0.09
System 4	2.9 ± 0.3	8.00 ± 0.02

D.2 Auxetic hydrogel scaffold

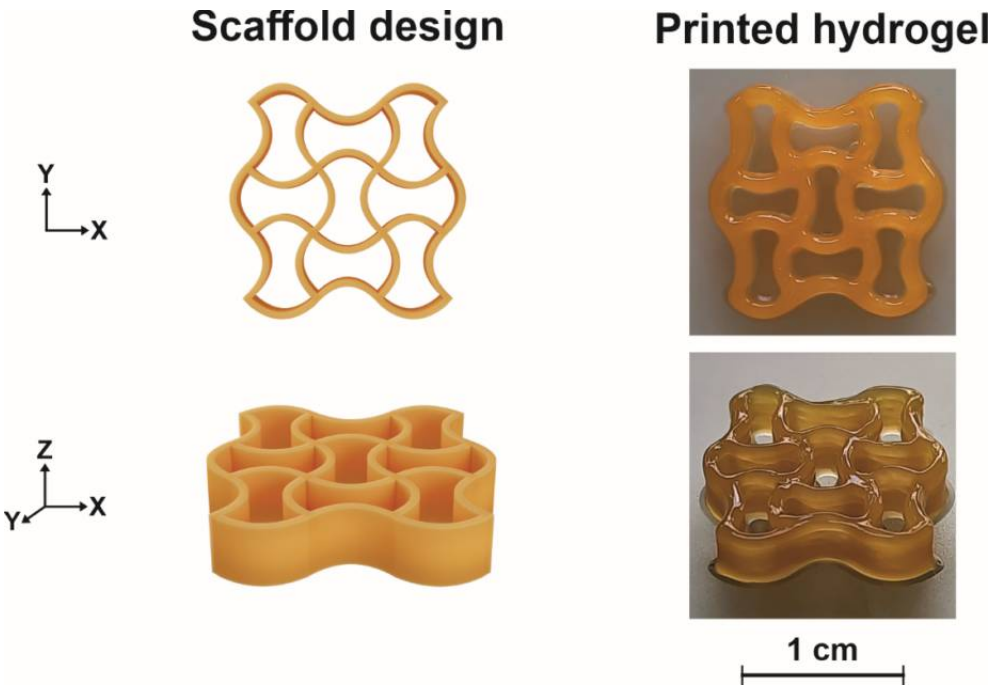

Figure D.2 – Design of the auxetic scaffold consisting of nine point-symmetrically arranged re-entrant honeycomb structures and one of the 3D printed auxetic protein-based hydrogels before drying

D.3 MRI parameters

Table D.3 – MRI device and experimental MRI parameters for the image acquisition of liquid systems 1 to 4

MRI parameter	Value
MRI probe providing the sample chamber	MIC WB40 RES 200 1H 040/025 QTR
Pulse sequence	Fast low-angle shot (FLASH) ortho
Field of view	25 mm x 25 mm
Matrix	128 px x 128 px
Number of Slices	10
Slice thickness	0.6 mm
Slice distance	0 mm
Repetition time	0.2 s
Echo time	1.88 ms
Number of averages	4
Acquisition time	1 min 42 s

D.4 MRI parameters for an optimized buffer-to-hydrogel contrast

Table D.4 – MRI device and experimental MRI parameters for the image generation for the optimized buffer-to-hydrogel contrast for liquid system 2.

MRI parameter	Value
MRI probe providing the sample chamber	MIC WB40 RES 200 1H 040/025 QTR
Pulse sequence	Rapid acquisition with relaxation enhancement (RARE)
Field of view	25 mm x 25 mm
Matrix	128 px x 128 px
Number of Slices	10
Slice thickness	0.6 mm
Slice distance	0 mm
Repetition time	2.13 s
Echo time	10 ms
Number of averages	4
RARE factor	8
Acquisition time	1 min 42 s